Department for
Business, Energy
& Industrial Strategy

Alternative Stores and Notional Development Plan

Key Knowledge Document

NS051-SS-REP-000-00022

This Key Knowledge Document (KKD) was generated as part of the pre-FEED project stage for NEP/NZT and completed in June 2021. This document release was put on hold to allow for the application process for the carbon dioxide licenses CS006 and CS007 by the North Sea Transition Authority to be completed and the licenses awarded in May 2022. The contents of the KKD does not fully reflect the subsequent work after drafting in June 2021.

May 2022

Acknowledgements

Any enquiries regarding this publication should be sent to us at:
enquiries@beis.gov.uk

Contents

Terms and Abbreviations

2D	Two-dimensional (seismic survey)
2DHR	Two-dimensional High Resolution (seismic survey)
3D	Three-dimensional (seismic survey)
AI	Acoustic Impedance
BCU	Base Cretaceous Unconformity
BEIS	Department of Business, Energy and Industrial Strategy
Capture	Collection of CO_2 from power station combustion process or other facilities and its process ready for transportation
Carbon	An element, but used as shorthand for its gaseous oxide, CO_2
CCGT	Combined Cycle Gas Turbine
CCUS	Carbon Capture, Utilisation and Storage
CO_2	Carbon Dioxide
DST	Drill Stem Test
FEED	Front-End Engineering Design
FFM	Full Field Model
FID	Final Investment Decision
GRV	Gross Rock Volume
HC	Hydrocarbon
HMG	Her Majesty's Government (UK government)
Key Knowledge	Information that may be useful, if not vital, to understanding how some enterprise may be successfully undertaken
MDT	Modular Formation Dynamic Tester
MM	Million
MMV	Monitoring, Measurement, and Verification
MT	Mega Tonne (10^6 metric tonnes)
MTPA	Mega Tonnes per Annum
NEP	Northern Endurance Partnership
NPV	Net Pore Volume
NUI	Normally Unmanned Installation
NZT	Net Zero Teesside
OBC	Ocean Bottom Cable
SCAL	Special Core Analysis
SNS	Southern North Sea
SPB	Southern Permian Basin
SPR	Seismic Phase Reversal
Storage	Containment in suitable pervious rock formations located under impervious rock formations usually under the seabed
TDRM	Top-Down Reservoir Modelling
TDS	Total Dissolved Solids
Transport	Removing processed CO_2 by pipeline from the capture and process unit to storage
TVDSS	True Vertical Depth Subsea
TWT	Two-way Time
UKCS	United Kingdom Continental Shelf
ZCH	Zero Carbon Humberside

Foreword

The Net Zero Teesside (NZT) project in association with the Northern Endurance Partnership project (NEP) intend to facilitate decarbonisation of the Humber and Teesside industrial clusters during the mid-2020s. Both projects will look to take a Final Investment Decision (FID) in early 2023, with first CO2 capture and injection anticipated in 2026.

The projects address widely accepted strategic national priorities – most notably to secure green recovery and drive new jobs and economic growth. The Committee on Climate Change (CCC) identified both gas power with Carbon Capture, Utilisation and Storage (CCUS) and hydrogen production using natural gas with CCUS as critical to the UK's decarbonisation strategy. Gas power with CCUS has been independently estimated to reduce the overall UK power system cost to consumers by £19bn by 2050 (compared to alternative options such as energy storage).

Net Zero Teesside Onshore Generation & Capture

NZT Onshore Generation & Capture (G&C) is led by bp and leverages world class expertise from ENI, Equinor, and TotalEnergies. The project is anchored by a world first flexible gas power plant with CCUS which will compliment rather than compete with renewables. It aims to capture ~2 million tonnes of CO2 annually from 2026, decarbonising 750MW of flexible power and delivering on the Chancellor's pledge in the 2020 Budget to "support the construction of the UK's first CCUS power plant." The project consists of a newbuild Combined Cycle Gas Turbine (CCGT) and Capture Plant, with associated dehydration and compression for entry to the Transportation & Storage (T&S) system.

Northern Endurance Partnership Onshore/Offshore Transportation & Storage

The NEP brings together world-class organisations with the shared goal of decarbonising two of the UK's largest industrial clusters: the Humber (through the Zero Carbon Humber (ZCH) project), and Teesside (through the NZT project). NEP T&S includes the G&C partners plus Shell, along with National Grid, who provide valuable expertise on the gathering network as the current UK onshore pipeline transmission system operator.

The Onshore element of NEP will enable a reduction of Teesside's emissions by one third through partnership with industrial stakeholders, showcasing a broad range of decarbonisation technologies which underpin the UK's Clean Growth strategy and kickstarting a new market for CCUS. This includes a new gathering pipeline network across Teesside to collect CO2 from industrial stakeholders towards an industrial Booster Compression system, to condition and compress the CO2 to Offshore pipeline entry specification.

Offshore, the NEP project objective is to deliver technical and commercial solutions required to implement innovative First-of-a-Kind (FOAK) offshore low-carbon CCUS infrastructure in the UK, connecting the Humber and Teesside Industrial Clusters to the Endurance CO2 Store in the Southern North Sea (SNS). This includes CO2 pipelines connecting from Humber and Teesside compression/pumping systems to a common subsea manifold and well injection site

at Endurance, allowing CO2 emissions from both clusters to be transported and stored. The NEP project meets the CCC's recommendation and HM Government's Ten Point Plan for at least two clusters storing up to 10 million tonnes per annum (Mtpa) of CO2 by 2030.

TEESSIDE (NZT)

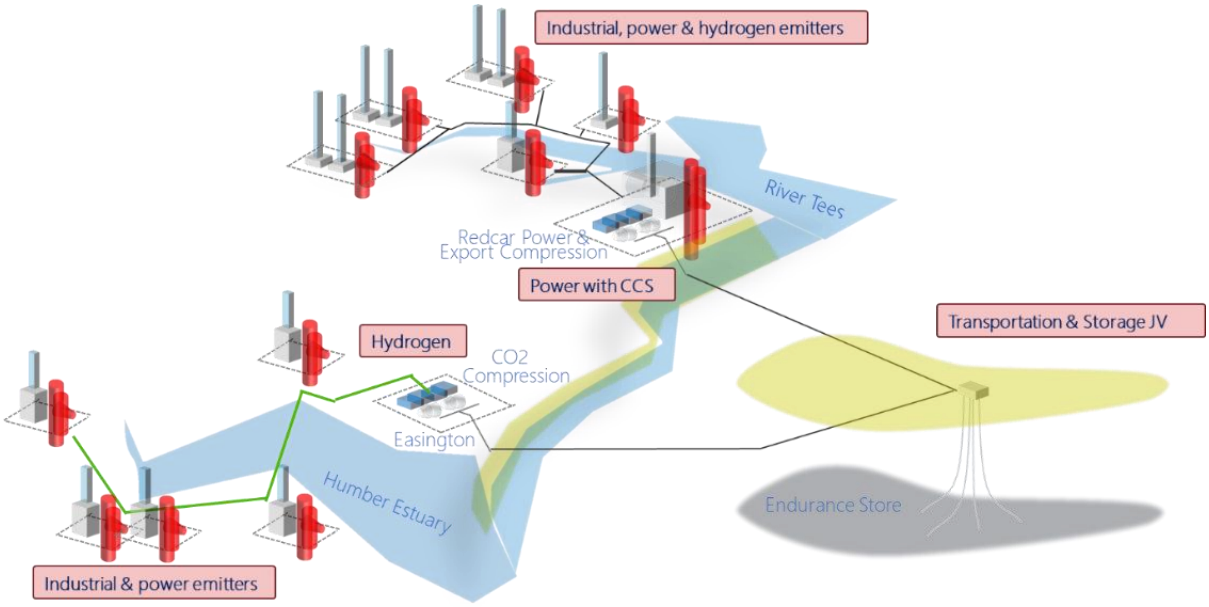

HUMBERSIDE (ZHC) NEP

The project initially evaluated two offshore CO2 stores in the SNS: 'Endurance', a saline aquifer formation structural trap, and 'Hewett', a depleted gas field. The storage capacity requirement was for either store to accept 6+ Mtpa CO2 continuously for 25 years. The result of this assessment after maturation of both options, led to Endurance being selected as the primary store for the project. This recommendation is based on the following key conclusions:

The storage capacity of Endurance is 3 to 4 times greater than that of Hewett.

The development base cost for Endurance is estimated to be 30 to 50% less than Hewett.

CO2 injection into a saline aquifer is a worldwide proven concept, whilst no benchmarking is currently available for injection in a depleted gas field in which Joule-Thompson cooling effect has to be managed via an expensive surface CO2 heating solution.

Following selection of Endurance as the primary store, screening of additional stores has been initiated to replace Hewett by other candidates. Development scenarios incorporating these additional stores will be assessed as an alternative to the sole Endurance development.

Executive Summary

The work programme for Net Zero Teesside includes the assessment of potential additional CO2 stores in the area for future expansion of CO2 storage capacity. Five stores are evaluated in this report: BC36, BC37, BC39, BC40 and BC3. The Alternative Stores are secondary in quality to the Endurance Store but cumulatively may offer up to an additional 1 GT of CO2 storage if pressure management is used (e.g. brine production).

The key conclusions from the assessment of these alternative stores for CO2 storage are as follows:

- Legacy wells without primary containment at Bunter Sandstone level are a significant problem because they pose a risk of potential CO2 leakage and are technically challenging to remediate. New technology in this area may be needed to progress BC36, BC37 and BC3 further.
- Reservoir quality appears to be poorer than Endurance (a higher degree of shale content and/or cementation).
- There is no core or well tests over the Bunter Sandstone in any of the structures, so permeability and injection rates have high uncertainty.

This assessment identified BC39 as the best candidate for CO2 storage. It is large, lies quite close to Endurance and has no legacy wells within the structural closure. However, it is lacking full seismic coverage and has no on-structure well penetration. Further appraisal is required. BC36 and BC37 both have legacy wells without containment at reservoir level and cannot be developed before this is resolved.

1.0 Introduction

The Bunter Closures (BC) in the Southern North Sea are some of the saline aquifer structures that have been identified as potentially suitable storage sites for CCUS. This report is one of a series of key knowledge documents (KKD), which describes the work program undertaken by the Net Zero Teesside & Northern Endurance Partnership (NZT/NEP) to characterise the subsurface at Bunter Closures BC36, BC37, BC39, BC40 and BC3 (the 'Alternative Stores').

1.1 Purpose

The purpose of this document is to summarize the work program completed on the integrated subsurface description of the Alternative Stores.

1.2 Location

The Alternative Stores are situated within the United Kingdom Continental Shelf (UKCS) in the Southern North Sea (SNS), about 100–150 km east offshore from Flamborough Head (**Figure 1**). They are located in quadrants 43, 44 and 49, to the east and southeast of the Endurance primary CO2 store.

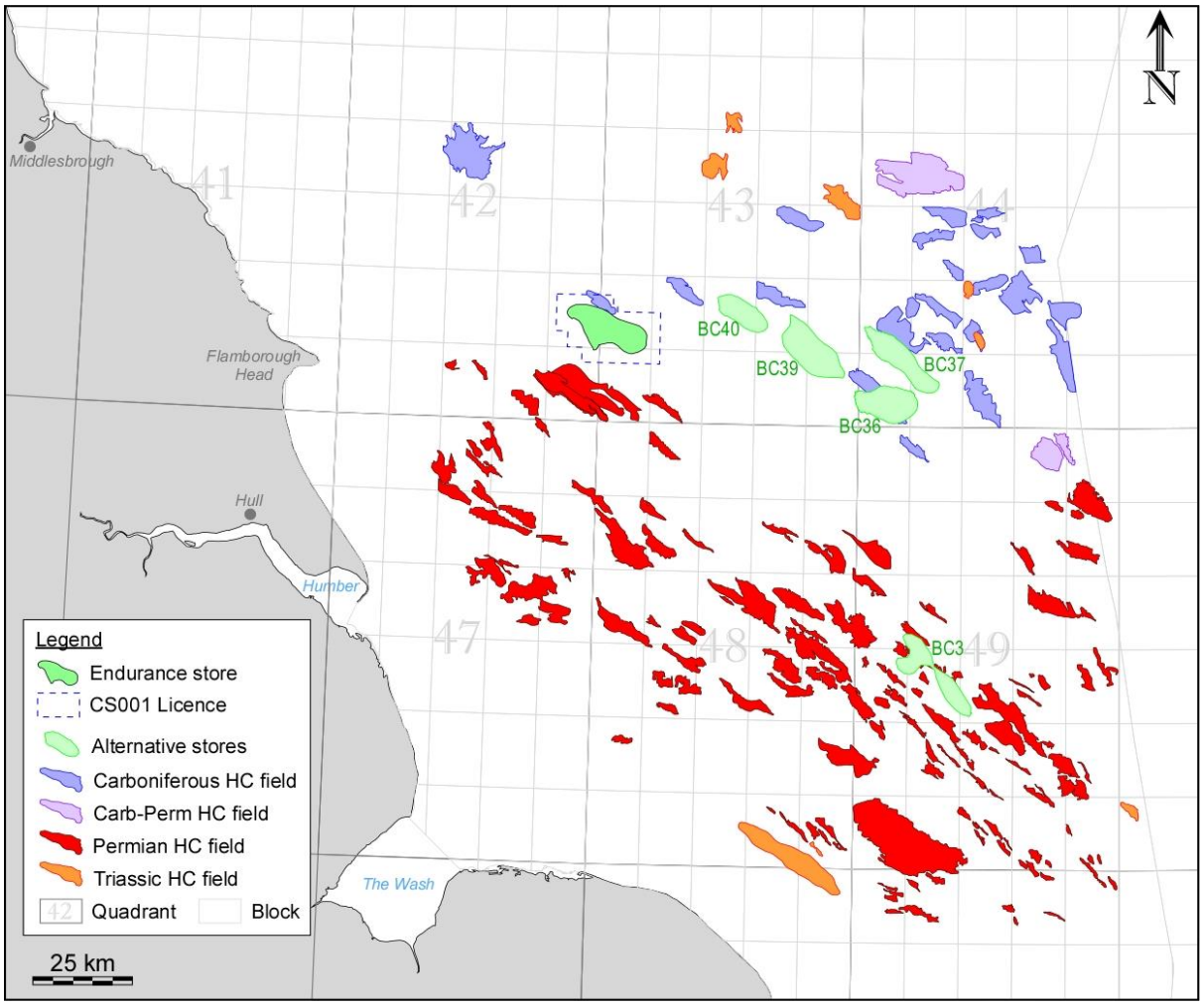

Figure 1 - Location map of the Alternative CO2 Stores in the Southern North Sea.

1.3 Geological Setting

The Alternative Stores are four-way dip-closed anticlines, formed above salt pillows, oriented NW–SE. They are located within the Silverpit and Sole Pit sub-basins at the western end of the much larger, E–W striking Southern Permian Basin (SPB). The basin is bound to the west by the Dowsing Fault Zone and to the east by the Cleaver Bank High. The northern limit is defined by the Mid North Sea High and the southern limit by the London-Brabant Massif (**Figure 2**).

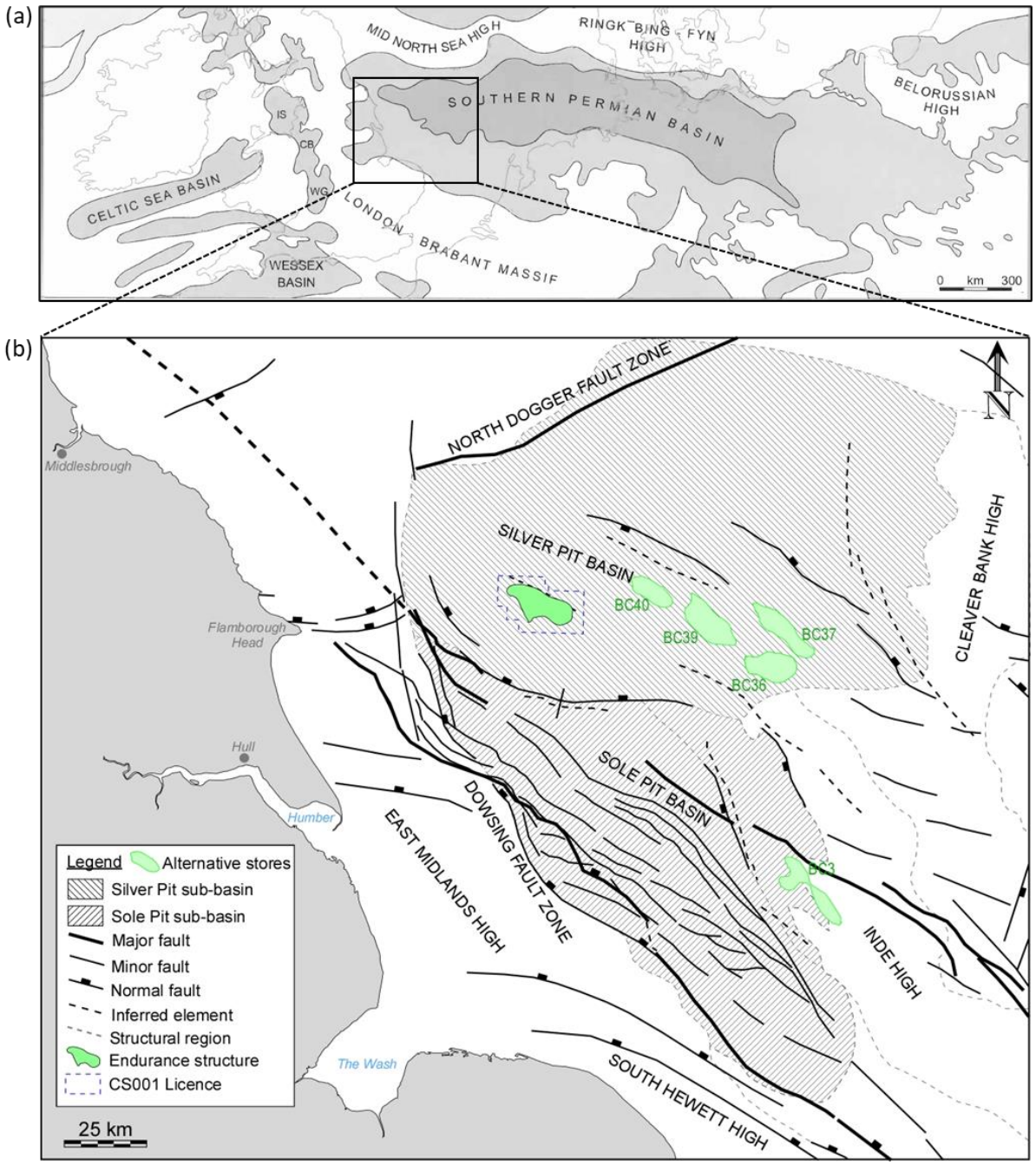

Figure 2 - Tectonic setting: (a) Extent of the Southern Permian Basin (modified from Underhill, 2003); (b) Structural elements of the Southern North Sea (modified from Richards, 2015; Pharoah et al., 2010).

1.3.1 Structural and Stratigraphic Evolution

The region has had a complex tectonic evolution but can be summarised into three key evolutionary periods: Palaeozoic continental collision and plate accretion (formation of Pangea), late Palaeozoic–Mesozoic intraplate subsidence and continental rift tectonics (break-up of Pangea), and late Mesozoic–Cenozoic inversion and thermal uplift (Alpine Collision). The regional tectonostratigraphy of the SNS is summarised in **Figure 3** and the lithostratigraphy is summarised in **Figure 4**. The oldest sediments penetrated within the Alternative Stores area are those deposited during the mid to late Carboniferous, unconformably overlain by a thick sequence of Permian, Triassic and early Jurassic sediments. A major unconformity separates the Jurassic from the Cretaceous to Cenozoic stratigraphy.

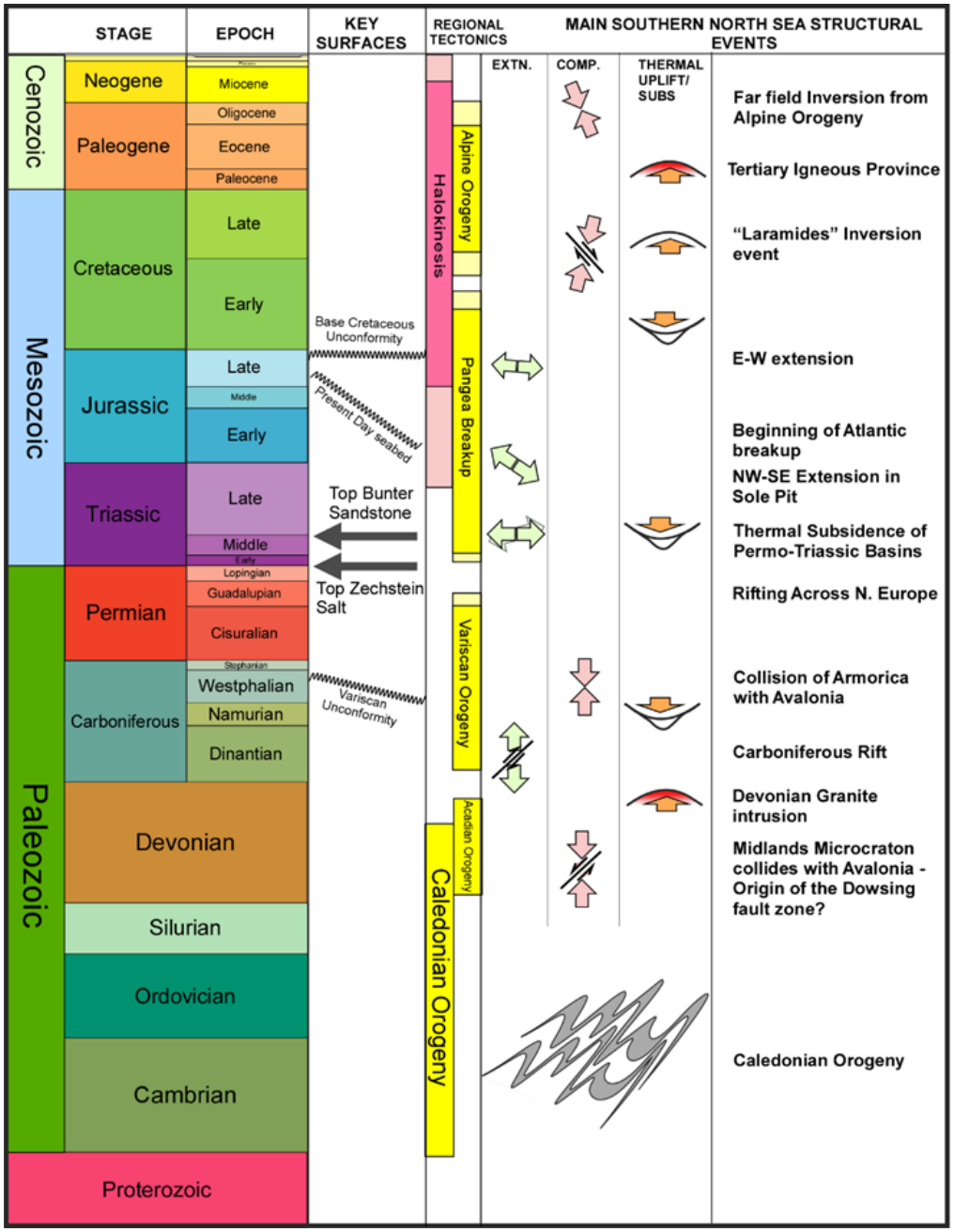

Figure 3 - Regional tectonostratigraphy of the Southern North Sea.

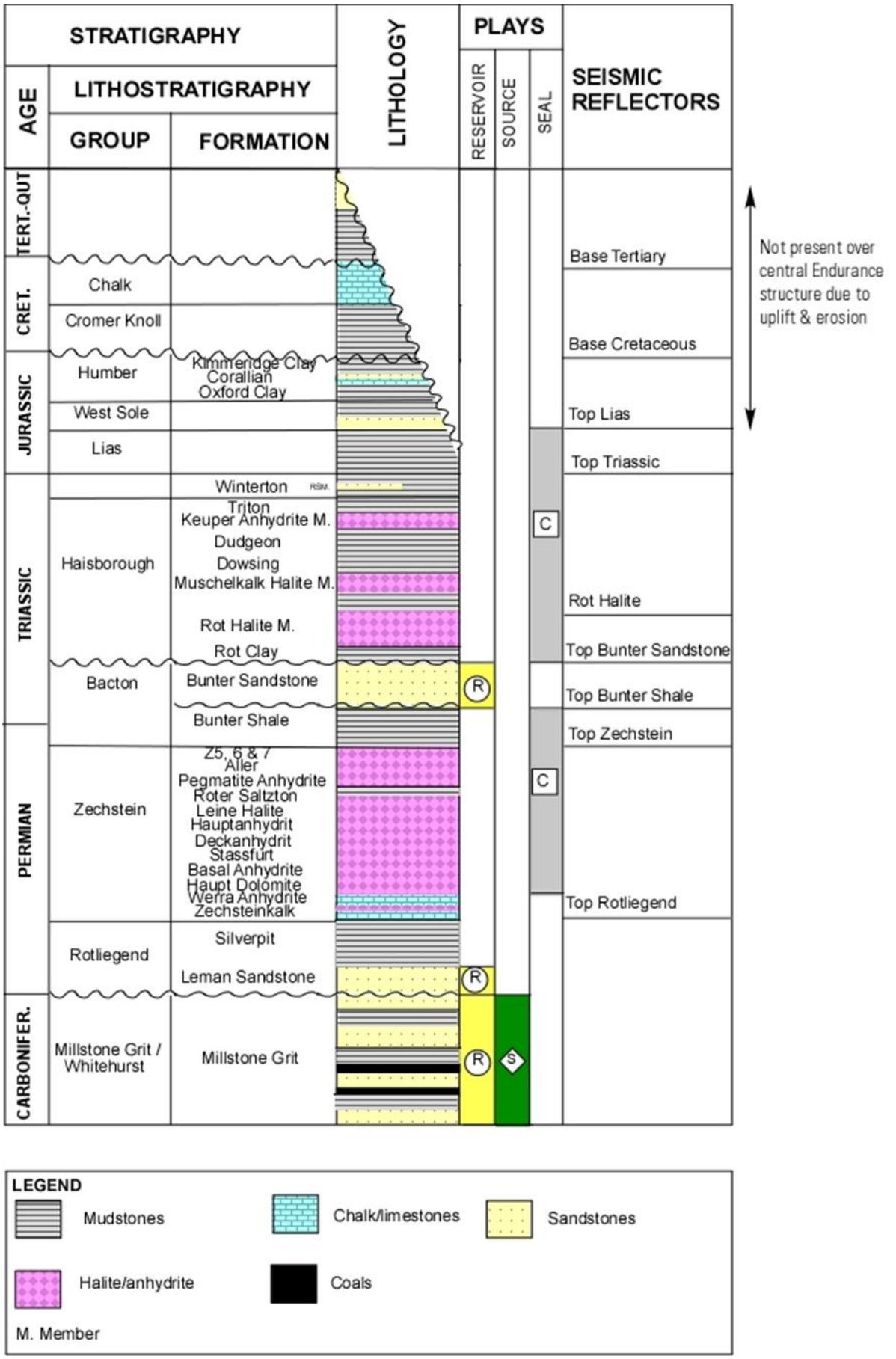

Figure 4 - Stratigraphic column for the Southern North Sea.

1.3.1.1 Ordovician to Carboniferous

Much of the structural fabric originates from the Caledonian and Variscan plate tectonic cycles during the Palaeozoic (Underhill, 2003). The Ordovician to Devonian Caledonian Orogeny influenced the development of NW–SE striking structures aligned with the northeastern boundary of the Midlands Microcraton during the Devonian (e.g. the Dowsing Fault Zone) (Guterch et al., 2010). Lithospheric extension and rifting commenced during the late Devonian to early Carboniferous, with active fault-bounded half grabens and tilted fault blocks developed in the Southern North Sea area, following the NW–SE trends of the older Caledonian basement (Coward et al., 2003; Moscariello, 2003). By the Late Carboniferous, the Southern North Sea area had transitioned to humid equatorial conditions and was an established deltaic province, characterised by deltaic to fluvio-lacustrine deposits with numerous coal layers (Underhill, 2003; Kombrink et al., 2010). Subsequent compression associated with the Variscan Orogeny resulted in fault reactivation, folding, uplift and erosion of the Carboniferous strata, with progressively younger Carboniferous-age rocks sub-cropping from west to east beneath the Variscan Unconformity (Moscariello, 2003; Grant et al., 2018).

1.3.1.2 Permian

Subsidence in the early Permian, in response to post-orogenic collapse and rifting at the end of the Variscan Orogeny, led to the development of the intracratonic Southern Permian Basin. This was an extensive basin which extended from the UK Southern North Sea eastwards as far as Poland (Underhill, 2003; Grant et al., 2018). Syn-sedimentary rifting occurred during the Permian, influenced by the NW–SE basement fault trends, which continued to be reactivated repeatedly during the Mesozoic and Cenozoic.

The ongoing plate tectonic movements meant that by the time the Southern Permian Basin was initiated it had drifted northwards of the equator to within the northern hemisphere desert belt (Glennie, 1997). An arid climate prevailed and the Permian Rötliegend Group deposition was within an entirely land-locked basin, with terminal playa and saline lakes developed in the central, deepest parts of the basin. Within the Southern North Sea area, the Rötliengend Group is represented by two key formations: the Leman Sandstone Formation and the Silverpit Formation. The Leman Sandstone Formation consists of cross-bedded, dune sandstones deposited within an aeolian desert environment, which laterally grade northwards into the Silverpit Formation, composed of mudstones and interbedded evaporites deposited within a playa lake environment (Gast et al., 2010; Underhill, 2003).

The Southern Permian Basin was flooded by marine waters during the late Permian. The Zechstein Group depositional environment reflects cycles of marine incursions which subsequently increased in salinity and progressively evaporated, leading to cyclic deposition of marine carbonates and mudstones followed by widespread evaporite deposits (Glennie, 1997; Underhill, 2003).

1.3.1.3 Triassic

The active basin extension in the Southern North Sea area waned through the late Permian and was succeeded by a phase of thermal subsidence, a period of tectonic quiescence which continued through the Triassic to Early Jurassic times (Underhill, 2003; Grant et al., 2018).

Semi-arid continental conditions also returned at the end of the Permian. Ephemeral fluvial systems drained northwards off the Variscan fold belt and the Triassic Bacton Group sediments (Bunter Shale Formation and Bunter Sandstone Formation) were deposited in predominantly fluvial, lacustrine and playa lake environments, which were subject to aeolian reworking (Bachmann et al.,2010; Geluk et al, 2018). In the mid Triassic, episodic marine incursions into partially restricted basins under dry climatic conditions resulted in the deposition of marine (and subordinate lacustrine) evaporites, mudstones and limestones of the lower Haisborough Group (Geluk et al;, 2018; Moscariello, 2003). In the late Triassic, more non-marine conditions returned, with deposition of clastics, evaporites and carbonates in emphemeral lake and fluvial systems (upper Haisborough Group). At the end of the Triassic (Penarth Group), there was a marine transgression and the depositional environments transitioned from non-marine, through paralic systems to marine conditions by the early Jurassic (Bachmann et al., 2018).

Subsidence in the Triassic–Jurassic was controlled by continued extension on the Dowsing Fault Zone, but sediment distribution was increasingly affected by salt tectonics, whereby the Zechstein Salt that had been deposited during the Late Permian formed into salt swells in response to the developing sedimentary load (Stewart & Coward, 1995; Pharaoh et al., 2010).

1.3.1.4 Jurassic to Early Cretaceous

Global sea level rise and flooding in the early Jurassic created a shallow epicontental basin into which shallow, open-marine, fine-grained mudstones of the Lias Group were deposited (Lott et al., 2010). In the mid Jurassic, thermal doming and uplift in the region of the North Sea Rift triple junction to the north of the Southern North Sea led to considerable erosion and removal of much of the Mesozoic section (Stewart & Coward, 1995; Pharaoh et al., 2010). The subsequent collapse of the thermal dome culminated in the extensional tectonics of the North Sea Rift during the Late Jurassic to Early Cretaceous, which was expressed as transtensional subsidence in NW-SE trending Sole Pit Basin, whilst rift flank uplift and erosion took place to the northeast, resulting in a combined complex of unconformities known as the Base Cretaceous Unconformity (Stewart & Coward, 1995; Pharaoh et al., 2010; Grant et al., 2018). The remainder of the Jurassic section after the Lias Group is absent in the area of interest due to the erosion associated with the Base Cretaceous Unconformity.

1.3.1.5 Late Cretaceous to Cenozoic

Open-marine depositional environments continued throughout the Cretaceous, with the deposition of shallow-marine argillaceous sediments of the Cromer Group in the Lower Cretaceous, followed by a thick sequence of chert-rich limestones, chalks and marls of the Chalk Group in the Upper Cretaceous (Moscariello, 2003). Post-rift thermal subsidence was established over the Southern North Sea area by the Late Cretaceous. Towards the end of the Late Cretaceous and throughout the Early Cenozoic, there was widespread basin uplift and several pulses of structural inversion related to the opening of the Atlantic Ocean and Alpine collision in Europe (Pharaoh et el, 2010; Grant et al., 2018). Within the Silverpit Basin, the structure is dominated by NW-trending Zechstein Salt pillows and walls, folding the post-Permian sequence into a series of NW-SE trending anticlines and synclines. Widespread halokinesis of the Zechstein salts was triggered by the Cenozoic inversion and reactivation of

basement faults under a dextral transpressional regime (Pharaoh et al., 2010; Conway & Valvatne, 2003; Moscariello, 2003). The final phase of inversion was in the Oligocene–Miocene, after which time thermal subsidence resumed and the remainder of the Cenozoic is characterised by marine and glacio-marine argillaceous sandstones, siltstones and clays (O'Mara et al., 2003; Moscariello, 2003).

1.4 Exploration and Appraisal History

Exploration for hydrocarbons first commenced in the Southern North Sea in the 1960s, targeting possible gas at the Triassic Bunter Sandstone 4-way structural closures. BC37 was drilled by well 44/21-1 in 1965 and BC36 by well 44/26-1 in 1968. Both wells failed to discover hydrocarbons at this stratigraphic level, due to a lack of charge. Subsequent hydrocarbon exploration in the licence application area in the 1980s and 1990s focussed on the gas targets in the Carboniferous. The Schooner gas field was discovered beneath BC36 structure in 1986 with exploration well 44/26-2 into Carboniferous Westphalian Coal Measures and Barren Red Measures formations, and was appraised by a further two wells, before commencing commercial gas production in 1996 (now ceased). BC40 was drilled by exploration well 43/23-3 in 1994, which was targeting the Triassic Bunter Sandstone, but was also a dry hole due to a lack of charge access through the Zechstein salt.

1.5 Storage Site Concept

The proposed CO2 injection reservoir is the Triassic-age Bunter Sandstone Formation within the structural closures of the BC36, BC37, BC39, BC40 and BC3 anticlines. Containment is provided by the overlying a Clay and Röt Halite (base Haisborough Group) as primary seals, plus secondary seals within the remainder of the Haisborough Group, Penarth Group and Early Jurassic.

2.0 Database

As the Southern North Sea has been a producing gas province for several decades, there is a significant amount of data that has been acquired over the years. The NZT/NEP project team had access to a PGS Megamerge 3D seismic dataset (stitched together from multiple surveys or varying vintages) as a seismic baseline for the extended area and well data from the publically-available Oil and Gas Authority's National Data Repository (NDR).

2.1 Seismic Database

The PGS Megamerge 3D seismic data has been utilised for interpretation over a wide area (**Figure 5**). Whilst there are some gaps in coverage (**Figure 6**), overall the imaging of the Triassic section is good for structural interpretation and accurate interpretation of the top Bunter Sandstone is possible. The data was provided with reverse polarity and has been phase shifted 180 degrees to follow the convention of a trough being a soft response and a peak being a hard response. The majority of the structures sit in the J07 volume. The details of the seismic over each structure are discussed below in Section 0.

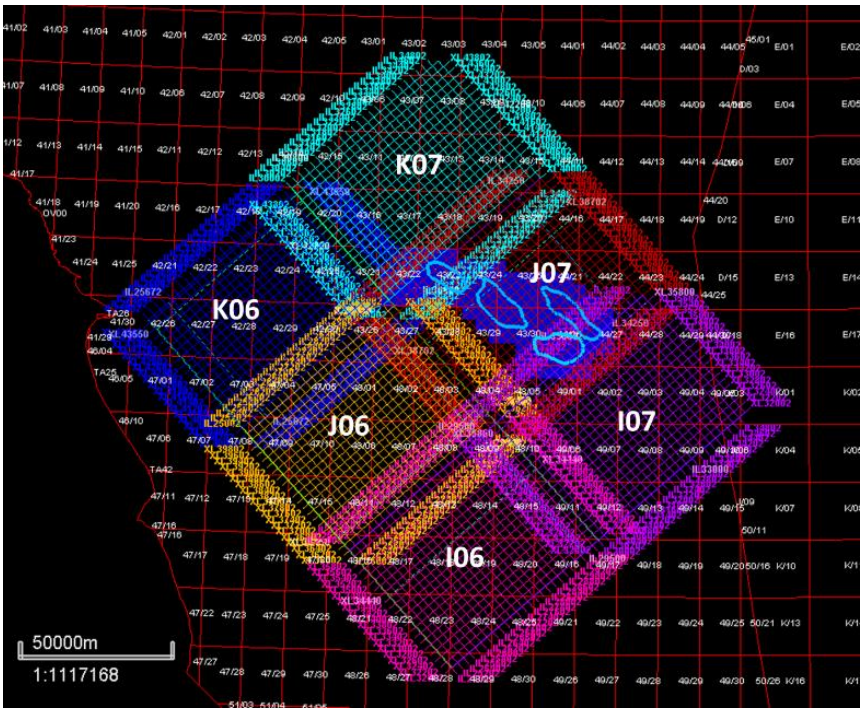

Figure 5 - PGS Megamerge 3D seismic volumes used for seismic interpretation.

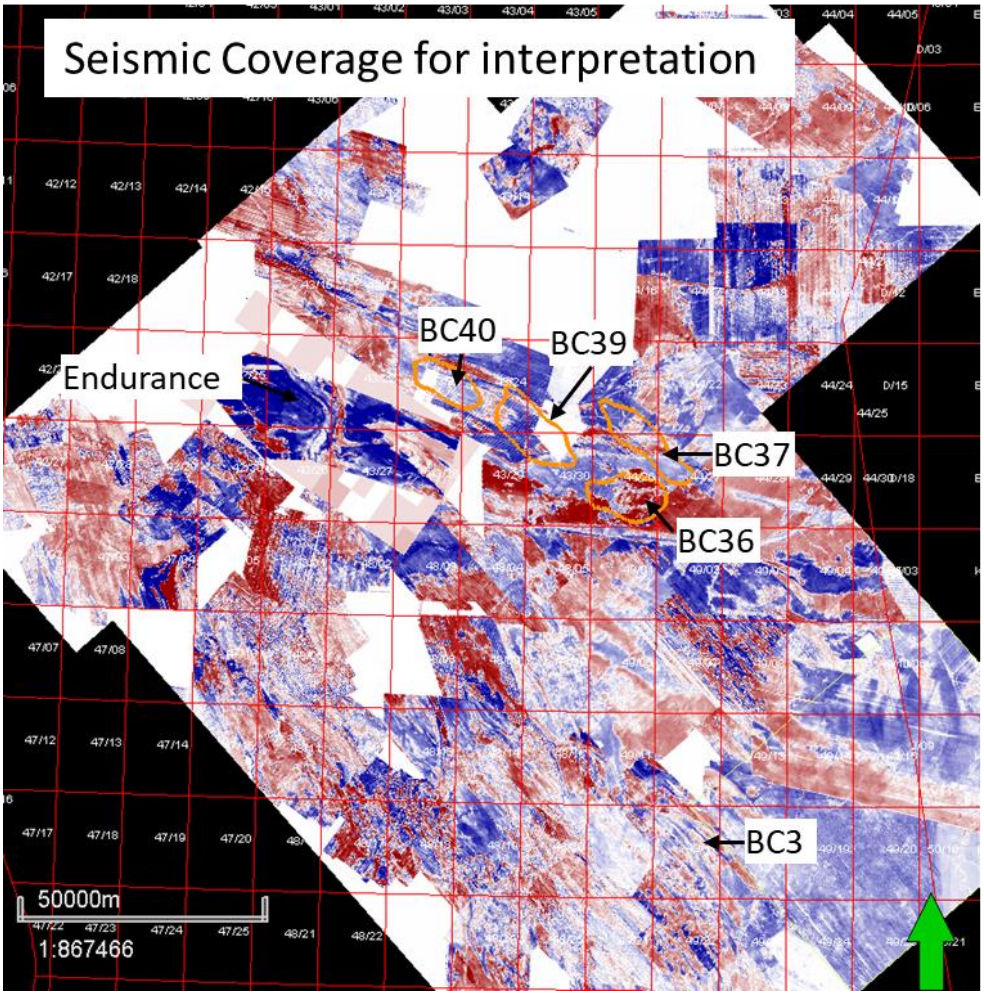

Figure 6 - Seismic coverage of the area: Areas in white have no available seismic data. Also note the patchwork of surveys with different acquisition styles.

2.2 Well Database

A large regional well database was assembled for depth conversion calibration (where applicable) and reservoir thickness calculations (**Table 1** and **Figure 7**).

Table 1 - List of wells used for depth conversion and Bunter Sandstone thickness calculations.

Well	Surface	X	Y	mTVDSS	mMD
42/15B-1	Top Bunter Sandstone	364429.81	6046061	-988.66	1025
42/25-1	Top Bunter Sandstone	368296.42	6011029	-1114	1114
42/25-2	Top Bunter Sandstone	357524.6	6014880	-1695.98	1733
42/30-1	Top Bunter Sandstone	361384.85	5992998	-1656.62	1686
43/11-1	Top Bunter Sandstone	373652.81	6050645	-820.03	856
43/12-1	Top Bunter Sandstone	394939.24	6041127	-1343.99	1383
43/15-B1	Top Bunter Sandstone	430053.87	6041123	-1605.91	1637
43/17-1	Top Bunter Sandstone	384498.46	6022562	-727.22	758
43/18-1	Top Bunter Sandstone	397706.45	6033439	-1250.57	1290.5
43/20-1	Top Bunter Sandstone	431954.32	6039279	-1589.82	1620
43/21-1	Top Bunter Sandstone	369943.96	6009606	-1023.17	1057
43/21-3	Top Bunter Sandstone	379426.43	6010241	-1572.04	1614

43/23-2	Top Bunter Sandstone	407597.25	6019963	-2163.03	2203
43/23-3	Top Bunter Sandstone	406915.81	6011170	-1563.63	1606
43/24-1	Top Bunter Sandstone	412770.3	6017822	-2062	2100.68
43/24-2	Top Bunter Sandstone	415673.76	6015934	-1949	1986.25
43/24-3	Top Bunter Sandstone	419496.62	6014988	-2205	2242.69
43/25-1	Top Bunter Sandstone	424437.26	6013266	-2357	2391.14
43/26-1	Top Bunter Sandstone	370196.47	5991172	-1425.66	1463
43/27-3	Top Bunter Sandstone	391394.71	5992992	-1584.63	1622
43/28-1	Top Bunter Sandstone	406041.35	5992797	-1530.31	1557
43/28-2	Top Bunter Sandstone	404433.29	5987317	-1504.02	1537
43/30-1	Top Bunter Sandstone	423989.31	5984479	-784.13	814
44/16- 1	Top Bunter Sandstone	442701.07	6024239	-891.38	931
44/19- 2	Top Bunter Sandstone	476238.51	6036565	-1680.13	1710
44/21- 1	Top Bunter Sandstone	443630.22	6004229	-1510.96	1539
44/21- 2	Top Bunter Sandstone	439776.06	6009440	-1797.2	1832
44/21a- 6	Top Bunter Sandstone	446676.03	6008279	-1822.3	1854

44/22- 3	Top Bunter Sandstone	453995.23	6015122	-1904.17	1938
44/22- 4	Top Bunter Sandstone	454869.47	6012568	-1900.56	1935
44/23- 3	Top Bunter Sandstone	464859.65	6006179	-1327.64	1363
44/23- 5	Top Bunter Sandstone	464923	6004649	-1373.12	1410
44/23- 7	Top Bunter Sandstone	461955.83	6008706	-1560.78	1594
44/26- 1	Top Bunter Sandstone	442724.93	5988943	-1237.04	1266
44/26- 2	Top Bunter Sandstone	437270.11	5993315	-1804.57	1832
44/26- 4	Top Bunter Sandstone	437191.35	5995539	-1918.68	1958
44/26-3	Top Bunter Sandstone	442280.18	5989813	-1282.48	1309
44/26c- 6	Top Bunter Sandstone	435579.87	5984979	-1781.86	1804.72
44/29- 2	Top Bunter Sandstone	476795.83	5990542	-1048.09	1074
44/29- 3	Top Bunter Sandstone	475737.29	5993255	-835.61	867
48/13B-3	Top Bunter Sandstone	397119.01	5930766	-1654.3	1686
48/14-1	Top Bunter Sandstone	412776.09	5935316	-1115.42	1152
48/6-26	Top Bunter Sandstone	370807.25	5963071	-1584.16	1627
48/6-28	Top Bunter Sandstone	381022.38	5963761	-1347.43	1388

48/9-1	Top Bunter Sandstone	417148.35	5957518	-2473.87	2506
49/01- 3	Top Bunter Sandstone	447118.52	5979453	-2835.86	2868.17
49/02- 1	Top Bunter Sandstone	459779.86	5976227	-425.69	458
49/02- 2	Top Bunter Sandstone	459106.45	5968907	-1151.18	1178
49/03- 3	Top Bunter Sandstone	470901.95	5983402	-1096.34	1132
49/08- 1	Top Bunter Sandstone	462643.08	5950544	-901.22	932
49/09a- 7	Top Bunter Sandstone	475026.74	5950807	-1747.78	1781
49/11a- 6	Top Bunter Sandstone	446737.36	5932747	-1515.42	1552
49/12- 3	Top Bunter Sandstone	448809.22	5932875	-1709	1741
49/16- 6	Top Bunter Sandstone	445366.46	5927044	-1514.42	1551
49/17- 1	Top Bunter Sandstone	454993.46	5921708	-1360.04	1389
49/17- 2	Top Bunter Sandstone	459824.94	5921723	-1570.79	1597
49/17- 2	Top Bunter Sandstone	459824.94	5921723	-1621.79	1648
49/17- 4	Top Bunter Sandstone	448129.32	5926817	-1376.61	1408
49/17- 7	Top Bunter Sandstone	458586.33	5919836	-1411.39	1444
49/17- 9	Top Bunter Sandstone	451578.18	5920293	-1702	1734

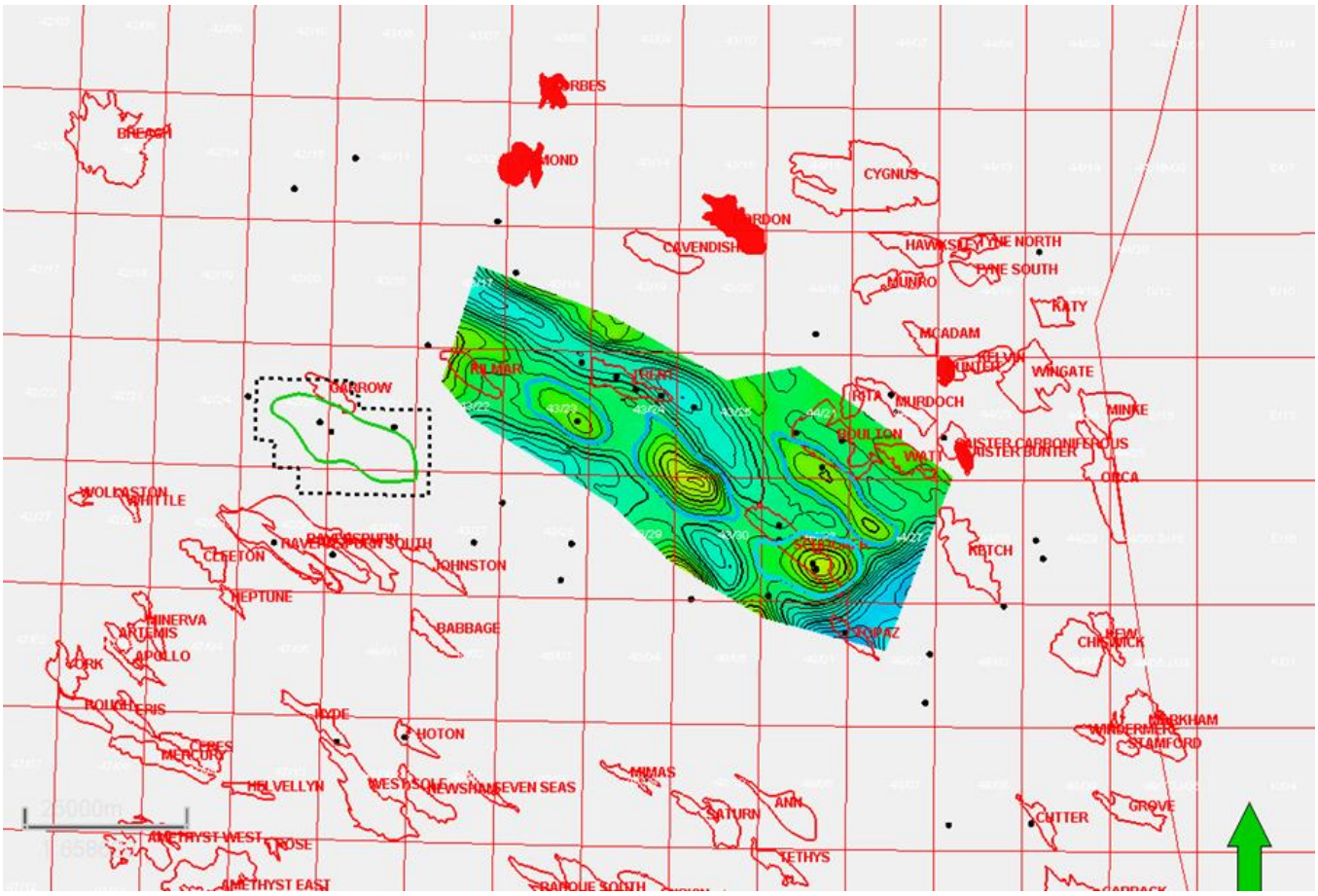

Figure 7 - Well data assembled for use in this study (black dots). Bunter gas fields are shown with red fill.

3.0 Regional Seismic Interpretation

Six horizons were interpreted regionally on the seismic data: Base Tertiary, Base Cretaceous Unconformity (BCU), Top Bunter Sandstone Formation, Top Bunter Shale Formation, Top Zechstein Group and Top Rötliegend Group. For the most part, the stratigraphy is clearly imaged on the seismic and is simple to interpret, except for the interpretation of the Top Bunter Shale Formation (which defines the base of the reservoir). The seismic lines in **Figure 8** and Figure 9 shows the isopachous nature of the Triassic section, even without good well control the error in the Top Bunter Sandstone interpretation would not be expected to be significant regionally.

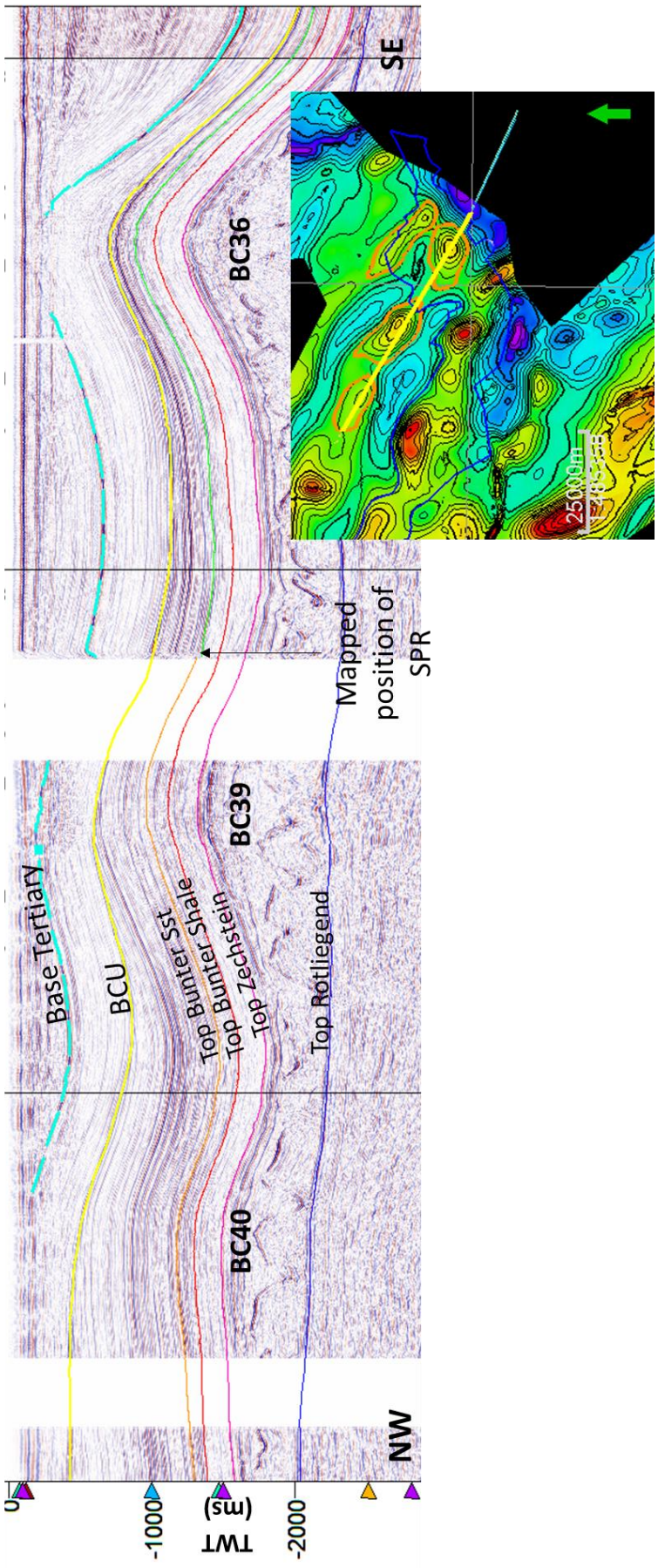

Figure 8 - NW-SE regional TWT seismic line through BC40, BC39 and BC36.

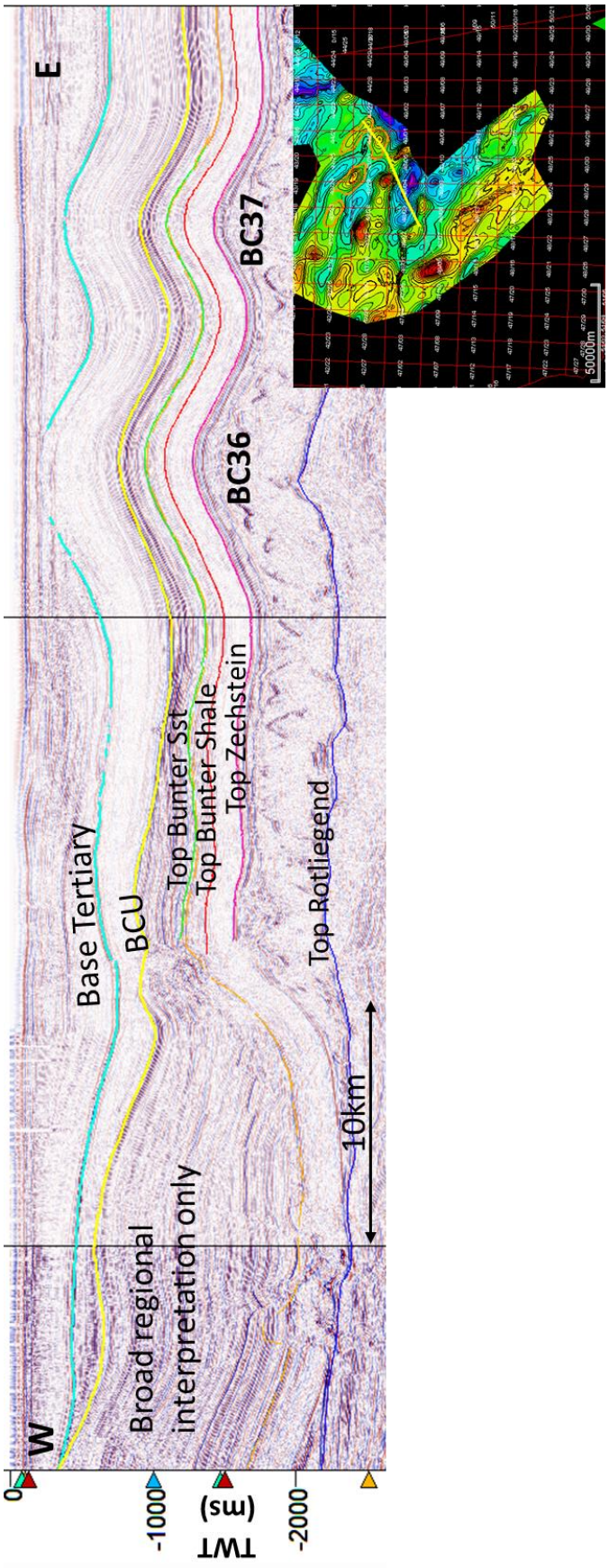

Figure 9 – W-E regional TWT seismic line through BC36 and BC37.

The structure of the Bunter Sandstone Formation is controlled by the underlying Zechstein salt. The salt forms pillow structures and ridges, which is the primary control on Triassic structure. In the area to the north and east of Endurance a number of salt pillow structures are found, which are the primary focus of this study. The seismic data closer to the coastline in the west is poorer in coverage and quality, and increased structural complexity makes interpretation more challenging (**Figure 10**). The northern interpretation is limited by a lack of seismic data available for this project over the Cavendish area (this data does exist and is owned by Western Geco) and the edge of the Bunter Sandstone facies. In the east the area is limited by the cutting down of the Base Cretaceous Unconformity (BCU), which gradually erodes the Triassic section including the Bunter Sandstone (**Figure 11**). The seal in this area would become the Cretaceous (rather than the Röt Halite) and the erosion reduces the thickness of the Sandstone significantly. Regional mapping was extended to the south as far south as Viking area. A map summary of the Bunter Sandstone Formation prospectivity for CO2 storage is shown in Figure 8. Depth conversion was done at prospect level and is described in each prospect section below (section 0).

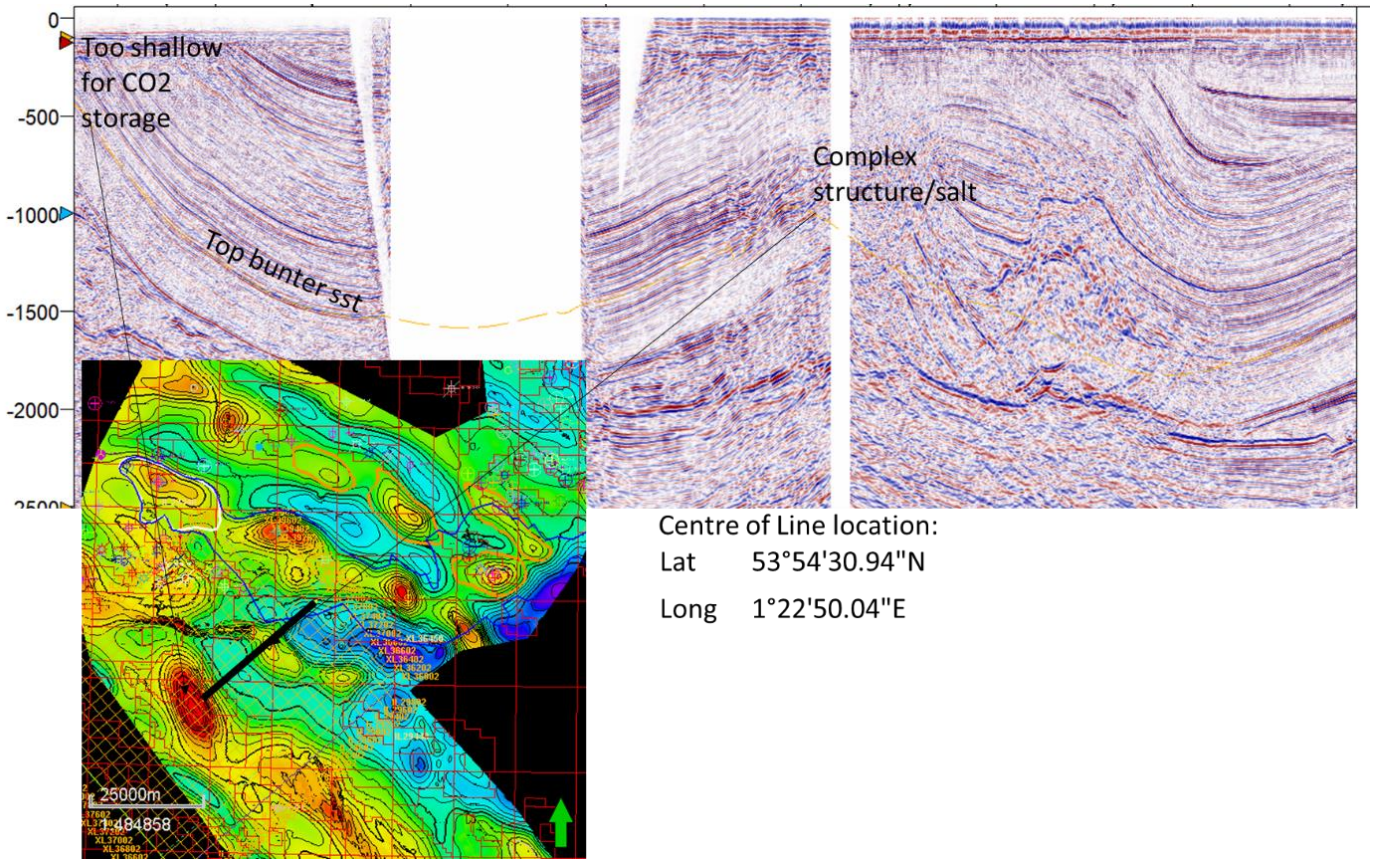

Figure 10 - South of Endurance there is some complex structure which has not been evaluated for CO2 storage with the current seismic data quality. Location of the seismic line is indicated by the black line on the map.

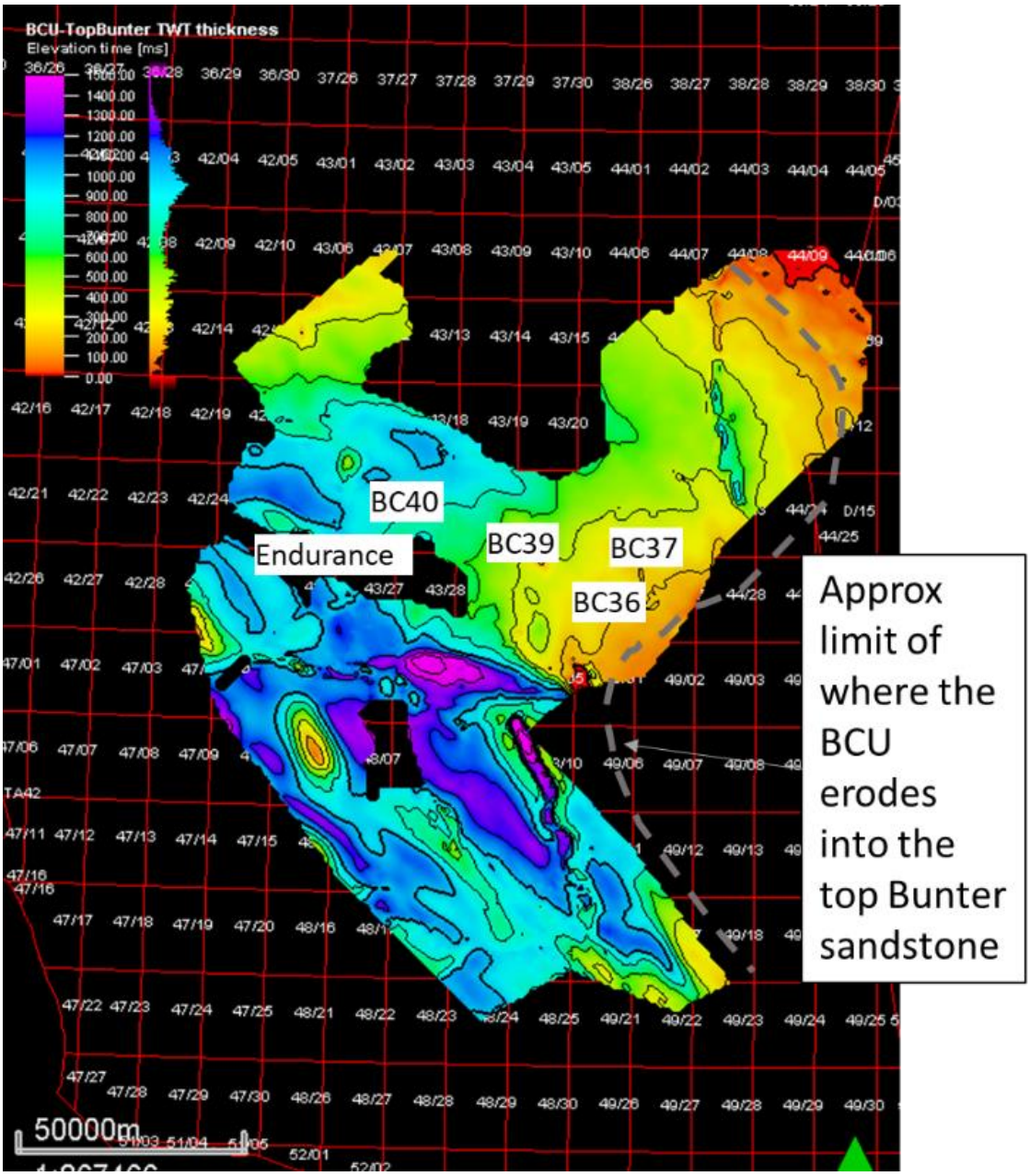

Figure 11 - Isochore map of BCU to Top Bunter Sandstone. The approximate limit of where the BCU erodes into the Top Bunter Sandstone is shown with a grey dashed line. This limits the eastern area of this study, but this is not the eastern limit of the Bunter Sandstone, which is present in Dutch and German sectors of the SNS.

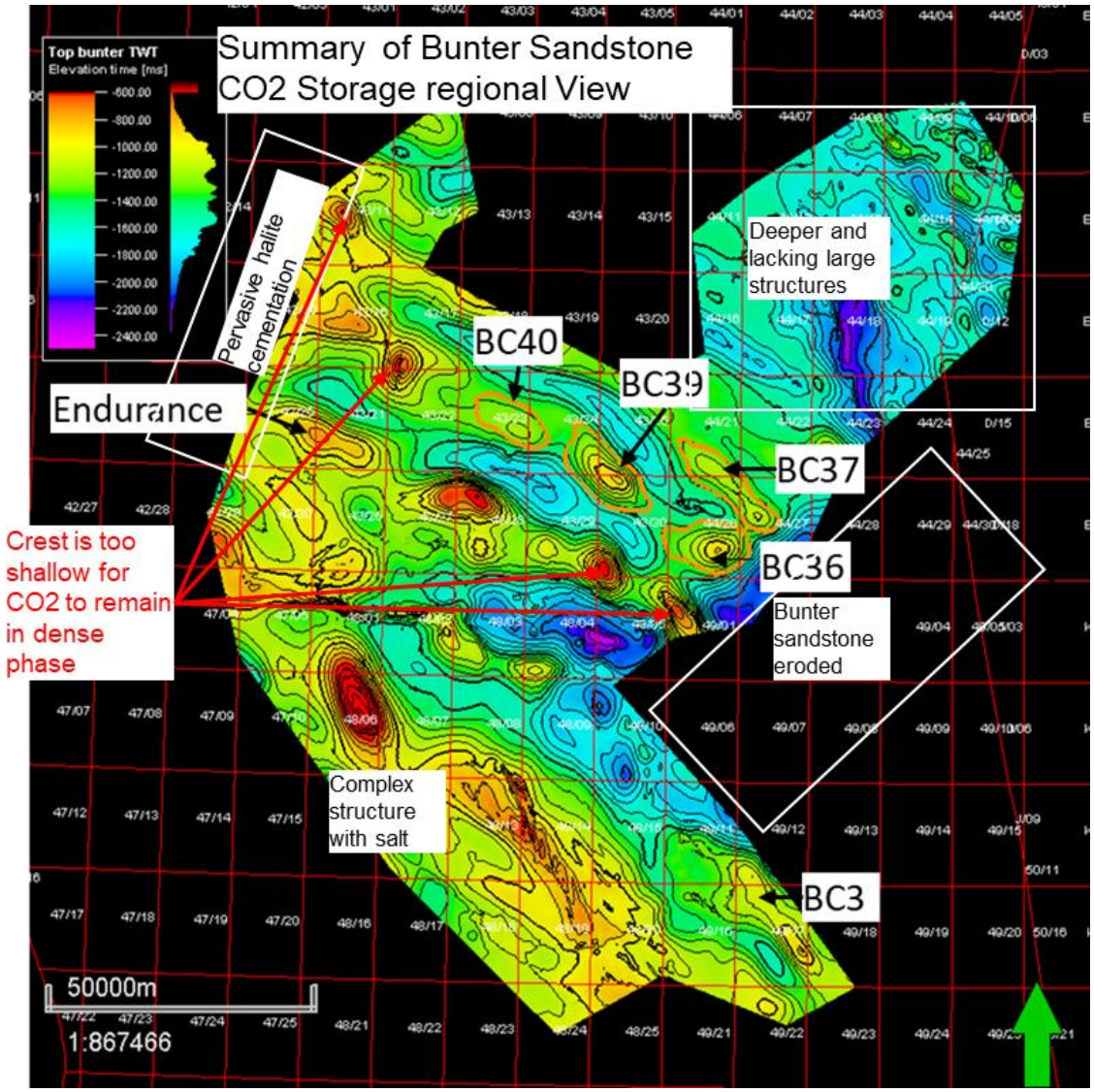

Figure 12 - Summary of regional understanding for CO2 storage in the Bunter Sandstone Formation.

3.1 Seismic Phase Reversal

The porosity at the top of the Bunter Sandstone Formation varies across the UK Southern North Sea. This is due to the presence of halite cementation in some areas. The halite cementation itself is described in more detail below in the petrophysical model (section 0). On the seismic data this difference in porosity causes a change from a trough at the top of the Bunter Sandstone where there is no halite cementation, to a peak where the halite cement makes the sandstone acoustically very hard. This is an important risk to understand as the halite reduces porosity and reservoir quality where it is present and may also cause baffling in the reservoir. The seismic phase reversal (SPR) has been mapped on this seismic volume and the polygon is shown in blue on the regional maps and in line view (**Figure 13**).

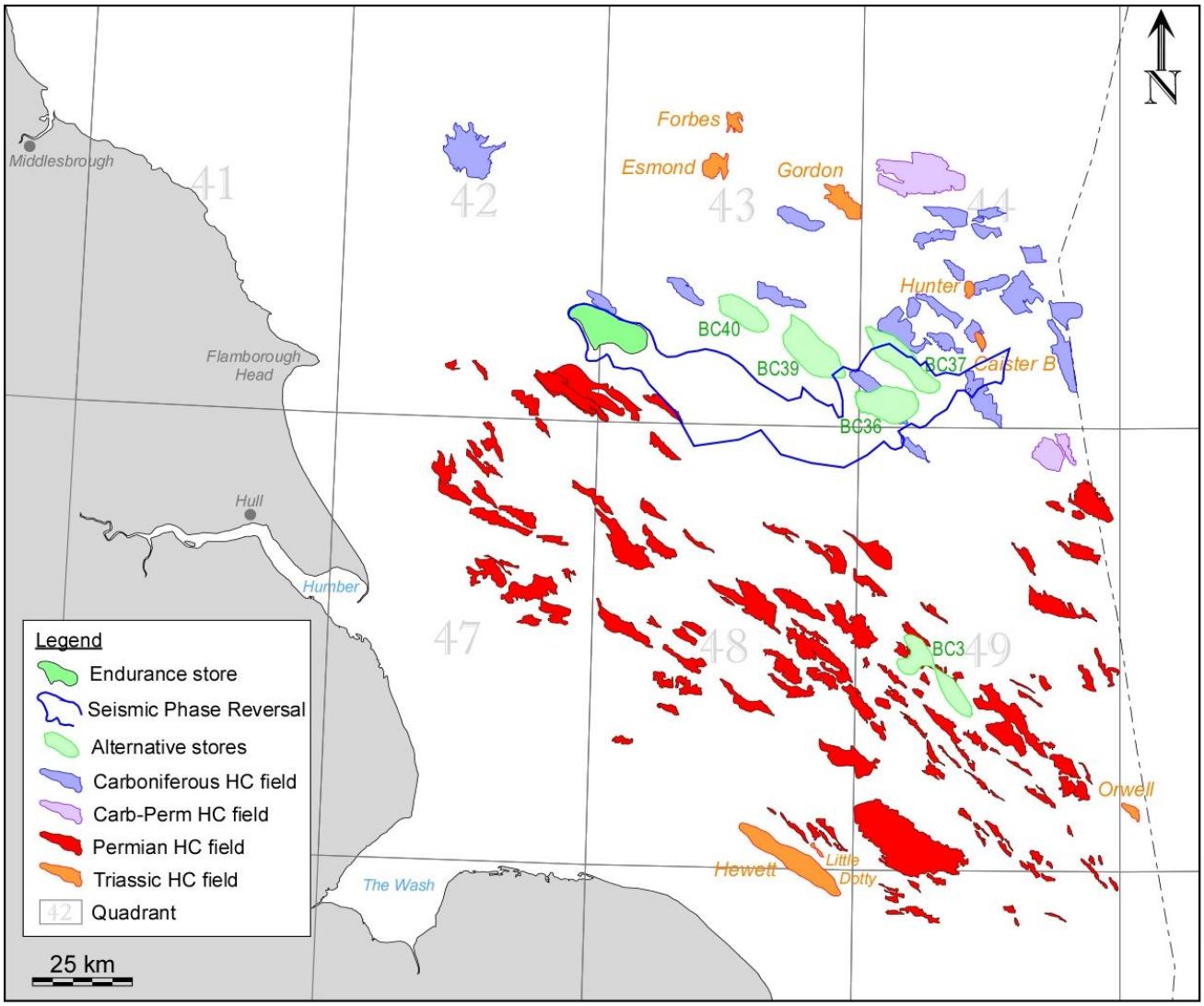

Figure 13 - Location of Triassic gas fields (orange), Endurance (dark green) and the structures being investigated for CO2 storage in this report (light green). The seismic phase reversal (SPR) is shown with a blue solid line – inside this polygon the Bunter Sandstone Formation appears to have no halite cementation and the top of the sandstone is soft, outside of it the top of the Bunter Sandstone Formation is pervasively cemented with halite and has a hard seismic response.

3.2 Structural Influence on Bunter Sandstone Deposition

If the deposition of the Bunter sandstone were influenced by pre-existing structure or halokinesis, facies or accommodation space may have been affected. Understanding any potential structural controls on Bunter Sandstone deposition therefore has the potential to enhance understanding of reservoir heterogeneity.

The top Bunter Sandstone reflector is well imaged on seismic and is close to parallel to the top Zechstein indicating little or no structurally controlled thickness variation in the entire Bunter package. The base of the Bunter Sandstone is poorly imaged. As interpreted, there is a subtle thinning of the Bunter sandstone towards the north and east (**Figure 14**). There are no

obvious lineaments or changes in isochore gradient that could be attributed to underlying linear structural features. It is concluded that there are no observable structural influences on Bunter sandstone deposition on the scale of this area.

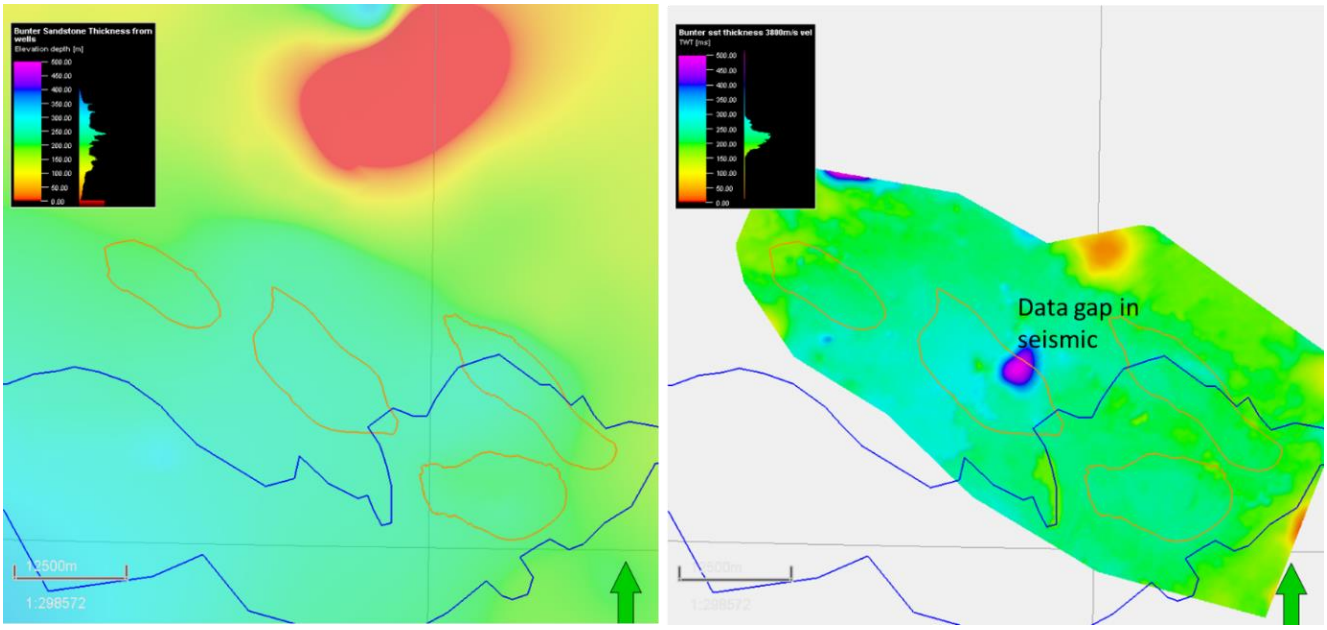

Figure 14 - Comparison of well gridding Bunter Sandstone thickness (left) and seismic interpretation using a constant 3800m/s velocity for the Bunter Sandstone (right).

The thickness of Bunter sandstone is strongly influenced by the large-scale geometry of the Sole Pit basin and the Dowsing fault zone. While there is no observable field-scale control on Bunter thickness, regional controls do exist, with evidence for increased subsidence within the Sole Pit basin during the Triassic. This may be an effect of thinned lithosphere responding to regional subsidence, or local control by faulting. No faults are observed that control this subsidence and any faulting in the pre-salt stratigraphy to be expected to be strongly detached from the post salt stratigraphy. A regional Bunter thickness gridded from well tops indicates a rough basin geometry (**Figure 15**).

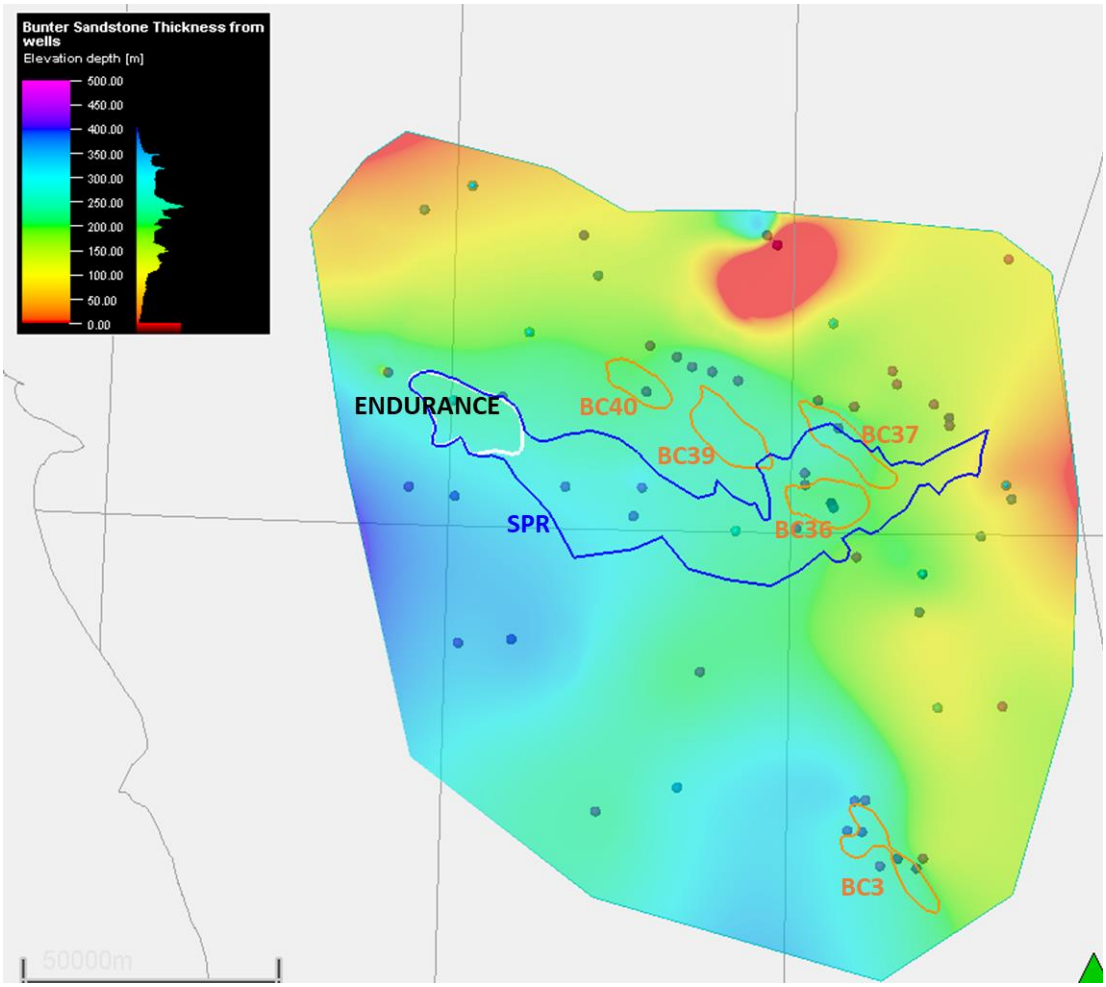

Figure 15 - Bunter Sandstone thickness gridded from well tops. The wells used to generate the map are shown as dots.

4.0 Regional Well Correlation

As discussed above, the Triassic section is approximately isopachous above the Zechstein salt. All the wells in the area show the Röt Clay, Röt Halite Dowsing Shale and Muschelkalk halite packages (**Figure 16**).

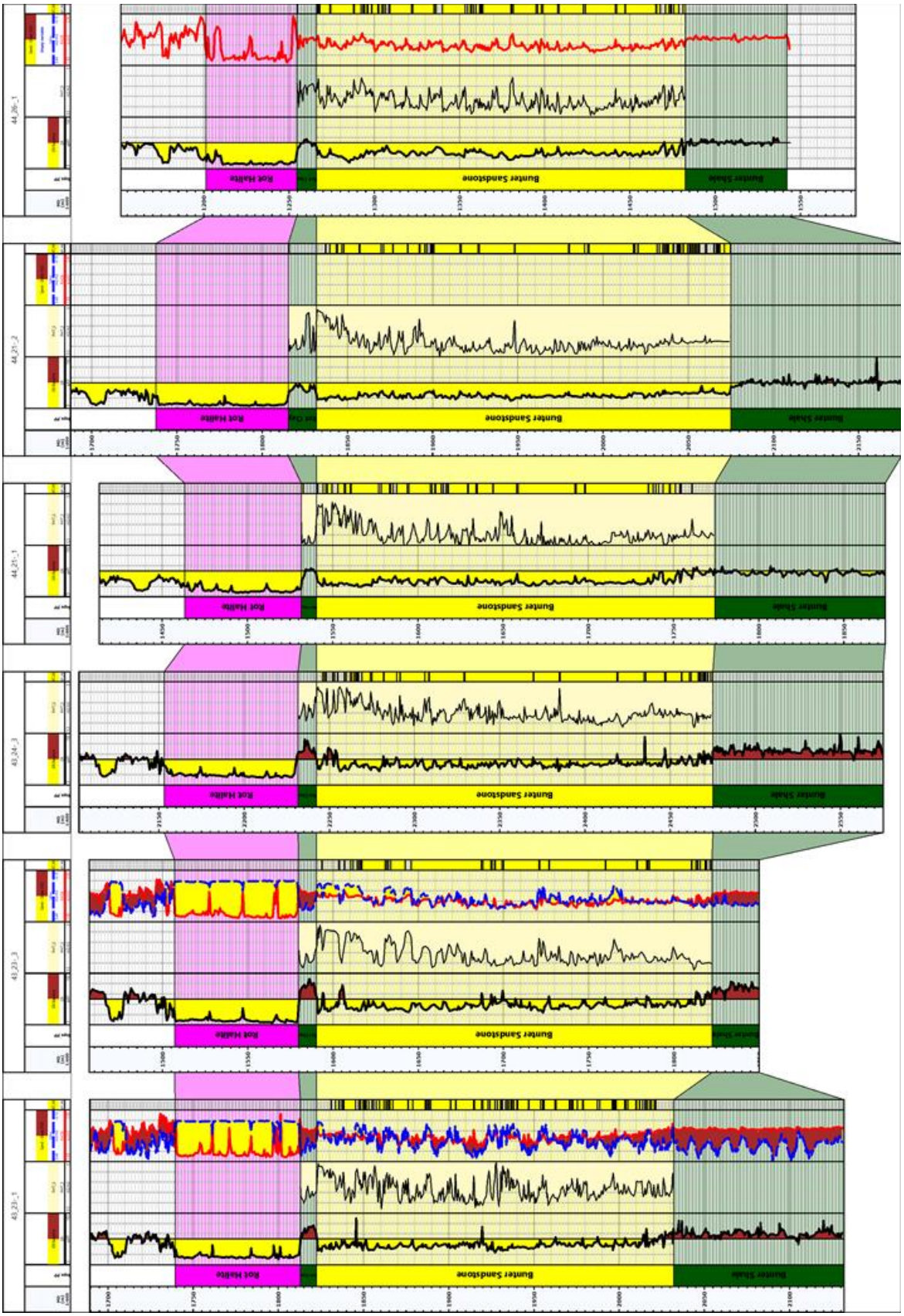

Figure 16 - Regional well correlation panel from NW to SE.

5.0 Sedimentology of the Bunter Sandstone Formation

There is a wealth of sedimentological description of the Bunter Sandstone reservoir that has previously been conducted on Endurance during earlier phases of work associated with the White Rose project. Leppard (2011) studied core acquired from ten regional wells in the Southern North Sea, and Blackbourn (2012) and Blackbourn & Robertson (2014) described the cores from the two wells on the Endurance structure (42/25-1 and 42/25d-3, respectively). Cuttings from well 43/28a-3 located on the outcrop, which penetrates Bunter Sandstone in the top ~400m of the well, were also described by Blackbourn (2014).

Those studies described the Bunter Sandstone as deposited in a semi-arid, land-locked basin with fluvial systems that terminated in playa lake, playa margin, aeolian dune and sabkha settings. Sedimentation rates were low (100m/3Ma) with considerable reworking and recycling via fluvial and aeolian processes. As a result, it was interpreted that irrespective of the final mode of deposition, many of these sediments have similar reservoir characteristics.

5.1 Analogues and Implications for Modelling

Modern and ancient analogues were reviewed to understand the depositional extents of the sedimentary facies observed in core at 42/25d-3. Modern analogues were identified in places such as Western Iran, Taklimakan Desert in China, Chott el Djerid in Tunisia, the Sistran Basin between Eastern Iran and Afghanistan and Khongoryn Els in Mongolia. An example of Khongoryn Els, in the extreme south of the Gobi Desert, Mongolia, is shown in **Figure 17**. Ancient analogues were provided by the existing Bunter Sandstone gas fields within the Southern North Sea and outcrop of analogous formations within onshore UK.

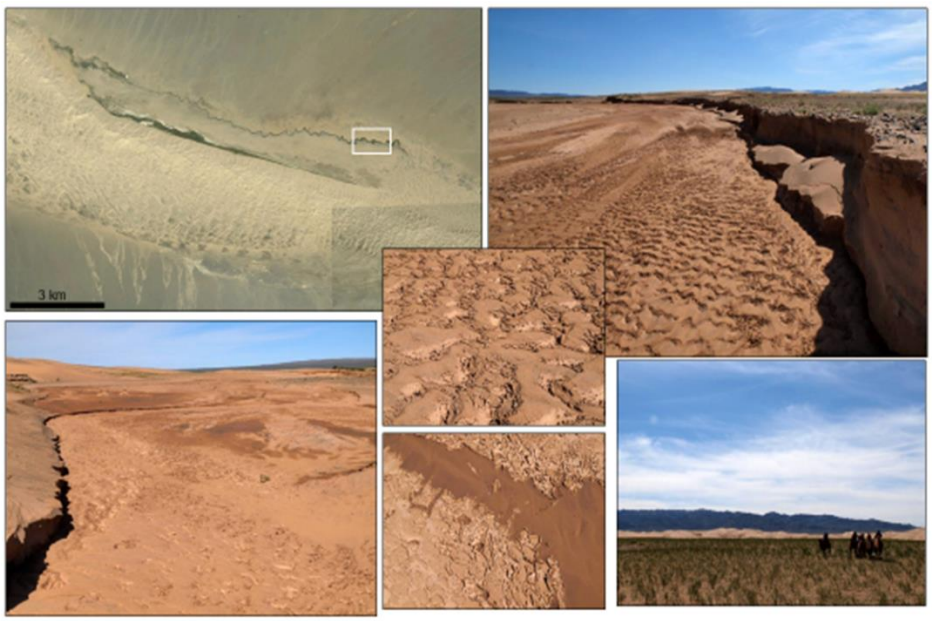

Figure 17 – Images from Khongoryn Els, Mongolia, showing small-scale features associated with small ephemeral lake systems, a modern analogue for the Bunter Sandstone Formation depositional environment.

Bunter Sandstone is the reservoir formation for eight fields in the UK Southern North Sea. A review of production performance from Bunter Sandstone gas reservoirs was conducted during the previous White Rose project on Endurance. In summary these studies concluded that depletion characteristics of Bunter Sandstone gas accumulations during production reflects a range of diagenetic and depositional controls on reservoir performance. In the east, the Caister and Hunter fields suggest that internal barriers to vertical flow are present where finer grained, more distal units are preserved and are able to support significant pressure differentials. To the north, the Esmond complex of fields in Bunter Sandstone reservoirs are more proximal to Endurance and data suggests fewer vertical barriers from pressure measurements and production data compared with Caister B field. An analysis of production and post-production pressure data has been modelled (see Dynamic Model KKD).

Onshore ancient analogues include the Cretaceous fluvial sandstones of the Weald Basin (Tunbridge Wells Sands unit). Whilst not a direct analogue, this may help as an illustrative aid. The high net sands of the Southern Sandstone consist dominantly of decimetre-scale fluvial cross-beds with some ripples. While the aeolian elements are absent here, the lateral continuity of any one set of cross-beds (around 1 – 3m) and the lack of any key bed-bounding surfaces to control the overall deposition may be a useful visual aid to demonstrate variability in the field.

Such modern and ancient analogues demonstrate the rapidly changing and extensively reworked nature of the depositional setting. The changeability of the lithotypes on the sub-metre scale and the lack of clear distinction between lithofacies determined that object-based modelling was not appropriate within the static model.

6.0 Regional Petrophysical Model: Analysis of Halite Cementation

Regional petrophysical analysis was conducted to review two key reservoir quality issues:

- How much halite cementation is present in the Bunter Sandstone in the wells in the Alternative Stores and surrounding area?
- What is the impact of halite cementation on reservoir properties?

6.1 Log Based Methodology

All of the wells in the area of interest were reviewed to see what log data was available (**Table 2**).

Table 2 - Log data coverage.

Log	Well coverage	Halite cemented response	Comment
GR	All wells	Low GR	Same as clean sandstone
Resistivity	All wells	High resistivity	Same as tight or gas bearing sandstone
Density	50%	Low density	Same as a high PHIT sand
Compressional sonic	Most wells	Fast sonic (67us/ft)	Same as a low PHIT sand
PEF	<25%	5 b/elec	Present in too few wells
Neutron porosity	<25%	0 v/v	Present in too few wells

From the log data coverage identified in **Table 2**, the clearest combination of data to produce a halite indicator was a density / compressional sonic combination (**Figure 18**). Over a halite cemented interval, the density would read low density (high porosity), whereas the sonic would read fast (low porosity). A significant difference between the two porosity calculations is therefore indicative of the presence of halite cements.

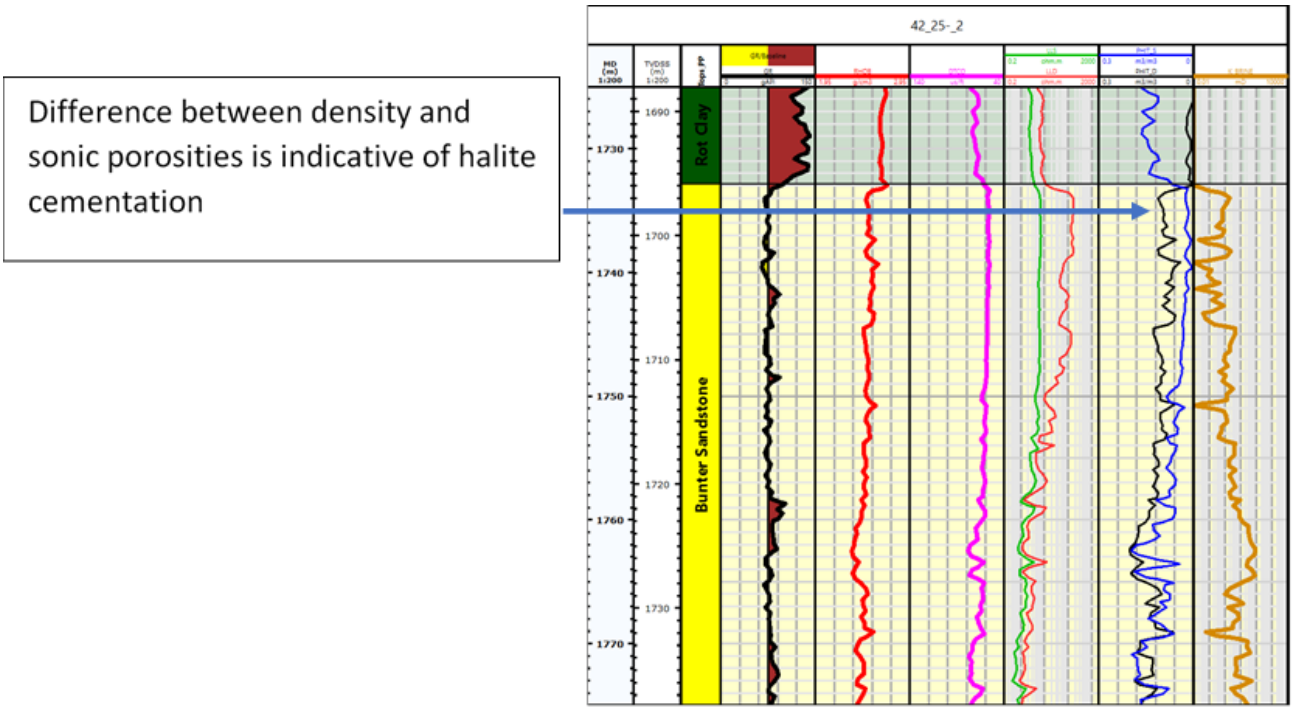

Figure 18 - Example of difference between density and sonic porosity, indicating halite cementation at well 42/25-2.

6.1.1 Bunter Sandstone Density / Compressional Sonic Response

From the main petrophysical model established at Endurance, there are porosity equations for both sonic and density. Using these equations, a characteristic trendline for the Bunter Sandstone can be derived. The equation of this line is:

$$RHOB = 1.2843 + 1.61 \times \sqrt{(\frac{55}{DTCO} - 0.26983)}$$

Crossplots between density and sonic are then created. Using the equation above, a trendline is calculated and clean Bunter Sandstone is expected to lie on this trendline. This is demonstrated on the **Figure 19** below (note: a filter of volume of clay (VCL)<10% was also applied), which has two wells with clean, high quality Bunter Sandstone (i.e. no halite cementation).

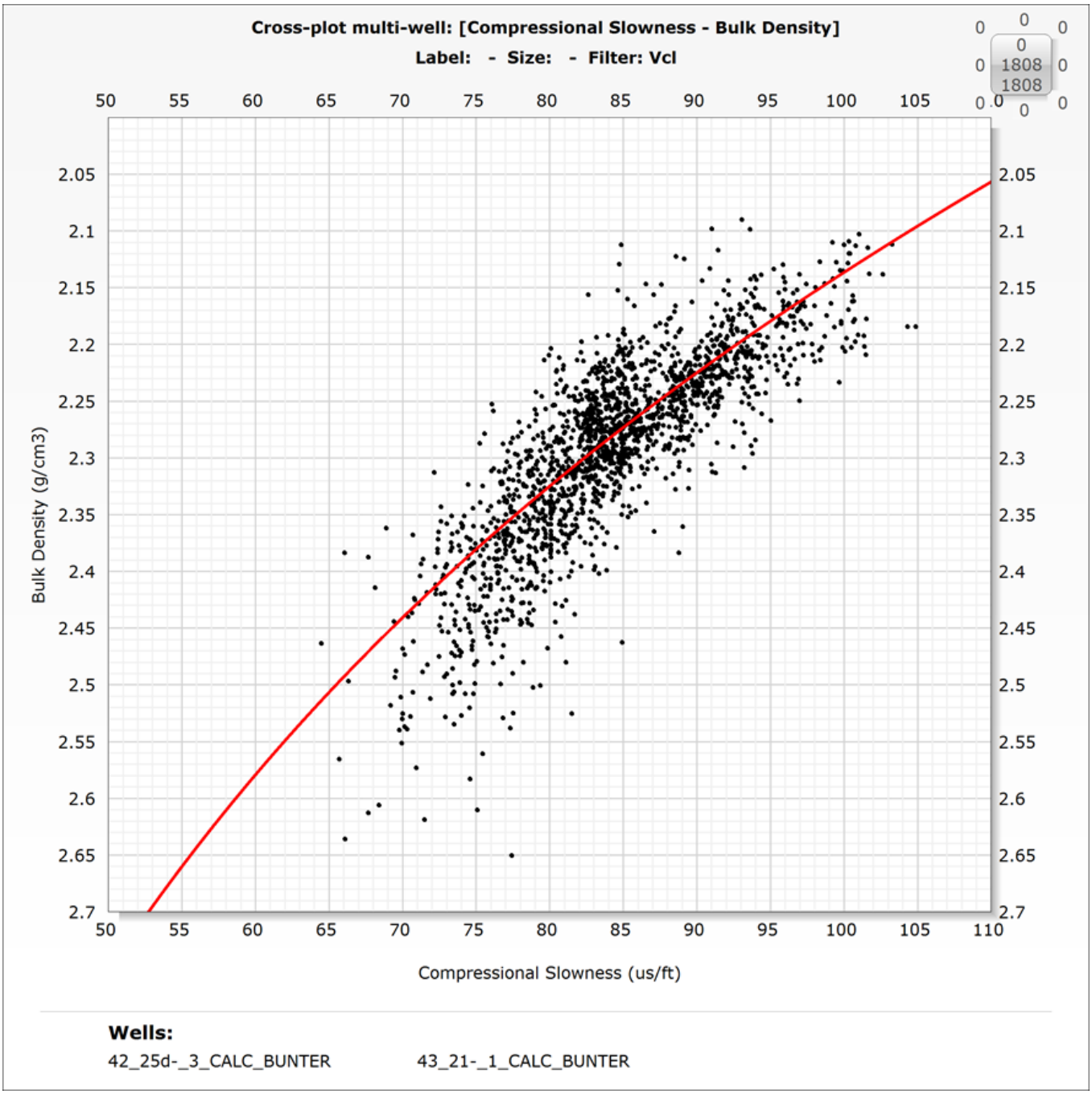

Figure 19 - Sonic - density cross plot for wells 42/25d-3 and 43/21-1.

6.1.2 Pure Halite Response

The log response of the Röt Halite was reviewed in several wells and plotted with the same variables and the same trendline as above. As observed in **Figure 20** below, the halite plots in a distinctive location, with a very characteristic sonic response and a low bulk density. Crucially, this plots in a significantly different area to the clean sandstone shown in **Figure 19**.

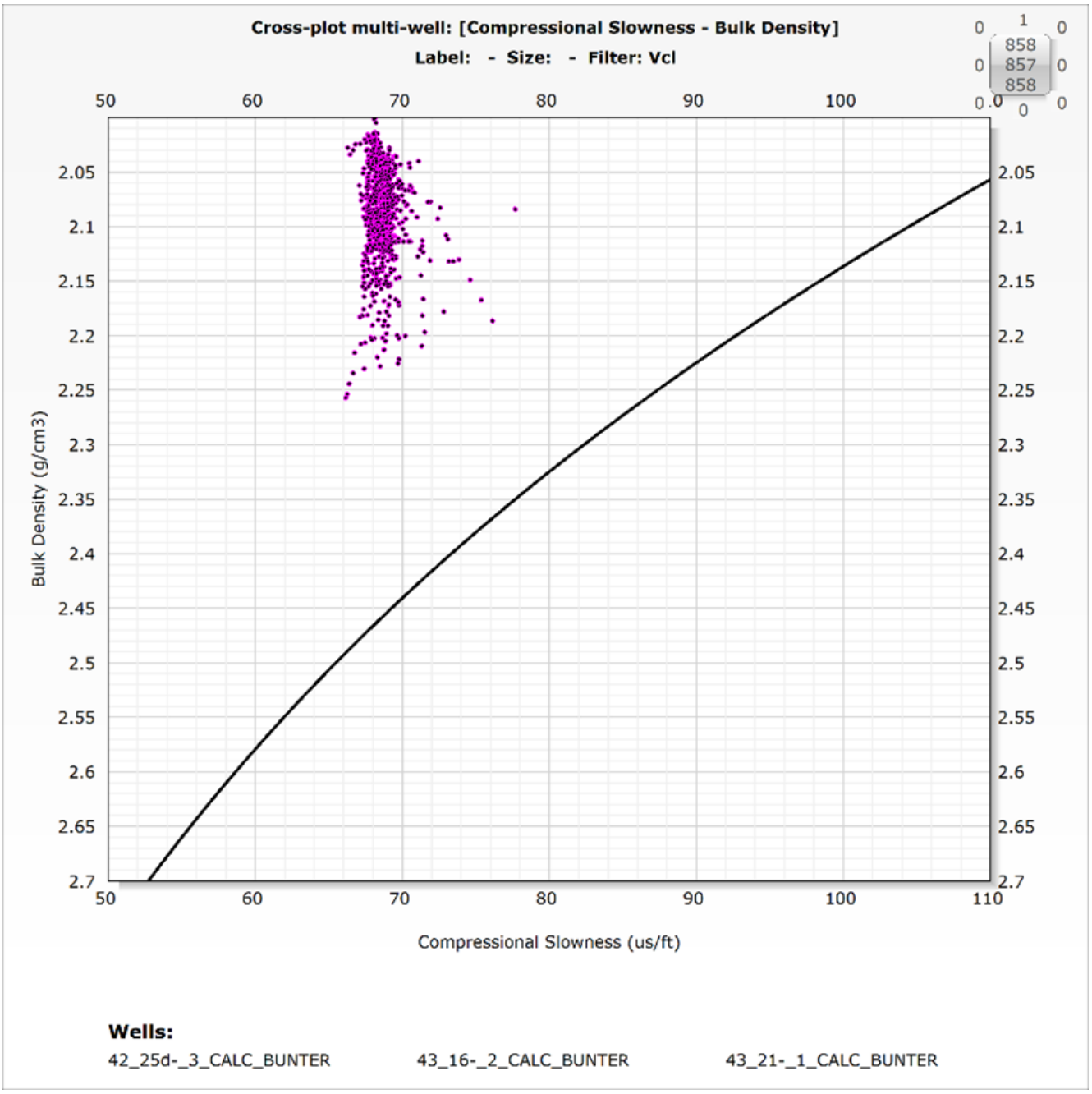

Figure 20 - Pure halite sonic-density character.

6.1.3 Picking the Halite Cemented Sandstones

The addition of halite cements to a normal Bunter Sandstone is expected to:

- Reduce porosity
- Move log response towards the halite “cloud”

The associated error in the Bunter Sandstone line was calculated using the uncertainty assessment from the petrophysical model. This was then used to produce an upper and lower bound for clean bunter sandstone (shown with the additional red lines on **Figure 21** below).

Halite cemented sands are expected to be low porosity. As there is also halite in the matrix, the data should plot between the “clean halite” and “low porosity sand”. This is shown graphically in **Figure 21** below.

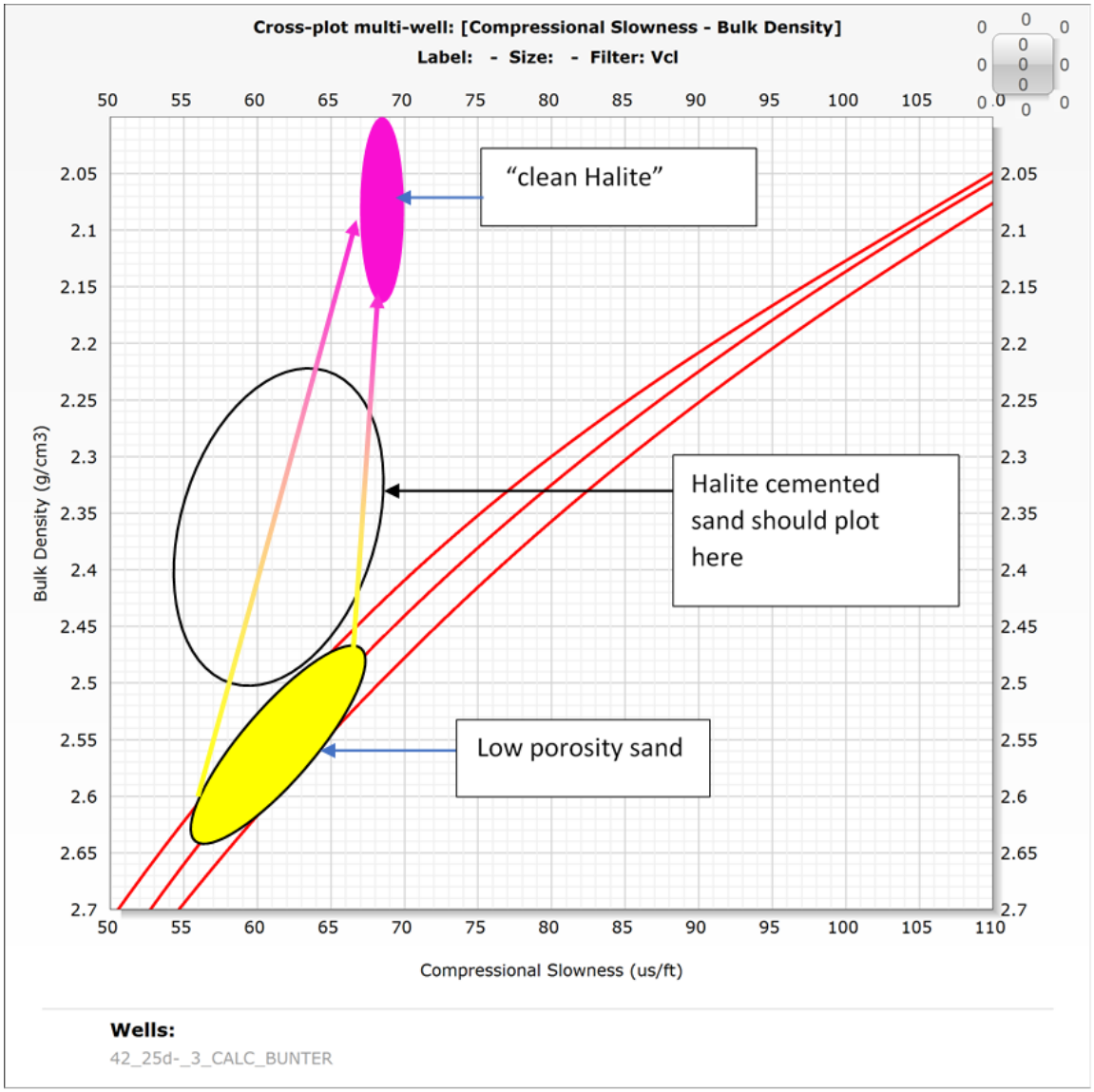

Figure 21 - Identifying halite on sonic-density cross plots.

To automate this process for application to well logs, the following constraints have been applied to identify halite cemented sands:

- Sonic porosity < 10%
- Data plots above the upper bound region for clean Bunter Sandstone.

This is shown graphically in **Figure 22**.

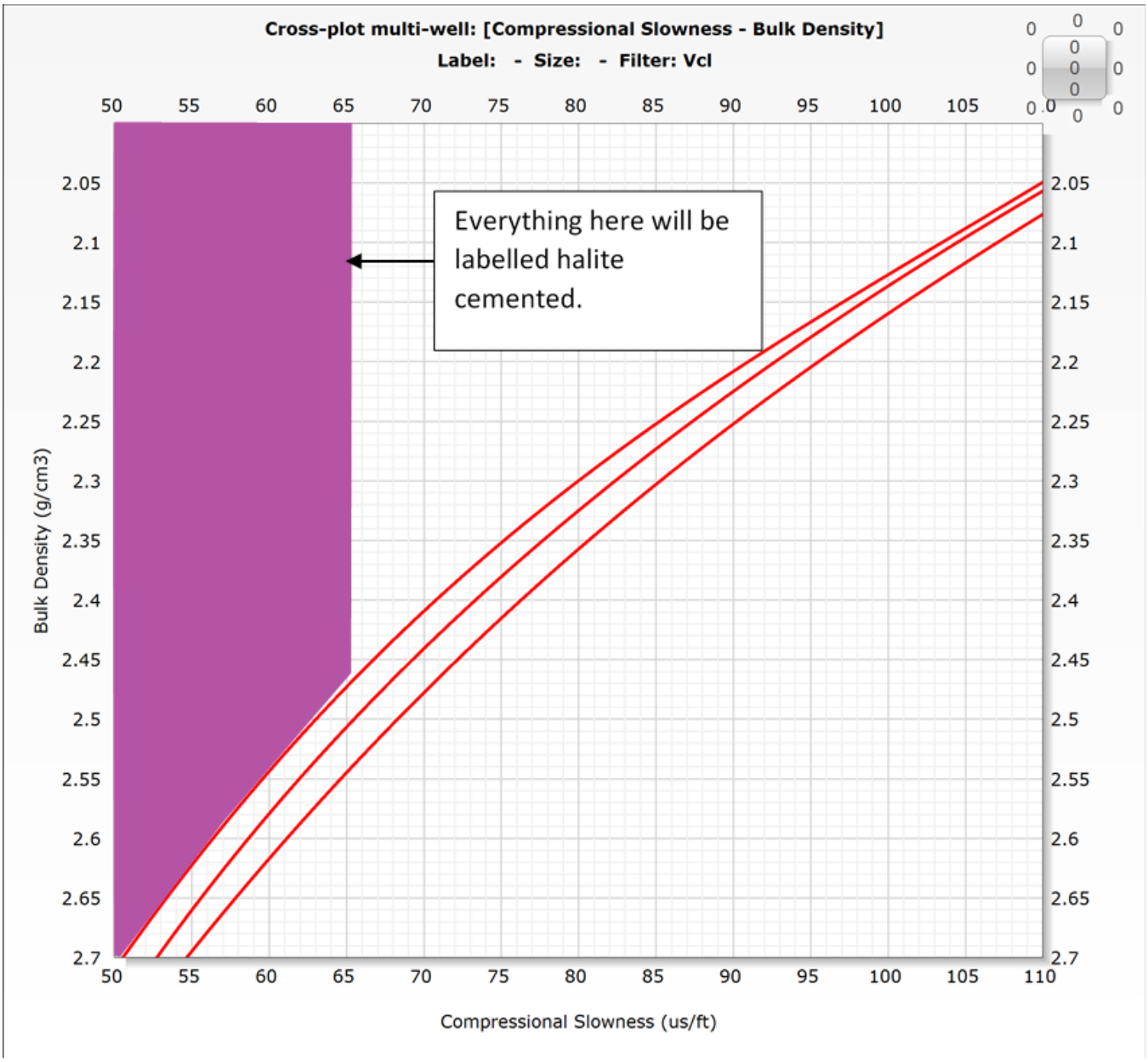

Figure 22 - Cut-off applied to log data to identify halite.

6.1.4 Results

The results of this routine are shown below for two wells with significant halite cementation (**Figure 23** and **Figure 24**). This automated routine was then applied to all of the wells in the area of interest. The resultant amount of halite cementation was then calculated and displayed in map form (**Figure 25**).

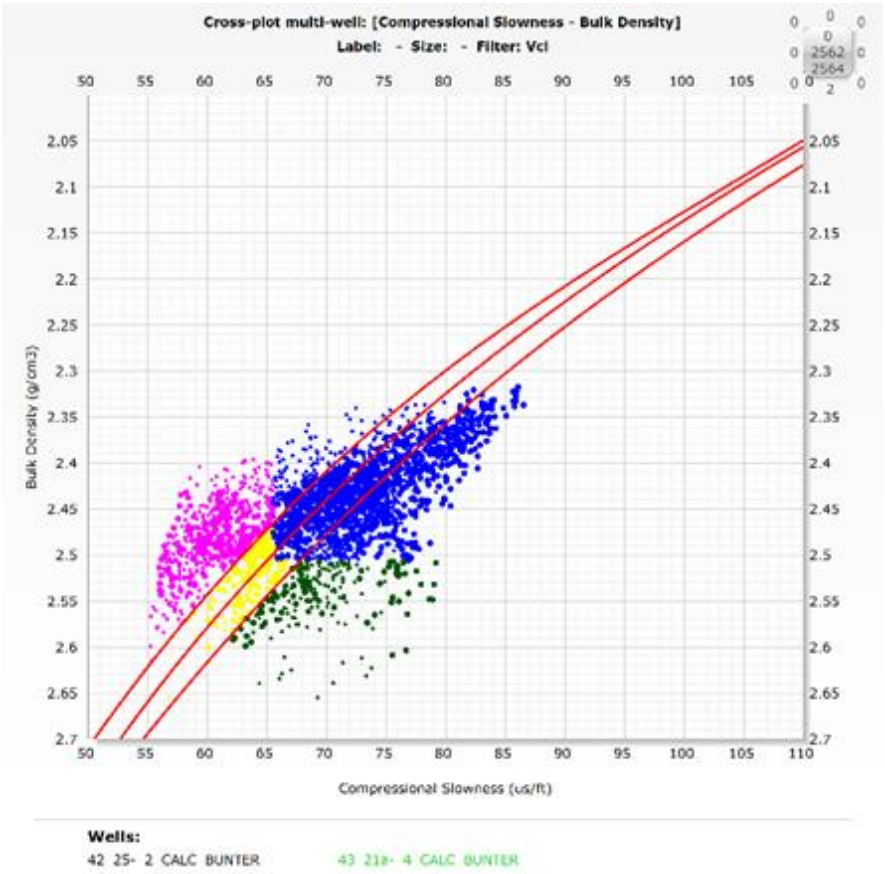

Figure 23 - Different styles of halite identified from logs.

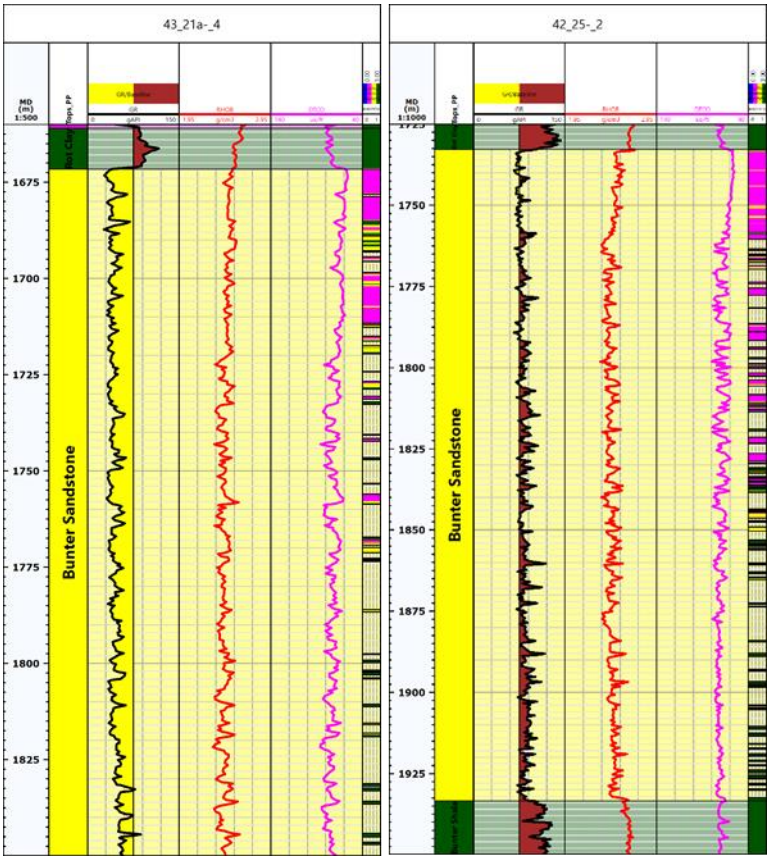

Figure 24 - Halite flags shown on log-view panel for well 43/21a-4 and 42/25-2.

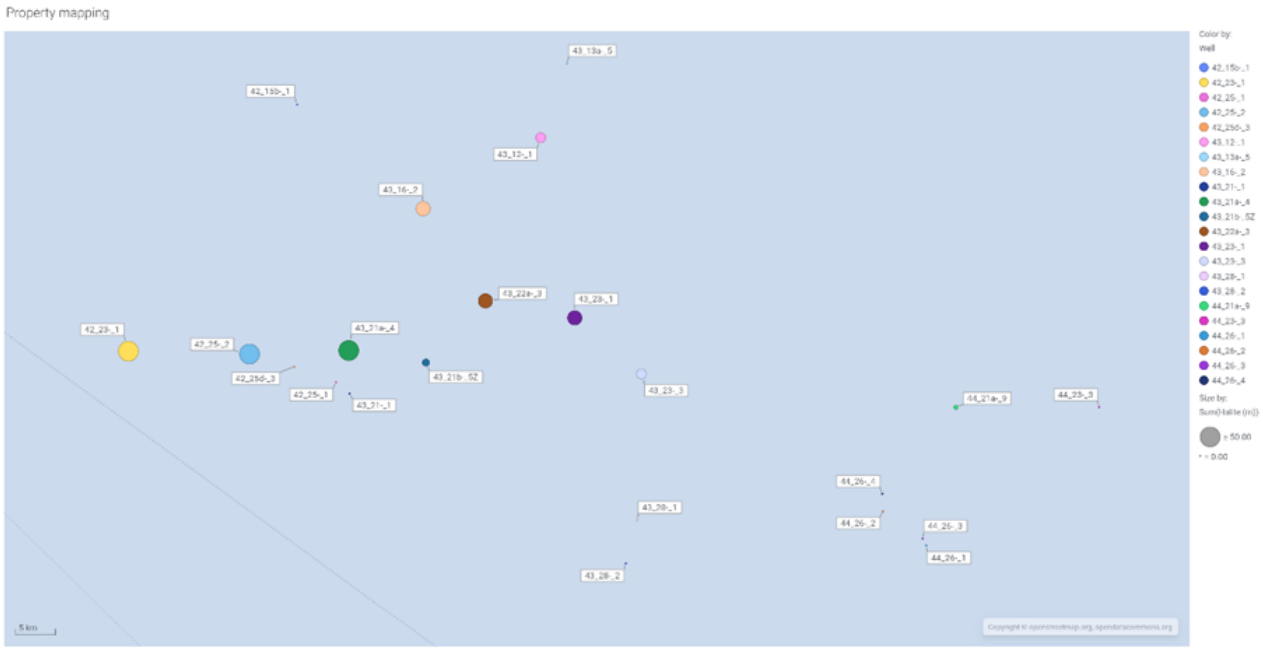

Figure 25 - Map of wells that halite log identification has been applied to.

6.1.5 Conclusions for Log-based Methodology to Identify Halite Cements

Well logs can successfully be used to pick large halite cemented beds (note: compressional sonic vertical resolution is usually ca. 2m). This well log process can be automated and systematically calculated for a large dataset.

6.2 Analysis of Core Data for Halite Cementation

6.2.1 Offset Well Database

The United Kingdom National Data Repository (NDR) and the Dutch equivalent were reviewed for regional core plug data in the Bunter Sandstone. The data listed in **Table 3** was found in this search and used for the core plug component of this study.

Table 3 - Regional core plug data identified.

Well	Number of RCA plugs	% of Bunter Sst cored	Data missing?
42/15b-1	120	50	No Klinkenberg
42/25-1	75	25	
42/25d-3	984	75	
43/11-1	28	75	No grain density
43/12-1	178	50	No Klinkenberg
43/18-1	23	10	No Klinkenberg
44/23-3	182	50	No Klinkenberg
44/26-1	12	10	No grain density
K13-02	574	90	No Klinkenberg

As Klinkenberg permeabilities are not available for a large portion of this dataset, the decision was taken to use air permeability measurements. As no stress corrections were available (other than those at the 42/25d-3 well), the decision was taken to also use unstressed measurements.

A quick review of plugging and cleaning methods was undertaken. All cores where the information was available recorded using hydrocarbon based lubricants for cutting the plugs. This is essential for preserving any halite within the samples.

6.2.2 Distinguishing Halite Containing Samples from Non-halite Containing Samples

Core plug descriptions were reviewed where available and then compared to the overall dataset. It was clear that the biggest quantitative discriminator of halite was the grain density.

From the core plug dataset over the Endurance Structure (wells 42/25d-3 and 42/25-1), the Bunter Sandstone grain density is taken to be 2.67 g/cc. Halite has a variety of quoted density values (ranging from 2.00 – 2.15 g/cc), however, the value that is assumed here is 2.04 g/cc (from Schlumberger “log interpretation charts”). Consequently, replacing pore space with halite will lower the matrix density of the core plugs. Assuming a two component matrix results in the following densities:

- 95% Bunter Sandstone, 5% Halite = 2.64 g/cc
- 90% Bunter Sandstone, 10% Halite = 2.61 g/cc
- 85% Bunter Sandstone, 15% Halite = 2.58 g/cc
- 80% Bunter Sandstone, 20% Halite = 2.54 g/cc

For the remainder of the study, the grain density will be used as a proxy for the amount of halite cementation present in the system.

6.2.3 Effect of Increasing Halite Content on Porosity

As the grain density decreases (and inferred percentage of halite increases) the amount of porosity in the core plugs also decreases (**Figure 26**). The most heavily cemented plugs have an average porosity of 5% and it is recommended that this should be used as a ‘ball park’ figure when quoting a halite cemented Bunter Sandstone porosity.

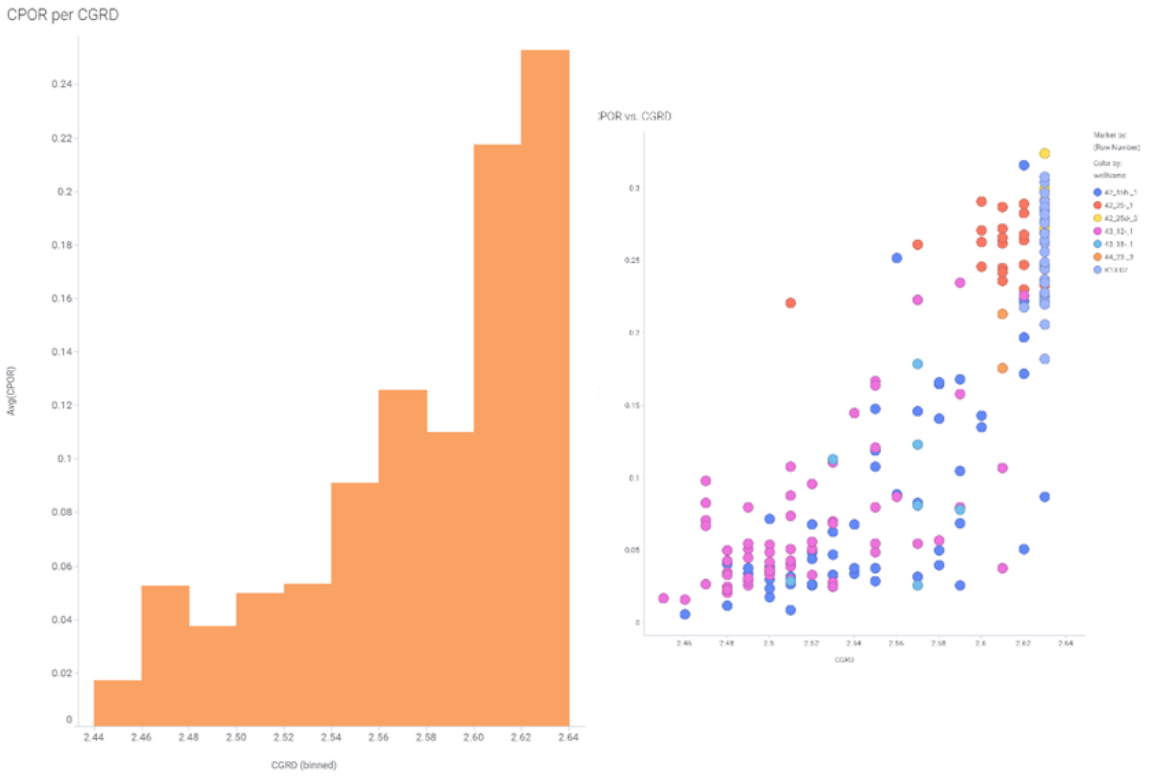

Figure 26 - Grain density versus core porosity. Left: histogram; right: scatter plot.

6.2.4 Effect of Increasing Halite Content on Permeability

As the grain density decreases (and inferred percentage of halite increases) the amount of permeability in the core plugs does decrease on average (**Figure 27**). However, the range of permeabilities possible at a given grain density are very large (at 2.5 g/cc, permeability of 0.01 – 300 mD is observed).

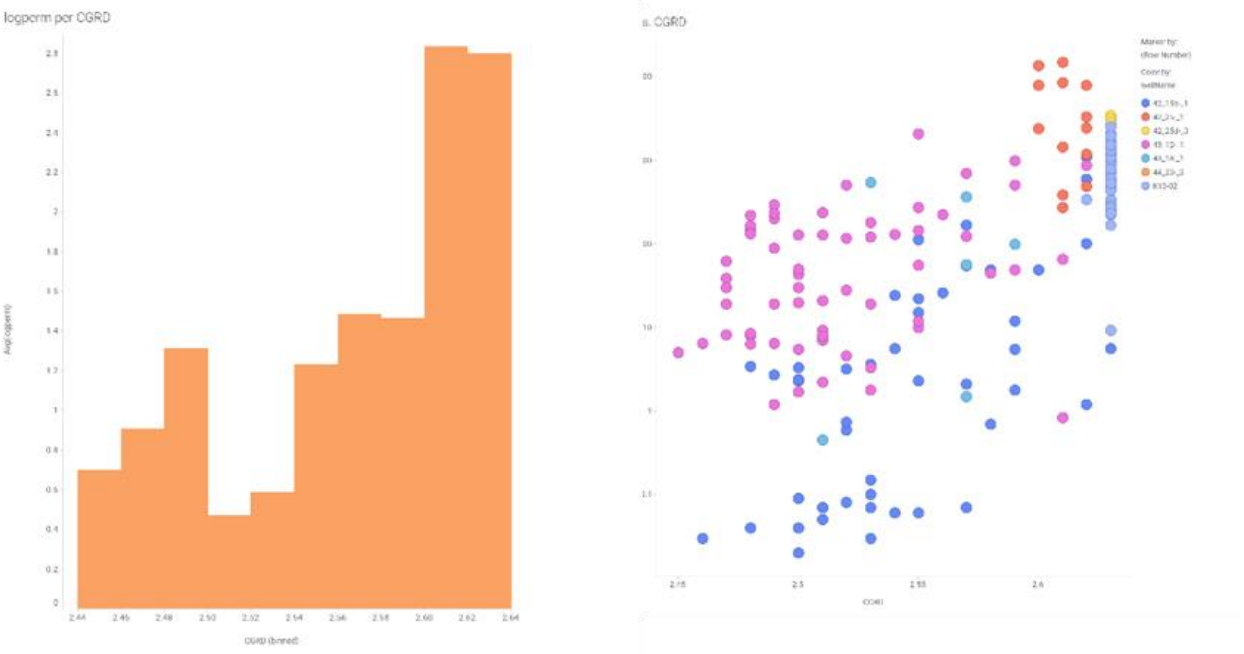

Figure 27 – Grain density versus core permeability. Left: histogram; right: scatter plot.

The current reservoir model uses a non-net approach for halite cemented layers (equivalent of 0 mD permeability). This is likely a pessimistic view as there appears to be several core plugs with reasonable permeabilities present in this dataset. A single representative value for a halite cemented facies is not recommended as permeabilities range from 0.01 – 300 mD.

6.2.5 Potential Models for Halite Distribution

Three potential groupings of core plugs have been established to investigate possible models for halite distribution:

1. Low porosity, high horizontal permeability, low vertical permeability
    - "Layered" distribution
2. Low porosity, high horizontal permeability, high vertical permeability
    - "Dispersed" distribution
3. Low porosity, low horizontal permeability, low vertical permeability
    - "Pervasive" distribution

Similar looking structures have been observed in the core photos (**Figure 28**).

Figure 28 - Three types of halite cementation: layered (left), dispersed (middle) and pervasive (right).

These three different models have been used to inform a range of different scenarios for halite cementation and have been given indicative permeabilities based on the core dataset outlined here. All of these cases to have a nominal 5% total porosity (arithmetic average of cemented plugs).

6.2.6 Porosity / Permeability Distribution of Analogue Core Data

All the core plug data for porosity and permeability was plotted on a crossplot and coloured by grain density to show how the halite cemented rock compares to the other facies seen in the Bunter Sandstone (**Figure 29**). The plot indicates that:

- The low grain density points (assumed halite) have low porosity and a large range of permeabilities
- The vast majority of the sandstone points (2.63–2.68 g/cc) have high porosity and high permeability.
- The higher grain density points have reasonable porosity, but lower permeabilities. This is caused by a combination of calcite, dolomite and clays.

Figure 29 - Core plug porosity/permeability measurements coloured by grain density.

6.3 Log based Approach Compared to Core Approach

Two wells have both core data, well logs and significant halite cementation (43/12-1 and 42/15b-1). These two wells were reviewed in detail to establish how well the log model predicted the amount of halite cementation. The results are presented below in **Figure 30**.

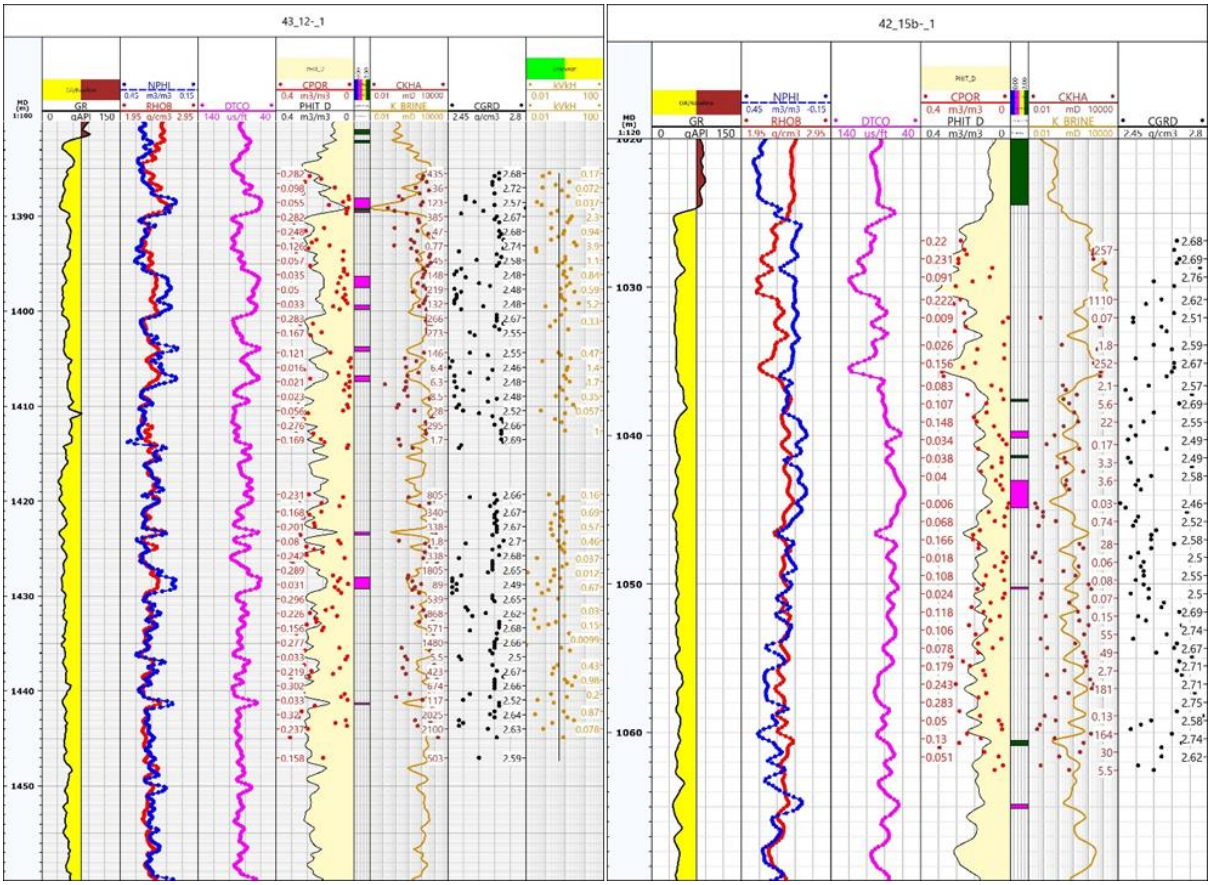

Figure 30 - Log-view panel comparing core data to log analysis.

The log model successfully identifies some thicker halite beds seen in the core plug data. However, the log model is unable to identify more interbedded sections with thinner halite beds present. Consequently, the log model is likely under-estimating the amount of halite in the system.

This is likely due to the poor vertical resolution of the compressional sonic curve. This is typically of the order of 2m, which is too coarse to identify some of the highly interbedded facies (beds seen on cm scale in core).

6.4 Conclusions on Petrophysical Model for Halite Cement

Key conclusions that can be drawn from the analysis of halite cements using the regional petrophysical model are as follows:

- Core data shows that halite cementation drastically reduces porosity (and therefore storage volume)
- Core data shows that halite cementation reduces permeability, but not as much as was expected
- Current reservoir model is likely pessimistic on this front
- The log model can identify thick halite cemented beds, but under-estimates the number of thin halite cemented beds.
- Sandstone with halite nearby doesn't seem to suffer property degradation
-

7.0 Use of Static Storage Efficiency Factor for Storage Capacity Estimates

Volumetric calculations for the high-graded prospects have been performed using Schlumberger's GeoX exploration risk, resource and value assessment software. Use of storage efficiency factor combined with accessible pore volume (dependent on reservoir sweep at various scales, and inversely correlated with reservoir complexity) can be used to estimate the storage capacity for aquifer storage on regional dip ("Migration Assisted Storage") or structural/stratigraphic closure. The storage efficiency factor is analogous to the use of recovery factor combined with hydrocarbon in-place volumetrics. This method is usually appropriate for early appraise stage screening and provides technical limits. These estimates should be sense-checked with additional tools such as numerical modelling.The volumetric method derived from the US Department of Energy (DOE) approach can be described as the storable quantity of CO2 for a given pore volume with a storage efficiency factor E (i.e. replacement of brine by stored CO2):

$$MCO2 = A \times h \times \emptyset \times \rho CO2 \times E$$

where: MCO2 is the storage capacity (mass) of CO2, A is the area of the reservoir screened for storage, h is the average net thickness of the reservoir, Ø is the average porosity of the rock, ρCO2 is the density of the CO2 at the average pressure and temperature of the portion of the reservoir, and E is the storage efficiency coefficient that reflects a fraction of the total pore volume that is filled by CO2. E is variable depending on heterogeneities, buoyancy, and displacement (sweep) efficiency.

E is typically in the range of 0.5 – 1% for closed/confined systems, and 5% and beyond for a storage area open to broader basin or into a geologic structure. The SPE SRMS Guidelines (Storage Resources Management System) document provides some useful ranges published

in the literature such as EU GeoCapacity project method to estimate the CO2 capacity for storage within a geologic structure (**Figure 31**).

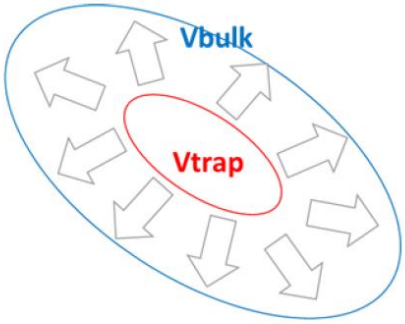

	V_{bulk} / V_{trap}				
Depth (m)	1	5	10	50	100
1000	0.10	0.5	1.0	5	10
1500	0.15	0.8	1.5	8	15
2000	0.20	1.0	2.0	10	20
2500	0.25	1.3	2.5	13	25
3000	0.30	1.5	3.0	15	30
3500	0.36	1.8	3.6	18	36

Figure 31 - EU GeoCapacity storage efficiency coefficients in a structural trap in percent (from the SPE SRMS Guidelines document). No pressure management is assumed.

The storage efficiency depends on the ratio of the geologic trap volume Vtrap (structural or stratigraphic) to the entire pore volume (Vbulk) hydraulically connected to trap volume (Vtrap), and the depth of the structural trap so as to avoid excessive pressurization (all Vbulk/Vtrap assume a closed boundary). Vbulk is strongly dependent on assumptions around the scale/extent and reservoir quality of the connected aquifer (e.g. amount of well/outcrop/analogue data available for the characterisation and mapping of the regional aquifer). Limited well or analogue data (resulting in large uncertainty in terms of long-distance connectivity assumptions) should lead to a conservative estimate for the Vbulk/Vtrap ratio.

This method results in storage efficiencies ranging from <1% for a confined system to 10% for a well-connected structure at the 1000-1500m depth range. As a check the efficiency factor determined using this method aligns with the output of the reservoir simulation study on Endurance. The simulation study indicates 3–5% as reasonable storage efficiency for a store in the 1000–1500m depth range and Vbulk/Vtrap circa 20–30 and is broadly aligned with the EU GeoCapacity methodology.

The use of pressure management, through brine production is expected to increase the storage efficiency. Reservoir modelling of the Endurance structure supports 15% storage efficiency for the reference case as shown in **Table 4**.

Table 4 - Static storage efficiency (E) used in the GeoX volumetric study for the alternative stores.

	Minimum	Mean	Maximum
No pressure management	0.5 (restricted system)	4	10 (well-connected system into greater Bunter aquifer)
With pressure management	5 (reservoir heterogeneities and/or compartmentalization impacting negatively pressure maintenance with brine extractors)	15 (based upon Endurance technical limits with reference model)	30 (excellent reservoir performance required limited brine extraction)

These parameters have been used in the GeoX assessment to provide preliminary estimates for the potential storage capacity of the storage site considered. Additional numerical simulation has been carried for BC39 and BC40 to specifically test a notional 4 MTPA subsea expansion from Endurance. Each structure has been assessed independently in GeoX, which discards any interference which could occur between the closest structure such as the southern edge of BC37 and BC36.

8.0 High-graded Prospects

Following initial screening of the Top Bunter Sandstone regional structure map, five structures were high graded for more detailed assessment. These were BC36, BC37, BC39, BC40 and BC3 (see summary map Figure 8). These all possessed the key criteria as defined below:

1. Deep enough for CO2 to remain in dense phase (i.e. below 1000 mTVDSS)
2. No significant faulting
3. Of moderate or greater size and/or located close to existing Endurance primary store.
4.

8.1 BC36

This structure is a four-way dip closure on the border of block 44/26 and 43/30. The structure overlies part of the deeper Carboniferous Schooner gas field.

8.1.1 BC36 Well Penetrations

There are exploration and development wells penetrating the BC36 structure, which could cause containment integrity problems (**Figure 32**). The wells are summarised in Table 5. At least one crestal well does not appear to have containment at the Bunter Sandstone level and could provide a leakage pathway. The latest status of the development wells is unknown and data is required from the operator to assess these.

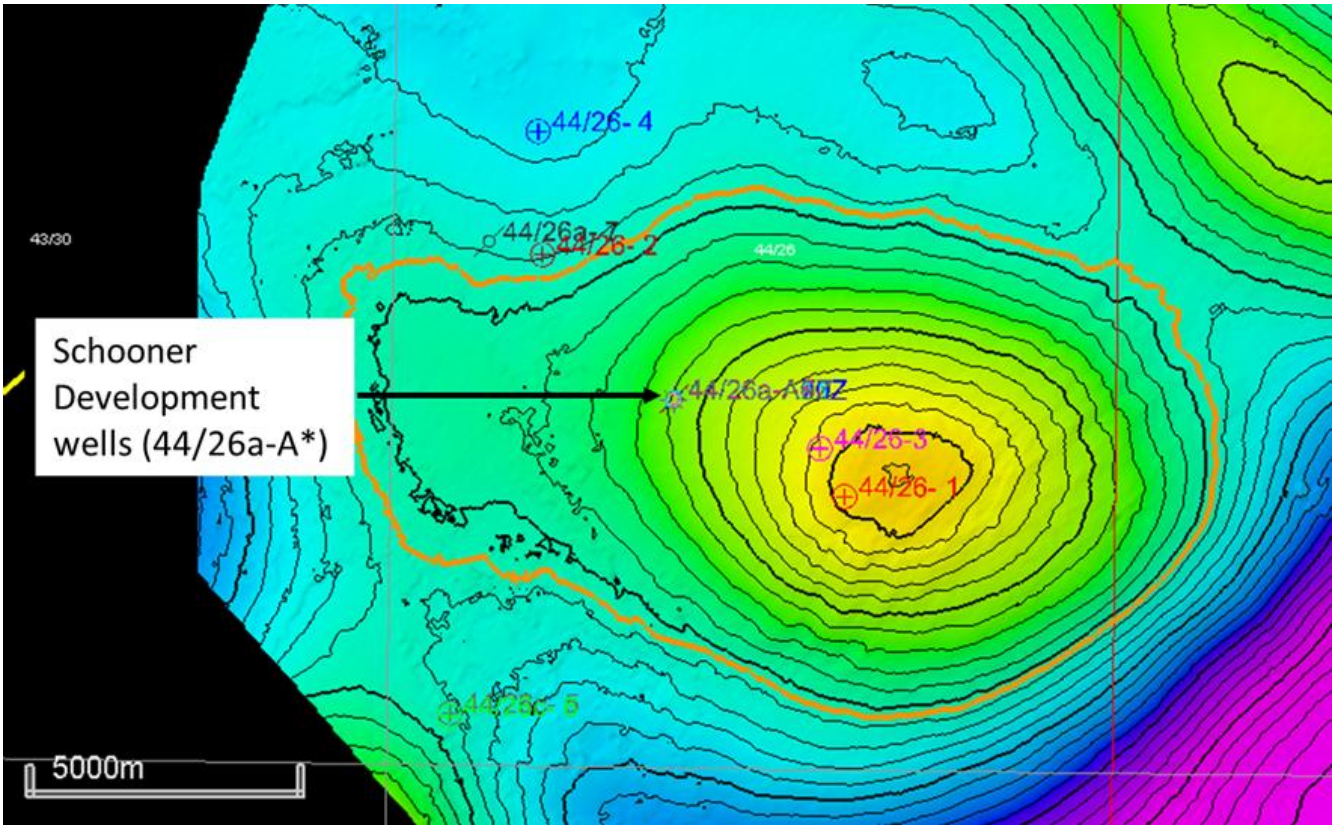

Figure 32 - Depth map of BC36 structure with spill point shown in orange. Well locations are indicated.

Table 5 - BC36 existing well penetrations.

Well		Status	Bunter containment
INSIDE SPILL POINT			
44/26-1		P&A	Good
44/26-3		P&A	Poor
46a-	A1	Shut in	Require CCS compliant P&A
	A2	Shut in	Require CCS compliant P&A
	A3	Shut in	Require CCS compliant P&A
	A44/2	Shut in	Require CCS compliant P&A
	A5	Shut in	Require CCS compliant P&A
	A6	abandoned phase 1	Require CCS compliant P&A
	A6Y	Shut in	Require CCS compliant P&A
	A6Z	abandoned phase 1	Require CCS compliant P&A
	A7	plugged	Require CCS compliant P&A
	A8	abandoned phase 1	Require CCS compliant P&A
	A8Z	Shut in	Require CCS compliant P&A
	A10	abandoned phase 1	Require CCS compliant P&A
	A10Z	Shut in	Require CCS compliant P&A
	A11	Shut in	Require CCS compliant P&A
OUTSIDE SPILL POINT			
44/26-2			
44/26a-7			

8.1.2 BC36 Reservoir Description

The BC36 structure sits within the mapped seismic phase reversal (SPR) and does not show any halite cementation of the sandstone reservoir. There are two wells near the crest of the structure: 44/26-3 was drilled with a large hole size which has created errors with absolute log values, so only data from 44/26-1 was available for reliable log analysis (**Figure 33**). Petrophysical analysis of the Bunter Sandstone at well 44/26-1 indicates that it is 215m thick with an average porosity of 21% (range from 17% to 26%). The average net-to-gross is 90% (range of 65% - 93%). Estimated average permeability is around 180mD. These reservoir properties are good but there is more clay content within the sandstone here than at Endurance, which may increase the chance of internal baffling.

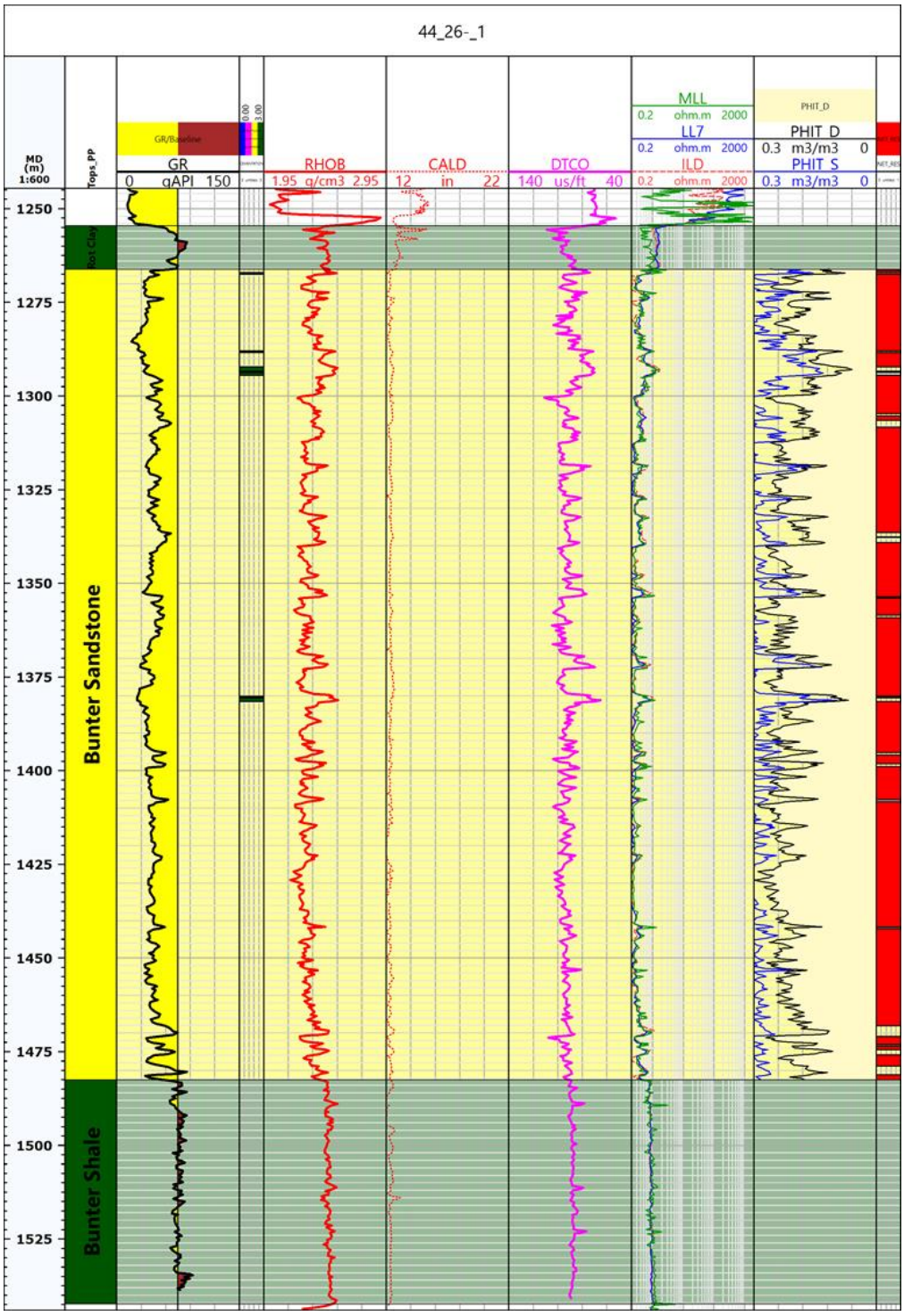

Figure 33 - Petrophysical interpretation for well 44/26-1.

8.1.3 BC36 Seal Description

The Base Cretaceous Unconformity (BCU) erodes quite deeply in this area and only the mid-lower Triassic section is preserved (**Figure 34**). However, this still provides around 230m of halites and shales as a top seal for the reservoir. Wells 44/26-1 and 44/21a-9 both possess the Röt Clay and Röt Halite primary seal package (**Figure 35**).

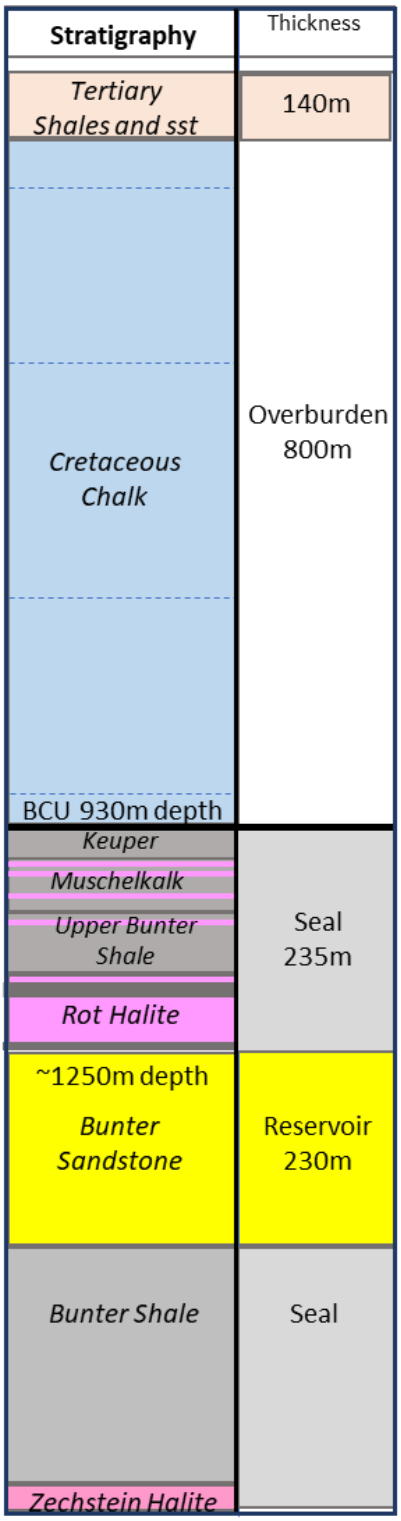

Figure 34 - Simplified stratigraphic column highlighting the stratigraphy present at the BC36 and BC37 locations.

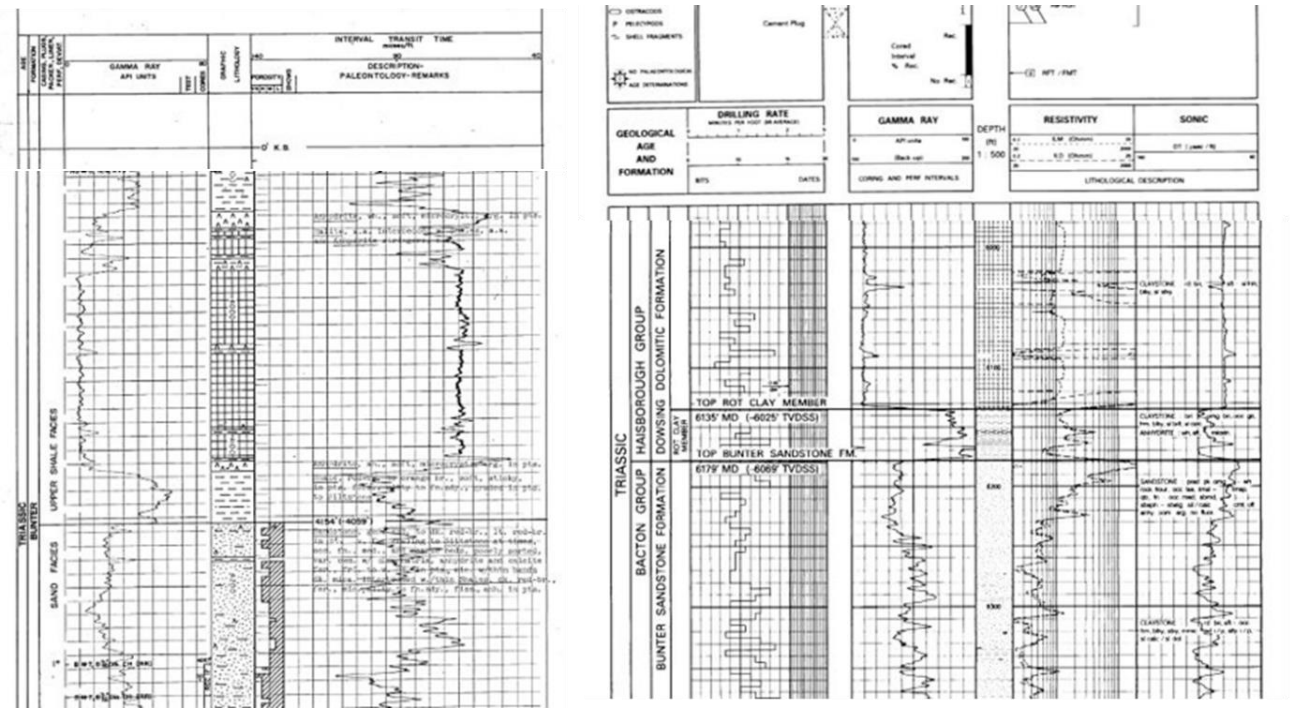

Figure 35 - Original composite logs for wells 44/26-1 (left) and 44/21a-9 (right) showing the Röt Clay and Röt Haite packages above the Bunter Sandstone Formation.

The thickness of the Röt Halite has been gridded from well tops, as the variable quality of the seismic data makes regional interpretation of the upper Röt Halite reflector challenging in this area. As seen in Figure 40 the thickness is very consistent averaging around 80–100m over the structures.

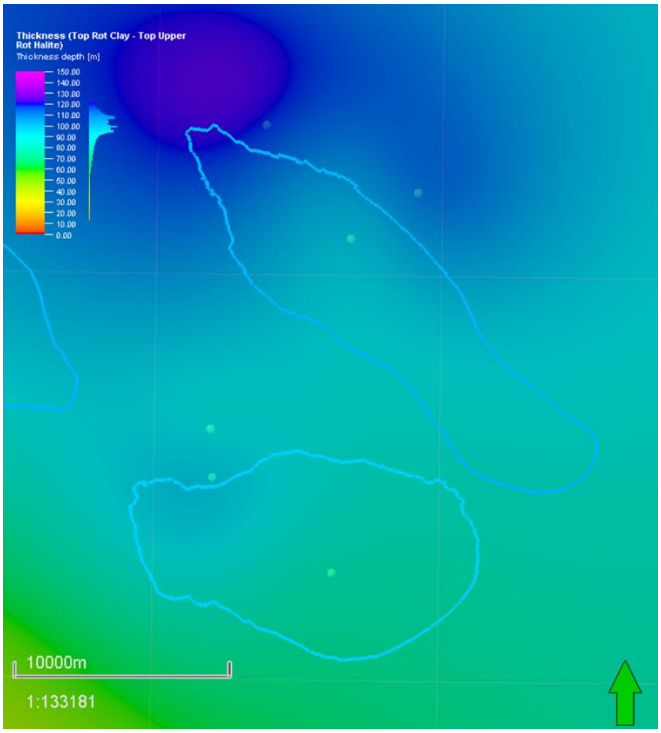

Figure 36 - Röt Halite thickness gridded from well tops. The wells used are shown as turquoise circles. BC36 (south) and BC37 (north) are outlined in blue.

8.1.4 BC36 Well Synthetic Seismograms

Synthetics were made for both exploration wells on structure (**Figure 37**). Note that the absolute values of well 44/26-3 are erroneous due to the large borehole, although the relative values are not as impacted, meaning that the seismic synthetic is still representative. The two wells are only 1 km apart and have a similar seismic response. At the base of the Röt Halite there is a thin anhydrite layer which is not seismically resolved, which somewhat complicates the seismic response at the top of the reservoir; it is showing a class IV AVO response. In general, the legacy seismic data available in the Southern North Sea is not optimised for Triassic imaging and there seems to be poor coverage of near offsets. This may explain why the strong Top Bunter Sandstone response dims regionally, and the amplitude change cannot be attributed to reservoir properties unless calibrated by well data. Given the thin layers with strongly different seismic rock properties in the overlying seal this will have a strong impact on the top reservoir seismic response.

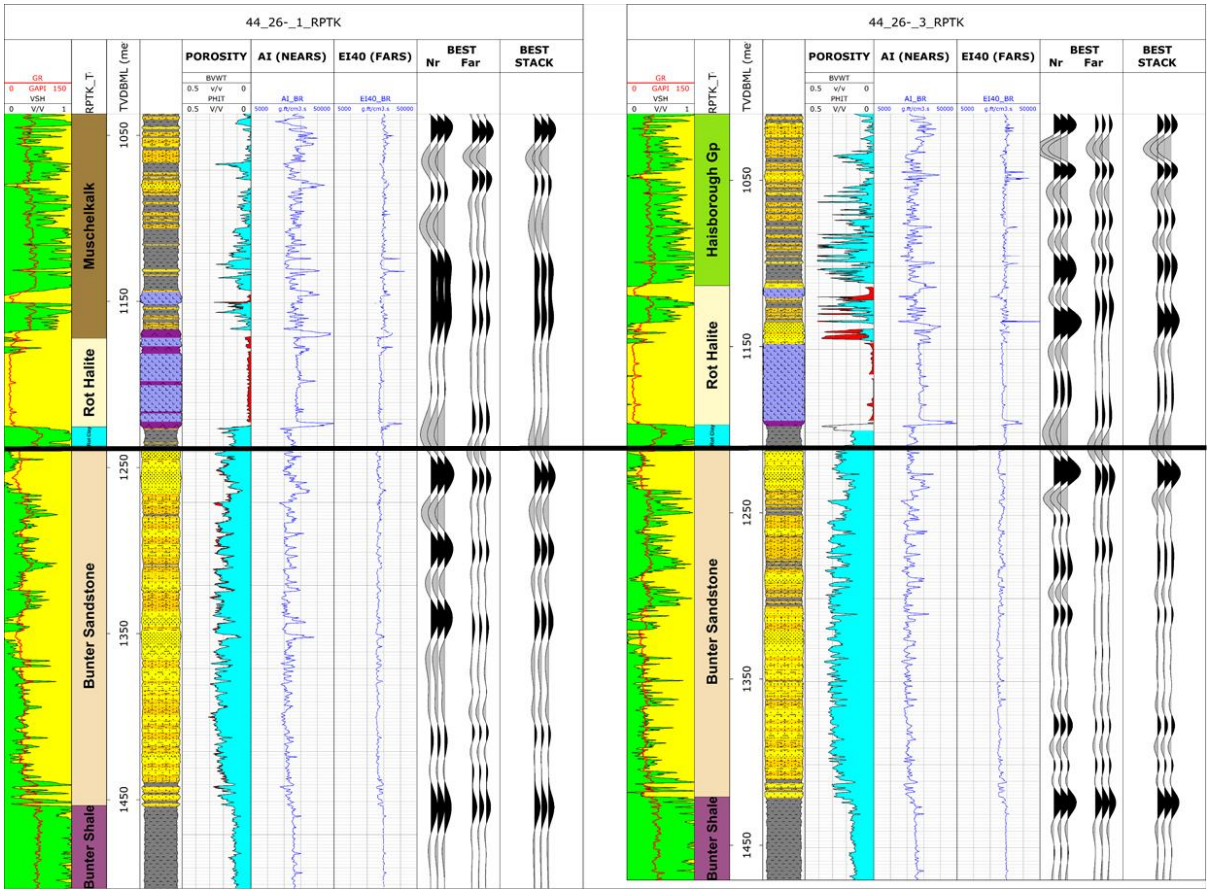

Figure 37 - Calculated well log synthetics for 44/26-1 and 44/26-3. Top Bunter Sandstone Fm is indicated with a thick black line. The wavelet used for the calculation is 4-8-50-90Hz.

8.1.5 BC36 Well-tie to Seismic

The 44/26-3 well-tie to seismic is shown in **Figure 38**. There were no check shots available for the well, which is evident with the mismatch at the Top Zechstein Halite. The lower bandwidth here compared to **Figure 37** makes the tuning with the thin anhydrite at the base of the Röt Halite disturb the Top Bunter Sandstone Formation event even more (**Figure 39**). The trough interpreted here on seismic is actually the top of the Röt Clay (which is ~10m thick and lies between the Röt Halite and the Bunter Sandstone).

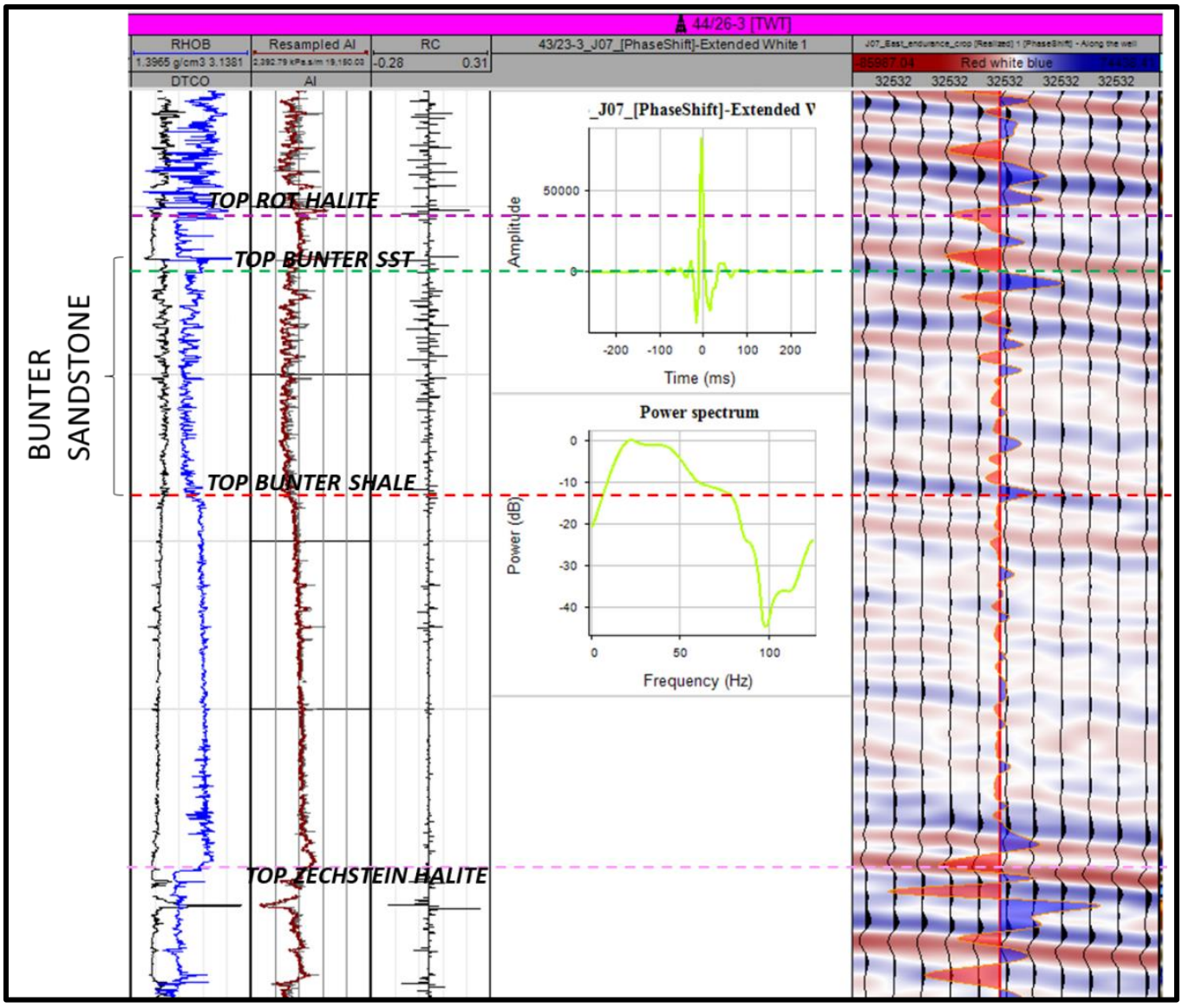

Figure 38 - Well-tie to seismic panel for 44/26-3.

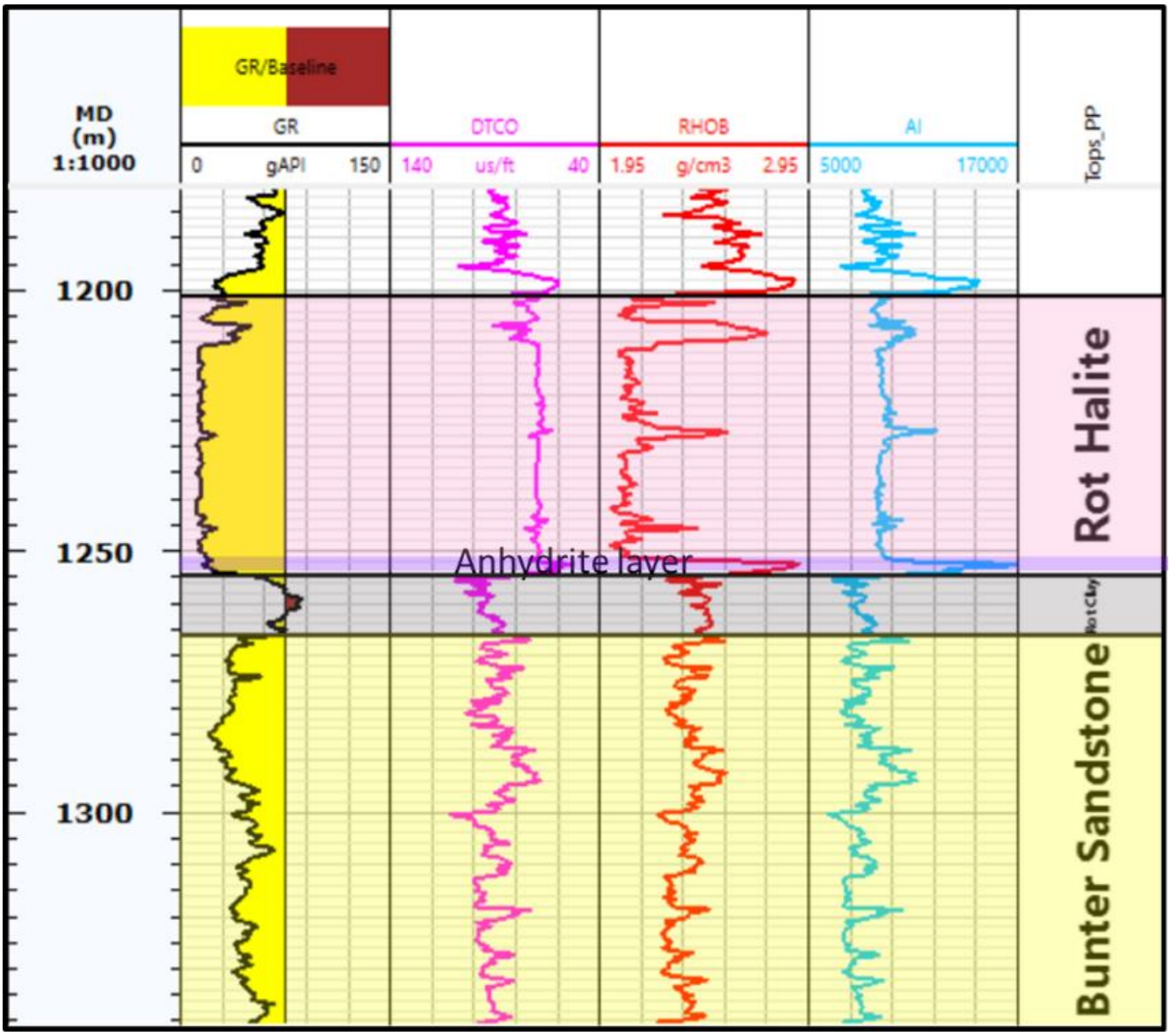

Figure 39 – Well log panel zoom-in to Röt Halite / Top Bunter Sandstone interface in 44/26-1. The hard anhydrite layer at the base of the Röt Halite has the largest acoustic impedance (AI) response in the section.

8.1.6 BC36 Horizon Interpretation

Figure 40 and **Figure 41** illustrate the horizon interpretation around the BC36 and BC37 structures. At the position indicated for the seismic phase reversal (SPR) the Top Bunter Sandstone response changes from trough (green horizon) to peak (orange horizon).

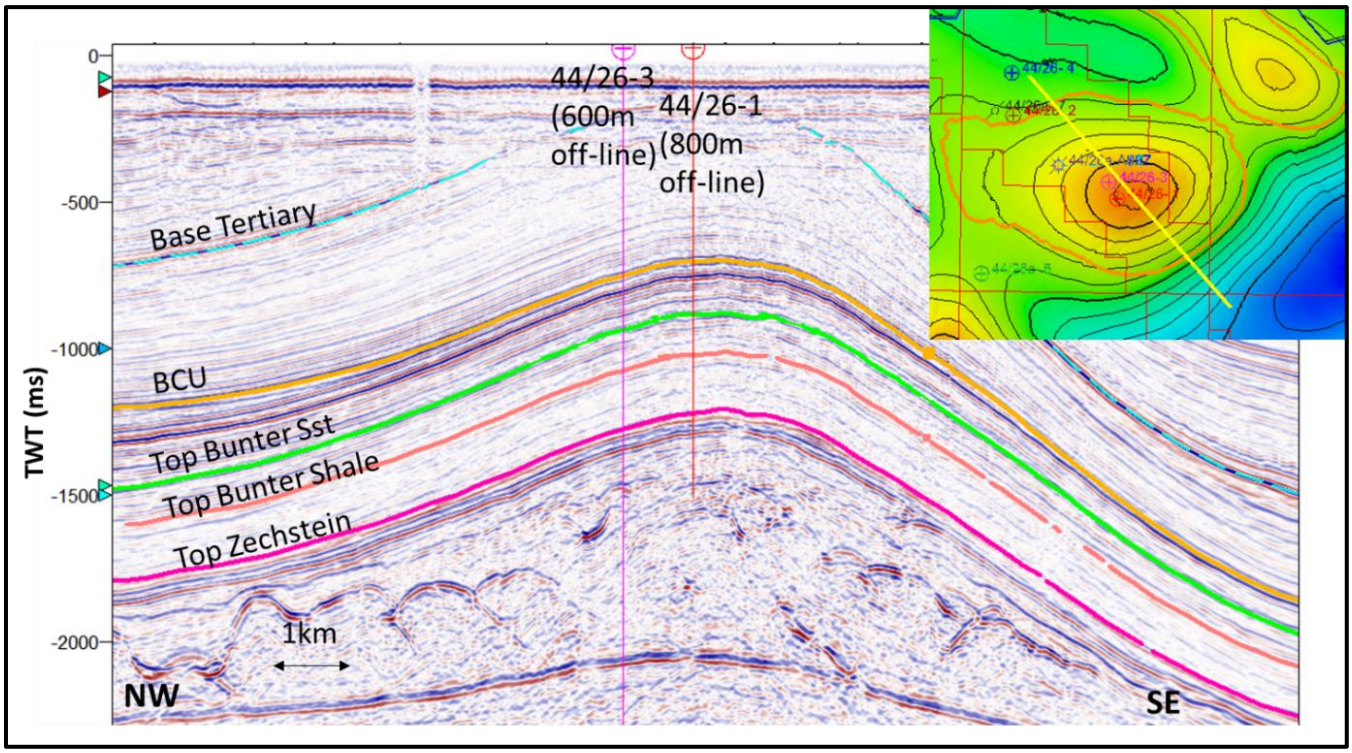

Figure 40 – NW-SE seismic section in TWT through BC36.

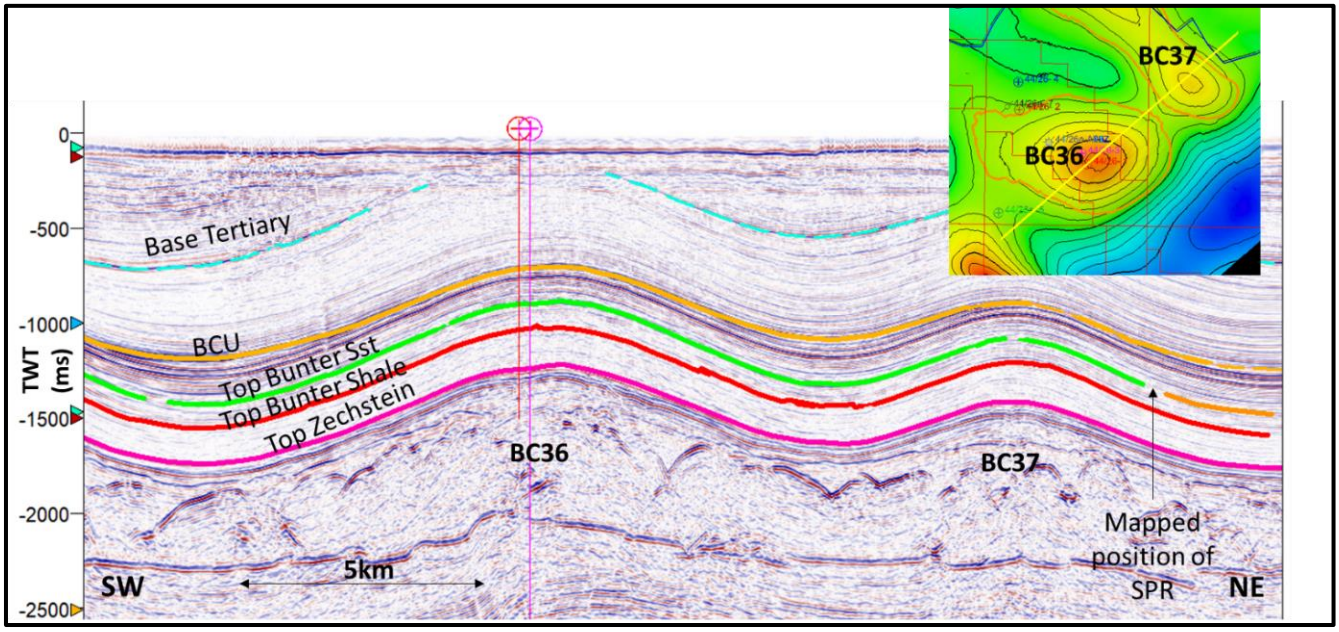

Figure 41 - SW-NE seismic section in TWT through BC36 and BC37.

8.1.7 BC36 Fault Interpretation

Seismic acquisition footprint is broadly aligned with the orientation of Triassic structural features and hampers detailed fault interpretation (**Figure 42**). When the variance is reviewed in detail it can be seen that there is faulting at the Triassic level that is slightly oblique to the acquisition direction. This corresponds to the much steeper dips on the SE limb of the structure. There is small-offset faulting present at all layers of the post-Zechstein stratigraphy but the faults do not appear to be connected all the way through the overburden. The faulting at the Top Bunter Sandstone cuts through both the Röt Halite and the Bunter Sandstone but the offsets are small (**Figure 43**). No faults are observed that displace the seal to an extent the seal continuity would be compromised. A potential risk is the extent to which the reservoir may be compartmentalised by this faulting, especially given the trend, which is parallel to dip and may inhibit updip plume migration.

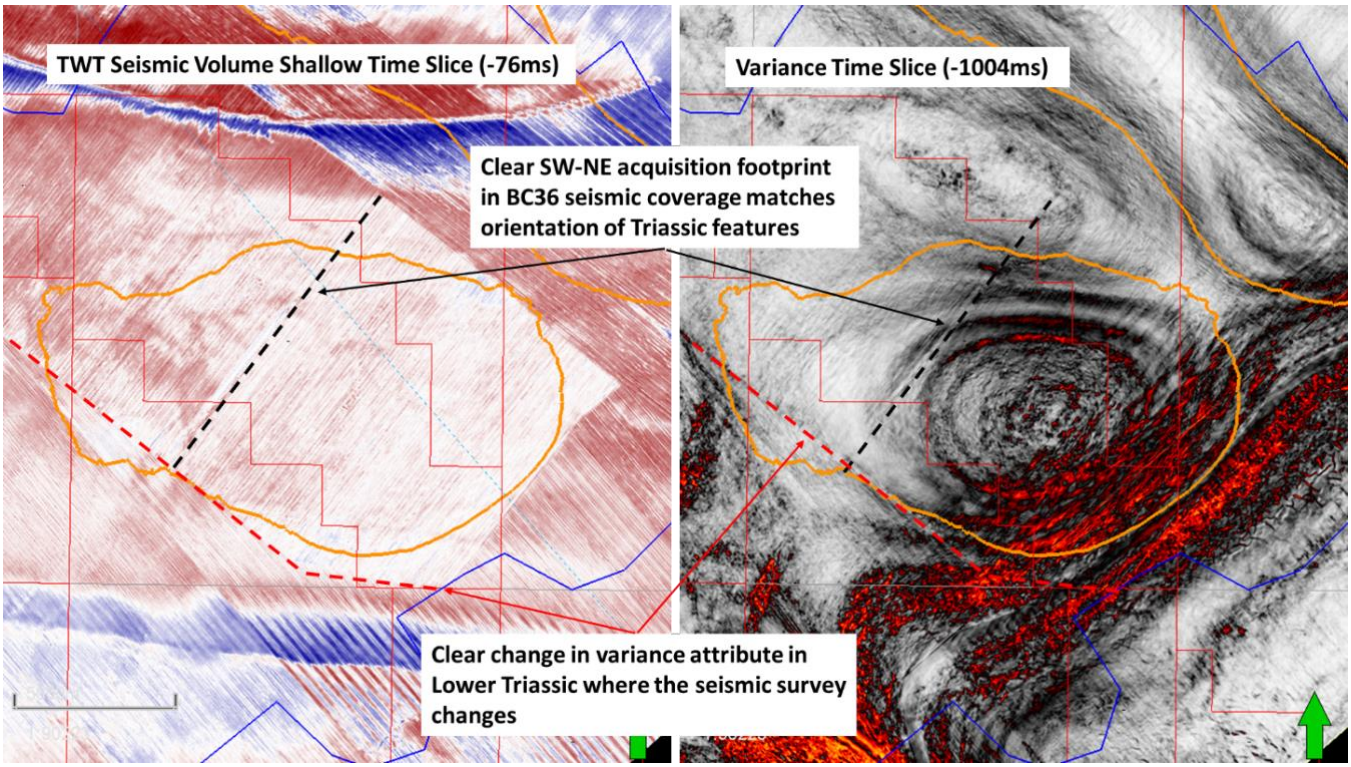

Figure 42 – Comparison of acquisition direction with seismic attributes: There is a strong overprint of acquisition direction observed at reservoir level.

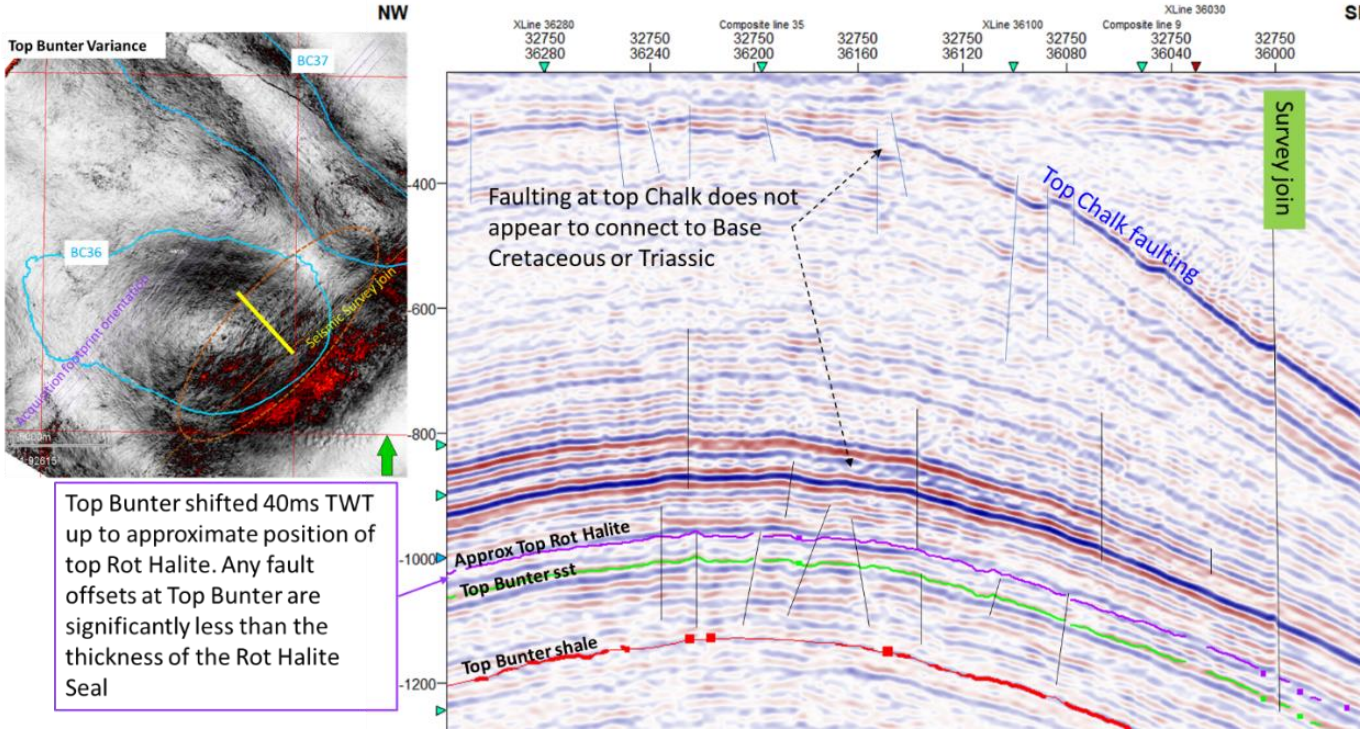

Figure 43 - Faulting at BC36: faulting at the top Chalk does not appear to connect down to the Triassic stratigraphy. Frequent small-scale faulting present at Top Bunter Sandstone but with throws much less than the thickness of the Röt Halite seal.

8.1.8 BC36 Depth Conversion

A regional velocity model was used for depth conversion, but locally this was not fully calibrated to the Triassic, so well top adjustments were applied to correct the depth surfaces. There is remaining uncertainty on exact depths and spill points and future work should include a new velocity model to reduce these errors. Some of the results are shown in **Figure 44**: when only the area around BC36 is used the resulting spill point is higher than when BC36 and BC37 are adjusted together. Because the saddle area between the two structures is small it seemed most appropriate to apply the adjustment to both structures to be able to assess the likelihood that BC36 and BC37 could be connected. The minimum curvature adjustment method was used after assessing some of the difference maps (Figure 45). This method provided a much smoother adjustment and seemed also more appropriate in areas of sparse well coverage and where overburden variations are long wavelength.

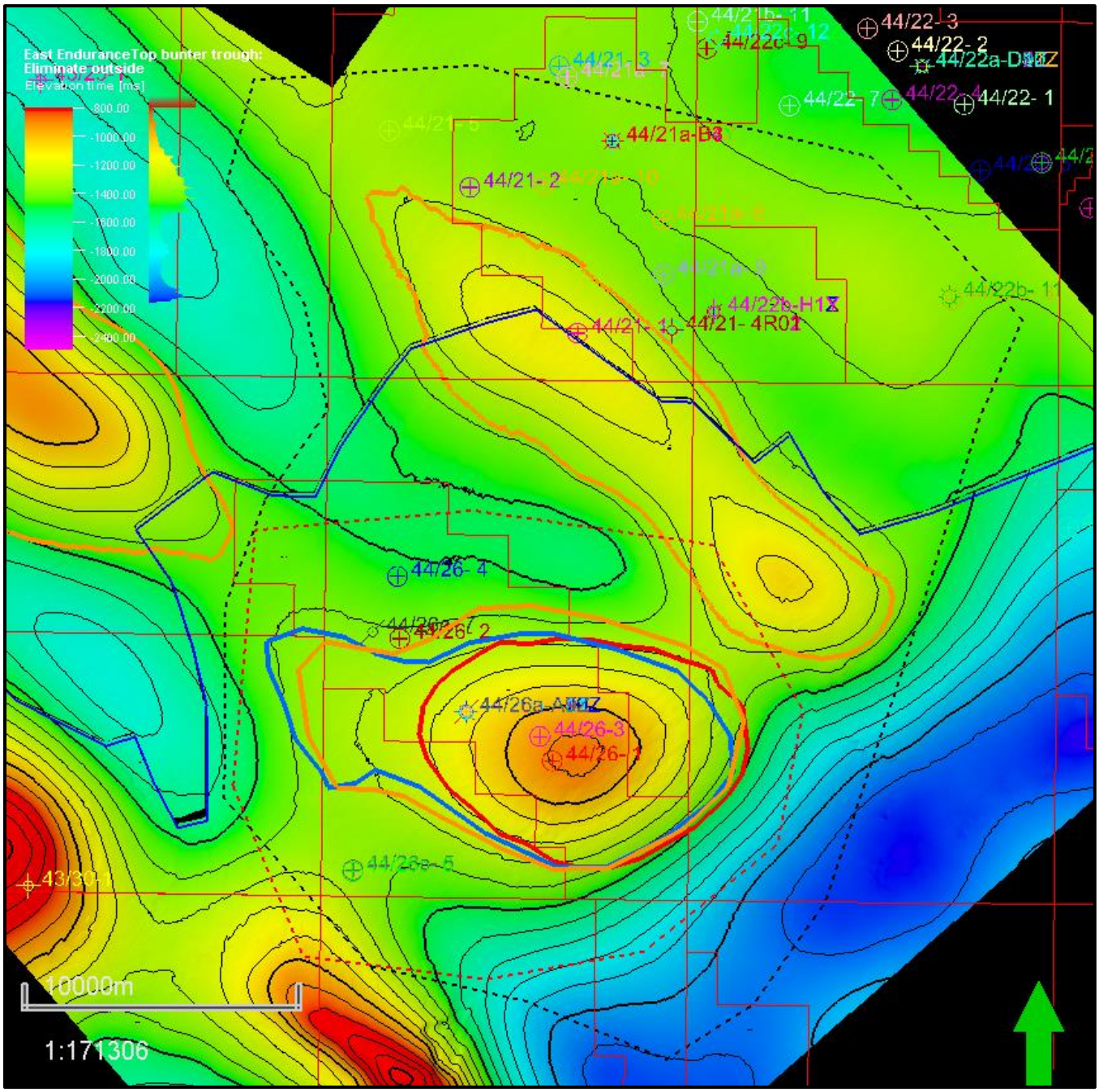

Figure 44 - Depth conversion uncertainty on spill point. The underlying map is the Top Bunter Sandstone TWT structure for reference. The red dashed line shows the area included in well top adjustment to get the red spill point. The black dashed line incorporates all of BC37 into the well top adjustment process and gives the blue (5km radius of adjustment) and orange (minimum curvature adjustment) spill points. The minimum curvature method was preferred as the adjustments are applied more smoothly.

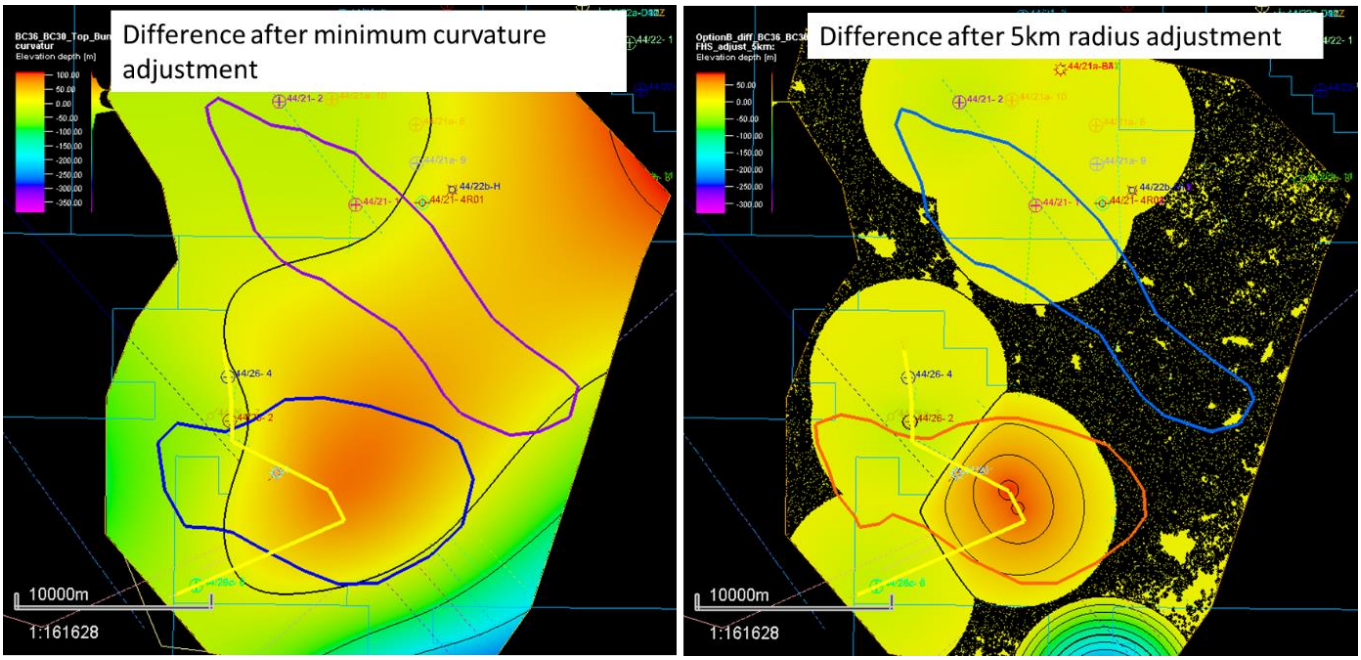

Figure 45 - Difference map after well top adjustment: comparison of methods.

8.1.9 BC36 Volumetric Calculations

Volumetric calculations have been performed using Schlumberger's GeoX exploration risk, resource and value assessment software. The P50 volume for BC36 is around 290MT CO2 (**Table 6**). This value assumes that the pressure increase from CO2 injection is managed, e.g. via brine production. If no pressure management is available, then the volume that can be stored by this structure reduces to around 80MT CO2.

Table 6 - BC36 volumetric calculations.

	Min	P90	P50	P10	Max
GRV [m3]	-	1.24E+10	1.48E+10	1.64E+10	-
Net-to-Gross	0.6	0.76	0.86	0.91	0.93
Porosity	0.16	0.18	0.21	0.24	0.26
Reservoir thickness [m]	200	206	221	244	275
Spill point depth [m]	1716	1747	1786	1824	1856
Crestal depth [m]	1175	1184	1195	1206	1215

Storage efficiency with pressure management	0.05	0.1	0.16	0.23	0.3
Storage efficiency no brine production	0.005	0.02	0.04	0.07	0.1
VOLUME CO2 WITH PRESSURE MANAGEMENT					
CO2 [MT]	-	167	293	461	-
VOLUME CO2 NO BRINE PRODUCTION					
CO2 [MT]	-	37	78	136	-

As a sensitivity, scenarios have also been calculated where the storage volumes are cropped to above the 44/26-3 legacy well and above the Schooner development wells to account for an eventuality where the legacy wells may not be able to be suitably remediated (Figure 46). This significantly reduces the potential volume available for CO2 storage (**Table 7**). It is clear that without remediation of legacy well 44/26-3 the structure is not likely usable for CO2 storage due to the very reduced volume. Correct abandonment of the Schooner wells is necessary to ensure BC36 is a suitable viable prospect for CO2 storage as a standalone structure.

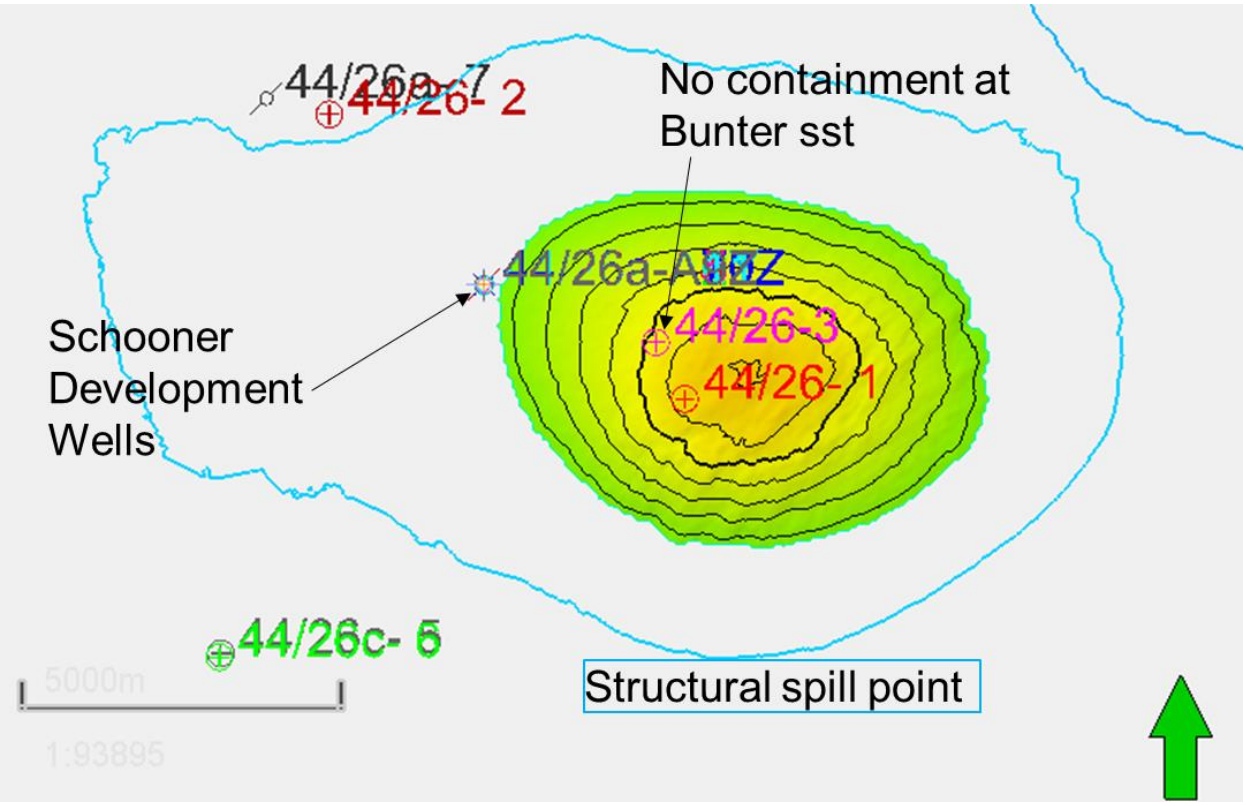

Figure 46 - Area of BC36 available above Schooner wells (44/26a-A**).

Table 7 – Sensitivity on BC36 volumetric estimations considering area above legacy wells only.

	P90	P50	P10
AVAILABLE CAPACITY ABOVE 44/26-3 LEGACY WELL			
CO2 [MT]	5	8	13
AVAILABLE CAPACITY ABOVE DEVELOPMENT WELLS WITH PRESSURE MANAGEMENT			
CO2 [MT]	48	81	125
AVAILABLE CAPACITY ABOVE DEVELOPMENT WELLS WITH NO BRINE PRODUCTION			
CO2 [MT]	10	22	39

8.1.10 BC36 Risk and Uncertainty

Risk and uncertainty for BC36 have been evaluated from the information available at the time. The risk matrix is shown in **Figure 47** and an uncertainty summary is presented in **Figure 48**. The structure has full seismic coverage with legacy 3D data and multiple well penetrations for evaluation. The primary concern for BC36 is the legacy well near the crest of the structure without primary containment at reservoir level. There is also additional risk posed by small scale faulting in the reservoir which could reduce the maximum pressure possible in the structure (and require earlier brine production). Due to this faulting being perpendicular to dip it may inhibit plume migration to the crest. Remediation of well 44/26-3 is key to enable this structure for CO2 storage.

Seismic Coverage: Full coverage with legacy 3D seismic
Well Coverage: Multiple wells in structure and close by

Top Down Evidence

Trap: Salt cored anticlines

Seal Capacity: Regionally the Rot clay and Rot Halite both provide an effective seal

Reservoir Presence: Bunter sst is a high NtG fluvial/aeolian system across a large part of the SNS

Reservoir Injectivity: High NtG sst, no halite cementation inside seismic phase reversal. Potential for baffling with clays/small scale faulting.

Legacy Well Risk: Wells drilled to Bunter targets are abandoned correctly for Bunter and don't post a leakage risk. Deeper target wells may not have correct abandonment. Remediation expensive and not guaranteed.

CO2 State: Regional data suggests crest below 800m TVDSS for dense phase CO_2 storage

Estimated Capacity Injection alone: 37-78-136MT
with brine production: 167-293-461MT
NEP Phase 2 notional plan: 2 injectors = 40MT
Total Risk Ps= 0%

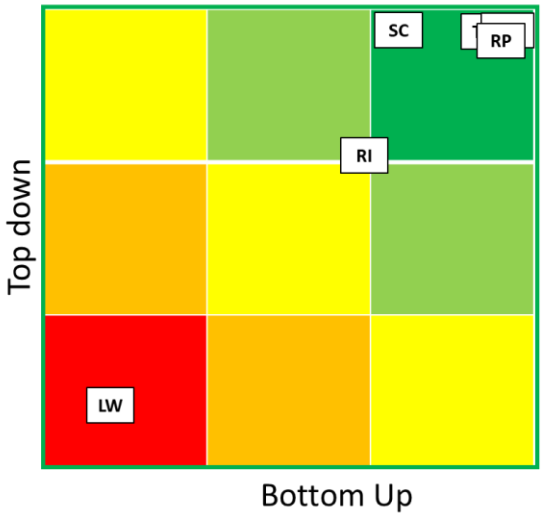

Bottom-Up Evidence

Trap: 4-way dip closure on 3D seismic in TWT and Depth. Some uncertainty on depth conversion but high relief structure

Seal Capacity: Rot Halite provides an effective seal. Small scale faulting at top reservoir present but does not offset seal.

Reservoir Presence: Bunter sst present in all wells on and off structure, regionally isopachous in this area, average thickness 220m.

Reservoir Injectivity: High NtG but thin clays may baffle. SE side of structure has faulting which may impede injectivity.

Legacy Well Risk: One well near crest with no Bunter containment; Carboniferous development wells mid-structure also unlikely to be correctly abandoned.

CO2 State: Crest at 1195m TVDSS

Figure 47 - BC36 risk matrix.

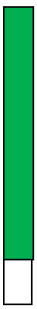

TRAP
- 4-way dip closure over salt-cored anticline
- >500m structural relief
- Depth conversion uncertainty on spill point

SEAL INTEGRITY AND CAPACITY
- Structure is overlain by Rot Clay, Rot Halite and other sealing lithologies
- Minor faulting at top Bunter, but does not offset seal
- Indications are that Rot Clay alone cannot hold back full column and may leak by capillary action but not fracture.
- Rot halite will be an effective seal.

RESERVOIR PRESENCE
- Bunter sandstone observed in all wells on structure and around
- Bunter sandstone thickness at crest of the structure is 215m.

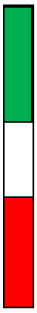

RESERVOIR INJECTIVITY
- Reservoir depth allows for CO2 injection in dense phase
- Bunter is high NtG sst
- Bunter sandstone appears to have some shalier sections which could baffle
- Extensive but small-scale faulting in SE side of reservoir may compartmentalise
- No core/well test in Bunter to confirm poro/perm

HYDROCARBON SYSTEM UNDERSTANDING
- Charge mechanism into Bunter from pre-Zechstein sources well understood and regional model exists; no charge pathway into Bunter
- No gas observed in well logs

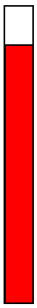

LEGACY WELL RISK
- At least 1 well (44/26-3) does not have primary containment at Bunter level
- Multiple penetrations of Bunter for development of deeper Schooner gas field
- Currently no remediation process is 100% reliable

Figure 48 - BC36 uncertainty summary.

8.2 BC37

The BC37 structure is a double-crested four-way dip closed anticline adjacent to BC36. The height of the structural closure is less than BC36 but the area inside the spill point is larger. One key uncertainty is reservoir quality, as it appears that the seismic phase reversal (SPR) cuts through this structure and the only on-structure well sits outside the SPR with halite cementation at the top of the sandstone.

8.2.1 BC37 Well Penetrations

There is only one well within the spill point, 44/21-1 (**Figure 44**). This well is believed to be lacking containment at Bunter level and is a potential leak risk.

8.2.2 BC37 Reservoir Description

Well 44/21-1 sits just outside of the seismic phase reversal (SPR) and halite cementation occurs within the top ~20m of the Bunter Sandstone, reducing the reservoir quality within that interval (**Figure 49**). However, as the majority of the BC37 closure sits within the SPR, well 44/21-1 is less likely to be representative and it is expected that reservoir properties would be similar to nearby BC36. Average reservoir thickness in 44/21-1 and 44/21-2 is 239m.

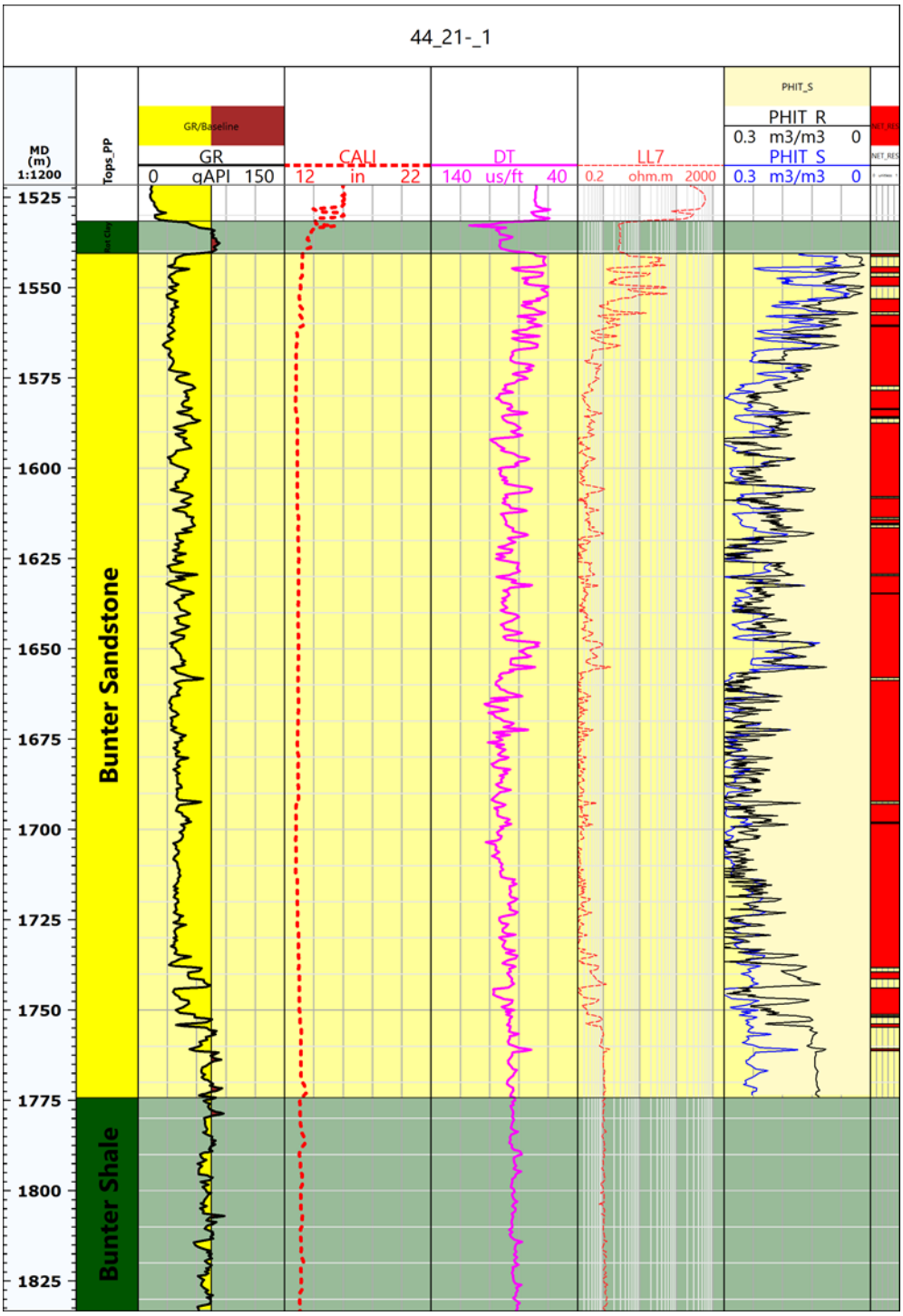

Figure 49 - 44/21-1 reservoir section. Halite cementation is present at the top of the Bunter Sandstone (approximately from 1540-1560m) and reduces porosity there.

8.2.3 BC37 Seal Description

The overburden stratigraphy at BC37 is very similar to BC36 (**Figure 34**). The wells show ~100m or greater of Röt Halite, with at least 70m of 'pure' halite facies at 44/21-1 (**Figure 50**).

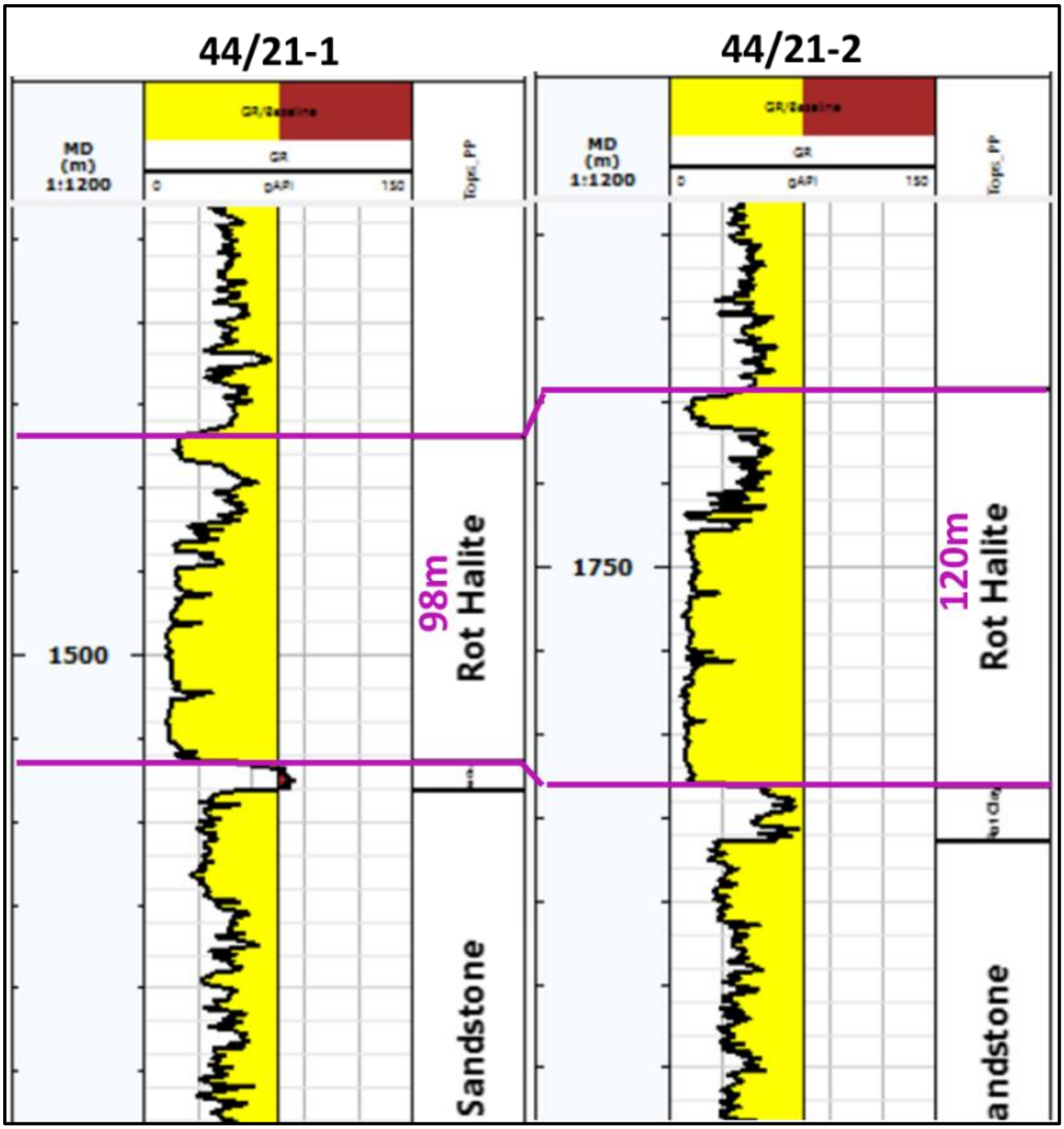

Figure 50 - Seal at BC37 in wells 44/21-1 and 44/21-1.

8.2.4 BC37 Horizon Interpretation

The re-interpretation of the seismic phase reversal (SPR) for this project has identified the SPR to cross the BC37 structure. The TWT seismic image in **Figure 51** shows the clear change in seismic character at the top Bunter level from trough in the west to peak in the east (and trough in the southeast to peak in the northwest in **Figure 52**).

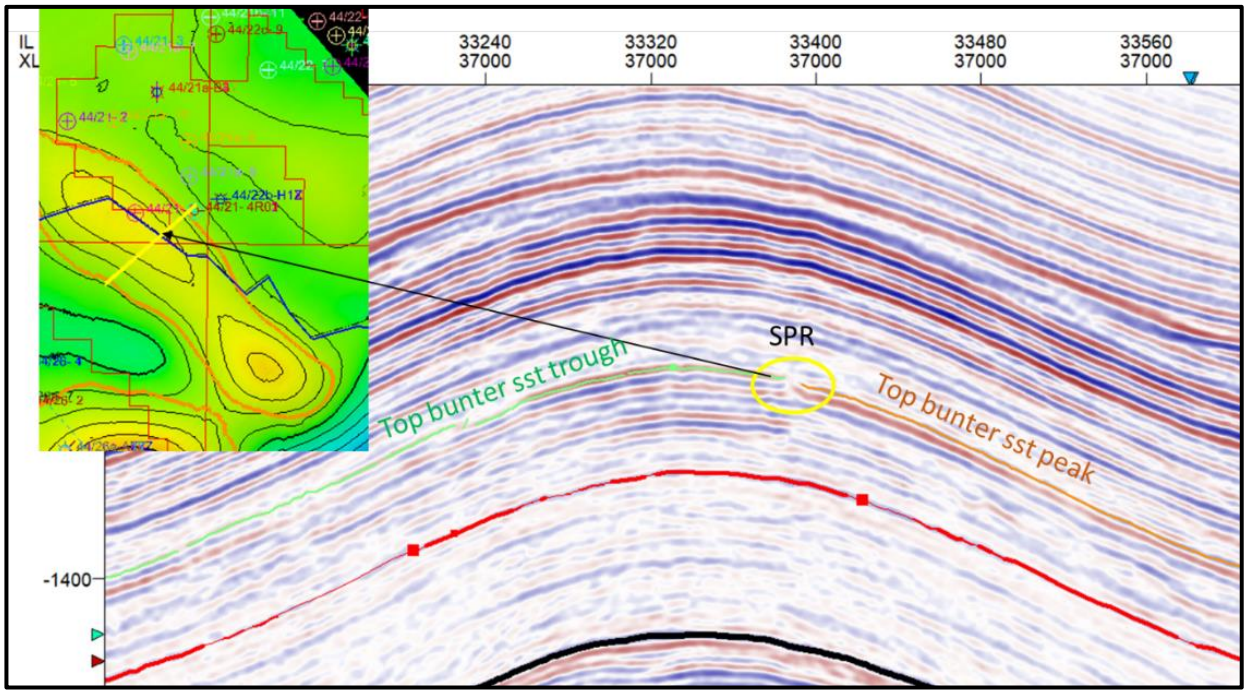

Figure 51 - West-east seismic line across BC37 showing the interpretation of the SPR on the structure. Note that the Top Bunter Sandstone character changes from trough-peak-trough in the west to peak-broad trough in the east.

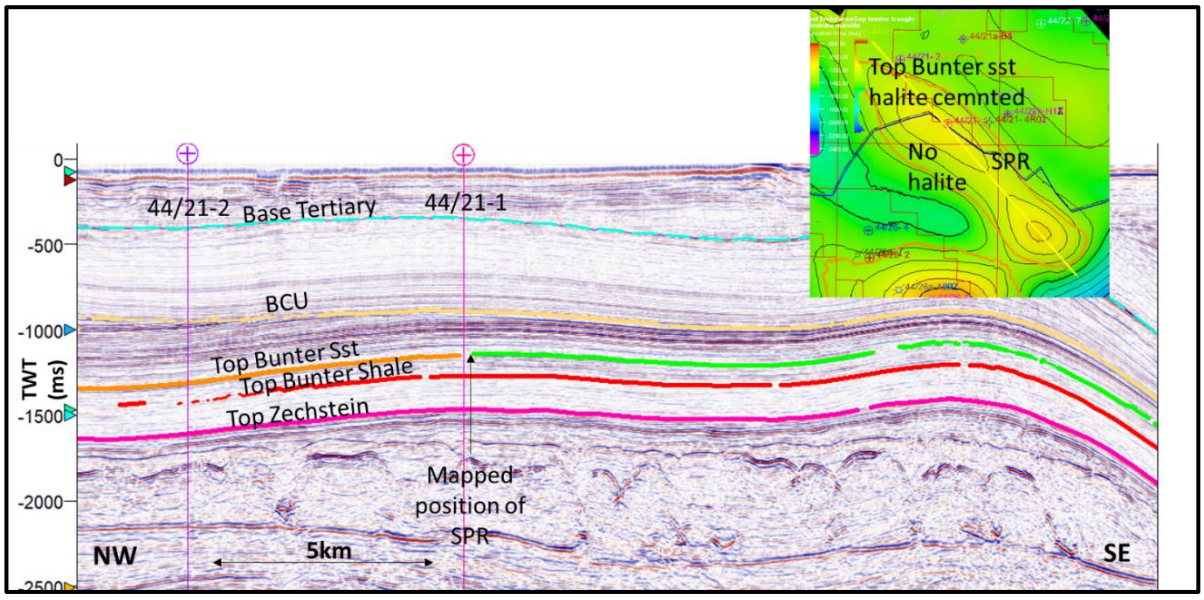

Figure 52 - TWT seismic line NW-SE through BC37. Top Bunter (orange) is halite cemented outside of the SPR, where this changes to green the Top Bunter Sandstone is higher porosity without halite cementation.

8.2.5 BC37 Fault Interpretation

There are no large faults at BC37 but some minor faulting is present in the southern half of the structure. Minor faulting is present at the Top Bunter Sandstone level (**Figure 53**), but offsets are small. There is also some perpendicular faulting (**Figure 54**, Line A) seen on the variance and seismic, but again, this is minor in offset and would not offset the Röt Halite seal. Variance data show a clear character change across the axis of the structure. To the NE this can be interpreted as the seismic phase reversal (**Figure 54**, Line B). To the SW, the variance change is apparent but there is no clear evidence of a seismic phase reversal. This has not been investigated further at this stage as there is no well calibration. Reprocessing of seismic data could possibly confirm if this is imaging-related or true reservoir character.

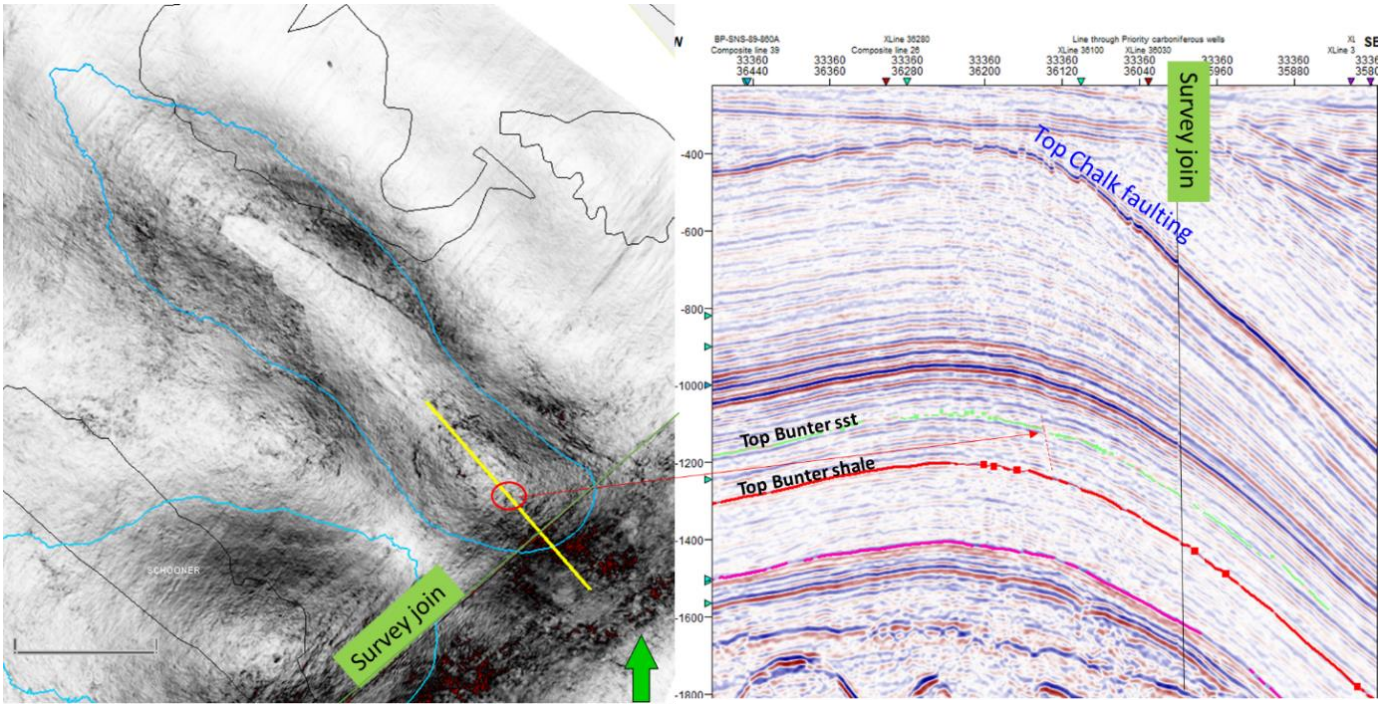

Figure 53 - Top Bunter Sandstone variance and seismic section in TWT. A small feature (red) is interpreted as a fault on the seismic.

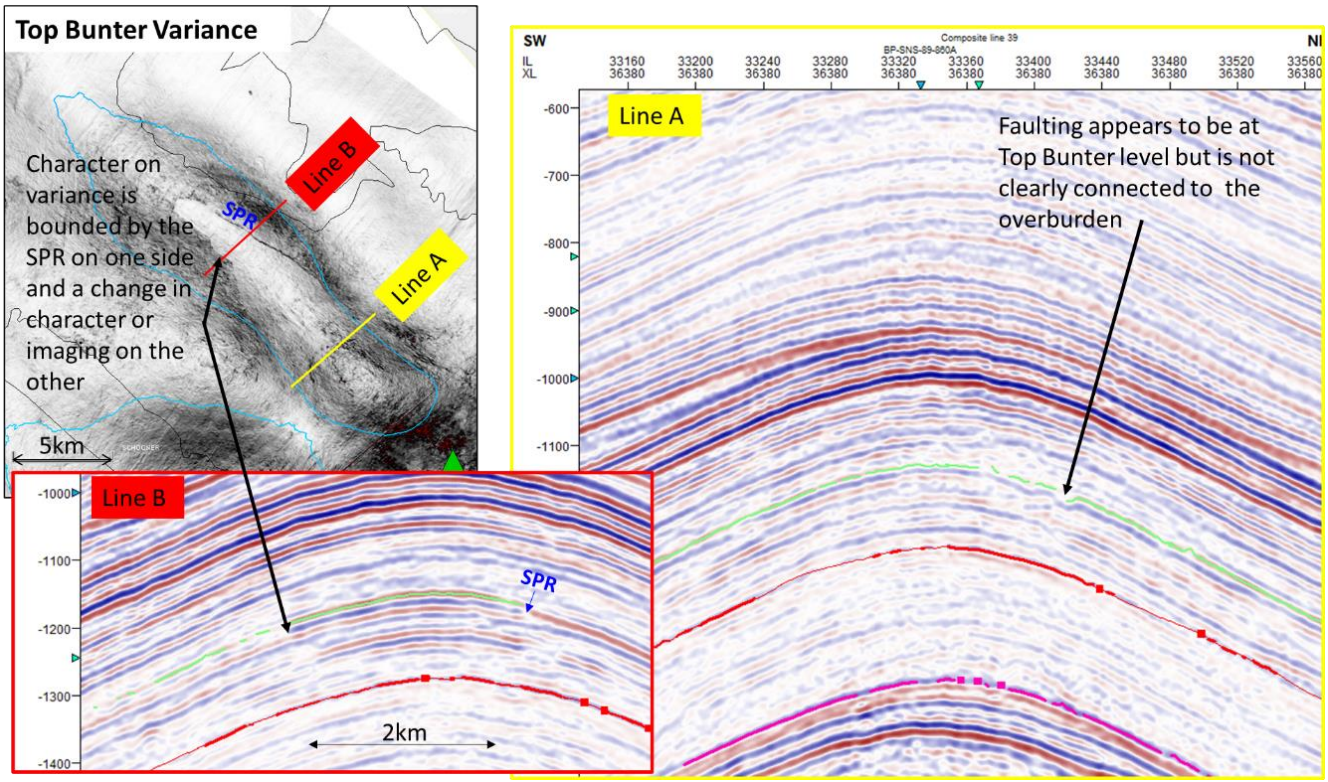

Figure 54 - BC37 variance and NW-SE orientated features (all maps are north orientated).

8.2.6 BC37 Depth Conversion

BC37 was depth converted together with BC36 as described above in section 0. For this structure there was not much difference between the two methods of well top adjustment (**Figure 55**).

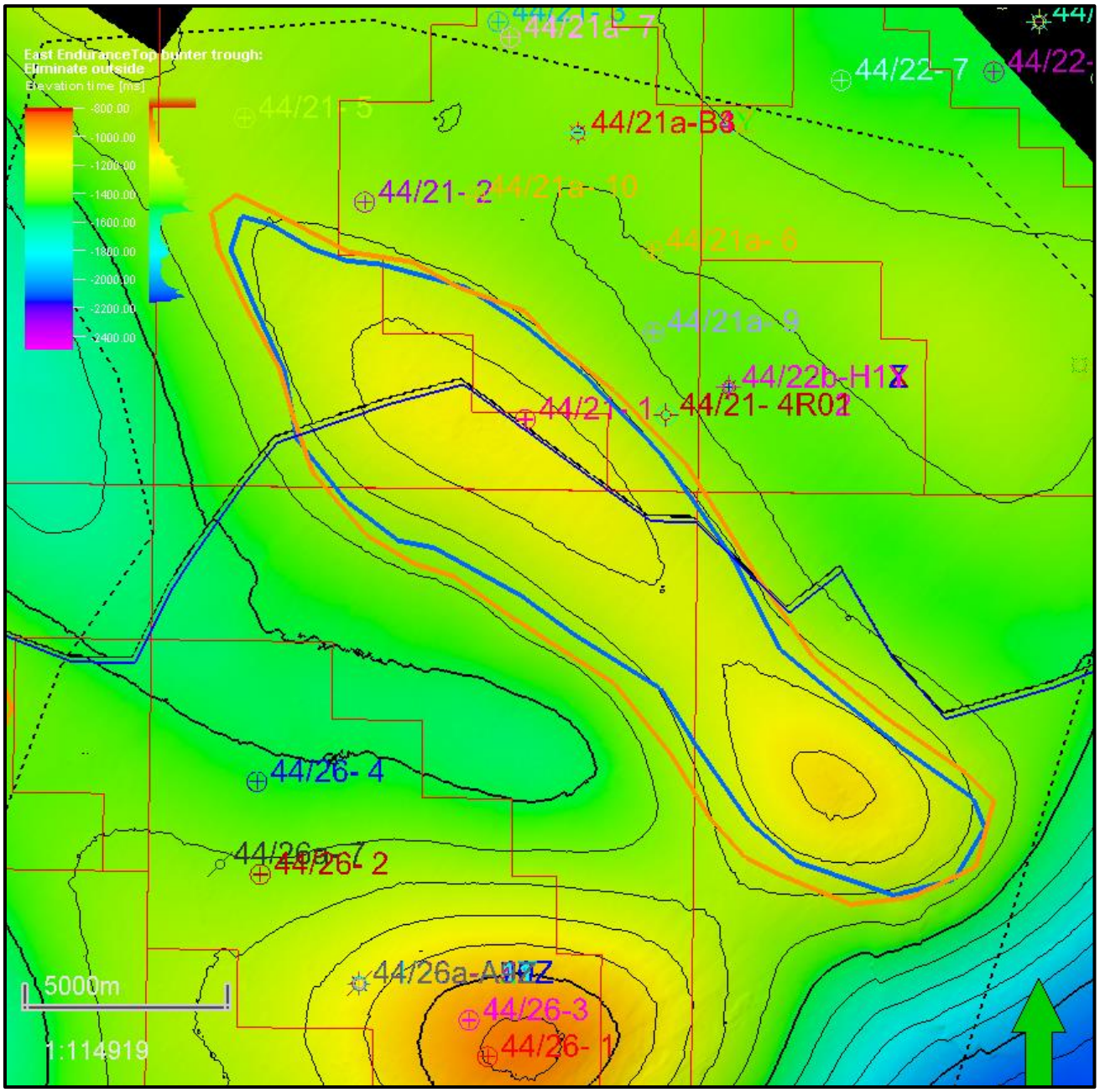

Figure 55 - Difference in spill point at BC37 using the minimum curvature (orange) and 5km radius (blue) algorithms. Base map is TWT top Bunter Sandstone structure map.

8.2.7 BC37 Volumetric Calculations

BC37 has only around 270m of structural closure but a large area. There is currently no analogue data available to understand the impact of vertical structural closure on storage efficiency. For this reason, the range for the storage efficiency has been kept the same for all calculations. The P50 volume is around 270MT CO2 (**Table 8**). If no pressure management is available (i.e. brine production), this reduces to 75MT CO2.

Table 8 - BC37 volumetric calculations.

	Min	P90	P50	P10	Max
GRV [m3]	-	1.04E+10	1.40E+10	1.76E+10	-
Net-to-Gross	0.6	0.74	0.83	0.88	0.9
Porosity	0.16	0.18	0.21	0.24	0.26
Reservoir thickness [m]	215	224	238	255	275
Spill point depth [m]	1667	1699	1737	1776	1807
Crestal depth [m]	1400	1422	1450	1478	1500
Storage efficiency with pressure management	0.05	0.1	0.16	0.23	0.3
Storage efficiency no brine production	0.005	0.02	0.04	0.07	0.1
VOLUME CO2 WITH PRESSURE MANAGEMENT					
CO2 [MT]	-	155	271	460	-
VOLUME CO2 NO BRINE PRODUCTION					
CO2 [MT]	-	36	74	134	-

The legacy well on the structure, 44/21-1, has no containment at the Bunter Sandstone level. The capacity above this well leak point has been calculated below (**Table 9**) to be on the order of 10–20MT. Without remediation of this well, the BC37 structure does not provide sufficient CO2 capacity to be developed.

Table 9 - BC37 capacity above level of 44/21-1 legacy well.

	P90	P50	P10
AVAILABLE CAPACITY ABOVE 44/21-1 LEGACY WELL			
CO2 [MT]	11	17	26

8.2.8 BC37 Risk and Uncertainty

The risk matrix for BC37 is shown in **Figure 56** and an uncertainty summary is presented in **Figure 57**. The key risk for BC37 at present is the 44/21-1 well, which does not have primary containment at the Bunter Sandstone level. The structure is relatively low relief (270m) which may reduce injectability over time and could necessitate earlier brine production. Part of the structure has been interpreted to lie outside the SPR on seismic and shows halite cementation in the well, although this is not thought to impact the majority of the reservoir (only top ~20m). There is no well within the structure to confirm reservoir quality inside the SPR.

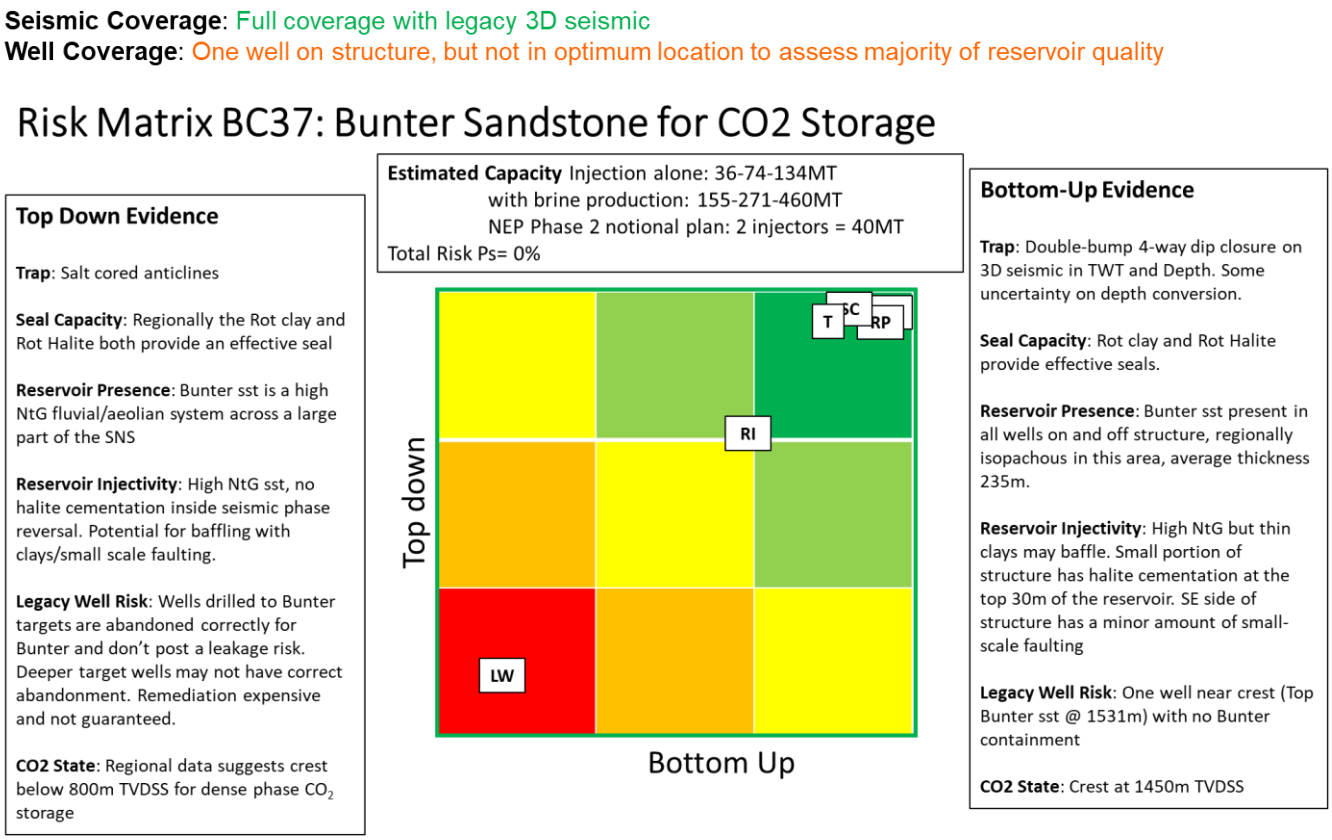

Figure 56 - BC37 risk matrix.

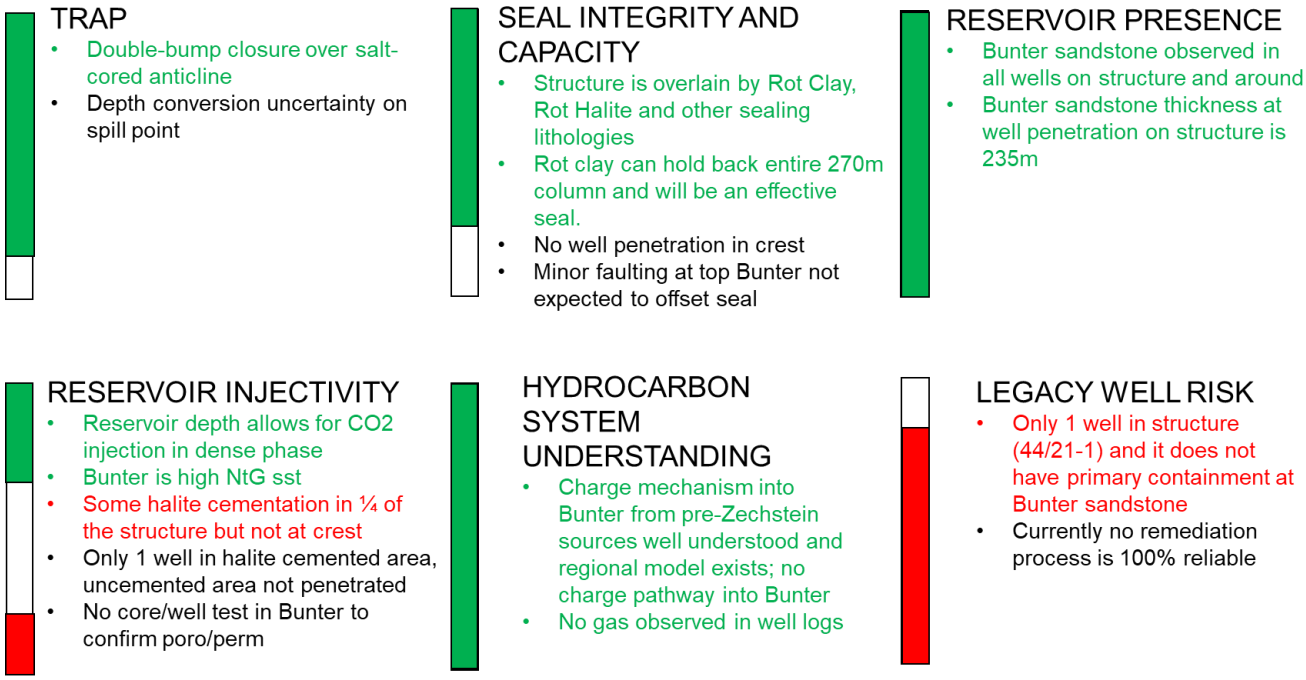

Figure 57 - BC37 uncertainty summary.

8.3 BC39

BC39 a four-way dip-closure structure that straddles blocks 43/24, 43/25, 43/29 and 43/30.

8.3.1 BC39 Well Penetrations

There are no well penetrations in the BC39 structure. Analysis of the structure relies on offset wells.

8.3.2 BC39 Reservoir Description

Seismic interpretation and offset wells suggest that there is some halite cementation at the top of the Bunter sandstone formation over much of the structure. There are indications that the seismic phase reversal cuts across the southern edge, however with the limited seismic coverage and join of two different datasets across the structure there is a lot of uncertainty on the amount of halite, the amount of shale and the distribution of these along with the thickness.

8.3.3 BC39 Seal Description

Regional understanding of the seal facies and distribution is good. Overall, the Triassic section is highly isopachous and the offset wells show little variation. Where the major uncertainty lies for BC39 is in the risk of faulting of the seal, because the lack of seismic coverage (**Figure 6**) means that this cannot be fully assessed.

At the location of BC39, the Base Cretaceous Unconformity (BCU) has cut a little deeper than at BC40 (**Figure 8**), reaching to around top Triassic level. Whilst the lowermost Jurassic is

missing, nearly all the Triassic package is in place and the primary sealing facies of the Röt Clay and Röt Halite, along with the other shale and halite layers of the Triassic are present.

8.3.4 BC39 Horizon Interpretation

Seismic horizon interpretation has been completed by correlating from the Endurance area and BC40, to over the BC39 structure and then down to BC36. The seismic quality impacts the interpretation at the edges of the surveys (**Figure 58** and **Figure 59**).

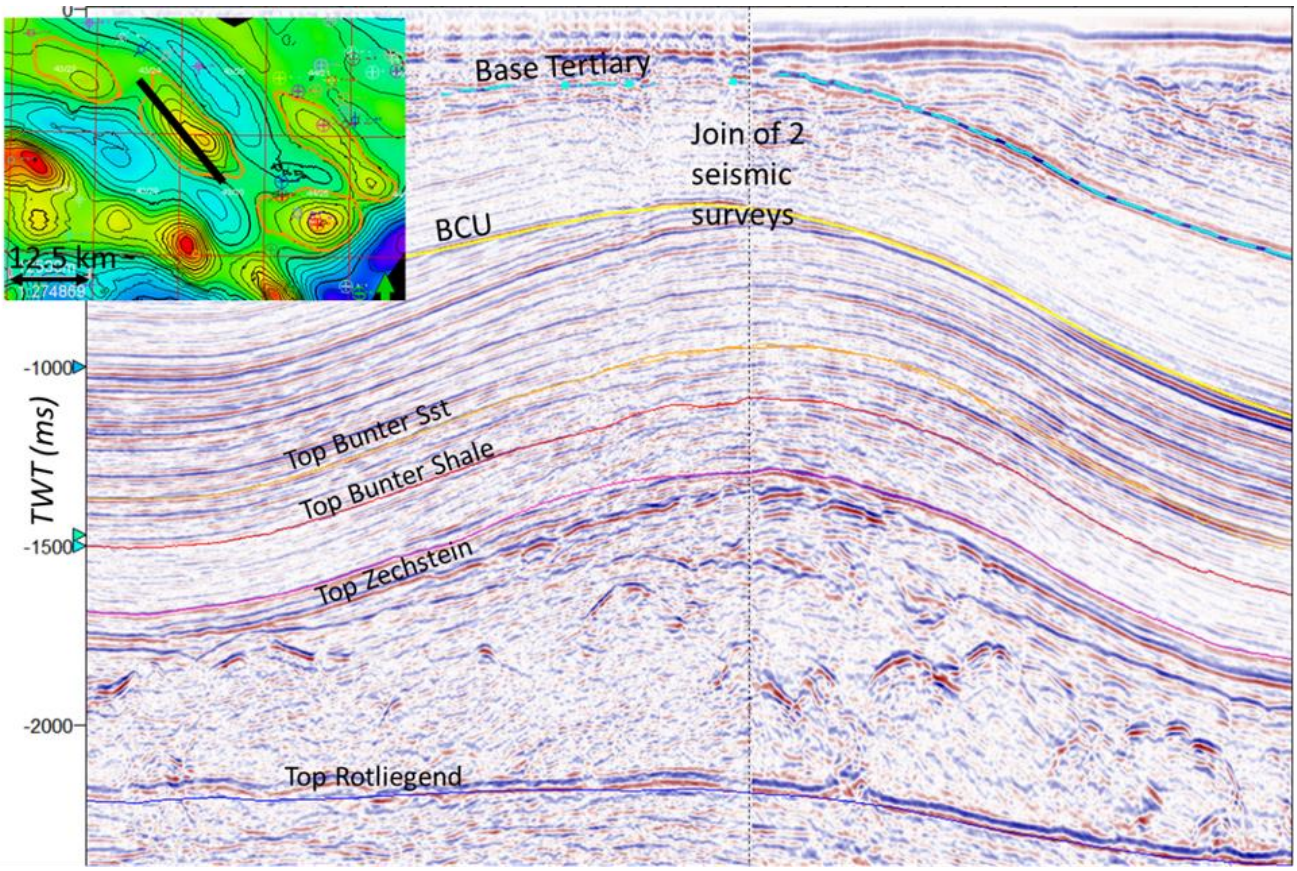

Figure 58 - NW-SE seismic line through BC39 to the west of the gap in seismic coverage.

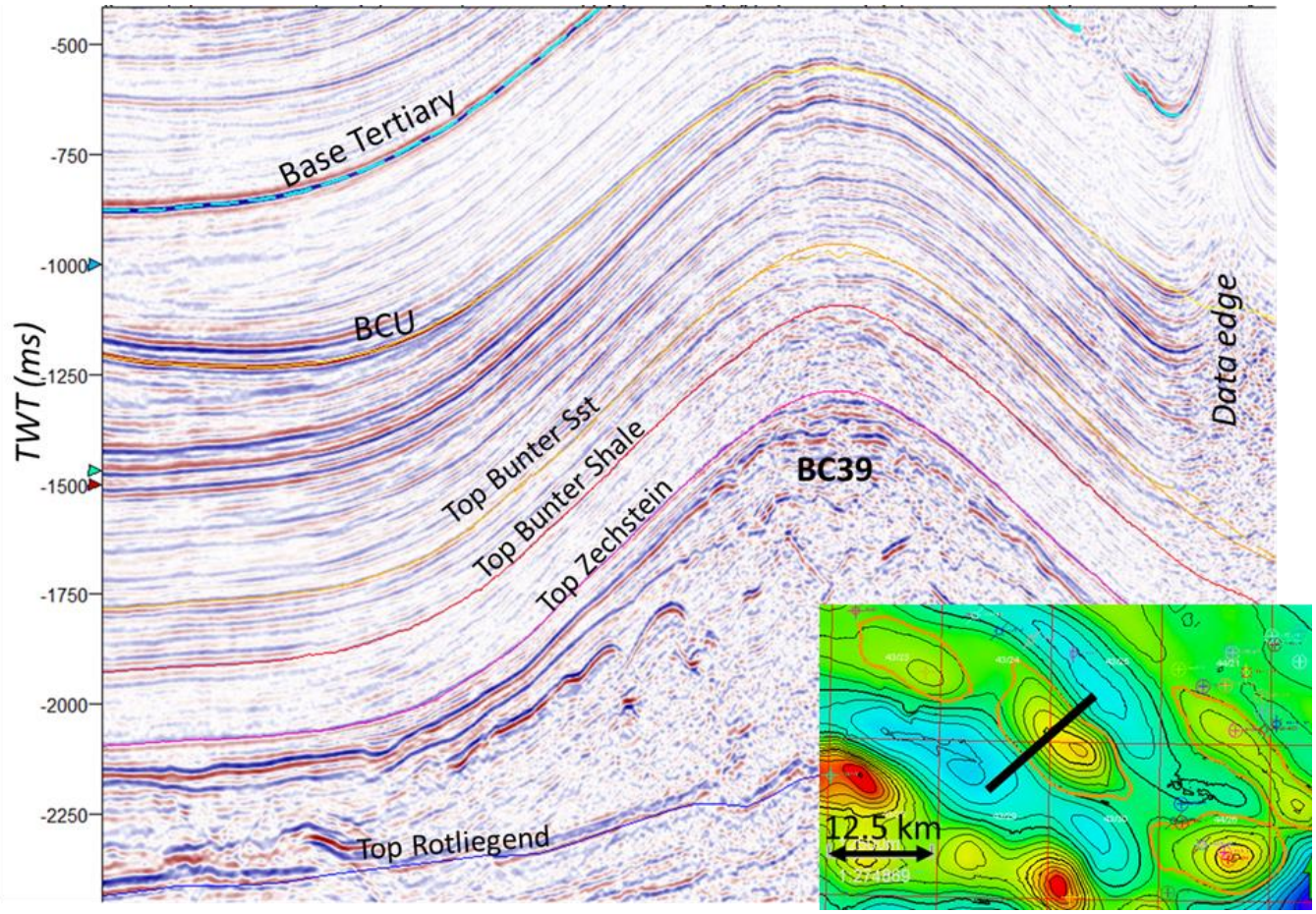

Figure 59 - SW-NE seismic line through BC39.

8.3.5 BC39 Fault Interpretation

Due to the lack of full seismic coverage and the merge of two seismic surveys, plus strong acquisition footprint in the data, faulting interpretation from attributes is not particularly usable (**Figure 60**). We can see hints of faulting on the seismic in section view (**Figure 59**) at the crest of the structure but they don't appear to create significant offset and it is difficult to evaluate if they are real. The upper Triassic level faulting is not significant, so it is unlikely that there are faults large enough to offset the seal package. Better quality seismic data is required to make a full evaluation.

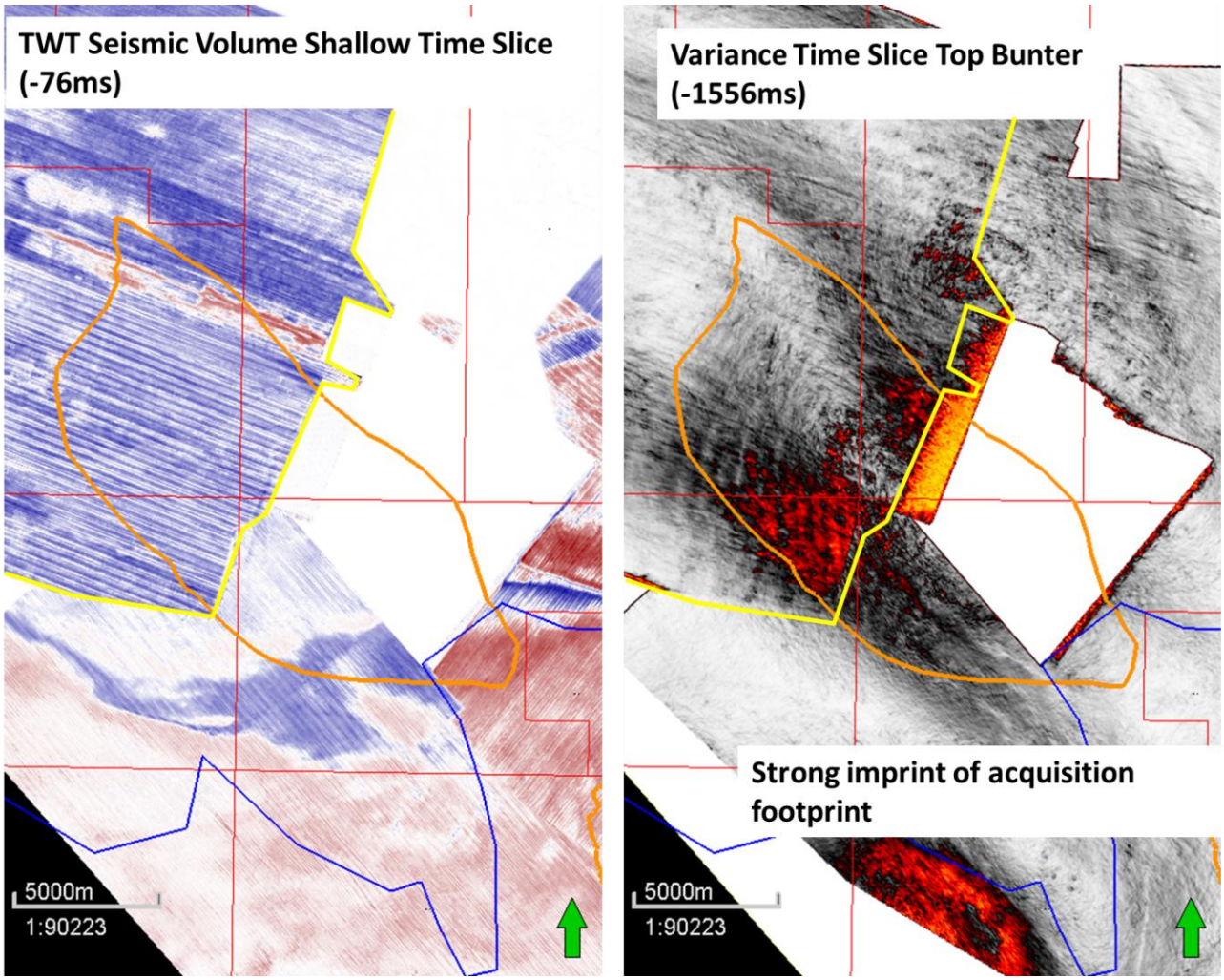

Figure 60 - Comparison of acquisition orientation and variance extraction at Top Bunter Sandstone over BC39.

8.3.6 BC39 Depth Conversion

The regional depth model was used for both BC39 and BC40 structures, with well adjustment provided by offset wells. As there is no well in the BC39 structure the depth of the crest has higher uncertainty. The average adjustment applied to correct the velocity model to the well tops was 32m. The wells included in the adjustment are shown in **Figure 61**.

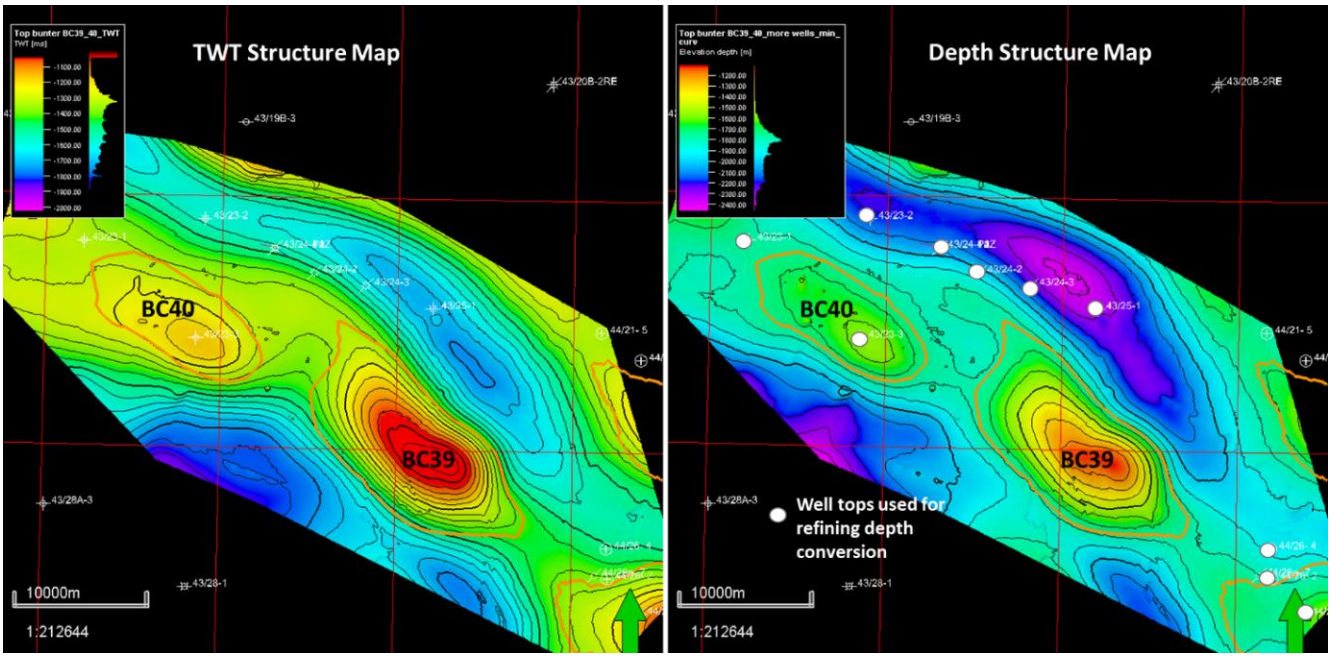

Figure 61 - Time and Depth Top Bunter Sandstone Fm structure maps. Wells used in the depth adjustment are shown with white circles.

8.3.7 BC39 Volumetric Calculations

The P50 volume for BC39 is 376MT CO2 (**Table 10**). If no pressure management is available this reduces to 83MT CO2. BC39 has the potential to be a store of significant size but the calculation is based upon offset data and more appraisal is required.

Table 10 - BC39 volumetric calculations.

	Min	P90	P50	P10	Max
GRV [m3]	-	1.83E+10	2.19E+10	2.61E+10	-
Net-to-Gross	0.45	0.63	0.77	0.85	0.9
Porosity	0.15	0.173	0.203	0.26	0.27
Reservoir thickness [m]	215	222	238	264	300
Spill point depth [m]	1707	1743	1787	1831	1867
Crestal depth [m]	1025	1070	1125	1180	1225
Column height [m]	321	510	676	808	900
Storage efficiency with pressure management	0.05	0.1	0.16	0.23	0.3
Storage efficiency no brine production	0.005	0.02	0.04	0.07	0.1
VOLUME CO2 WITH PRESSURE MANAGEMENT					
CO2 [MT]	-	217	376	622	-
VOLUME CO2 NO BRINE PRODUCTION					
CO2 [MT]	-	49	83	183	-

8.3.8 BC39 Risk and Uncertainty

The risk matrix for BC39 is shown in **Figure 62** and an uncertainty summary is presented in **Figure 63**. The lack of full seismic coverage and no well in structure means that we have larger uncertainties for BC39 compared to the other structures. It may be impacted by halite cementation as the structure is mostly outside of the seismic phase reversal area but the surrounding offset wells do now show this to be pervasive. In addition, the reservoir and petrophysics analysis has shown that halite cement may not inhibit permeability substantially, so it may not be a large concern. Seismic and well data is required to reduce uncertainty.

Seismic Coverage: 75% coverage with legacy 3D seismic, survey join in centre of structure
Well Coverage: No well in structure

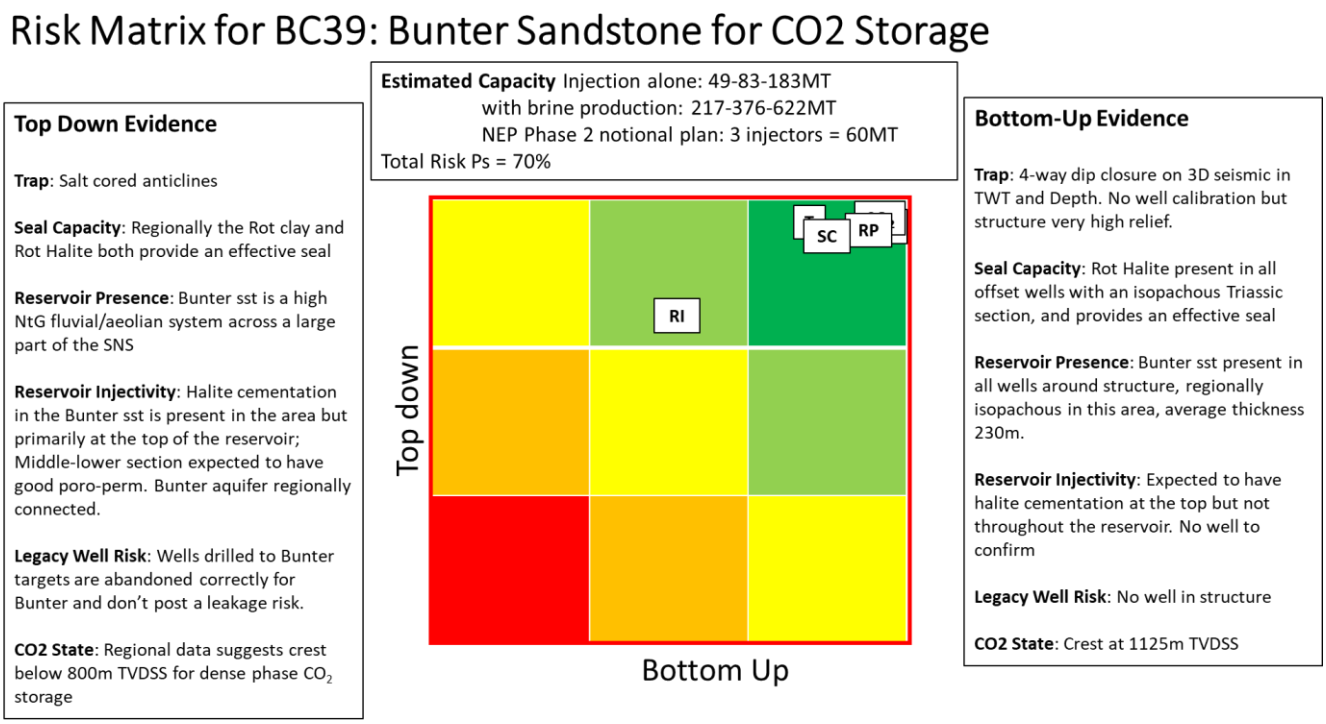

Figure 62 - BC39 risk matrix.

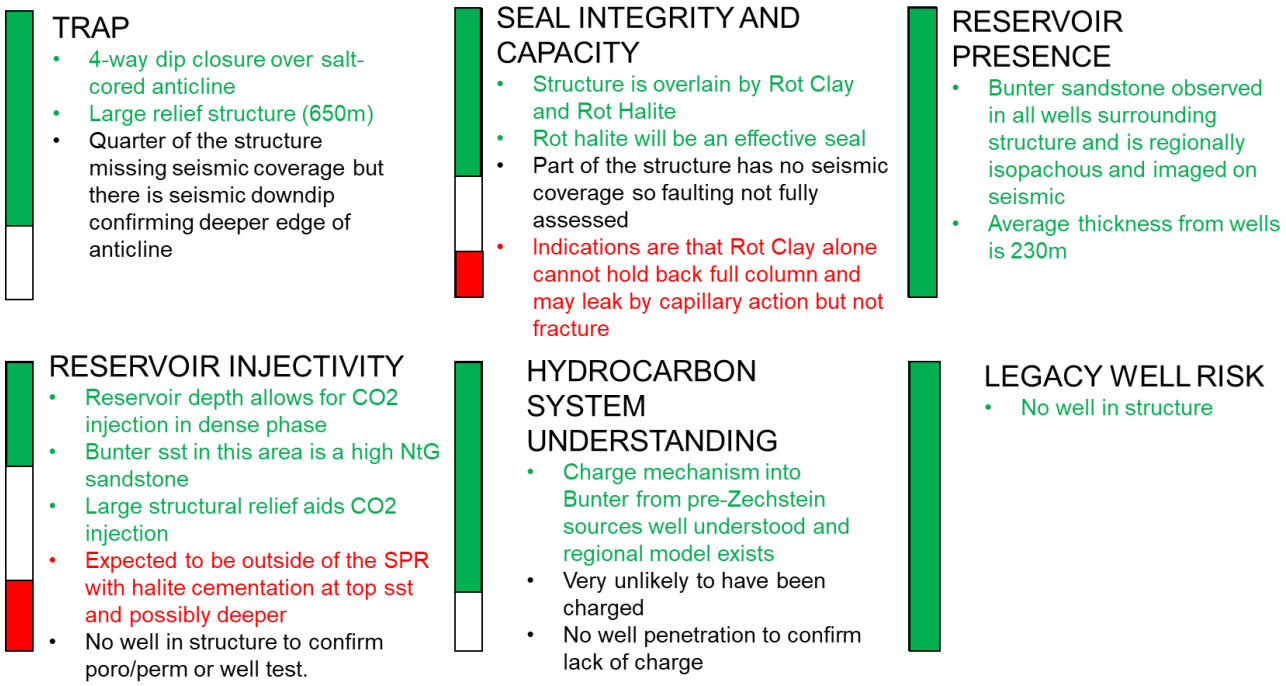

Figure 63 - BC39 uncertainty summary.

8.4 BC40

BC39 a four-way dip-closure structure that straddles blocks 43/23 and 43/24.

8.4.1 BC40 Well Penetrations

There is one well in the structure: 43/23-3 drilled by Chevron in 1994. This well targeted the Bunter Sandstone Fm and TD'd in the upper Bunter Shale Formation. It was abandoned with one laterally extensive primary barrier to isolate the Bunter Sandstone. The status of any secondary barrier is uncertain due to lack of data.

8.4.2 BC40 Reservoir Description

Well 43/23-3 shows halite cementation at the top of the Bunter Sandstone, as well as indications of halite cemented layers at deeper levels within the reservoir (**Figure 64**). Halite cementation appears to dramatically reduce porosity where it is present within the reservoir but the impact on permeability is not expected to be as strong. Both the 43/23-3 and 43/23-1 (**Error! Reference source not found.**) wells lie outside the seismically defined phase reversal p olygon where we anticipate greater halite cement. However, the impact on these two wells is variable with 43/23-3 showing average porosity of 21% and a net-to-gross of around 85%, while 43/23-1 lying further downdip of the structure shows poorer reservoir properties with an average of 17% porosity and a net-to-gross of 74%.

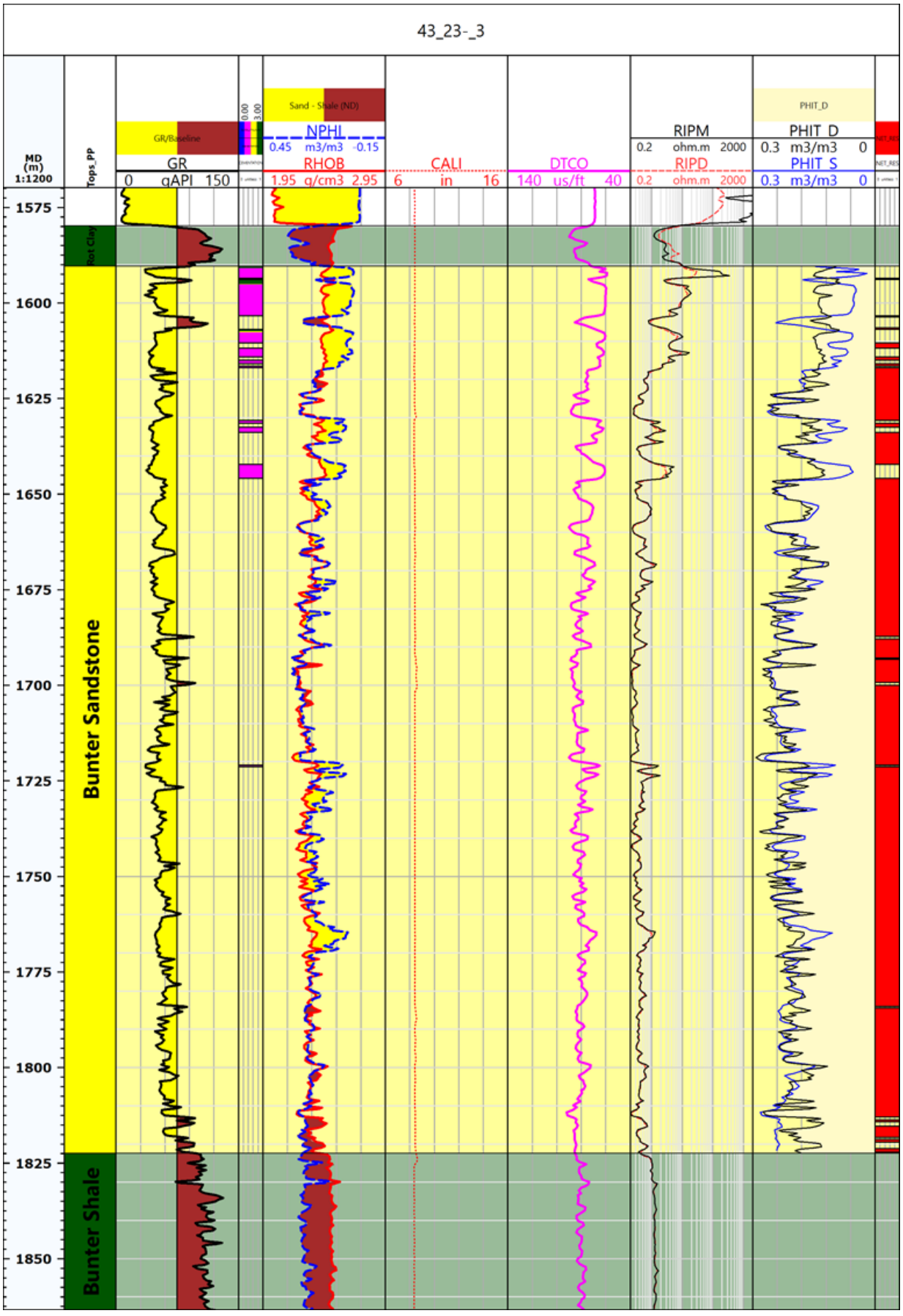

Figure 64 – Well 43/23-3 in the crest of BC40. Halite is shown by the pink flag in the column next to Gamma Ray (GR). Net pay flag is in red on the far right.

8.4.3 BC40 Seal Description

The seal package at BC40 is similar to the Endurance structure. The Base Cretaceous Unconformity (BCU) cuts down into the mid Jurassic section, leaving the lowermost Jurassic and the full Triassic sequence in place. The Röt Clay and Röt Halite primary seals are 10m and 73m thick, respectively (**Figure 65**).

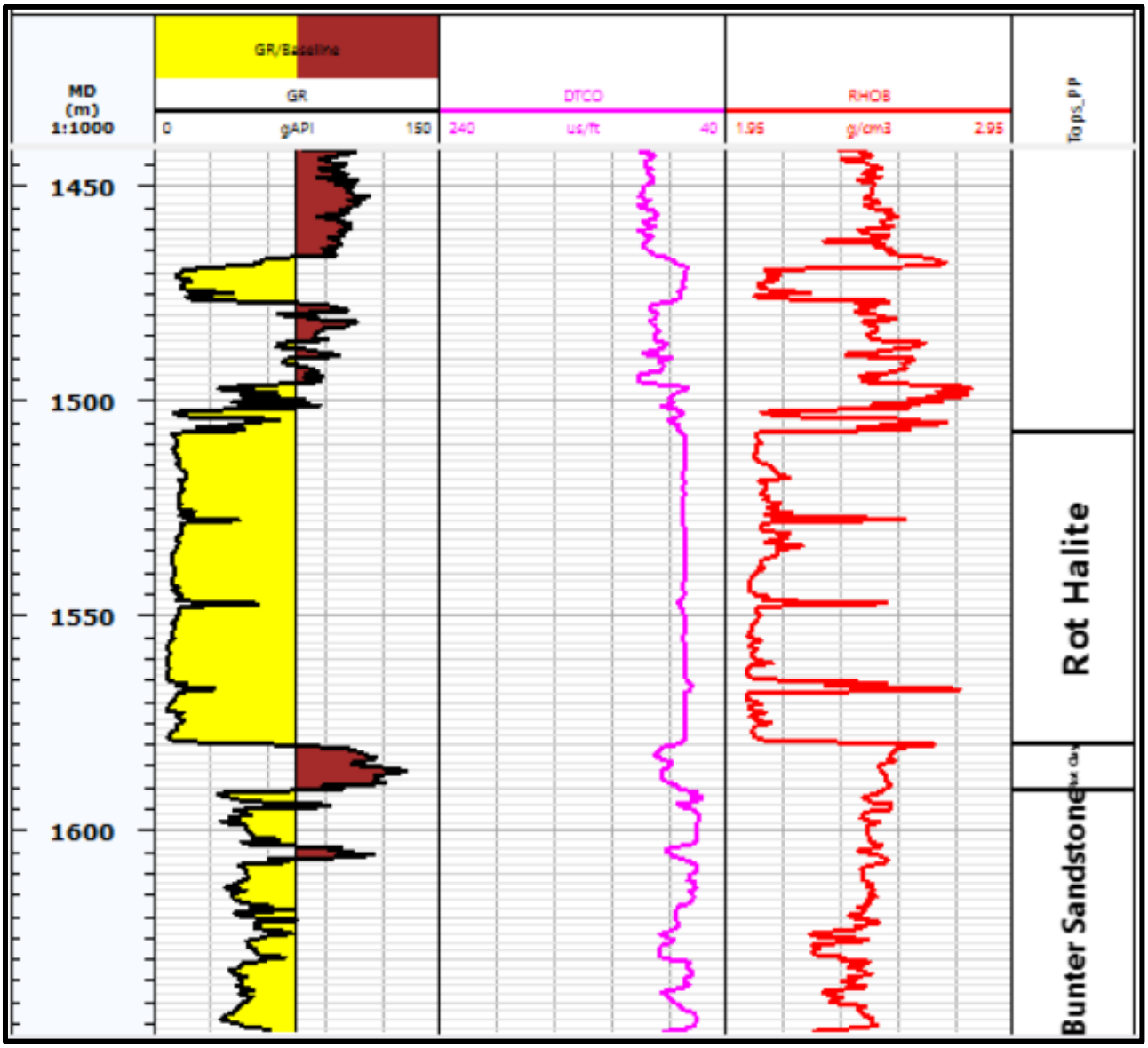

Figure 65- BC40 Seal package at 43/23-3. The Röt Halite is 73m thick.

8.4.4 BC40 Horizon Interpretation

Seismic horizon interpretation at BC40 was tied to the interpretation at Endurance and calibrated with the 43/23-3 well at the crest of the structure (**Figure 66** and Figure 67). The structure is outside the seismic phase reversal (SPR) and the top Bunter Sandstone is interpreted as a peak. The base of the reservoir (top Bunter Shale) was interpreted with moderate confidence.

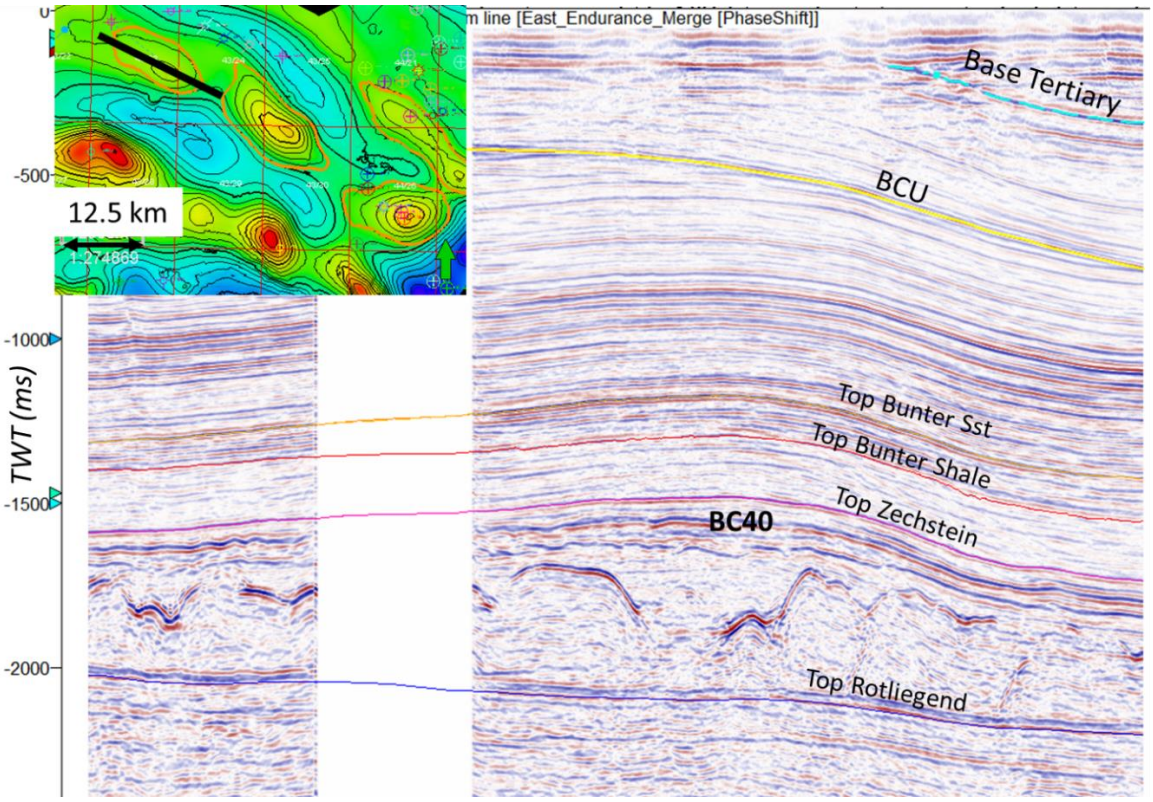

Figure 66 - NW-SE seismic line through BC40 structure.

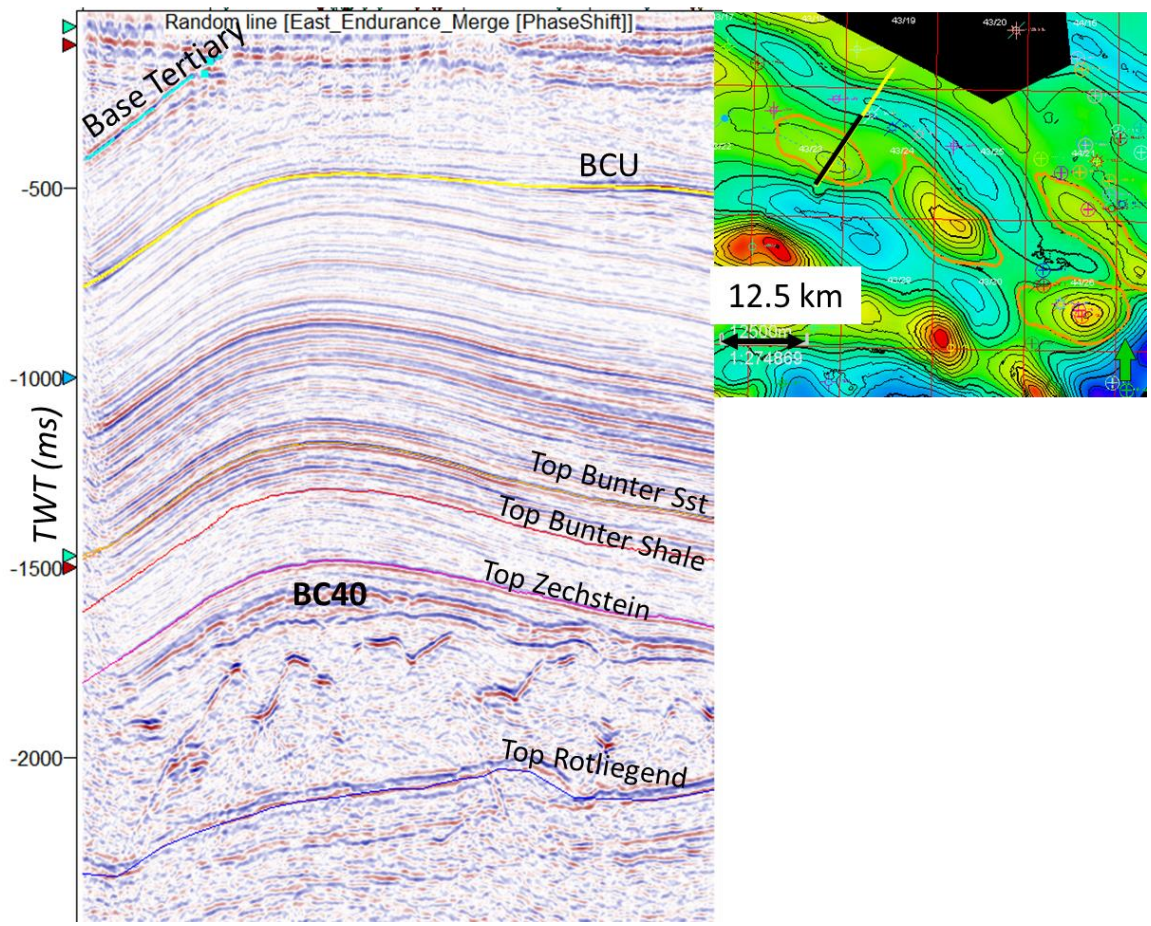

Figure 67 - SW-NE seismic line through BC40 structure.

8.4.5 BC40 Fault Interpretation

The gentle dips of the BC40 structure have created very little faulting. No strong indications of faulting at the top Bunter Sandstone are present (**Figure 68**) and there is also very little overburden faulting. There is a small gap in the seismic coverage of BC40 but given the nature of the imaged structure faulting is not believed to be a risk. The only linear feature on the variance appears to be seismic survey acquisition related.

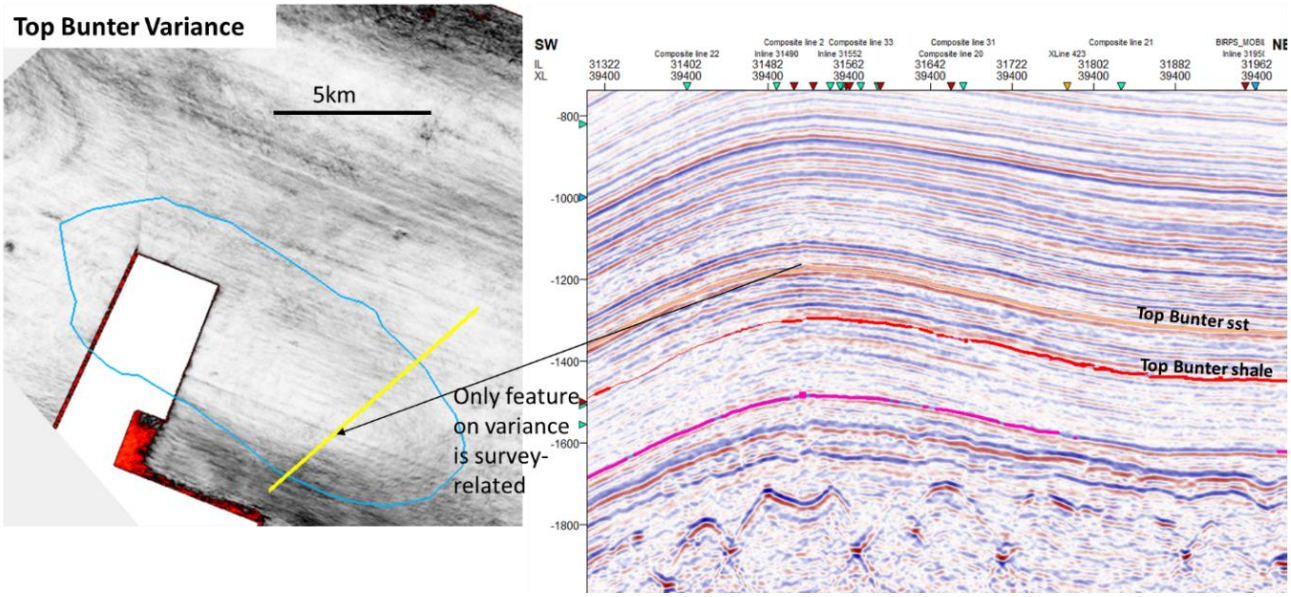

Figure 68 - BC40 variance attribute (left) at Top Bunter Sandstone.

8.4.6 BC40 Depth Conversion

The regional depth model was used for both BC40 and BC39 structures, with well adjustment provided by offset wells. The average adjustment applied to correct the velocity model to the well tops was 32m. The wells included in the adjustment are shown in **Figure 61**.

8.4.7 BC40 Volumetric Calculations

The structural closure for BC40 is estimated to be about 220m, which is quite low and may reduce the storage efficiency factor further, pushing the range lower than the stated P50 here. There is no data available to accurately assess the impact of shallow versus tall structures, so the range has been kept the same for all evaluations. It is estimated that the structure could hold in the order of 90MT CO2 with brine production, and 25MT CO2 without brine production (**Table 11**).

Table 11 - BC40 volumetric calculations.

	Min	P90	P50	P10	Max
GRV [m3]	-	3.30E+09	5.50E+09	8.00E+09	-
Net-to-Gross	0.45	0.63	0.77	0.85	0.9
Porosity	0.15	0.172	0.2	0.23	0.25
Reservoir thickness [m]	215	222	234	252	275
Spill point depth [m]	1690	1721	1760	1799	1830
Crestal depth [m]	1540	1549	1560	1571	1580
Storage efficiency with pressure management	0.05	0.1	0.16	0.23	0.3
Storage efficiency no brine production	0.005	0.02	0.04	0.07	0.1
VOLUME CO2 WITH PRESSURE MANAGEMENT					
CO2 [MT]	-	43	93	168	-
VOLUME CO2 NO BRINE PRODUCTION					
CO2 [MT]	-	10	25	49	-

8.4.8 BC40 Risk and Uncertainty

The risk matrix for BC40 is shown in **Figure 69** and an uncertainty summary is presented in **Figure 70Figure 63**. The main risk at BC40 is reservoir injectivity. The capacity of the structure is small and the low structural relief combined with the possibility that the halite cementation creates baffling in some parts of the reservoir (especially towards the top where the halite is concentrated) means that it may be difficult to utilise the full structure.

Seismic Coverage: 85% coverage with legacy 3D seismic
Well Coverage: 1 well in crest of structure

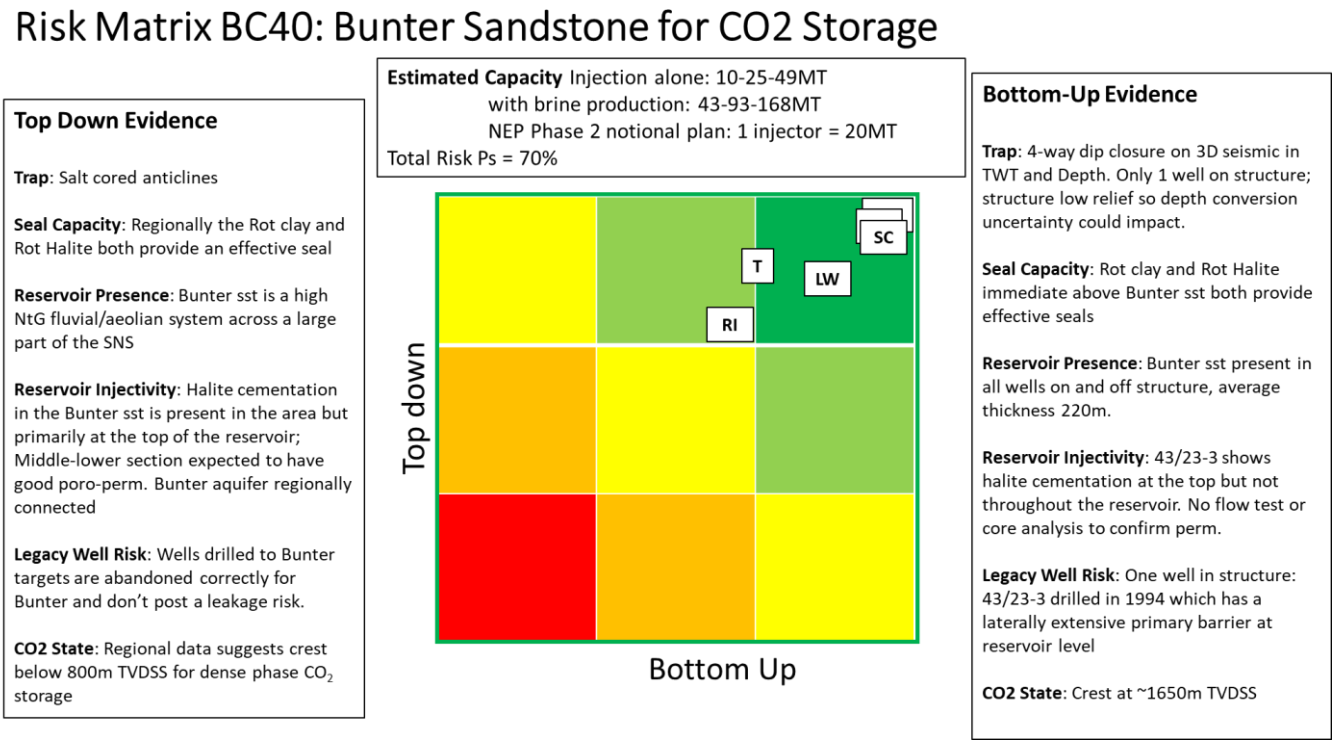

Figure 69 - BC40 risk matrix.

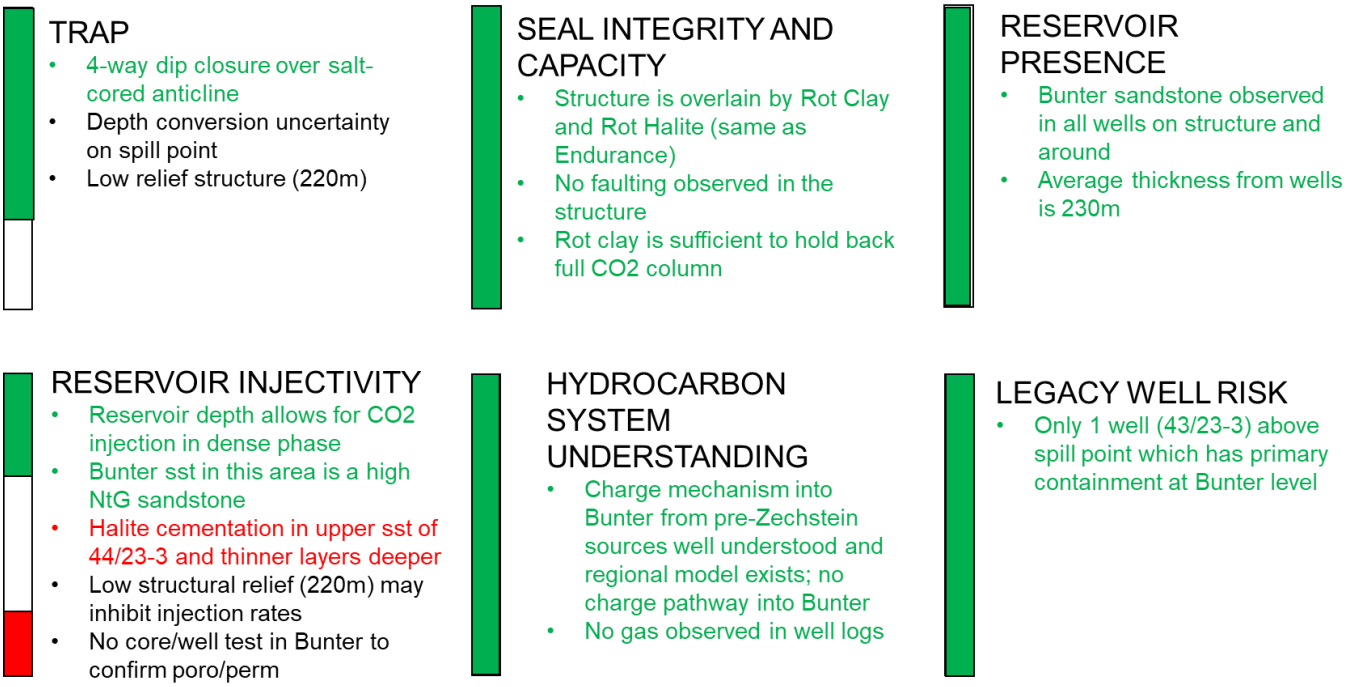

Figure 70 - BC40 uncertainty summary.

8.5 BC3

BC3 lies above the Viking (Viking A, Viking B, Viking E) and Victoria Permian gas fields in Quadrant 49. As such there are multiple development locations and legacy wells across the area. This structure was not the main focus of this study, but is included for completeness, albeit not to the same level of detail of the BC structures closer to Endurance. Primarily this was because it is too far from Endurance to be a satellite but is not large enough to be a standalone store (its estimated capacity is around half of Endurance). It has many legacy wells penetrating the structure, which will need more detailed assessment.

8.5.1 BC3 Well Penetrations

Status of Bunter Sandstone containment in wells on the BC3 Structure (**Figure 71**):

- South
    - 49/17-B5 (edge): Unknown
    - 49/17-1 (1963 wildcat to Permian): Good
    - 49/17-15 (2008 exp to Leman): Good
    - 49/17-7: Unknown
    - 49/17-C3 dev wells: Unknown
- Saddle
    - 49/17-14: Good
- North
    - 49/17-6 (edge): Good
    - 49/17-L2 dev wells: Good
    - 49/17-4: Poor
    - 49/12a- dev wells: Good

Further investigation is needed into the wells in the south. It appears that at least one well in the northern area is likely to have poor isolation.

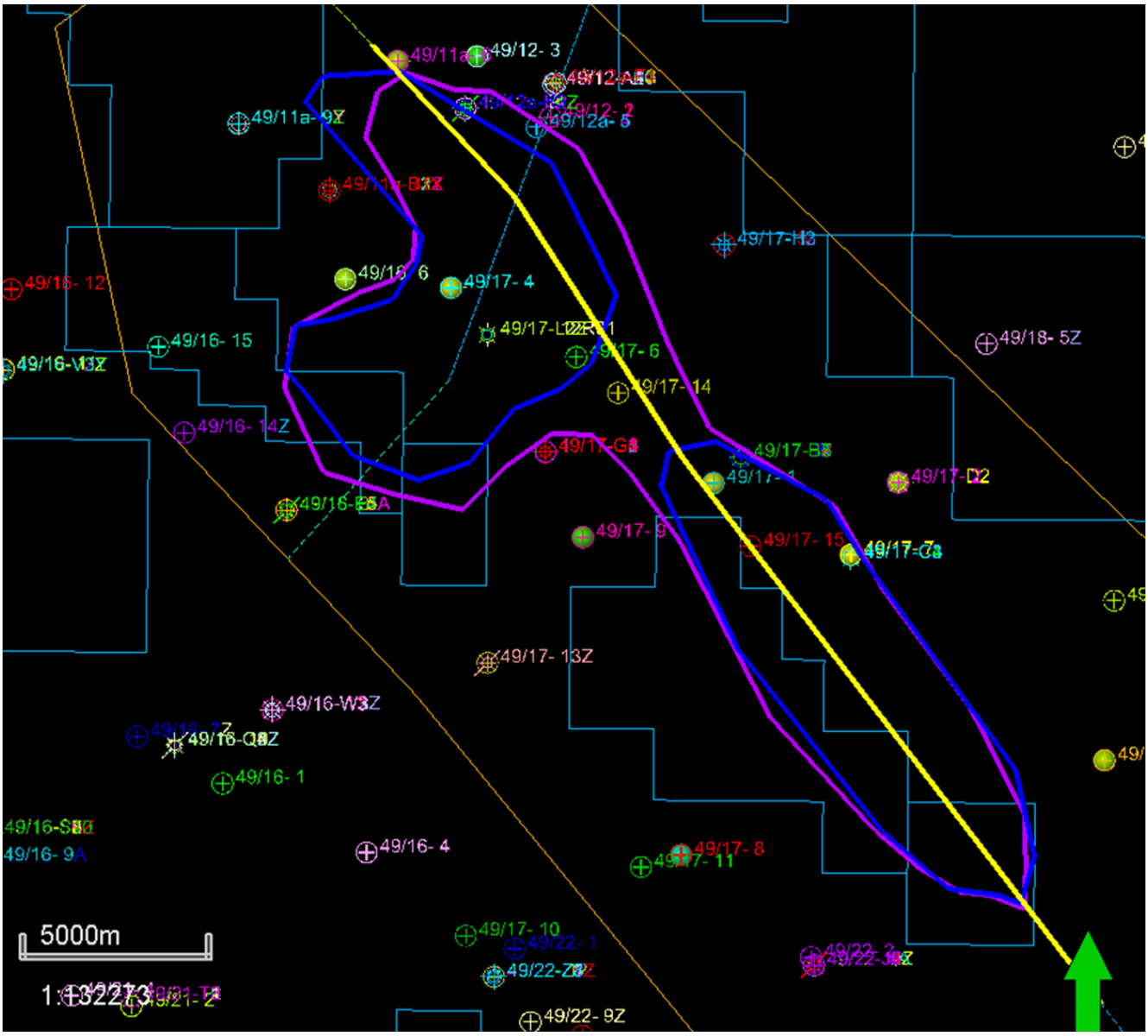

Figure 71 - Legacy wells around the BC3 structure.

8.5.2 BC3 Reservoir Description

A typical Bunter Sandstone description is shown in **Figure 72** and the some of the variability is shown in **Figure 73**.

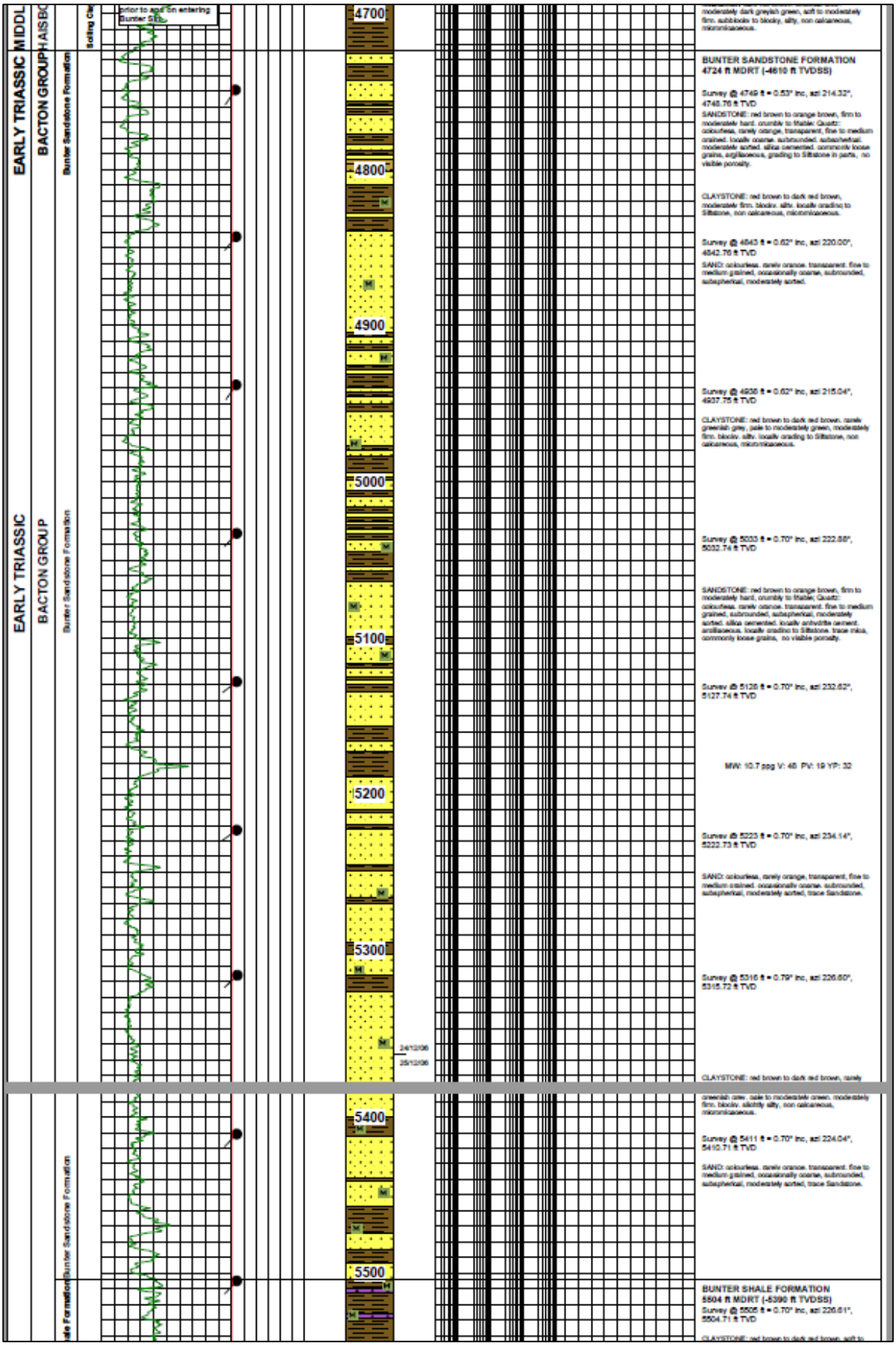
EARLY TRIASSIC
BACTON GROUP
Bunter Sandstone Formation
4700
4800
4900
5000
5100
5200
5300
5400
5500
BUNTER SANDSTONE FORMATION
4724 ft MDRT (-4610 ft TVDSS)
BUNTER SHALE FORMATION
5504 ft MDRT (-5390 ft TVDSS)
MW: 10.7 ppg V: 48 PV: 19 YP: 32

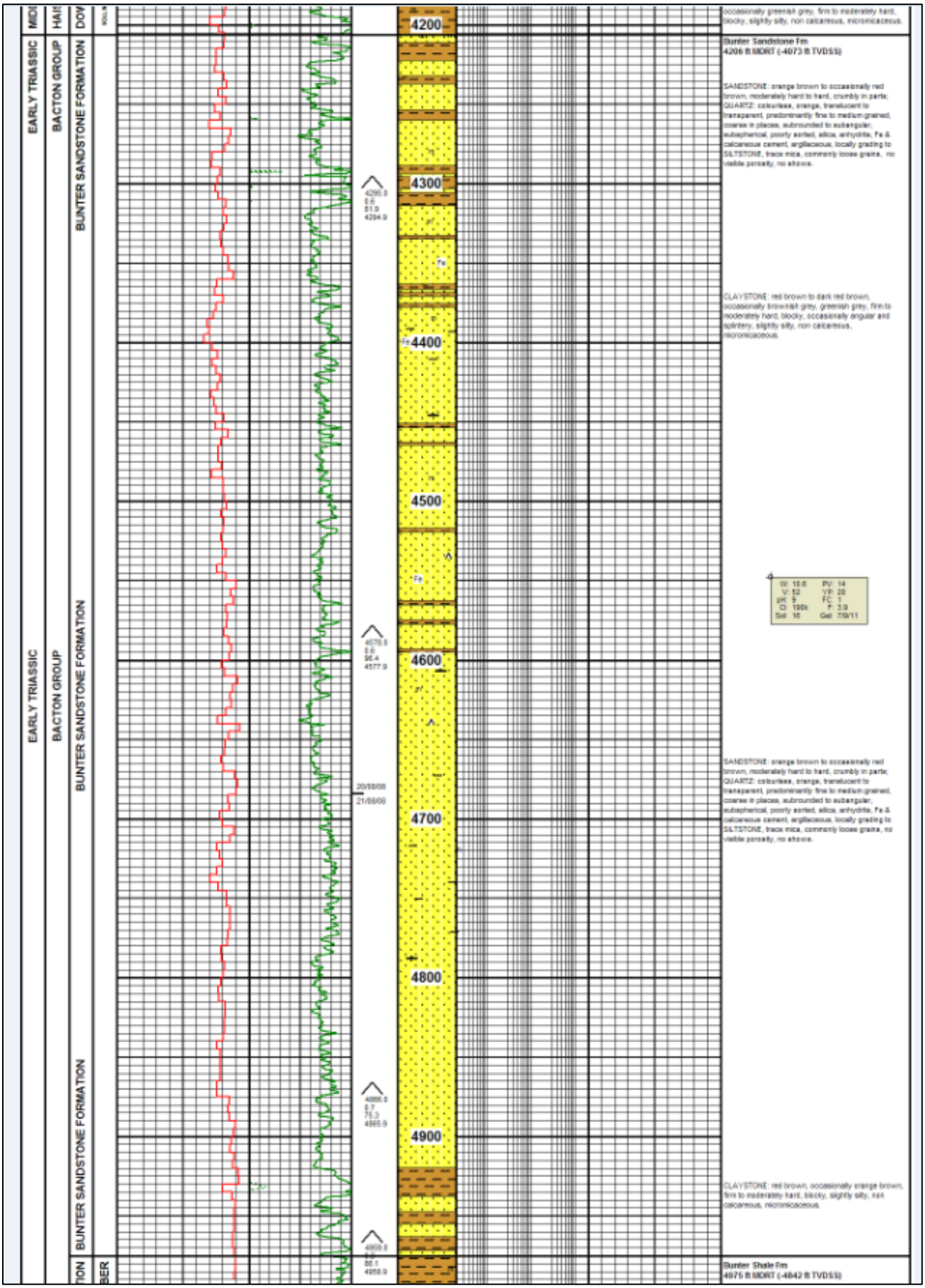

Figure 72 - Reservoir composite log for well 49/17-15, showing 234m of Bunter Sandstone Fm with higher proportions of claystone at the top and base of the unit.

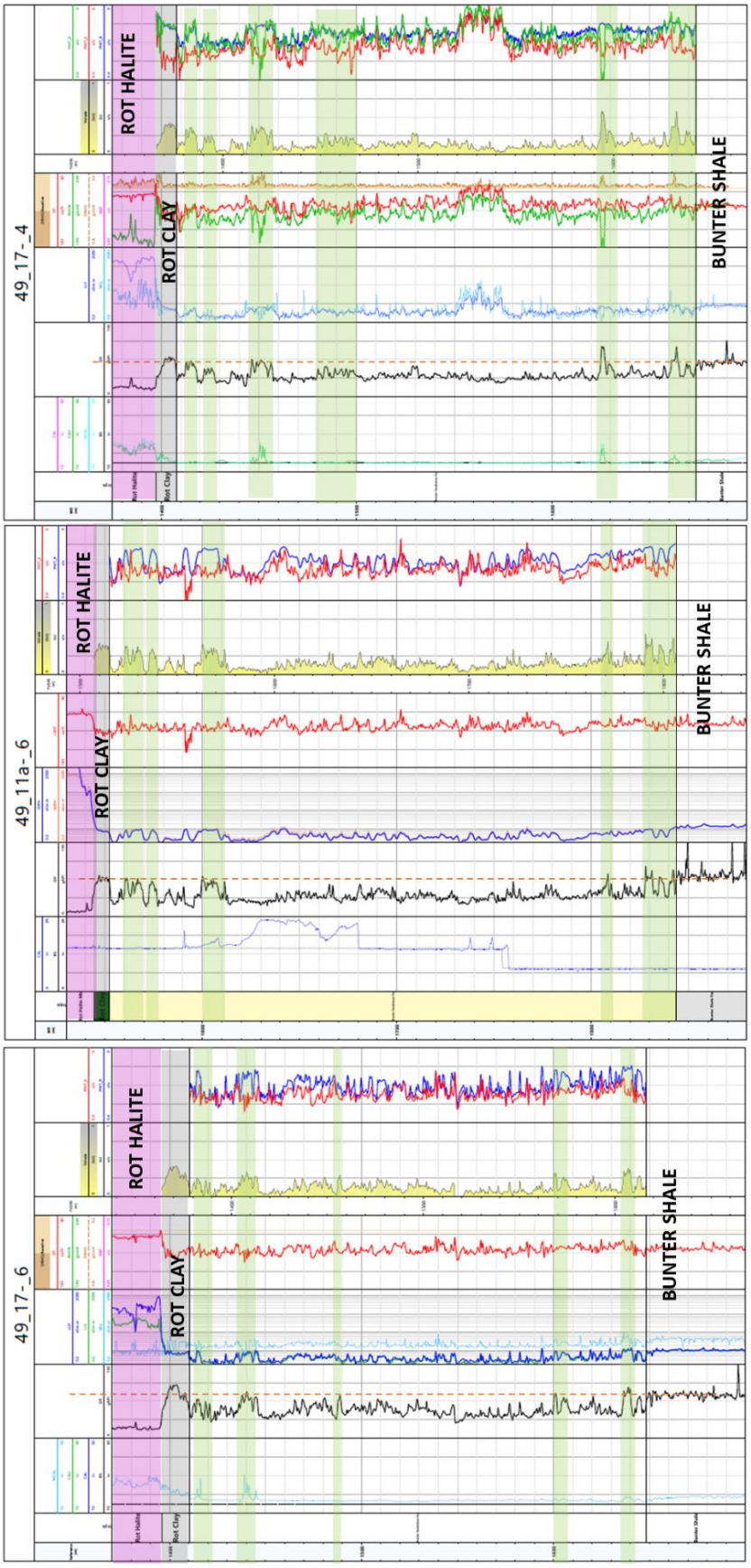

Figure 73 - BC3 wells: 49/17-6, 49/11a-6 and 49/17-4. Potential shales in the reservoir section are highlighted in green. There is variation across the area in the amount of shale in the middle Bunter Sandstone.

8.5.3 BC3 Seal Description

Typical Röt Clay and Röt Halite descriptions are shown in **Figure 74** and **Figure 75**.

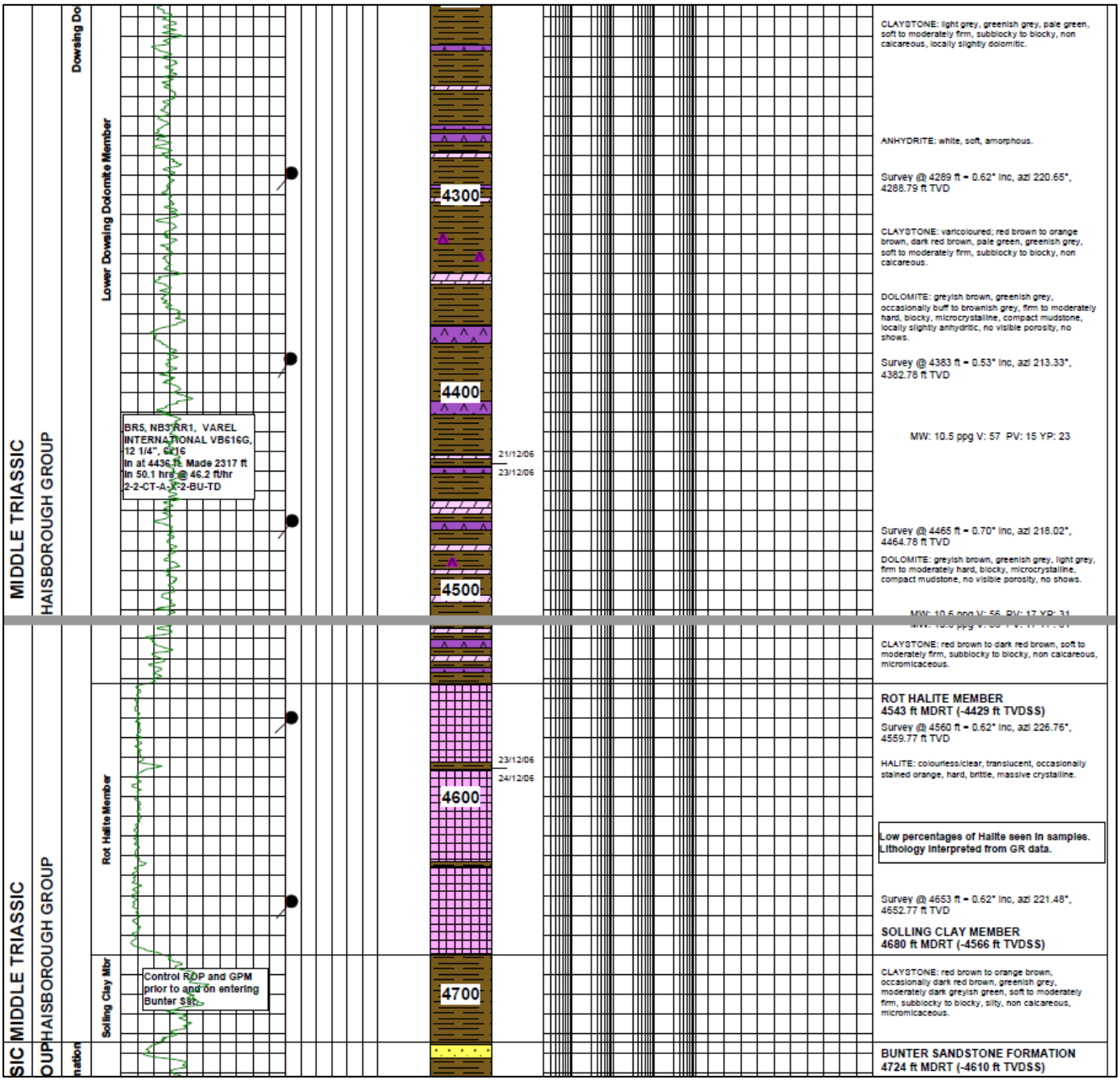

Figure 74 - Seal package at well 49/17-14.

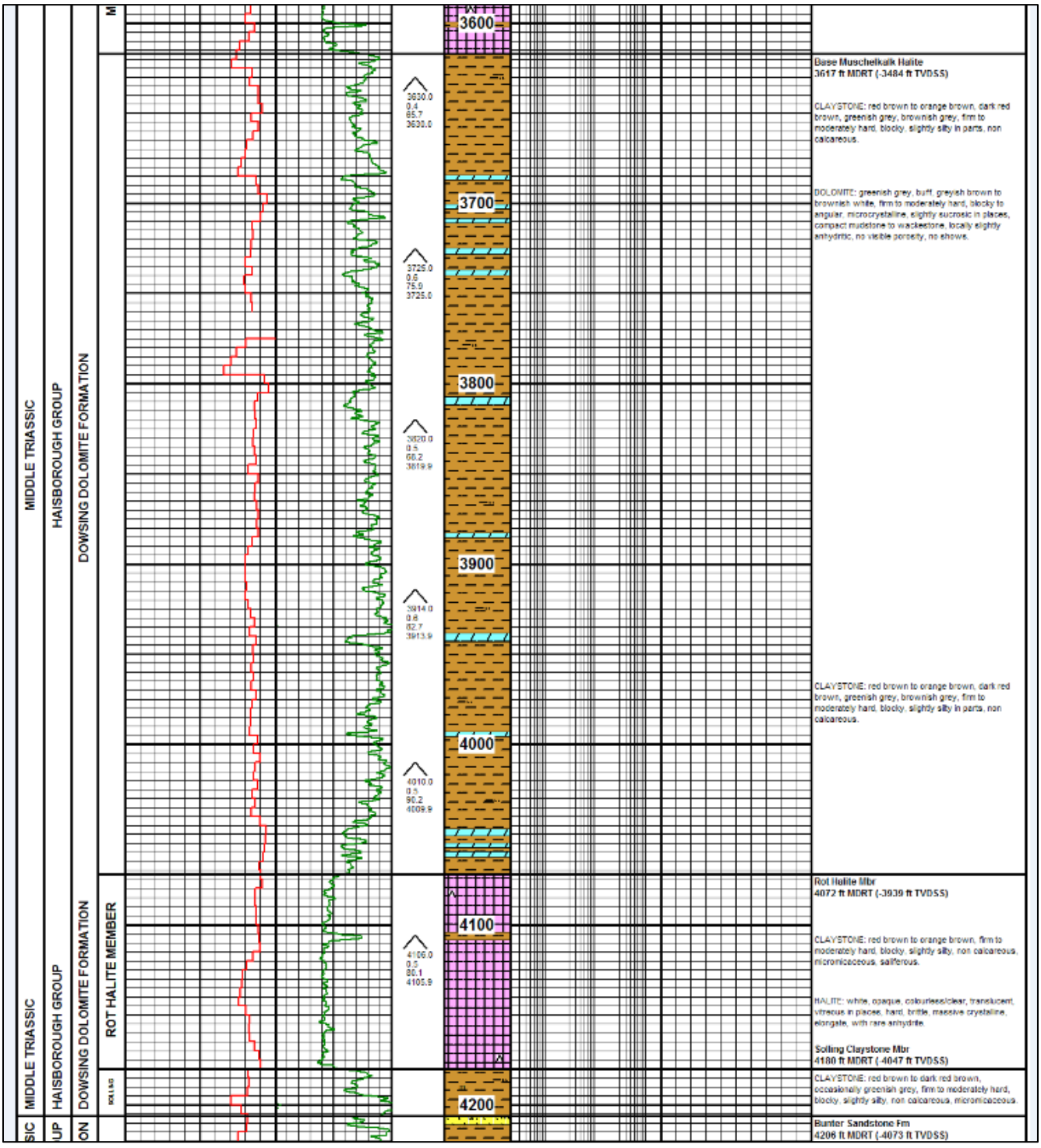

Figure 75 - Seal at well 49/17-15. The Röt Clay, Röt Halite and Dowsing formations are all present.

8.5.4 BC3 Horizon Interpretation

The top of the Bunter Sandstone was interpreted across the BC3 structure. The top of the Bunter Shale is not clearly imaged on seismic and reservoir thicknesses from wells were used instead in volumetric calculations.

8.5.5 BC3 Fault Interpretation

There is clear faulting at the crest of the southern bump of the BC3 structure. The faults appear to have maximum throw around top Bunter Sandstone and this throw decreases shallower into the overlying Triassic. The throw observed in **Figure 76** may be enough to offset the Röt Halite seal.

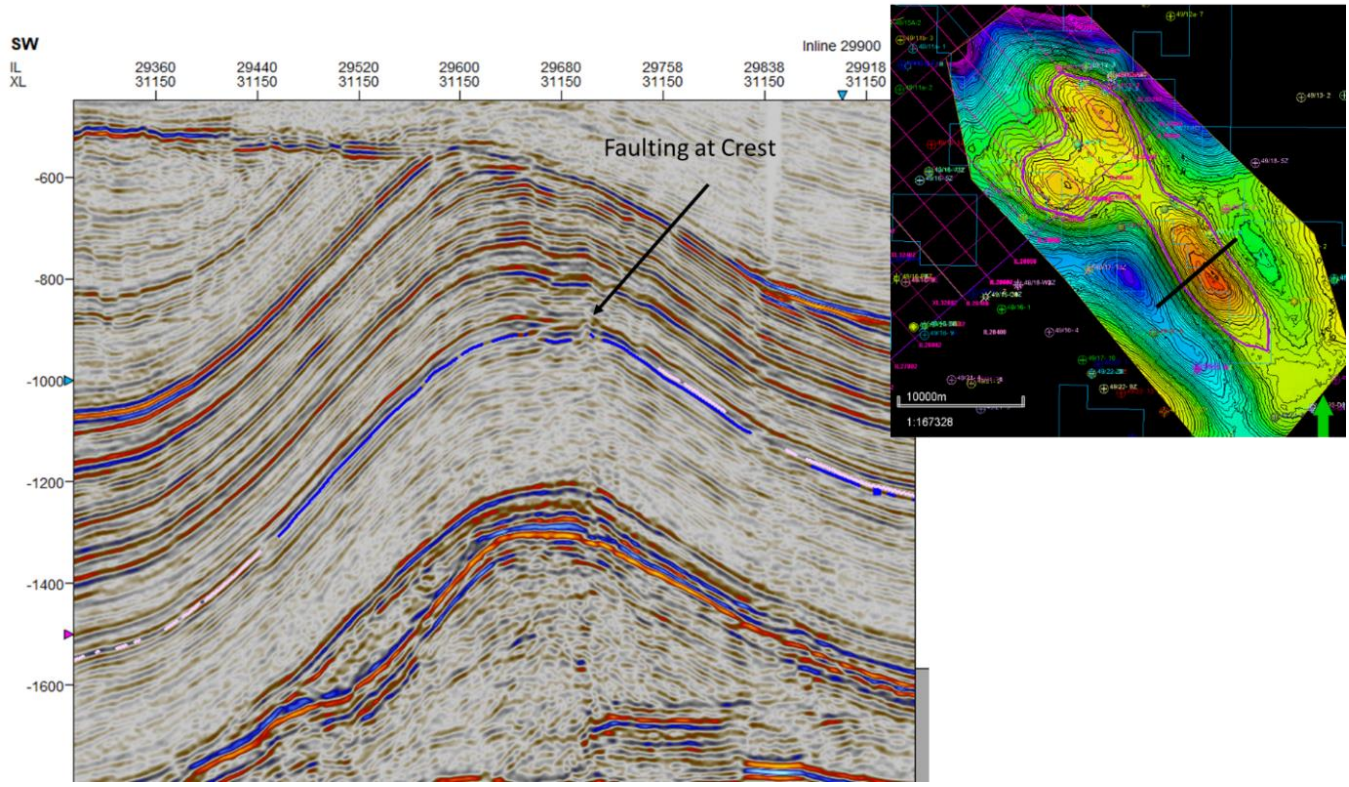

Figure 76 – Seismic line across the southern crest of BC3, showing faulting in the crest of the structure.

8.5.6 BC3 Depth Conversion

The Bunter Sandstone structure at BC3 is a combination of two structures which may be joined, but there is some uncertainty in the depth conversion (**Figure 77**). The regional velocity model is not tied to many wells in this area, so a well adjustment was applied. The wells used for the adjustment are shown in **Figure 78**. There is quite a large uncertainty about the connection between the two structural crests.

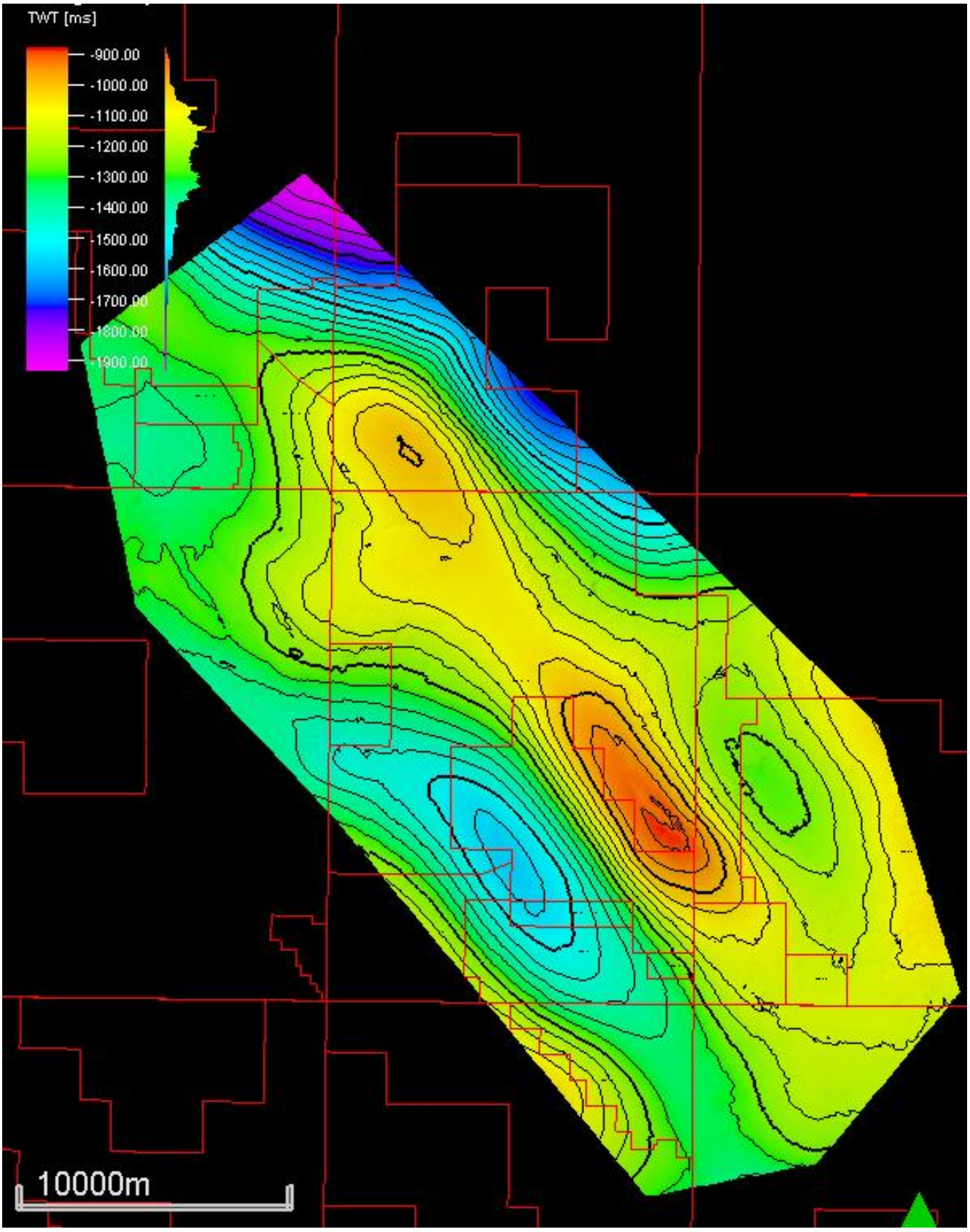

Figure 77 - BC3 Top Bunter Sandstone TWT Structure.

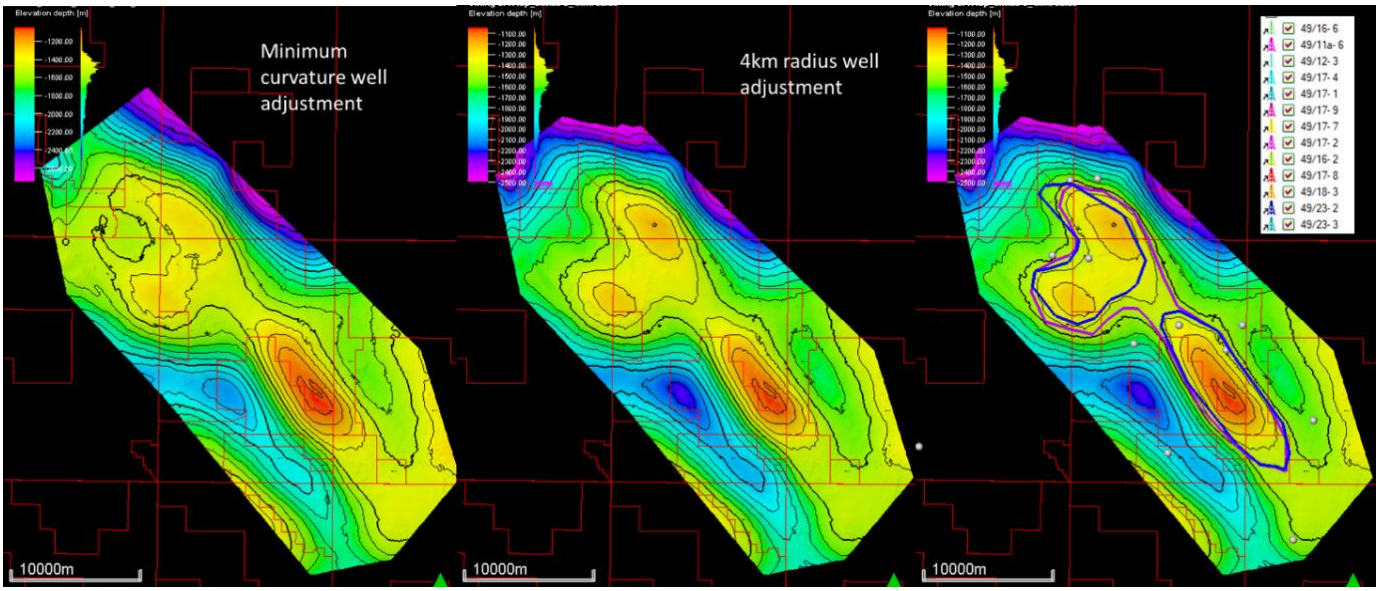

Figure 78 - Depth converted BC3. Left hand map after minimum curvature adjustment, middle after 4km radius adjustment. The right-hand map shows the location of the wells used to adjust and the spill points of the two methods. The minimum curvature result is the blue spill point, where the structure is split into two. In the 4km radius option the two crests are joined in the saddle.

8.5.7 BC3 Volumetric Calculations

The volumetric calculation is using the structure from the 4km radius well adjustment depth surface. However, to make the range realistic the spill point was reduced to be the mean between the two depth conversion methods (min: 1350m, mean: 1450m, max: 1500m). The P50 volume is calculated to be 218MT CO2; without pressure management this could reduce to 59MT CO2 (**Table 12**). To reduce uncertainty on these numbers a new velocity model needs to be built with all the available well data and updated seismic surfaces.

Table 12 - BC3 volumetric calculations.

	Min	P90	P50	P10	Max
GRV [m3]	1.25E+10				
Net-to-Gross	0.7	0.75	0.8	0.86	0.9
Porosity	0.16	0.18	0.2	0.22	0.24
Reservoir thickness [m]	200	209	221	235	250
Spill point depth [m]	1350	1389	1437	1473	1500
Crestal depth [m]	1000	1022	1050	1078	1100
Storage efficiency with pressure management	0.1	0.12	0.15	0.18	0.2
Storage efficiency no brine production	0.02	0.03	0.04	0.05	0.06
VOLUME CO2 WITH PRESSURE MANAGEMENT					
CO2 [MT]	-	130	218	322	-
VOLUME CO2 NO BRINE PRODUCTION					
CO2 [MT]	-	35	59	89	-

8.5.8 BC3 Risk and Uncertainty

The uncertainty summary for BC3 is presented in **Figure 79Figure 63**. The southern crest has good structural relief but apparent faulting at the crest. The northern crest has lower structural relief and at least one legacy well without primary containment at Bunter Sandstone level. If these concerns are not deemed ‘show-stoppers’ to this this prospect, then a new velocity model should be constructed to assess the connection between the north and south structural crests, which will reduce the uncertainty on storage volume. The most significant risk for this area is the large number of legacy wells penetrating the structure, many of which still require further evaluation.

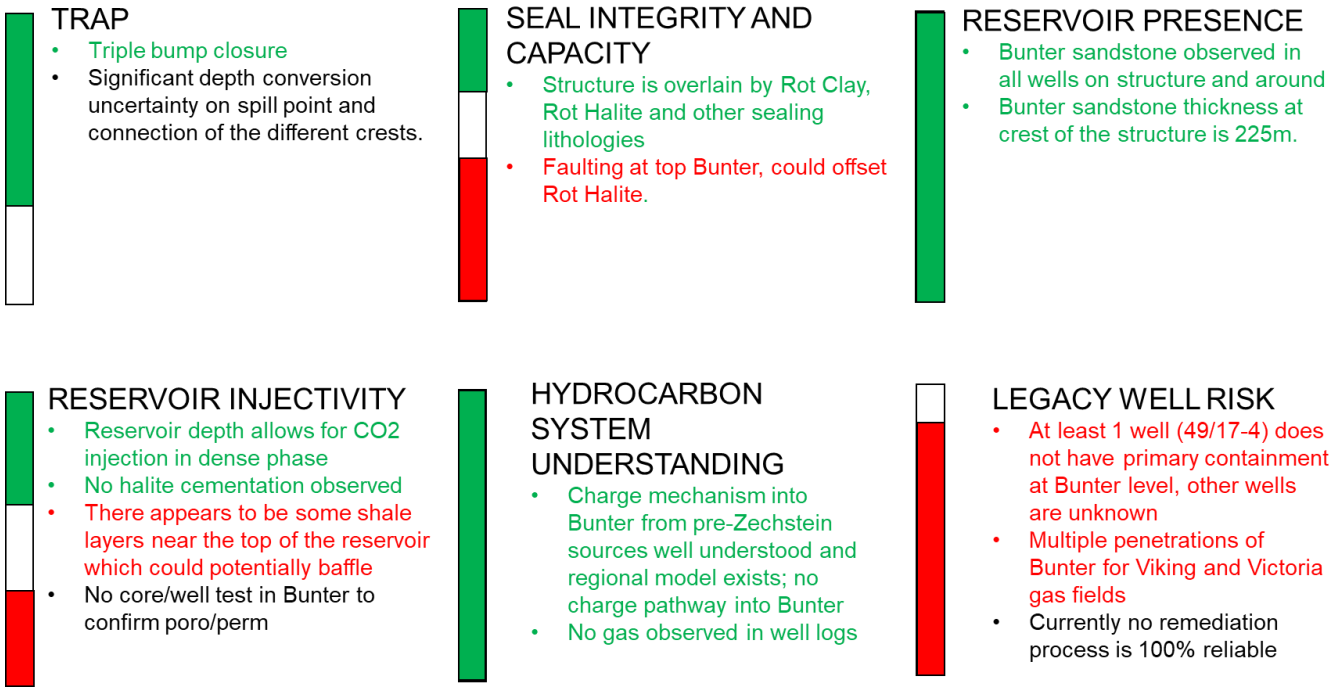

Figure 79 - BC3 uncertainty summary.

9.0 Reservoir Modelling for BC39 and BC40 Stores

Reservoir modelling efforts were carried out to evaluate the potential for the unpenetrated BC39 structure to be developed with a notional 4 MTPA subsea expansion (1 MTPA for BC40 and 3 MTPA for BC39) as shown in **Figure 80**.

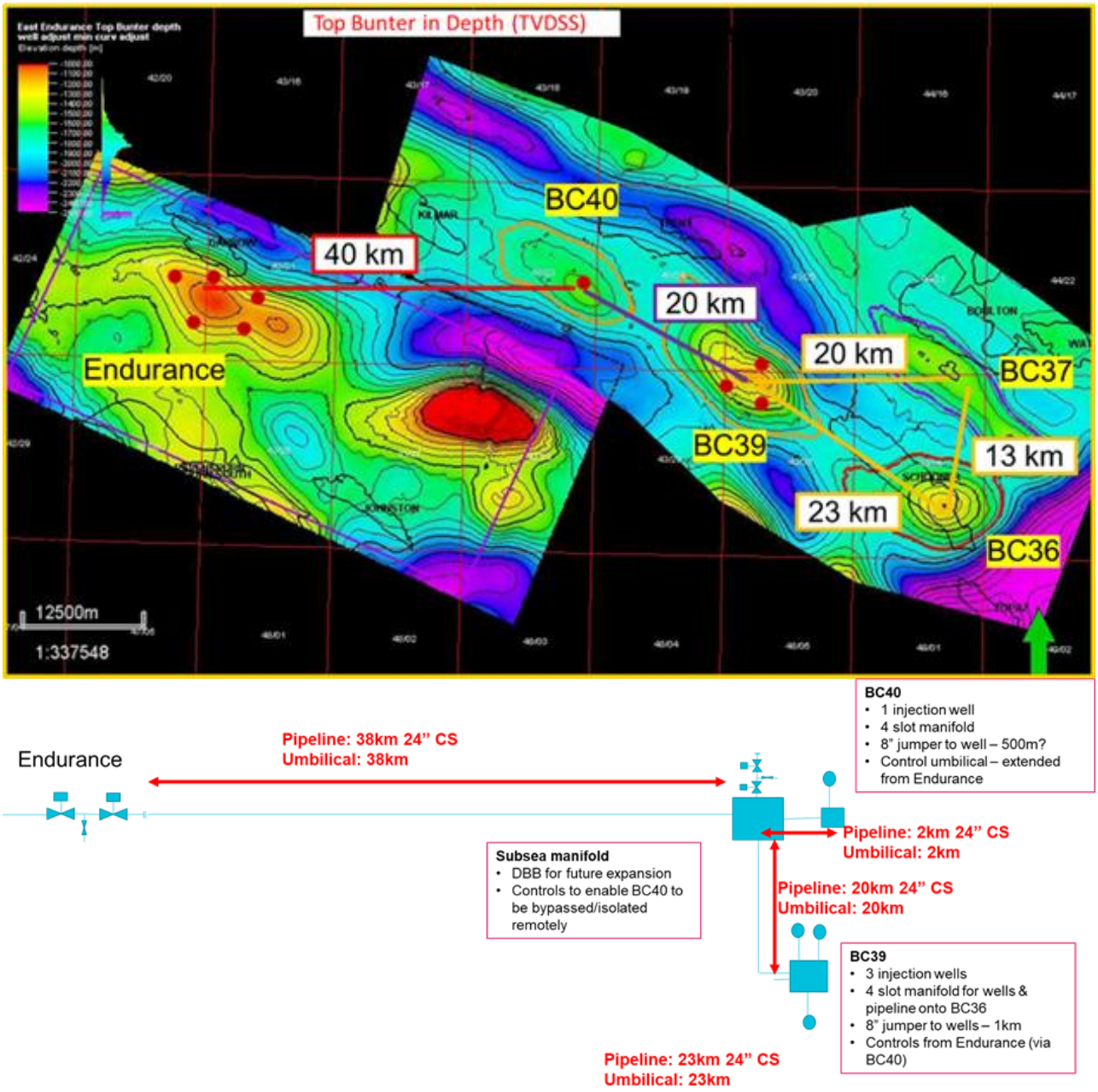

Figure 80 - Notional subsea expansion from Endurance to BC40 and BC39.

Significant uncertainties remain for the combined BC39/BC40 super structure in terms of reservoir injectivity, connectivity to the broader Bunter Sandstone aquifer, and the extent of the halite cementation over the area. A series of mechanistic full-field models were therefore built

in Petrel and Nexus to assess these uncertainties and quantify their impact on pressurisation and CO2 sweep.

9.1 Area of Interest and Gridding Scheme for the Reservoir Model

The area of interest was defined in a similar fashion as Endurance reservoir model to ensure the inclusion of sufficient volume of aquifer around the BC39 and BC40 structures as shown in **Figure 81**. Regional mapping of the top Bunter Sandstone structure was used to generate a simple grid in Petrel with constant gross thickness of 230m (230m shift was used to generate the base of the grid).

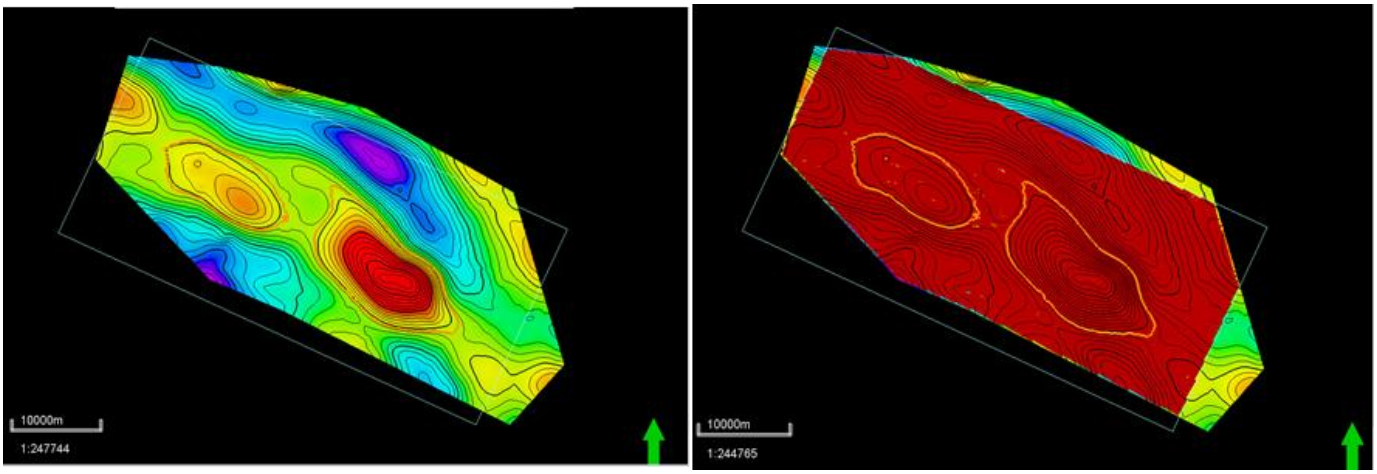

Figure 81 - Gridding AOI for the BC39/40 model.

Grid dimension is NX=252*NY=110*NZ=92 with cell size of 200m*200m*~2.5m (~1.9 million active cells) offering manageable run time. Simplistic zoning scheme has been generated to model separately the upper Bunter Sandstone (with halite cementation ~30m thick, zone 1), the upper-middle Bunter Sandstone section (~30-50m thick accounting for the transition between the upper cemented zone and the middle to lower Bunter Sandstone, zone 2), and the middle-lower Bunter Sandstone (150m to 185m thick, zone 3) as shown in **Figure 82**.

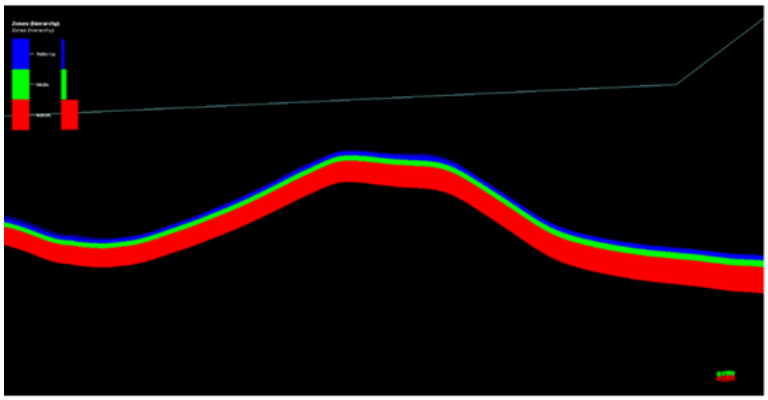

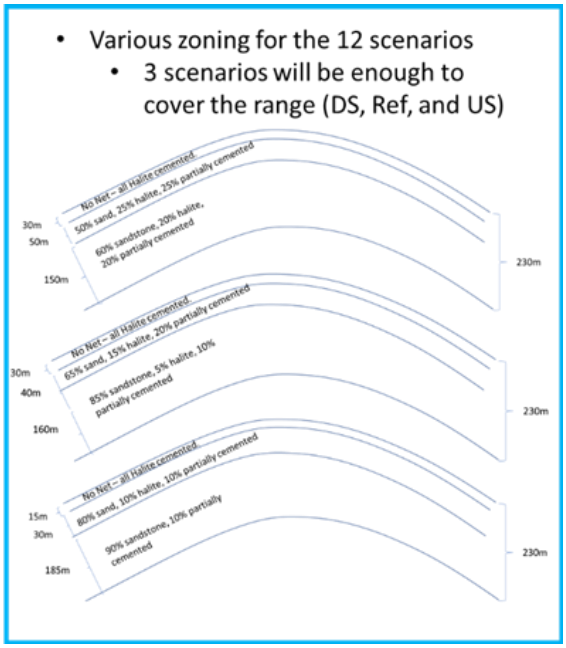

Figure 82 - Layering and zoning for the reservoir model with 92 confirmable later split into 3 zones (zone 1 in blue: halite cemented, zone 2 in green: transition, zone 3 in red: preserved Bunter section).

9.2 Facies Modelling

Three notional scenarios have been created to investigate the impact of various degree of cementation across the Bunter Sandstone (**Figure 83**). The cases do follow the zoning scheme described above with the upper 15 to 30 meters of the formation being fully cemented (non-net) overlying a transition zone (from 30 to 50 m with significant fraction of cemented or partially cemented facies) and the middle to lower Bunter Sandstone with reasonable reservoir properties.

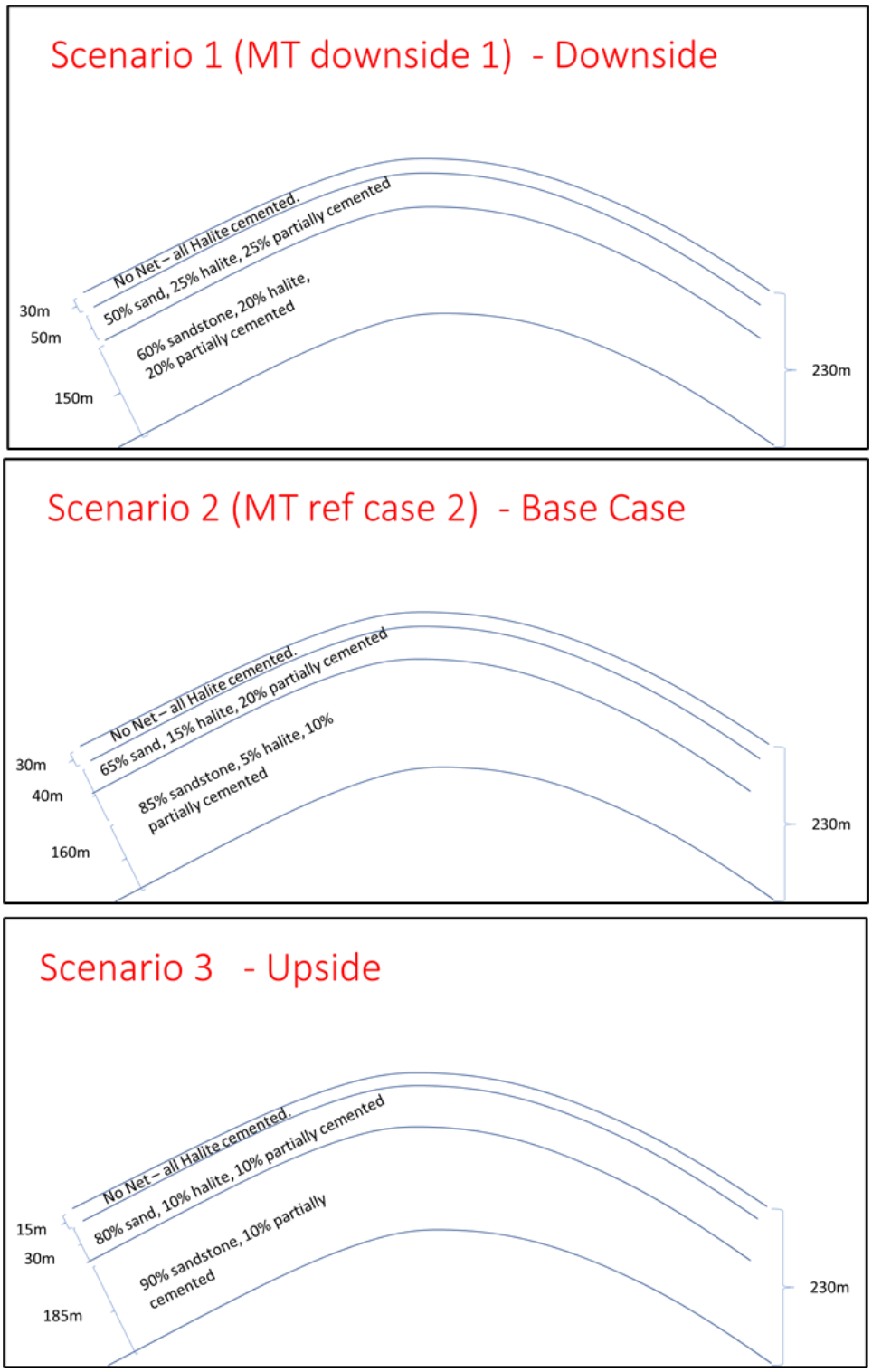

Figure 83 - Notional Halite cementation scenarios considered for the facies modelling.

The Sequential Indicator Simulator (SIS) technique has been used in Petrel to populate the three petrofacies considered for the model, i.e. pervasive halite cementation facies, partially cemented sandstone, and good sandstone. The scheme is de facto similar to the one used for the reservoir model in Endurance alongside the variogram lengths (**Figure 84**).

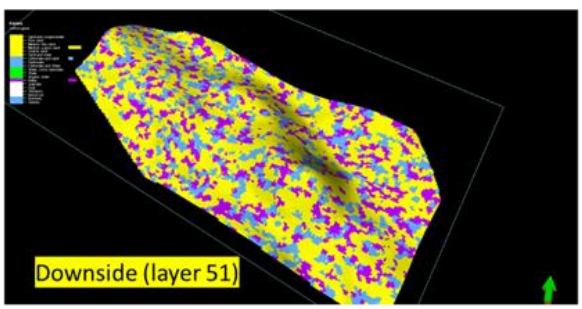

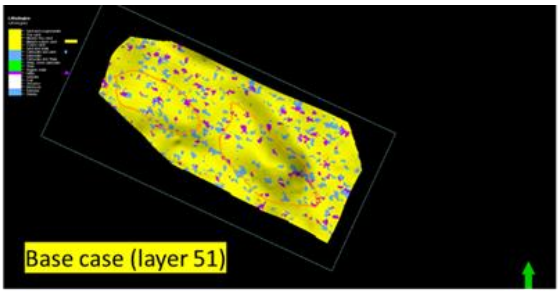

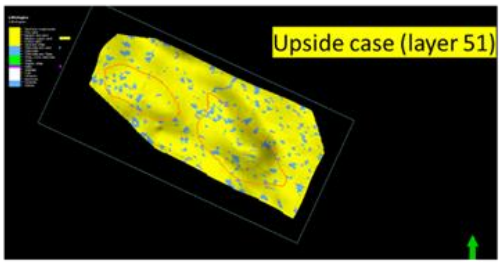

Items		BC 39 Variograms		
		Lateral X	Lateral Y	Vertical
Facies	Good Sand	1000	750	3
	Partially Cemented	1000	750	3
	Plugged & cemented 'Halite' non-net	1000	750	3

Use same variogram as Plugged & cemented for partially cemented

Figure 84 - Facies modelling for the BC39/40 reservoir model using the Petrel SIS facies modelling module.

The three notional halite distribution scenarios, especially the downside case, offer an appropriate range in terms of degree of halite precipitation that might be encountered in the unpenetrated BC39 structure. The drilling and coring of an appraisal well in BC39 would be required to understand the eventual presence of the halite precipitation throughout the Bunter Sandstone and characterise its potential impact on flow (**Figure 85**, **Figure 86** and **Figure 87**).

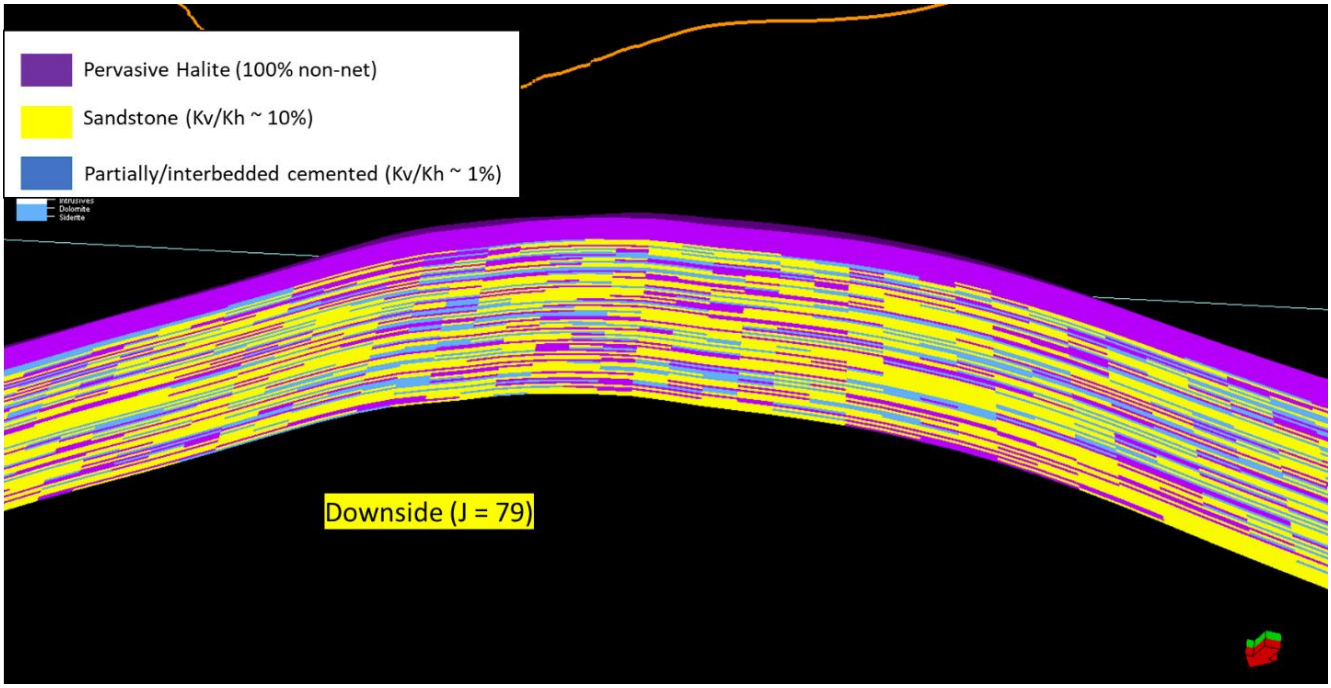

Figure 85 - Facies model for downside scenario with significant degree of halite cementation present throughout the reservoir. Note: the upper Bunter Sandstone is fully cemented (magenta).

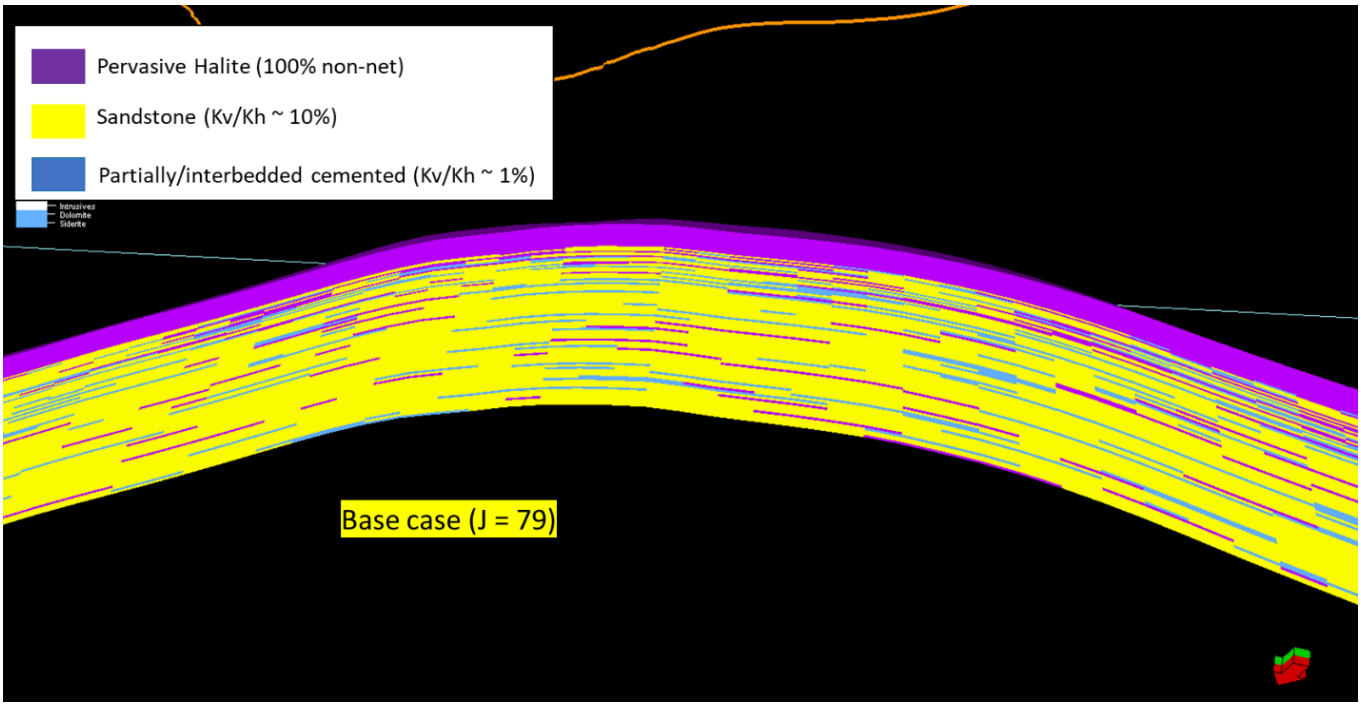

Figure 86 - Facies model for base case scenario with limited degree of halite cementation present throughout the reservoir beyond the upper 30 metres. Note: the upper Bunter Sandstone is fully cemented (magenta).

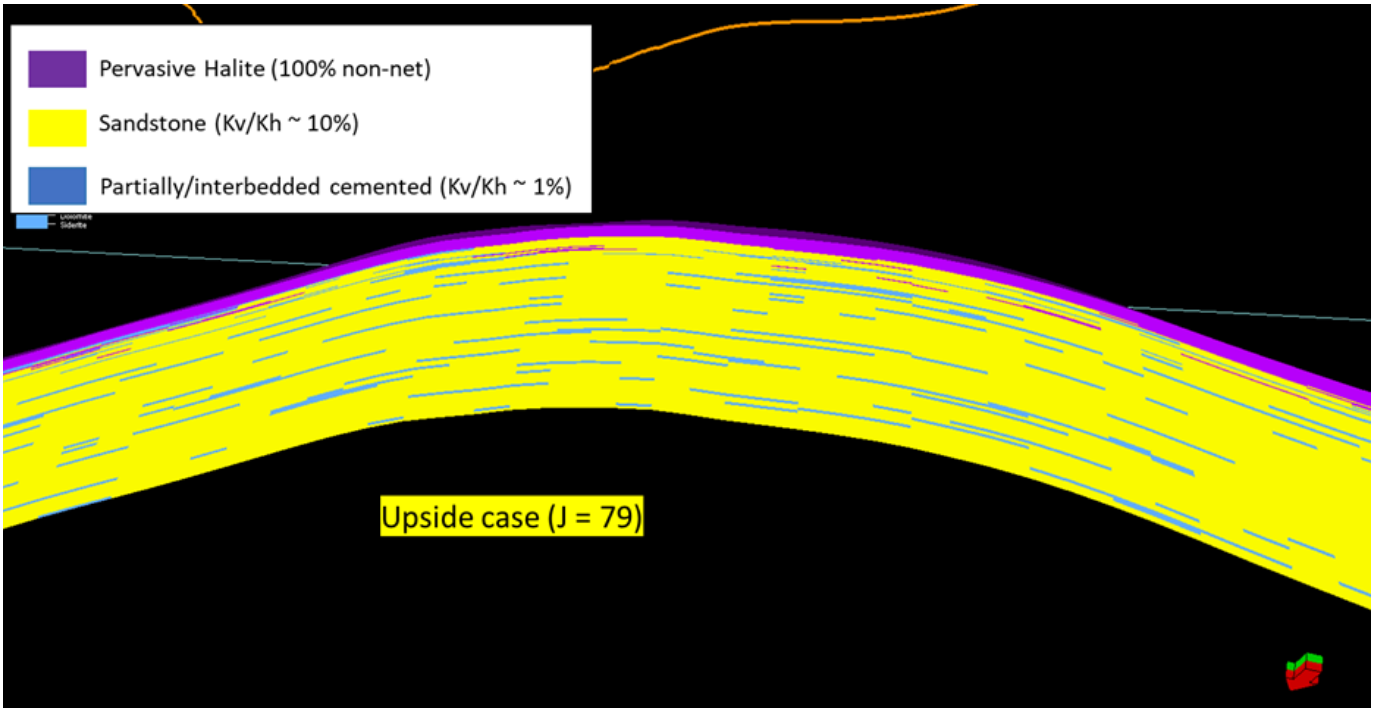

Figure 87 - Facies model for base case scenario with absence of diffuse halite cementation beyond the upper 30 meters (with some partially cemented lenses present which would still provide vertical baffling to flow). Note: the upper Bunter Sandstone is fully cemented (magenta).

9.3 Property Modelling

Reservoir properties were based upon property distribution and statistics from the Endurance reservoir model (model v1.5), i.e. the porosity distribution for the good sand and partially cemented sand petrofacies as shown in **Figure 88**. The pervasive halite petrofacies is considered non-net (**Figure 89**) and is in effect a barrier to flow wherever present throughout the reservoir. **Figure 90** and **Figure 91** show the impact of the facies distribution on the porosity modelling.

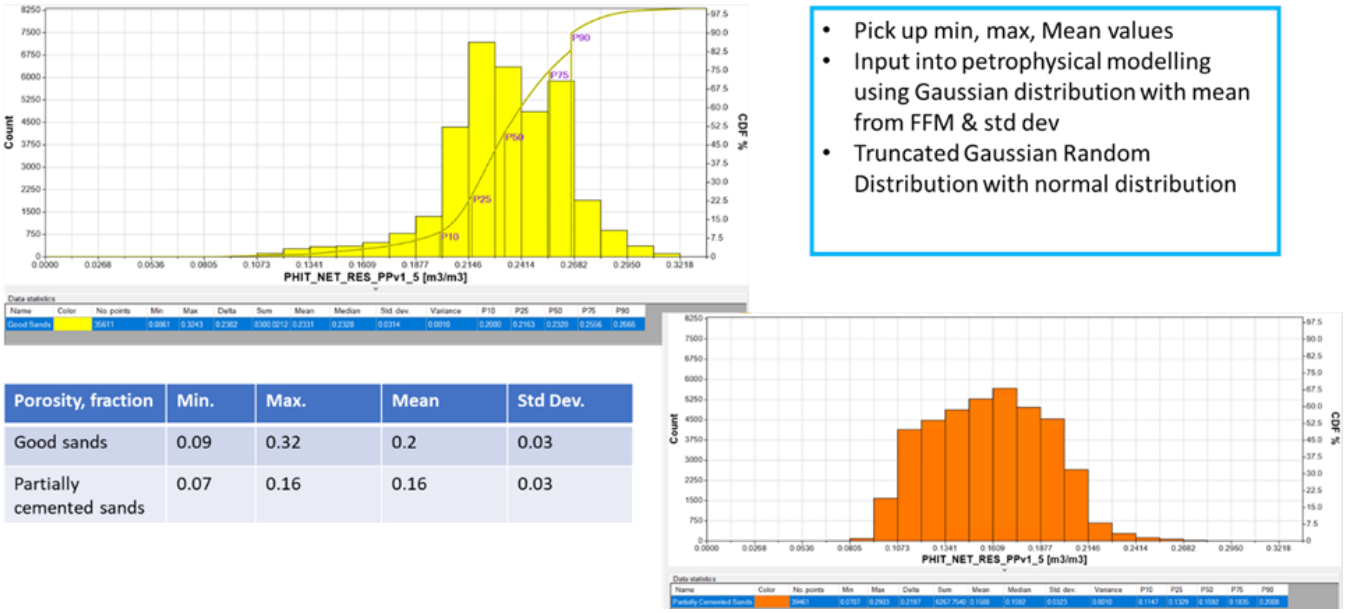

Porosity, fraction	Min.	Max.	Mean	Std Dev.
Good sands	0.09	0.32	0.2	0.03
Partially cemented sands	0.07	0.16	0.16	0.03

Figure 88 - Porosity properties extracted from Endurance reservoir model for use in the property modelling for BC39.

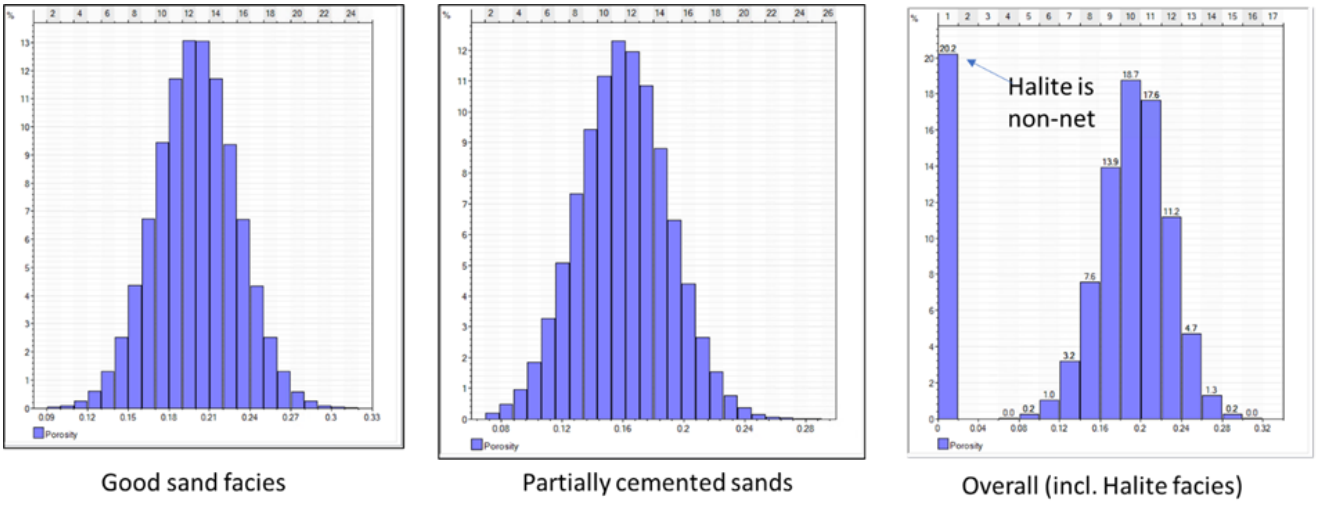

Figure 89 - Modelled porosity distribution for model facies (base case facies model).

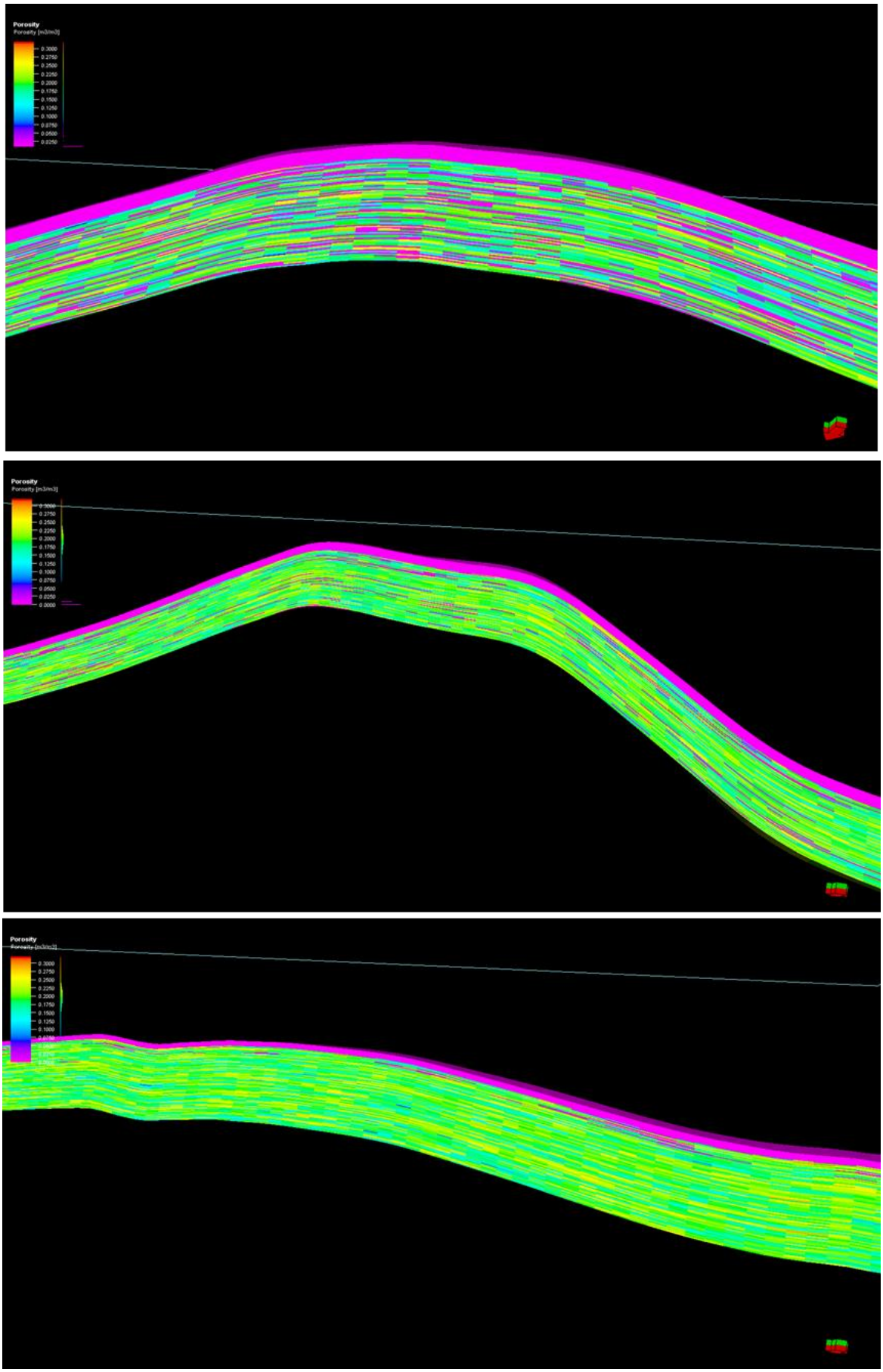

Figure 90 - Porosity modelling for the three reservoir architecture scenarios: downside (above), base case (middle), and upside (bottom).

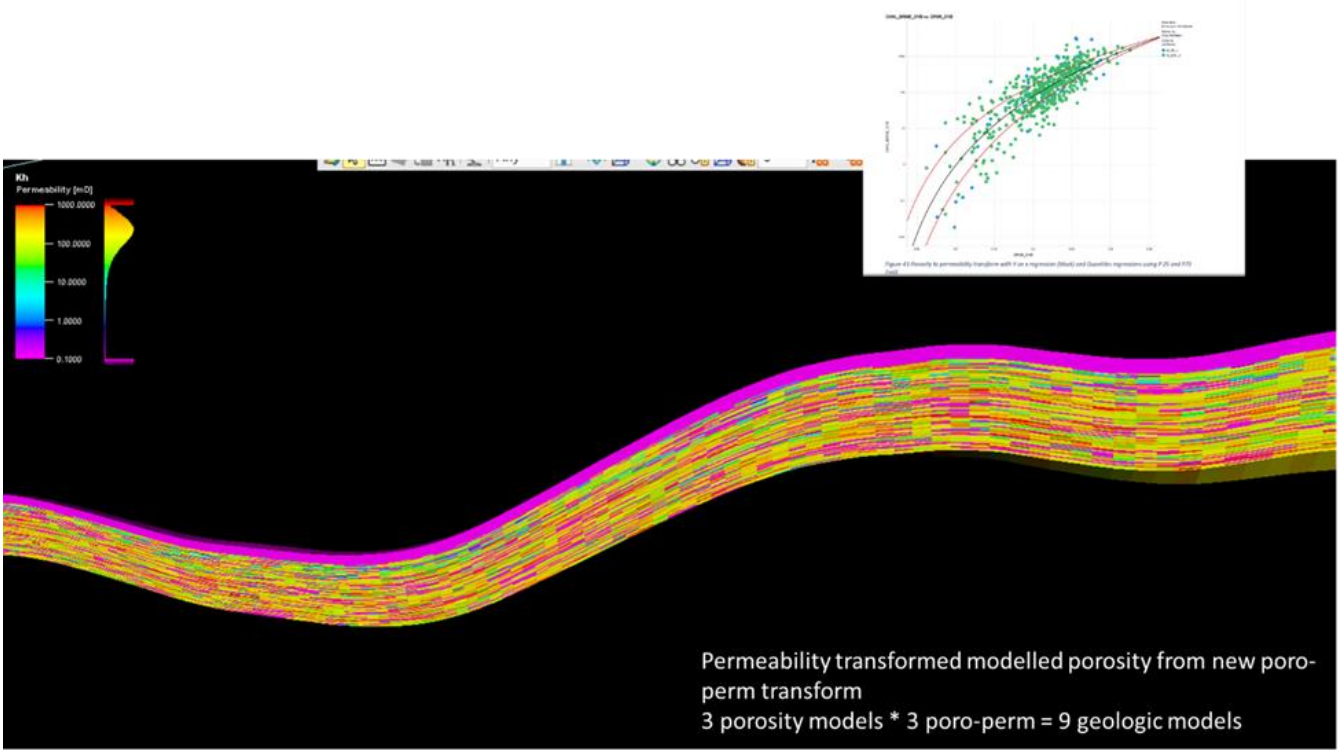

Figure 91 - Permeability modelling for the BC39/40 model using P25/P50/P75 porosity-permeability transform from Endurance core data (model v1.5).

Horizontal (X and Y directions) permeability was modelled by using the simple porosity permeability transforms generated from the Endurance petrophysical model v1.5, i.e. P25, P50, and P75. A total of nine models were generated. Vertical to horizontal permeability ratios (Kv/Kh) were based upon the Endurance model with KV/Kh = 10% for the good sand facies and 1% for the partially cemented facies. The volumetric fraction of pervasive halite (non-net) and partially cemented sands does control the overall vertical permeability and the gravity-driven migration of the CO2 plume to the crest. The combination of significant halite cementation and poor to medium reservoir properties would constitute a downside geologic outcome and would be a limiting factor in terms of storage capacity for the structure.

9.4 On structure Compartmentalisation

Notional faulting patterns have been generated for both structures (BC39 and BC40) based upon the framework utilized for Endurance modelling (**Figure 92**). Inter-region transmissibilities have been used as an ITRAN array in the Nexus model to account for notional lateral baffling across the structure which could potentially limit the connectivity to the broader aquifer area.

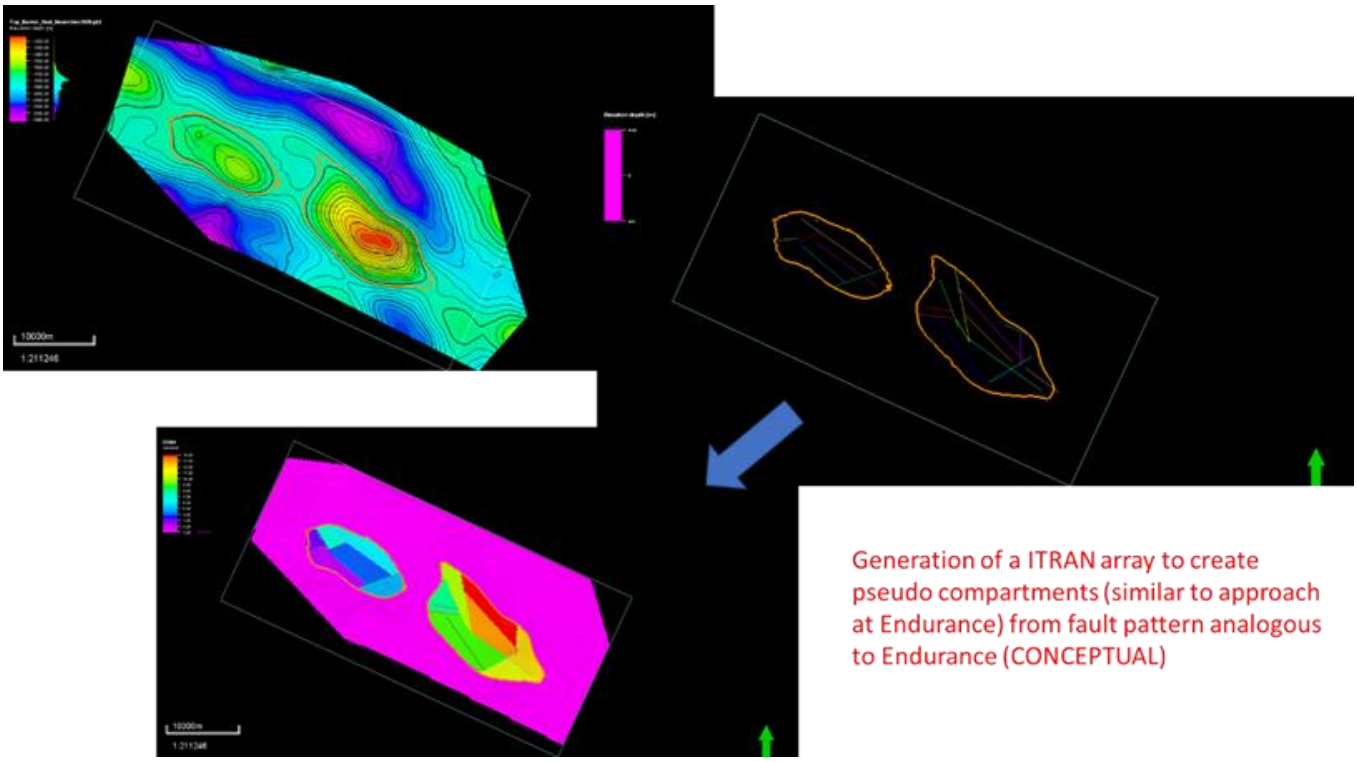

Figure 92 - Notional regions used for reservoir modelling for BC39/BC40 reservoir models.

It is important to consider these regions as notional rather than actual features mapped from the seismic (no faults have been observed on seismic on these structures, see sections above). Further seismic acquisition will be required for BC39/40 with additional characterisation required regarding eventual compartment presence, which is considered unlikely considering the structural characterisation carried out at Endurance (see Geophysical Model KKD for Endurance).

9.5 Model Volumetrics

For reference, volumetrics have been exported from the Nexus model using a spill point at 1775 m TVDSS as follows (Figure 93**,** Table 13 **and Table 14):**

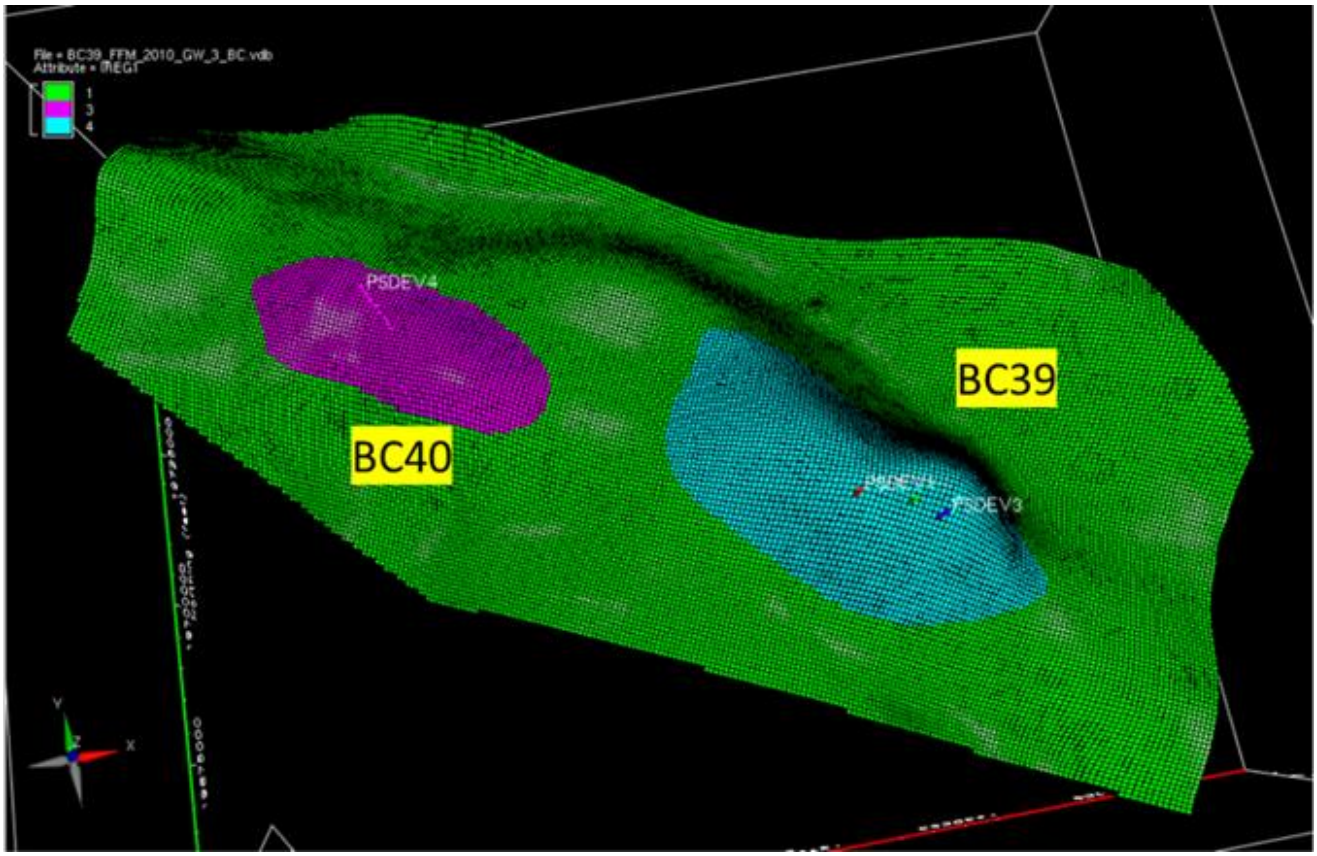

Figure 93 - Regions used for volumetric calculations.

Table 13 - Net pore volume for BC40 above spill point 1775 mTVDSS.

Model	Net Pore Volume* (billion reservoir barrels)	Net Pore Volume* (billion reservoir cubic meters)
Downside Architecture	4.23	0.672
Base case Architecture	5.01	0.796
Upside Architecture	5.34	0.849

Table 14 - Net pore volume for BC39 above spill point 1775 mTVDSS.

Model	Net Pore Volume* (billion reservoir barrels)	Net Pore Volume* (billion reservoir cubic meters)
Downside Architecture	15.8	2.5
Base case Architecture	19.2	3.06
Upside Architecture	20.4	3.25

For reference, the Net Pore Volume for Endurance above spill point (at 1450m TVDSS) is 4.2 billion reservoir m3.

9.6 Nexus Dynamic Model Key Assumptions and Inputs

The dynamic modelling approach is broadly similar to the strategy used for Endurance. A simple gas-water model (immiscible gas-water) was used for BC39 and BC40 as brine salinity is assumed to be similar to samples from well 42/25d-3 (250,000 ppm %w) which would result in limited CO2 solubility into the brine (of the order of 1 to 1.5% per mass). BC39 and BC40 structures are deeper than Endurance so a gas-water table was re-generated with Petroleum Expert PvTp for a datum temperature of 143.6°F (at 1500m TVDSS datum). Brine PVT tables were kept the same as in the Endurance model with three brine PVT tables. The pressure datum was set at 2365 psia at 1500 m TVDSS using in effect the pressure at 42/25d-3 corrected for the depth difference with 0.51 psi/ft hydrostatic gradient (**Figure 94**).

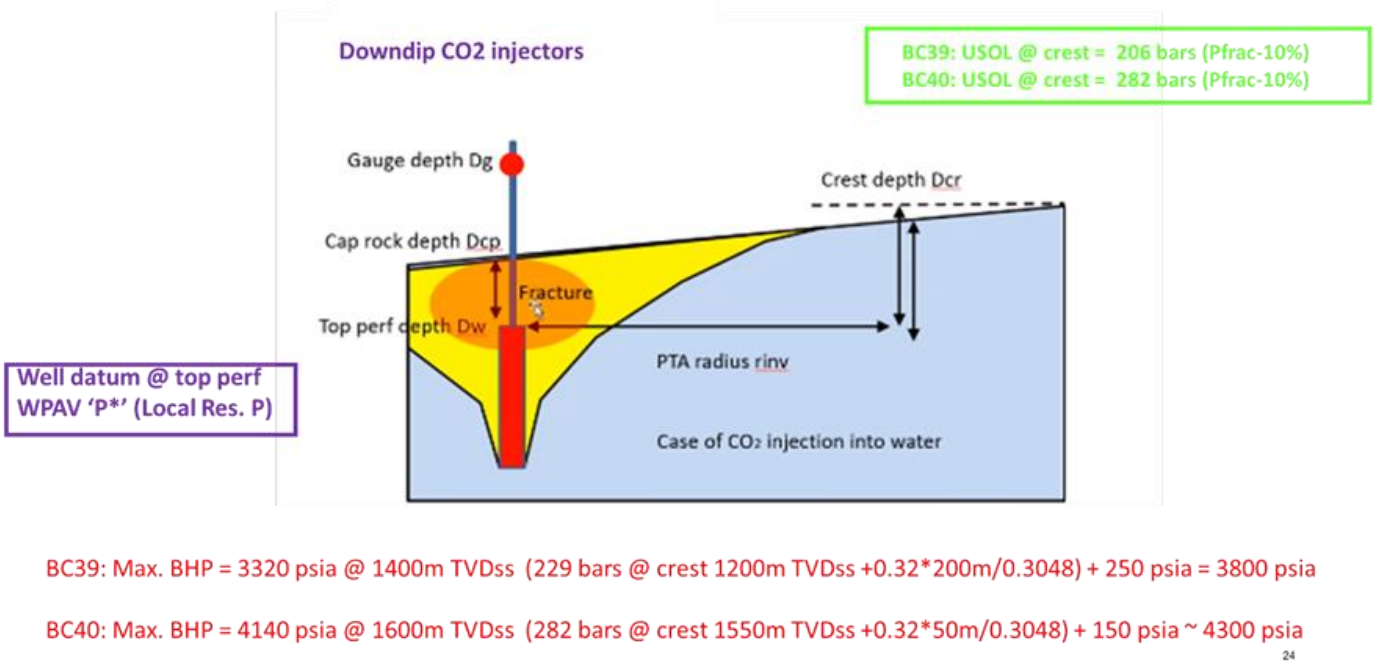

Figure 94- Pressure constraints for the BC39/BC40 modelling.

A notional subsea development scheme with three wells drilled over BC39 and one well drilled over BC40 was tested across a range of models generated from Monte Carlo workflow in bp proprietary tool TDRM™. The wells are operated with maximum BHP values as no lift curves were used for this study (uncertainty on network modelling and arrival pressure from Endurance). Preliminary fracture pressure at crest for the Röt Halite at BC39 and BC40 (from overburden) were calculated respectively to be 229 bars and 313 bars (note that these are not final numbers and require update and/or confirmation). The Nexus dynamic model is shown in Figure 95.

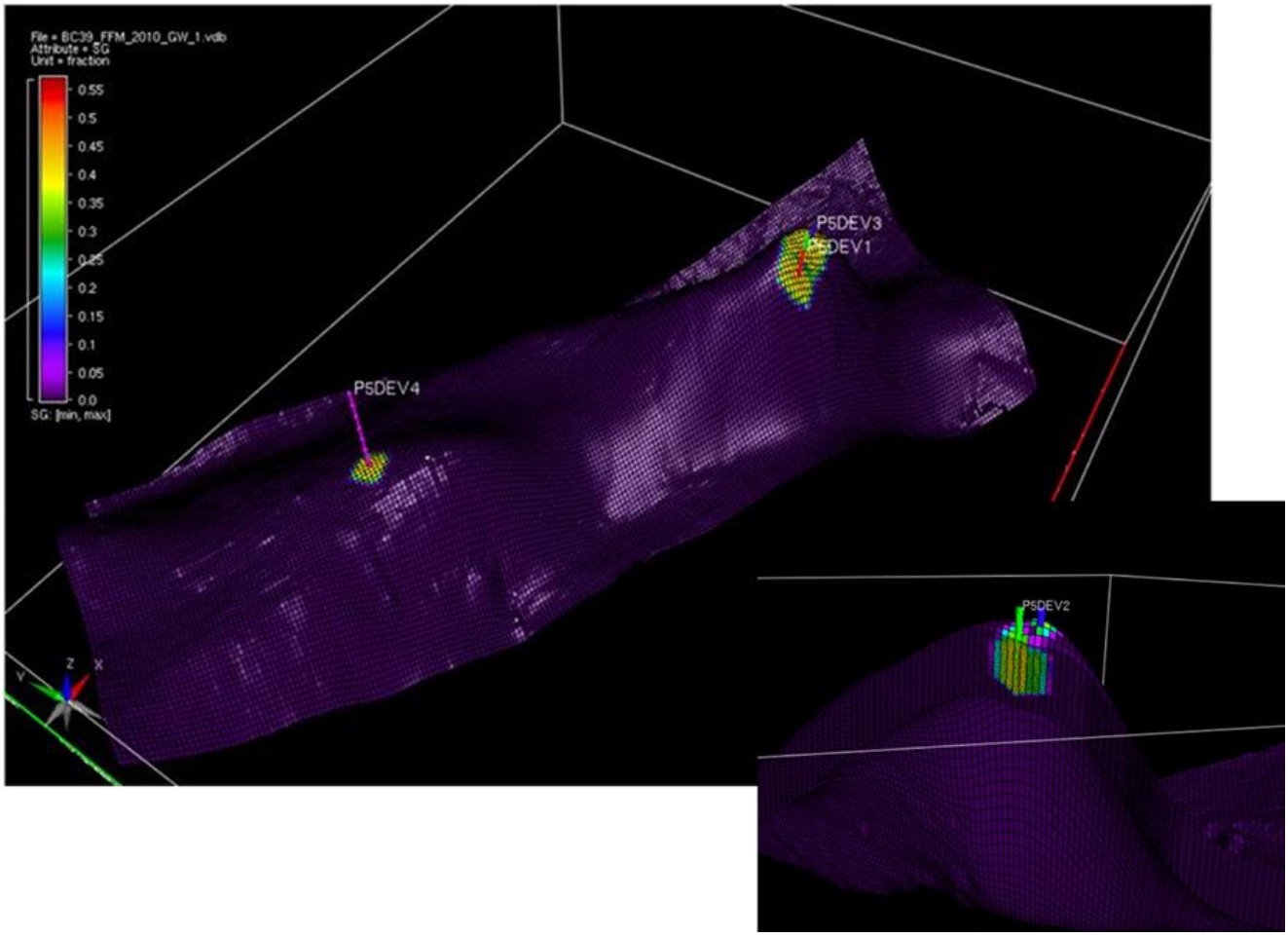

Figure 95 - Nexus reservoir model for BC39 and BC40.

9.7 Reservoir Uncertainties Considered

The connectivity to the greater Bunter Sandstone aquifer in the BC39/BC40 remains to be tested through actual CO2 storage development. Various scenarios were therefore assessed via the use of pore volume multipliers at the edge of the model as shown in **Figure 96**.

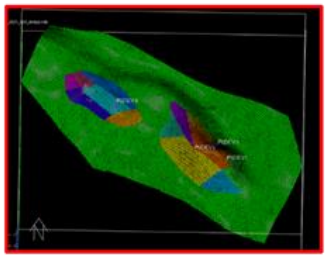

Downside
Closed system beyond AOI

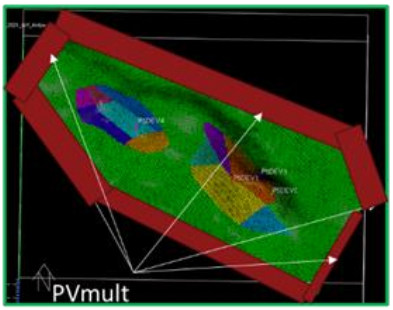

BC: AOI aquifer (with seabed outcrop)
WIP = 222 billion STB

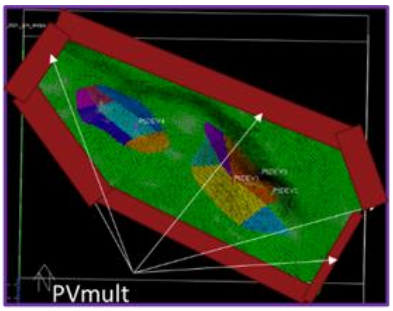

US: Greater Bunter aquifer (with seabed outcrop)
use of PV at edge
to obtain Esmond-like radius i.e. 20 km)

FOR REFERENCE in ESMOND: connected volume of 115 billion barrels of brine (Bentham et al)

Uncertainty	Downside	Base Case	Upside
Aquifer extent – EACH EDGE CONSIDERED INDEPENDENT	Closed system, no PV	Current AOI + PV at edges to have 4 km	Greater Bunter Aquifer (Esmond-like extent): Current AOI + PV at edges to have 20 km

Figure 96 - Aquifer connectivity/extent beyond AOI.

Petrophysical uncertainty was dealt with via the use of multiple porosity-permeability transforms as described in section 0 and shown in **Figure 97**. Inter-region transmissibility multipliers were also considered to ensure that potential lateral baffling scenarios are considered (**Figure 98**). Relative permeability model was based upon Endurance displacement model (**Figure 99**). Uncertainty in bulk rock volumes (variable gross thickness in Bunter observed at Endurance not explicitly modelled with the grid in the BC39/BC40 model, i.e. 230 m) was accounted for with global +15%/-15% multipliers applied for respectively downside and upside cases.

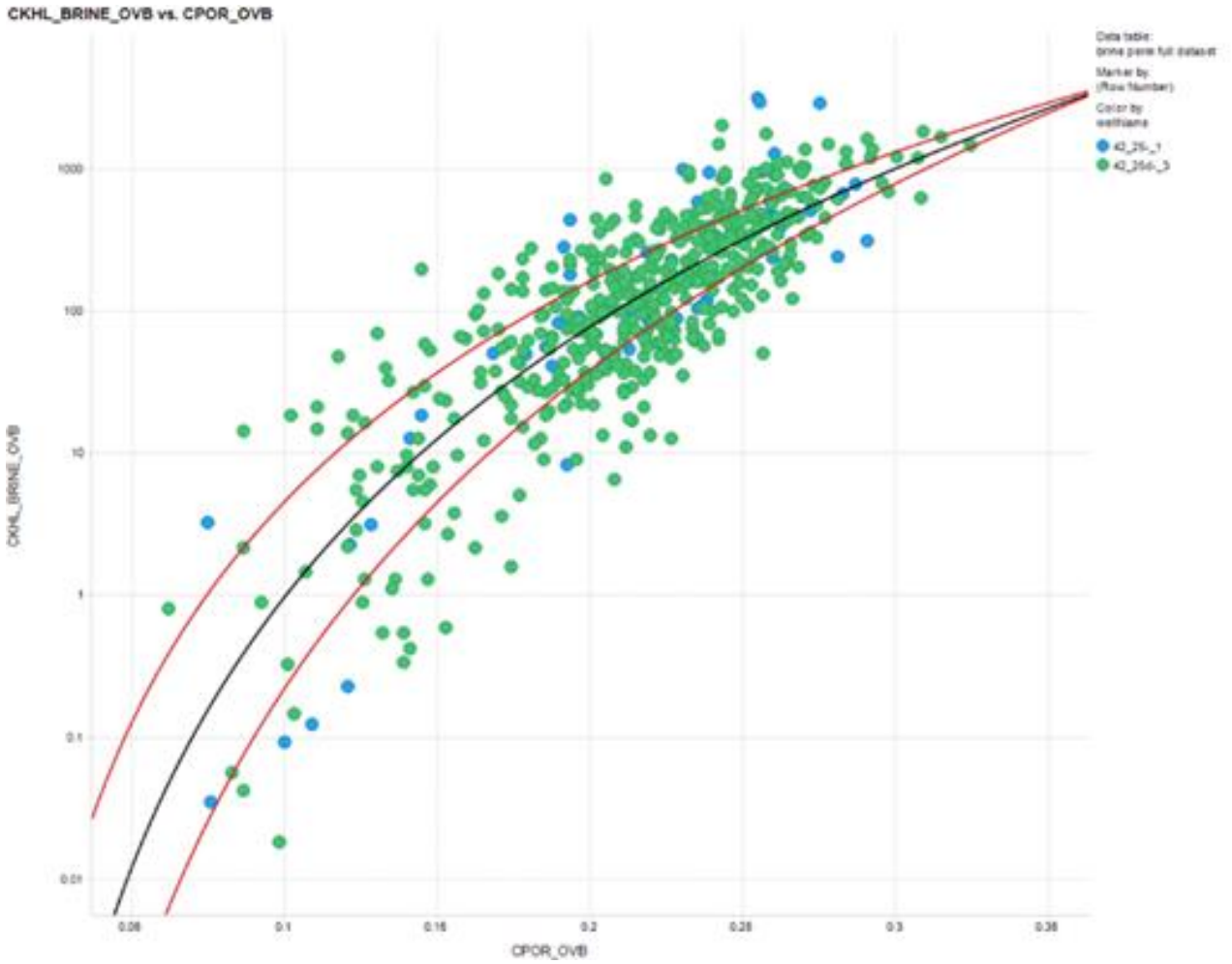

Figure 97 - Porosity-permeability transform (P25 considered as downside case, P50 considered as base case, P75 considered as upside).

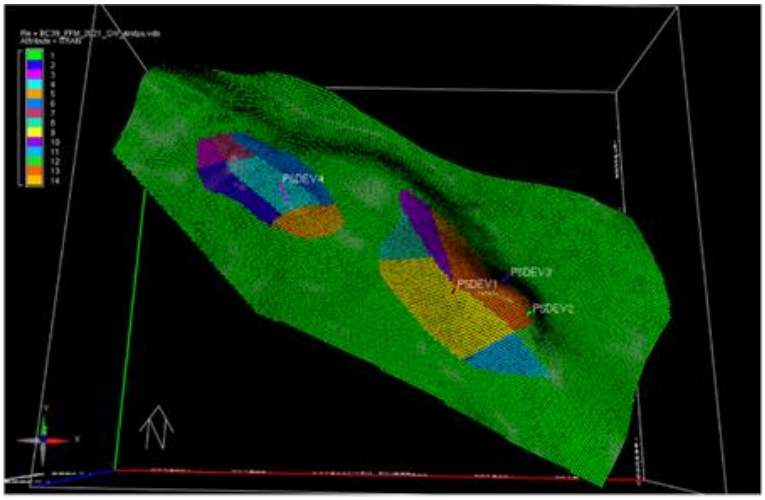

Uncertainty	Downside 1	Downside 2	Base Case	Upside
Inter-region transmissibility	0.02	0.16	0.44	1

Figure 98 - Potential on-structure baffling based upon Endurance structural framework study.

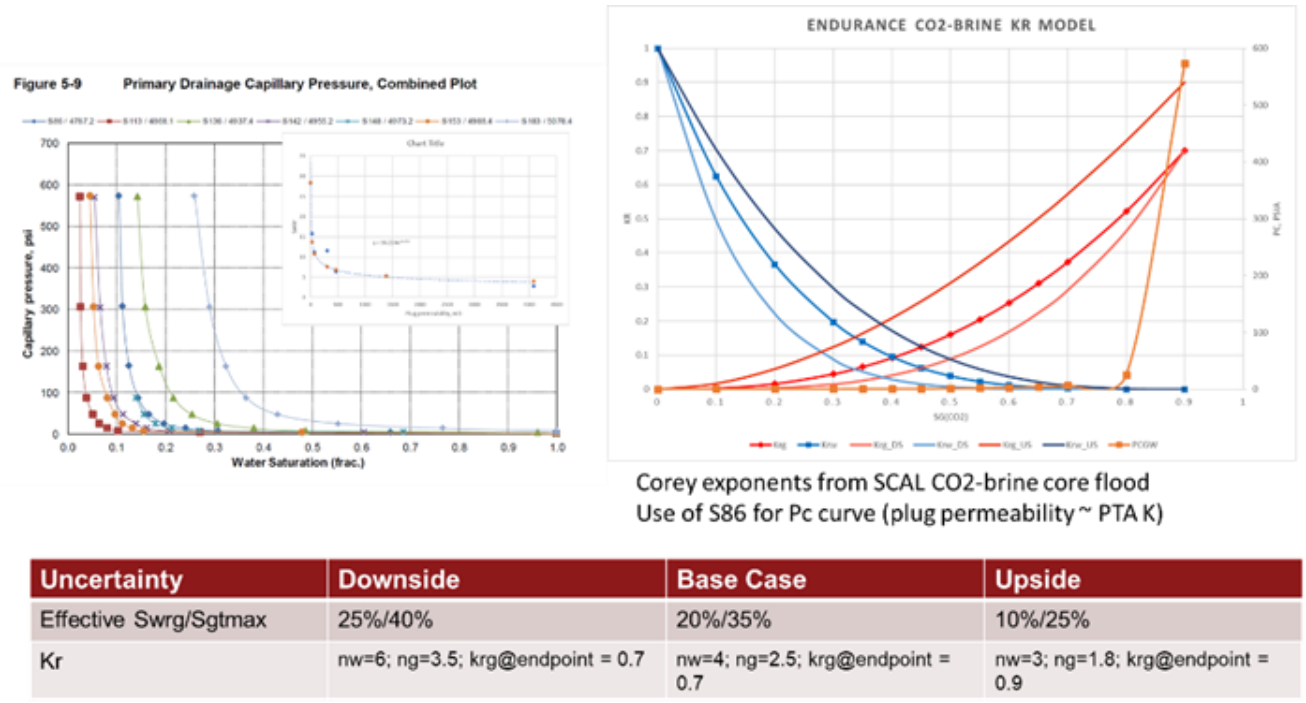

Uncertainty	Downside	Base Case	Upside
Effective Swrg/Sgtmax	25%/40%	20%/35%	10%/25%
Kr	nw=6; ng=3.5; krg@endpoint = 0.7	nw=4; ng=2.5; krg@endpoint = 0.7	nw=3; ng=1.8; krg@endpoint = 0.9

Figure 99 - Relative permeability model for Endurance used for the BC39/BC40 modelling.

9.8 Uncertainty Analysis and Identification of Relevant Downside, Base and Upside Cases

A series of Monte Carlo workflows were run with TDRM™ to assess the impact of various geologic outcomes on the considered development as shown in **Figure 100**.

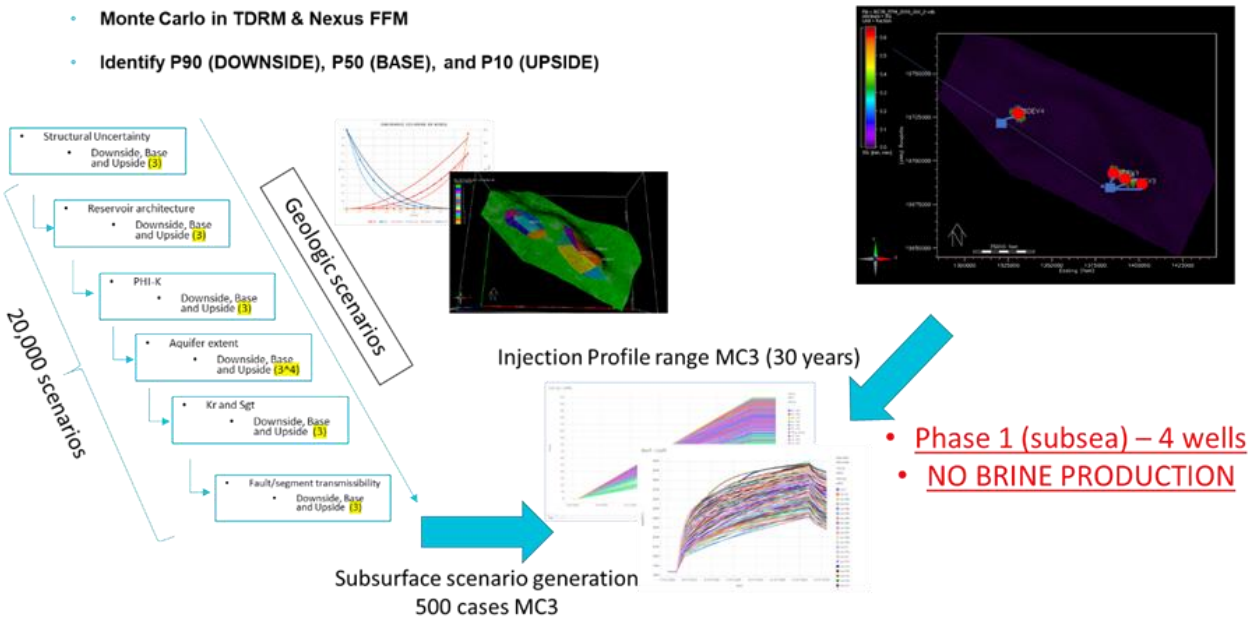

Figure 100 - Monte Carlo workflow with TDRM™ for BC39 & BC40 reservoir models.

Results of the Nexus dynamic simulations are shown in **Figure 101** to **Figure 105**. 4 MTPA (3 MTPA in BC39 and 1 MTPA in BC40 – 'Phase 1 for BC39/40') appears largely achievable for if reservoir properties are demonstrated to be sufficient: a well test and core acquisition programme for the BC39 appraisal well would help eliminate some downside scenarios, e.g. the mc.242 case presented in this study (downside/P90). Indeed, downside reservoir architecture coupled with poor rock properties (P25 transform, K in the order of 10's of mD) would present challenges to maintain 3 MTPA plateau with the crestal pressure for the downside case approaching the upper safe limit set in the study (fracture pressure for the halite with 10% safety factor). In spite of its limited size, BC40 store presents potential upside with the anticipated abandonment pressure significantly below the set safe limit. Further study will be required to evaluate the additional storage capacity (**Figure 102**).

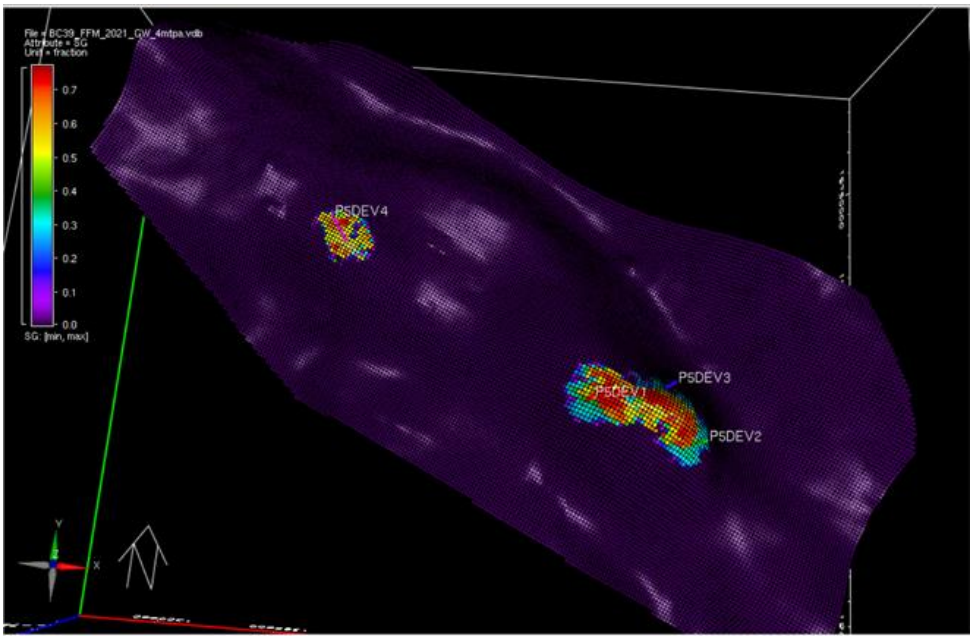

Figure 101 - CO2 saturation 150 years after the end of injection (mc.225 base case).

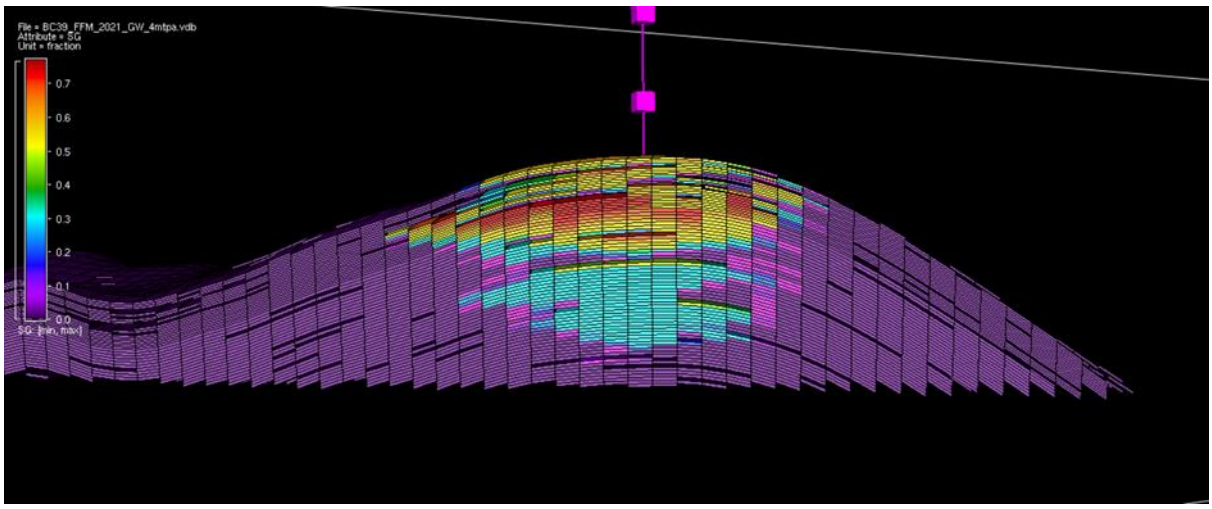

Figure 102 - CO2 saturation across BC40 150 years after cessation of injection for mc.225 (base case).

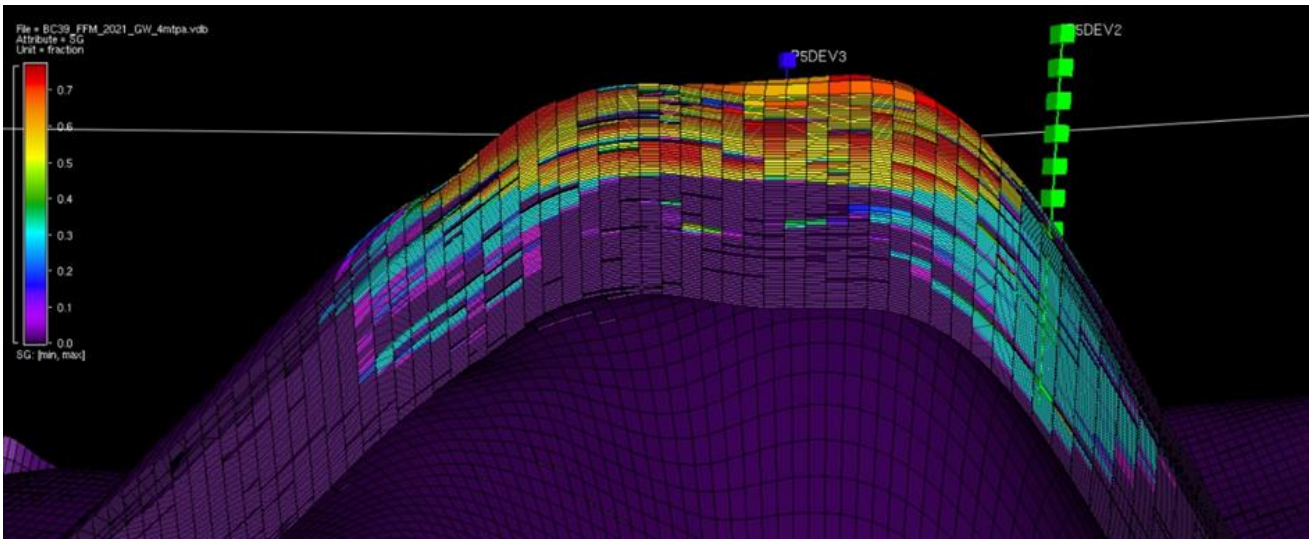

Figure 103 - CO2 saturation across BC39 150 years after cessation of injection for mc.225 (base case).

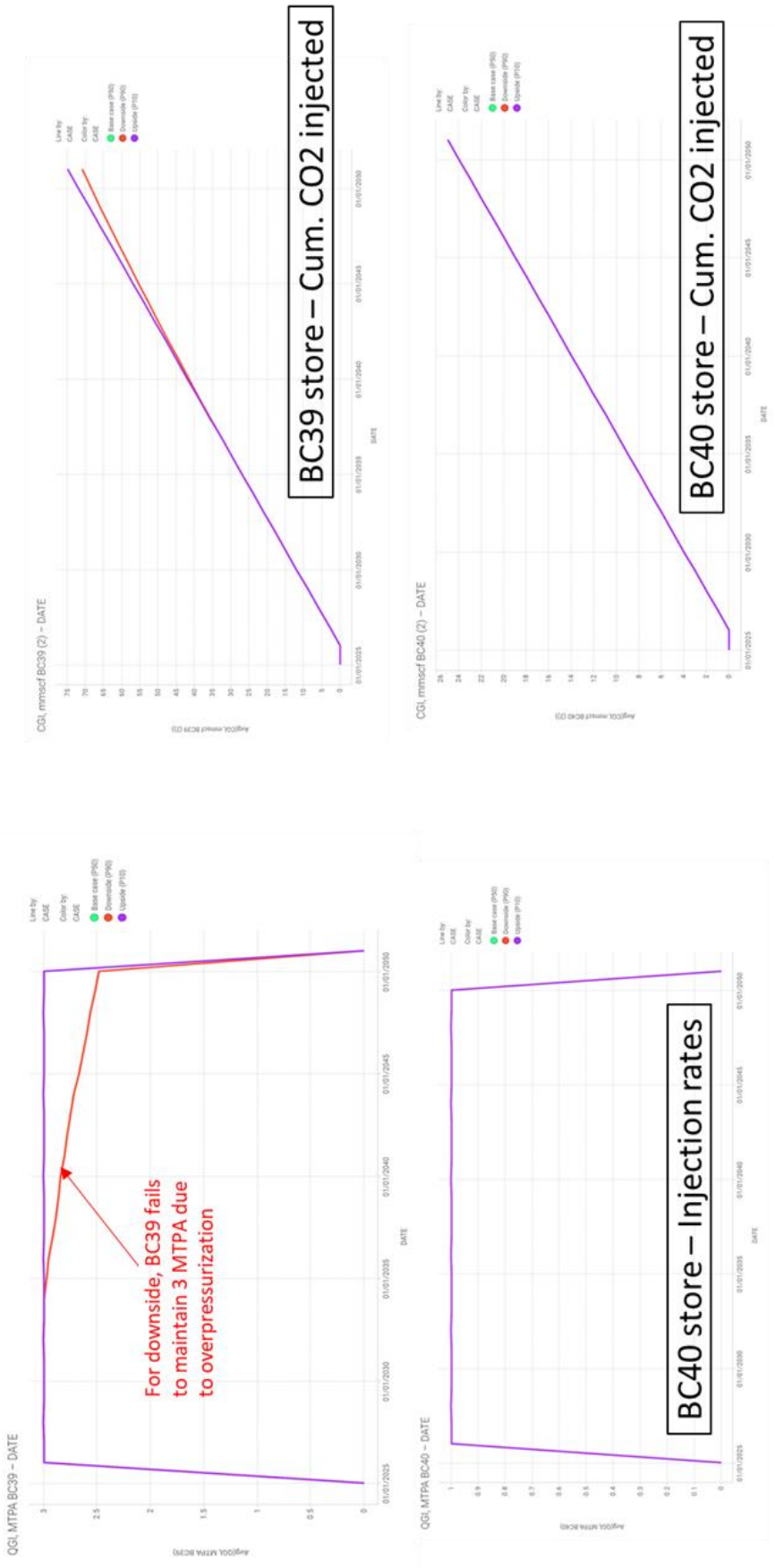

Figure 104 - Total cumulative injected CO2 volumes for BC39 and BC40; Total injection rates for BC39 (3 MTPA plateau) and BC40 (1 MTPA).

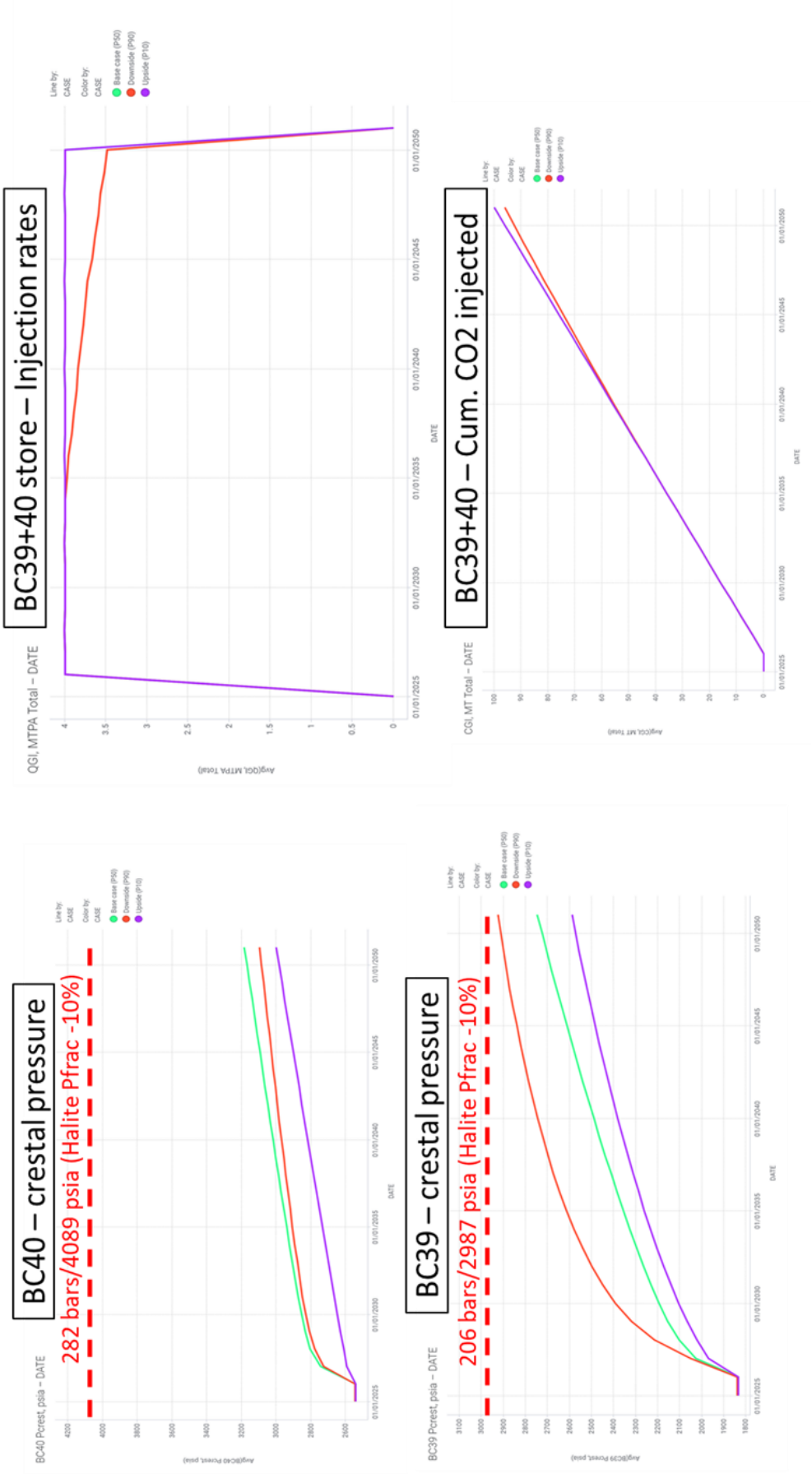

Figure 105 - Crestal pressure over time for stores BC39 and BC40; Total cumulative injected CO2 volumes for BC39+40; Total injection rates for BC39+40 (4 MTPA plateau).

10.0 Notional Development Plan (NEP Phase 2 and Beyond)

There is reasonable confidence in the ability of the Endurance structure to store c.100 million tonnes or the equivalent of 4MTPA average injection over 25 years as part of Phase 1. Beyond that, e.g. in order to reach 10 MTPA plateau, brine production would be required depending on the level of localised pressurisation in the reservoir. Alternatively, Endurance could serve as the hub to access analogous Bunter Closure stores BC36, BC37, BC39 and BC40 whilst delaying brine production. Given the brine production technical solution cannot be determined definitively until further data is obtained during Phase 1 production, having the alternative of accessing expansion stores provides optionality to NZT/NEP to manage a more rapid ramp up should that be required. Endurance brine production together with the expansion stores therefore provides line of sight to a potential storage volume of close to 1 billion tonnes at an injection rate of up to 27 MTPA.

Utilisation of the nearby Bunter Closures BC36, BC37, BC39 and BC40 may enable a cost effective and low risk expansion beyond the phase 1 development of Endurance to reach 10 MTPA (average), as well as providing further opportunities for longer term expansion (23 MTPA). A proposed expansion scenario has been developed based on 4 phases (**Figure 106**):

- Phase 1: 4 MTPA average (5.6 MTPA peak) from 2026: no brine, Endurance store only, 5 subsea wells + 1 observation well.
- Phase 2: 10MTPA average (14 MTPA peak) from 2030: expansion to 10 MTPA with the development of the alternative stores east of Endurance (Figure 107).
- Phase 3: 16MTPA average (20 MTPA peak) from 2034 with expansion of Endurance to 10 MTPA
- Phase 4: 23MTPA average (27 MTPA peak) from 2038

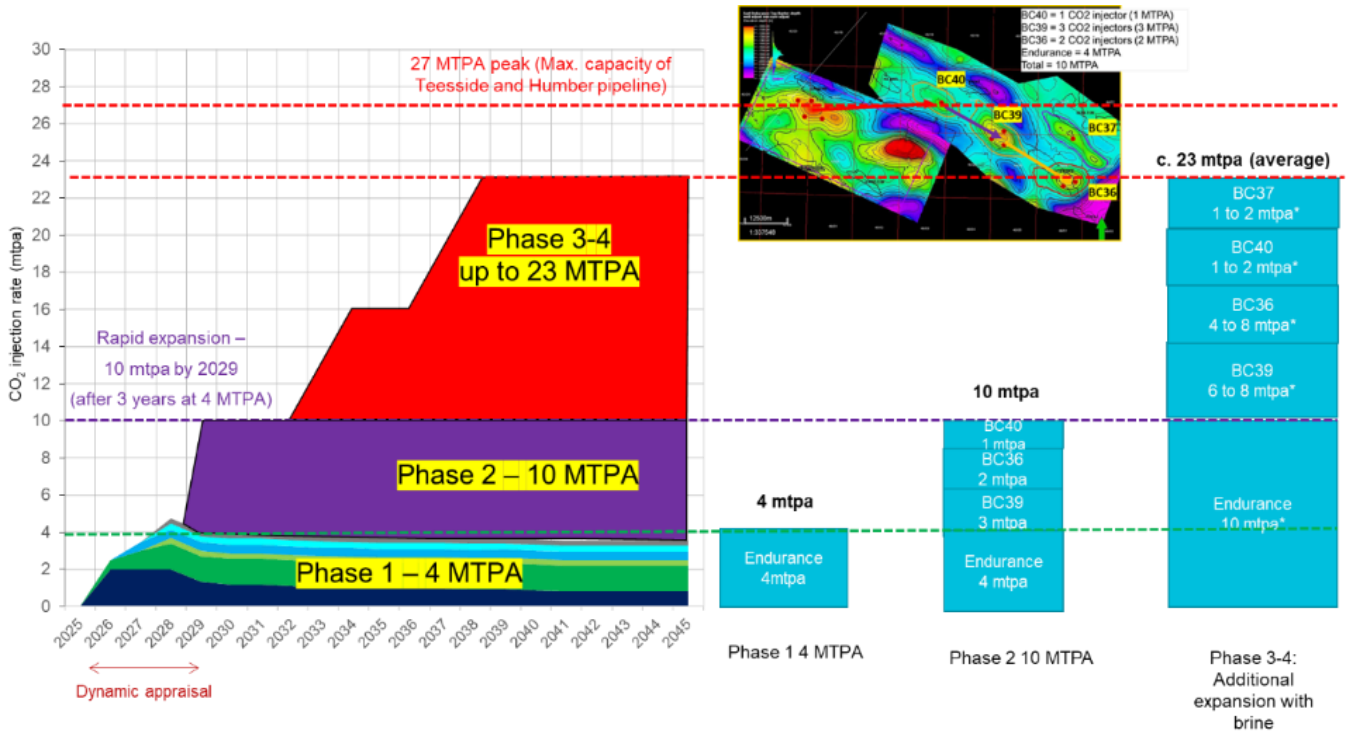

Figure 106 - Notional NEP expansion strategy from 4 to 10 MTPA to 23 MTPA.

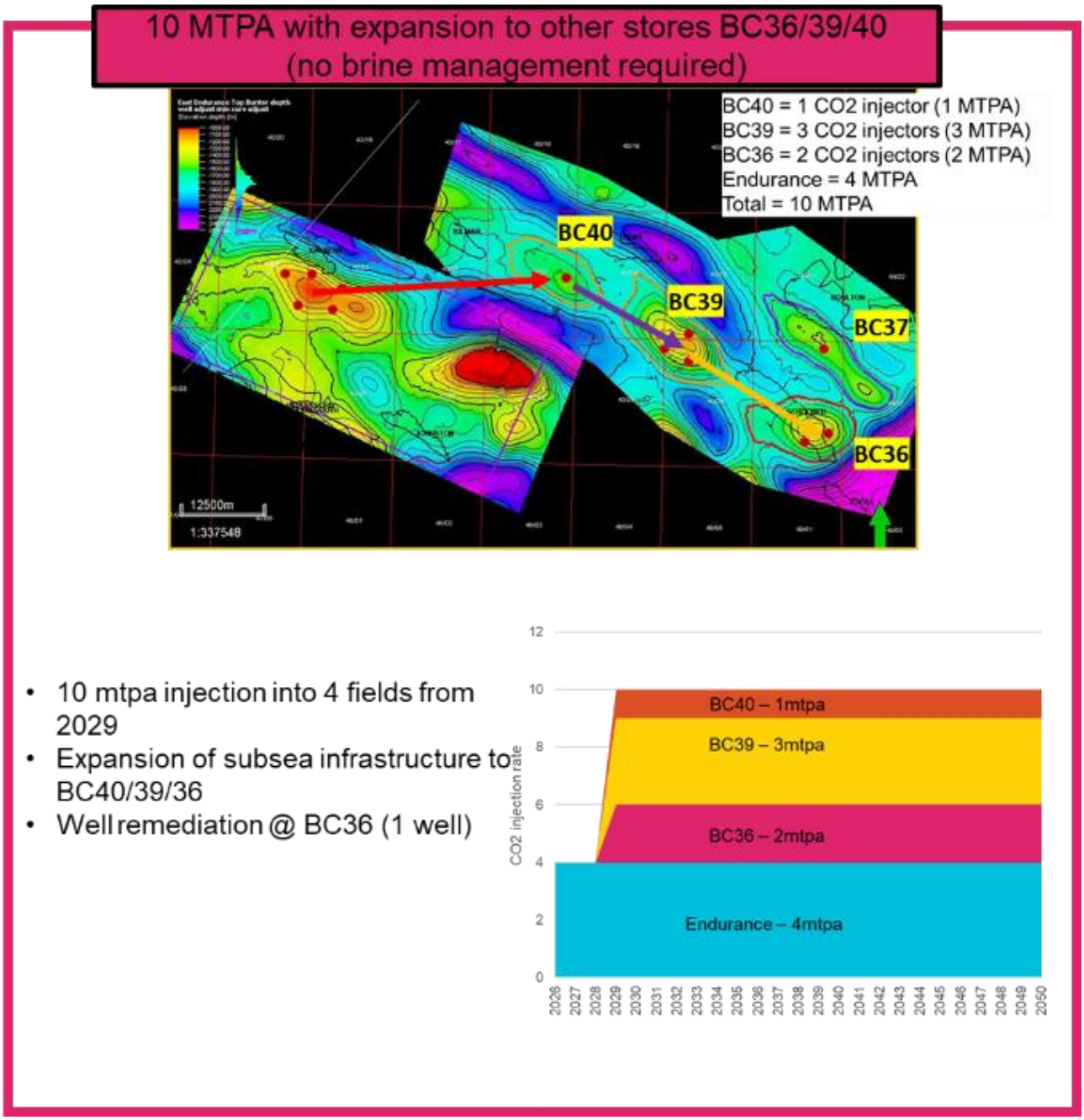

Figure 107 - Path to 10 MTPA (Phase 2) from Phase 1 (4 MTPA at Endurance) with the expansion into additional stores (BC36/39/40) to add 6 MTPA capacity (no brine would be expected).

The expansion to 10 MTPA with the development of BC36, BC37, BC39 and 40 (Phase 2 10 MTPA - provisional on successful license application and completion of the required work program) would notionally comprise (**Figure 107**):

- Increased onshore compression capacity to 10MTPA (average)
- Six new injection wells (6 MTPA capacity)
    - Two in BC36 (or BC37 alternatively in lieu of BC36)
    - Three in BC39 (contingent on successful appraisal of the structure)
    - One in BC40

New subsea infrastructure to connect the additional stores to the existing subsea network at Endurance

A well remediation operation in BC36 targeting one of the two crestal legacy wells over the structure (i.e. 44/26-3)

An agreement with DNO to remediate to integrity risks of the 10 development wells targeting Schooner gas field.

A summary of the notional expansion concept is given in Figure 108. An expansion of the NZT/NEP development through utilization of the nearby Bunter Closure reservoirs may enable the following benefits to be realized:

- It enables “appraisal while developing” for Endurance, significantly improving subsurface understanding and the forecast of brine production timing, volumes, and rates.
- Earlier incorporation of additional reservoirs provides mitigation of the geological risks by using a multistore approach rather than a single store.
- An opportunity to demonstrate a regional basin approach that maximises UKCS storage resource as per OGA and BEIS’ ambition
- Benefit from pipeline pre-investment and development 150 MT of storage capacity at a lower cost

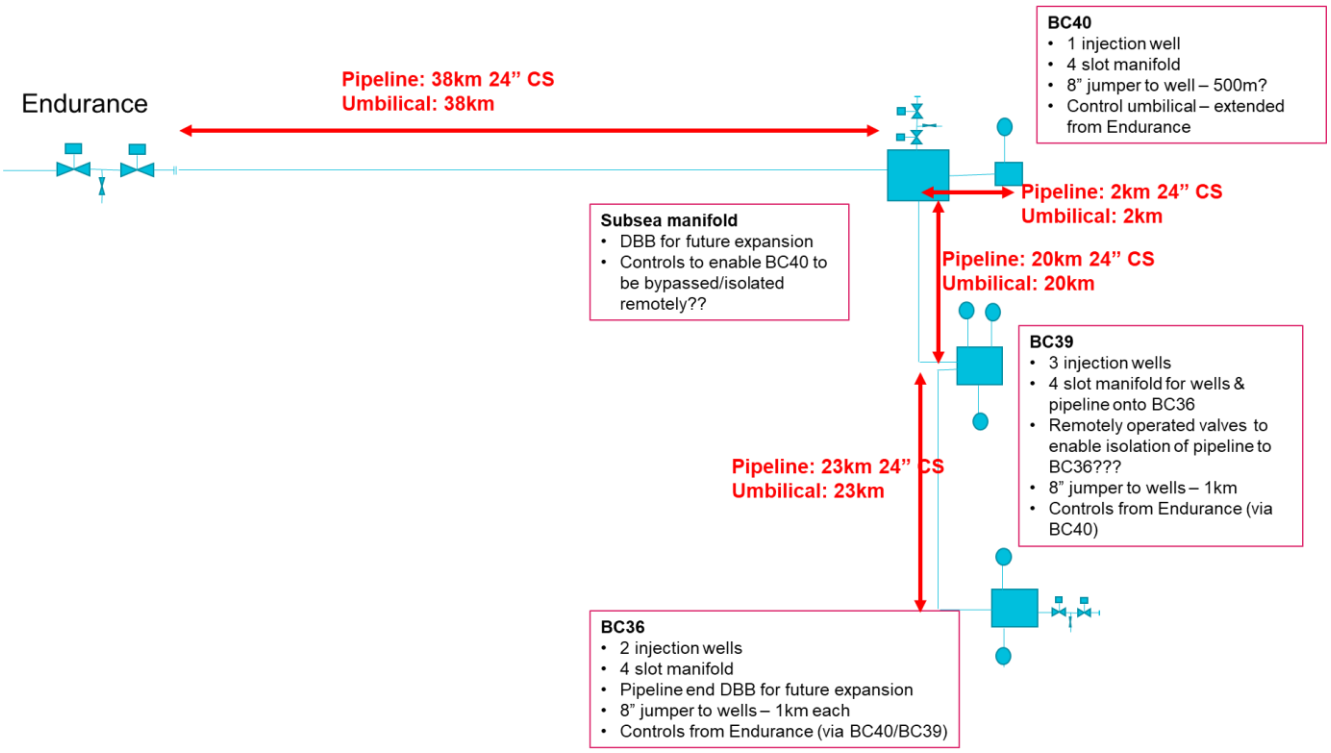

- Figure 108 - Notional subsea expansion from Endurance to BC40, BC39, and BC36 (subsea system will have the ability to be connected to BC37 as well to support future phases).

The development of the alternative Bunter Closure stores will be facilitated by the ability to connect the flowlines back to Endurance subsea infrastructure (5 subsea injectors and 2 manifolds) as shown in **Figure 109**. The tie-in point at the Wye will allow the use of Endurance and existing pipeline infrastructure for injection further east.

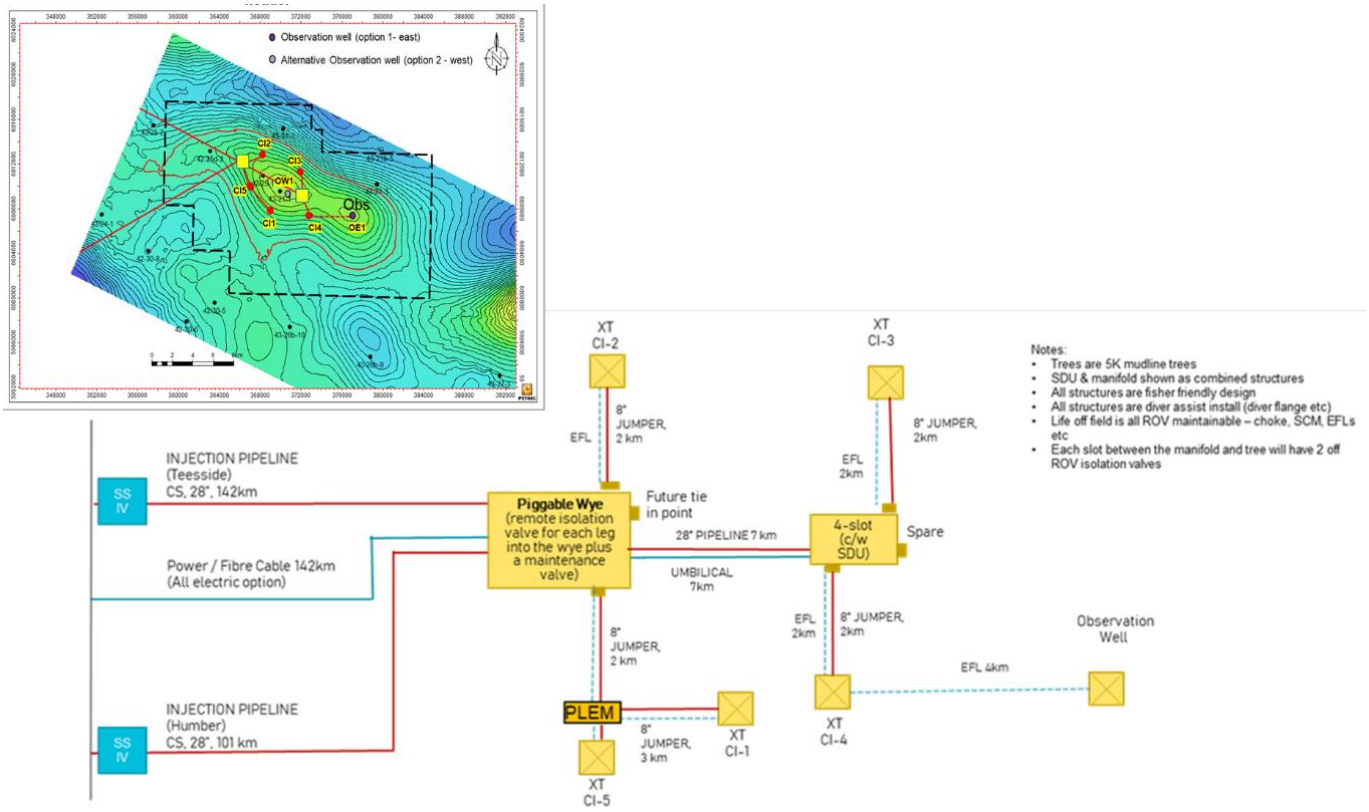

Figure 109 - Endurance Phase 1 subsea development.

For reference, from the booster compression discharge at Teesside the CO2 will be exported through a 142 km carbon steel 28'' pipeline to the Endurance CO2 storage site (capacity 10 MTPA). An additional 101km carbon steel 28'' pipeline from Humber to Endurance will be used, to transport and store up to additional 17 MTPA peak form Humber emitters with 1.7 MTPA CO2 initially (Phase 1). Both pipelines will join at the Wye as shown above in **Figure 109**.

Beyond Phase 2, additional ramp-up from 10 MTPA to 23 MTPA will be accommodated via expansion at Endurance (which would have benefited from a longer dynamic appraisal period circa 8 years) and expansion at the additional Bunter Stores through Endurance infrastructure. Dynamic learnings from the portfolio of stores will allow the NZT/NEP to refine performance understanding for the various store and ramp-up injection across the pool of CO2 stores in an efficient manner and allow an optimised Brine production.

11.0 References

Bachmann G.H., Geluk, M.C., Warrington, G., Becker-Roman, A., Beutler, G., Hagdom, H., Hounslow, M.W., Nitsch, E., Rohling, H.G., Simon, T. and Szulc, A., 2010. Triassic. In: J.C. Doornenbal and A.G. Stevenson (Eds.) Petroleum Geological Atlas of the Southern Permian Basin Area, EAGE Publications, Houten, 149–173.

Blackbourn, G.A., 2012. Petrography of seven core samples from the Bunter Sandstone of well 42/25-1, UK North Sea. Blackbourn Geoconsulting, report prepared for National Grid Carbon in consultation with AGR Petroleum Services, 35pp.

Blackbourn, G.A., 2014. Petrography of cuttings samples from the Bunter Sandstone of well 43/28a-3, UK North Sea. Blackbourn Geoconsulting, report prepared for National Grid Carbon in consultation with AGR Petroleum Services, 46pp.

Blackbourn, G.A. and Robertson, L.F., 2014. Sedimentology, petrography and burial history of the cored Triassic section in National Grid Carbon well 42/25d-3, UK North Sea. Blackbourn Geoconsulting, report prepared for National Grid Carbon in consultation with AGR Petroleum Services, 163pp.

Conway, A.M. and Valvatne, C., 2003. The Boulton Field, Block 44/21a, UK North Sea. In: J.G. Gluyas and H.M. Hichens (Eds.) United Kingdom Oil and Gas Fields Commemorative Millennium Volume, Geological Society, London, Memoir, 20, 671–680.

Coward, M.P., Dewey, J., Hempton, M. and Holroyd, J., 2003. Tectonic evolution. In: D. Evans, C. Graham, A. Armour and P. Bathurst (Eds.) The Millennium Atlas: Petroleum Geology of the Central and Northern North Sea, Geological Society, London, 17–23.

Doornenbal, J.C. and Stevenson, A.G. (Eds.), 2010. Petroleum Geological Atlas of the Southern Permian Basin Area, EAGE Publications, Houten, 342pp.

Fossen, H., Soliva, R., Ballas, G., Trzaskos, B., Cavalcante, C. and Schultz, R. A., 2018. A review of deformation bands in reservoir sandstones: geometries, mechanisms and distribution. Geological Society, London, Special Publications, 459, 9-33.

Gast, R.E., Dunsar, M., Breitkreuz, C., Gaupp, R., Schneider, J.W., Stemmerik, L., Geluk, M.C., Geisbler, M., Kiernsnowski, H., Glennie, K.W., Kabel, S. and Jones,N.S., 2010. Rötliegend. In: J.C. Doornenbal and A.G. Stevenson (Eds.) Petroleum Geological Atlas of the Southern Permian Basin Area, EAGE Publications, Houten, 101–121.

George, G.T. and Berry, J.K., 1997. Permian (Upper Rötliegend) synsedimentary tectonics, basin development and palaeogeography of the southern North Sea. In: K. Ziegler, P. Turner and S.R. Daines (Eds.) Petroleum Geology of the Southern North Sea: Future Potential, Geological Society, London, Special Publication, 123, 31–61.

Geluk, M., McKie, T. and Kilhams, B., 2018. An introduction to the Triassic: current insights into the regional setting and energy resource potential of NW Europe. In: B. Kilhams, P.A. Kukla, S. Mazur, T. McKie, H.F. Munlieff and K. Van Ork (Eds.) Mesozoic Resource Potential in the Southern Permian Basin, Geological Society, London, Special Publication, 469, 139–147.

Glennie, K.W., 1997. History of exploration in the southern North Sea. In: K. Ziegler, P. Turner and S.R. Daines (Eds.) Petroleum Geology of the Southern North Sea: Future Potential, Geological Society, London, Special Publication, 123, 5–16.

Grant, R.J., Underhill, J.R., Hernandez-Casado, J. and Barker, S., 2019. Upper Permian Zechstein Supergroup carbonate-evaporite platform palaeomorphology in the UK Southern North Sea, Marine and Petroleum Geology, 100, 484–518.

Guterch, A., Wybraniec, S., Grad, M., Chadwick, R.A., Krawczyk, C.M., Zeigler, P.A., Thybo, H. and De Vos, W., 2010. Crustal structure and structural framework. In: J.C. Doornenbal and A.G. Stevenson (Eds.) Petroleum Geological Atlas of the Southern Permian Basin Area, EAGE Publications, Houten, 11–23.

Ingram, G. M. and Urai, J. L., 1999. Top-seal leakage through faults and fractures: the role of mudrock properties. Geological Society, London, Special Publications, 158 (1), 125-135.

Kombrink, H., Besly, B.M., Collinson, J.D., Den Hartog Jager, D.G., Drozdrewski, G., Dunsar,M., Hoth, P., Pagnier, H.J.M., Stemmerik, L., Waksmundzka, M.I. and Wrede,V., 2010. Carboniferous. In: J.C. Doornenbal and A.G. Stevenson (Eds.) Petroleum Geological Atlas of the Southern Permian Basin Area, EAGE Publications, Houten, 81–99.

Lott, G.K., Wong, T.E., Dunsar, M., Andsbjerg, J., Monnig, E., Feldman-Olszewska, A. and Verreussel, R.M.C.H., 2010. Jurassic. In: J.C. Doornenbal and A.G. Stevenson (Eds.) Petroleum Geological Atlas of the Southern Permian Basin Area, EAGE Publications, Houten, 175–193.

Moscariello, A., 2003. The Schooner Field, Blocks 44/26a, 43/30a, UK North Sea. In: J.G. Gluyas and H.M. Hichens (Eds.) United Kingdom Oil and Gas Fields, Commemorative Millennium Volume, Geological Society, London, Memoir, 20, 811–824.

O'Mara, P.T., Merryweather, M., Stockwell, M. and Bowler, M., 2003. The Trent Gas Field, Block 43/24a, UK North Sea. In: J.G. Gluyas and H.M. Hichens (Eds.) United Kingdom Oil and Gas Fields, Commemorative Millennium Volume, Geological Society, London, Memoir, 20, 835–849.

Pharaoh, T.C., Dusar, M., Geluk, M.C., Kockel, F., Krawczyk, C.M., Krzywiec,P., Scheck-WendeRöth, M., Thybo, H., Vejbaek, O.V. and Van Wees, J.D., 2010. Tectonic evolution. In: J.C. Doornenbal and A.G. Stevenson (Eds.) Petroleum Geological Atlas of the Southern Permian Basin Area, EAGE Publications, Houten, 25–57.

Price, N. J. and Cosgrove, J. W., 1990. Analysis of geological structures. Cambridge University Press.

Richardson, S., 2015. Key structural elements, tectonostratigraphy and lineament analysis of the Southern North Sea. BP internal report, 40pp.

SPE, 2020. Guidelines for Applications of the CO2 Storage Resources Management System.

Stewart, S.A. and Coward, M.P., 1995. Synthesis of salt tectonics in the southern North Sea, UK, Marine and Petroleum Geology, 12 (5), 457–475.

Underhill, J.R., 2003. The tectonic and stratigraphic framework of the United Kingdom's oil and gas fields. In: J.G. Gluyas and H.M. Hichens (Eds.) United Kingdom Oil and Gas Fields, Commemorative Millennium Volume, Geological Society, London, Memoir, 20, 17–59.

White Rose, 2016. K40: Subsurface geoscience and production chemistry reports. Capture Power Limited, 300pp., https://assets.publishing.service.gov.uk/government/uploads/system/uploads/attachment_data/file/531045/K40_Subsurface_Geoscience_and_Production_Chemistry.pdf

This publication is available from: www.gov.uk/beis

If you need a version of this document in a more accessible format, please email enquiries@beis.gov.uk. Please tell us what format you need. It will help us if you say what assistive technology you use.